Department of AERONAUTICS and ASTRONAUTICS
STANFORD UNIVERSITY

John A. Sorensen

PRECISION MAGNETIC ATTITUDE CONTROL OF SPINNING SPACECRAFT

This work was performed in association with research sponsored by the National Aeronautics and Space Administration under Research Grant NSR 05 020 379

AUGUST 1969

SUDAAR NO. 380

Department of Aeronautics and Astronautics
Stanford University
Stanford, California

PRECISION MAGNETIC ATTITUDE CONTROL OF SPINNING SPACECRAFT

by

John A. Sorensen

SUDAAR No. 380

August 1969

This work was performed in association with research sponsored
by the National Aeronautics and Space Administration
under Research Grant NSR 05 020 379

ABSTRACT

This dissertation presents a study of the precision magnetic attitude control of rigid, earth orbiting spacecraft which are nominally spinning about their maximum axes of inertia. Specifically, control systems for accurately pointing the satellites' spin axes and maintaining nearly constant spin speed are investigated. The effects of environmental disturbances and incorrect vehicle parameters upon obtainable pointing accuracies are evaluated.

The first control system studied is for axisymmetric vehicles operating in highly eccentric orbits, each with its spin axis constrained to point normal to the orbit plane. One application of this type of spacecraft and orbit configuration is to measure the unknown tesseral harmonic coefficients of the earth's gravitational potential; an analysis of the selection of orbital elements for this purpose is included. Next, the Kalman filtering of horizon-sensor measurements of roll error is shown to provide an effective means of lowering the overall attitude error of the satellite. An algebraic solution of the quadratic matrix equation governing the minimum power controller is derived and used to generate a pointing control law suitable for the spacecraft with or without a nutation damper. It is shown that this control law can be mechanized magnetically by either three orthogonal coils or a single coil skewed 45° to the spin axis. Spin speed control is simultaneously provided by incorporation of a unique three-mode logic into the mechanization.

Another magnetic attitude control system investigated points the spin axis of a spacecraft precisely at a star. The vehicle considered has a circular, polar orbit, and attitude error measurements are made by means of an optical star tracker. A reduced-order observer is developed to estimate disturbance torques acting upon the spacecraft and these estimates are utilized to cancel the torques' effect. Performance evaluation of this magnetic controller indicates that it compares quite favorably with other precision control devices.

Finally, a method is developed for synthesizing continuous attitude control laws for nonsymmetric spinning vehicles. This technique allows the designer to provide arbitrary dynamic response to the vehicle and has direct application to magnetic attitude control.

CONTENTS

CONTENTS (Cont)

TABLES

LIST OF ILLUSTRATIONS

LIST OF ILLUSTRATIONS (Cont)

LIST OF ILLUSTRATIONS

LIST OF ILLUSTRATIONS

LIST OF SYMBOLS

A	matrix formed from F_1 in Appendix D
A_c	area of coil
A_{ls}	a_{ls} plus jb_{ls}
A_r	matrix of a quadratic matrix equation
A_s	moment of inertia ratio $(I_{zz} - I_{xx})/I_{yy}$
$A_{1,2,3,4}$	coefficients used to compute ρ as a function of T_m
A_α	magnitude of $\alpha_x + j\alpha_y$
a	orbit semi-major axis
a_e	mean earth radius
$a_1, \ldots, a_n$	coefficients of characteristic equation of F
a_{ls}, a_{Os}	coefficients of complex symmetric equations
a_p	3-hour magnetic activity index in units of $2\gamma_m$
a_s	moment of inertia ratio $(I_{zz} - I_{xx})/I_{xx}$ for a symmetric satellite
B	magnitude of $\vec{B}$
$\vec{B}$	the earth magnetic field
B_O	a nominal value of B
B_i	induced magnetic flux in satellite material
B_{ls}	$a_{Os} + jb_{Os}$
B_r	matrix of quadratic matrix equation
B_s	the moment of inertia ratio $(I_{zz} - I_{yy})/I_{xx}$
B_{x_O}	constant value of B
$B'_{x,y,z}$	the cartesian components of $\vec{B}$
$B_{x,y,z}$	measured values of $B_{x,y,z}$

B_α	amplitude parameter of $\lvert\phi + j\theta\rvert$
b	column matrix $M_1^{-1} A^{-1} K$
b_i	bias of the i^{th} horizon-sensor pair
b_{1s}, b_{0s}	coefficients of complex symmetric equations
$b_{x,y,z}$	bias terms of the magnetometers
C	a matrix of arbitrary elements which reduces the output of a multivariable system to the minimum output required to build a system state estimator
$C_{B/R}$	orthogonal transformation matrix from reference frame to body frame
C_{d1}, C_{d2}	deadband boundaries on spin speed
C_p	value of $\dot{\sigma}$ at the point of the semilatus rectum
C_r	matrix of a matrix quadratic equation
C_0	optimal control law gain matrix
$C_1 - C_5$	constants
$\vec{C}_3$	earth-reflected radiant flux per unit area
C_{10}	$\dot{\omega}_p + \dot{M} + m(\dot{\Omega} - \dot{\theta}_e)$, a constant dependent upon the orbit's mean elements
c	column matrix
c_i	column of C
c_ℓ	speed of light in a vacuum
c_1	$-0.5\,[d_p + j(n - D)]$
D	$(I_{zz}/I_{xx})\dot{\psi}$, the normalized satellite angular momentum
D_m	declination angle of the magnetic field (Fig. A.1)
D_n	sub-block of error system matrix of reduced-order observer
D_r	drag force magnitude
D_s	$(B_s/A_s)^{\frac{1}{2}}$

$\vec{D}_3$	total reflected radiant flux
d	days from January 1
$\vec{d}$	vector from origin to $d\vec{s}$
dA	incremental area of earth or satellite surface
d_p	nutation damper time constant
$d\vec{s}$	$\hat{n}dA$, the incremental area of the satellite surface
d_w	satellite wall thickness
E	kinetic energy of satellite
e	eccentricity of orbit
$\hat{e}$	arbitrary unit vector
$\hat{e}_{1,2}$	unit vectors
F, F(t)	system matrix
$F_{cx,y}$	translational control force
$F_{\ell mp}(i)$	the inclination function (Eq. 2.46)
F_1	$M_1 F M_1^{-1}$
F_2	$AM_1 F M_1^{-1} A^{-1}$
$F_{10.7}$	the 10.7 cm decimetric flux from the sun in units of 10^{-22} Watts/m^2/cps bandwidth
$\bar{F}_{10.7}$	monthly average of $F_{10.7}$
$F_{11}, F_{12}, F_{21}, F_{22}$	sub-blocks of F
f	true anomaly
f_n	empirical function used to determine ν_n as a function of h_a and $\alpha_\odot$
$\vec{f}_p$	force of gravitational attraction on a particle at point p
f_τ	function used to compute shear force S_{cyl}

$G, G(t)$	distribution matrix
$G_{\ell pq}(e)$	the eccentricity function (Eq. 2.47)
G_2	$T_1 G$
G_{11}, G_{21}	sub-blocks of G
g_e, g_{eo}	gravitational acceleration
g_n^m, h_n^m	coefficients corresponding to multiple of the associated Legrendre function describing the earth magnetic field
$H, H(t)$	output matrix
$\vec{H}$	satellite angular momentum
H_a	hour angle of sun
H_i	scale height corresponding to the i^{th} element
H_m	horizontal component of the magnetic field (Fig. A.1)
H_o	orbital angular momentum
H_2	PHT_1^{-1}
h_a	altitude
h_p	altitude of perigee
$h_1, h_2, \ldots$	rows of H
I	identity matrix
$\vec{\vec{I}}$	satellite moment of inertia dyadic
$\mathbf{I}_B$	$\vec{\vec{I}}$ coordinatized in body frame
I_m	identity matrix of order m or dip angle of the magnetic field (Fig. A.1)
I_{xx}, I_{yy}, I_{zz}	satellite moments of inertia about the $\hat{x}_B$, $\hat{y}_B$, and $\hat{z}_B$ axes
I_{xo}	nominal value of I_{xx}
I_{zo}	nominal value of I_{zz}
I_{xy}, I_{xz}, I_{yz}	cross products of inertia

i	inclination of orbit
i_c	current in coil
$i_{x,y}$	currents in the skewed coil controller
J	Jordan matrix
$J_{a,b,c}$	sub-blocks of J
J_f	cost function or performance index
$J_{\ell m}$	magnitude of tesseral harmonic of degree ℓ and order m
$J_{2,3,\cdots}$	zonal harmonic terms of earth gravitational potential
j	$\sqrt{-1}$
K	gain matrix of state estimator
K_{Bz}	gain equal to time average value of $1/B_z$
K_d	constant determining rate of change of kinetic energy due to the nutation damper
$K_g(t)$	time varying gain matrix
K_{IB}	control gain to cancel body-fixed torque
K_{II}	control gain to cancel inertially-fixed torque
$K_{\ell 1}$, $K_{\ell 2}$	limit cycle effect on translational control jet torque
K_{OB}	time average value of $1/B^2$
K_p, K_{p1}, K_{p2}	position control gains
K_{pu}	pulse estimator gain
K_v	rate control gain
K_{v1}	translational control gain
K_w	wind constant
K_z	spin control gain
$K_{1,2}$	lower and upper bounds on $K_g(t)$
k_B	Boltzmann constant
k_c	constant

$k_{fx,y,z}$	scale factor errors of the magnetometers
k_m	maximum value of $k_1(t)$
$k_{nx,y,z}$	quadratic nonlinearities of the magnetometers
$k_1(t) \ldots k_p(t)$	diagonal elements of $K_g(t)$
k_2	constant
$k_{10}, \ldots k_{p,\alpha p}$	elements of the matrix K
$k_{11}, \ldots k_{1p}$	diagonal elements of K_1
$k_{21}, \ldots k_{2p}$	diagonal elements of K_2
L	gain matrix of reduced-order observer equal to bc^T
L_1	distribution matrix for $\vec{v}_1$
$\vec{L}_\odot$	vector from observable illuminated increment of earth dA to satellite
ℓ	length of cylindrical satellite or an index
ℓ_1, ℓ_2, ℓ_3	components of complex matrix L
M	mean anomaly
M_L	lateral component of $\vec{M}_s$
M_r	positive definite matrix
$\vec{M}_s$	spacecraft dipole magnetic moment
M_z	spin component of $\vec{M}_s$
M_1	observability matrix defined in Appendix D
$\vec{m}$, m	magnetic moment or an index
m_i	molecular or atomic mass
m_p	particle of mass at point p
m_r	mass of radiant energy
m_s	$0.5(D_s + 1)(\phi + j\theta)$
$m_{x,y,z}$	the cartesian components of $\vec{m}$
$m'_{x,y,z}$	actual magnetic moment generated by the magnetic coils
$m_{1,2,3,4}$	elements of M_r

N	number of turns of wire in coil
N_r	matrix used in deriving Lyapunov function
N_s	$(B_s A_s)^{\frac{1}{2}} / \dot{\psi}$
$N_{x,y,z}$	fluctuations of the magnetic field components not detected by the magnetometers
n	mean orbital rate or an index
$\hat{n}$	outward normal vector from dA
n_i	gas concentration
n_1, n_2	constants used to define $\dot{\sigma}$ variation
P_c	effective leak force
$\vec{P}_{cyl}$	total atmospheric normal force on side of cylindrical satellite
$\vec{P}_{end}$	total atmospheric normal force on end of cylindrical satellite
P_m	transformation matrix for modifying H
$P_n^m(\cos \theta_p)$	multiple of the associated Legendre function
$P^{n,m}(\cos \theta_p)$	Gauss normalized multiple of the associated Legendre function
P_r	matrix used in deriving Lyapunov function
$P(t)$, P, P_1	positive definite matrices used to determine power optimal control law
P_w	power used by coil to generate a magnetic moment
P_2	covariance matrix which is expected value of $\vec{\epsilon}_1 \vec{\epsilon}_1^T$, i.e., $E\{\vec{\epsilon}_1 \vec{\epsilon}_1^T\}$
P_3	matrix with sub-blocks of A_r, B_r, and C_r
P_∞	steady-state value of P(t)
p	semilatus rectum of orbit
$\vec{p}$	atmospheric normal force per unit area
p_s	$0.5(D_s + 1)(\phi + j\theta)$

Q	covariance matrix of $\vec{v}_1(t)$
$Q_o(t)$	observability matrix of time varying system
Q_r	positive definite matrix
Q_2	matrix in J_f
q_n	$\omega_x + jD_s\omega_y$
$q_{1,2}$	elements of Q and Q_2
R	$\lvert\vec{R}\rvert$
$\vec{R}$	radius vector from geocenter to satellite mass center
$\hat{R}$	unit vector pointing from geocenter to satellite
$\hat{R}_\odot$	unit vector pointing from geocenter to sun
R_a	magnitude of $\vec{R}_{a1}$, $\vec{R}_{a2}$, or $\vec{R}_{a3}$
$\vec{R}_{a1}$	direct solar radiation
$\vec{R}_{a2}$	earth emitted radiation
$\vec{R}_{a3}$	earth reflected radiation
$R_{\ell mpq}$	element of the harmonic expansion of the earth gravitational potential
R^n	n-dimensional Euclidean space
$\vec{R}_p$	position of each particle m_p of satellite with respect to the geocenter
R_s	I_{zz}/I_{xx}
R_1	variance of w(t)
R_2	matrix in J_f
r	radius of cylindrical satellite or index
r_j	electrical resistance of the j^{th} coil
r_p	radius of perigee
r_s	$p_s \exp\left[-j(N_s + 1)\psi/2\right]$

S	complex version of matrix P
$\vec{S}_{cyl}$	total atmospheric shear force on side of cylindrical satellite
$\vec{S}_{end}$	total atmospheric shear force on end of cylindrical satellite
$S_k(t)$	column of matrix $Q_o(t)$
S_n	subspace of R^n
S_r	flux of radiant energy crossing unit area
$S_\odot$	function of $x_\odot$ used to compute temperature as a function of T_∞ and altitude
s_s	$m_s \exp(-j(N_s - 1)\,\psi/2)$
s_{11}, s_{12}, s_{22}	elements of matrix S
$\vec{T}$	the total applied torque
T_∞	T_∞' modified to account for geomagnetic activity
T_∞'	T_o modified to account for variations from the solar bulge
T_B	$\vec{T}$ coordinatized in the body frame
T_{Baero}	B body-fixed torque due to the atmosphere
T_{BM}	body-fixed component of $\vec{T}_{mag}$
$\vec{T}_c$	control torque
$T_{cx,y,z}$	cartesian components of $\vec{T}_c$
$\vec{T}_D$	the desired torque
$T_{Dx,y,z}$	the cartesian components of $\vec{T}_D$
$\vec{T}_e$	eddy-current torque
$\vec{T}_{gg}$	gravity gradient torque
$\vec{T}_{Iaero}$	inertially-fixed torque due to the atmosphere
T_{Ij}	magnitude of average inertially-fixed torque due to misaligned or leaky jet

T_{IM}	inertially-fixed component of T_{mag}
$\vec{T}_k$	torque equivalent to that required to move satellite away from reference frame at the rate of the frame's kinematic motion with respect to inertial space
T_m	temperature in degrees Kelvin
$\vec{T}_{mag}$	magnetic disturbance torque
T_{mi}	temperature of incident molecules of air
T_{mr}	temperature of reflected molecules of air
T_{mw}	temperature of the satellite's outer surface
T_n	$T_{x1} + jD_s T_{y1}$
T_r	matrix which transforms P_2 to Jordan canonical form
$\vec{T}_{Saero}$	spin torque due to the atmosphere
$T_{sj1}, \cdots T_{sj4}$	magnitude of average spin torque due to misaligned or leaky jet
T_x, T_y, T_z	components of $\vec{T}$ coordinatized in body frame
T_{x+}, T_{x-}	pulse torques about the $\hat{x}_B$ axis due to misalignment of the $\hat{y}_B$ axis translational control jets.
T_{xo}	a body-fixed torque about $\hat{x}_B$
T_{x_1}	T_x normalized as T_x/I_{xx}
T_{x_2}, T_{y_2}	functions of T_x, T_y, I_{xx}, I_{yy}, and ψ
T_{y+}, T_{y-}	pulse torques about the $\hat{y}_B$ axis due to misalignment of the $\hat{x}_B$ axis translational control jets
T_{y1}	T_y normalized as T_y/I_{yy}
T_0	$\bar{T}_o$ with semiannual and 27-day effects
$\bar{T}_0$	night-time minimum temperature at 1000 km altitude
$\bar{T}_0'$	fluctuation in $\bar{T}_0$ caused by 27-day effect
T_1	transformation matrix AM_1
T_{*x}, T_{*y}	inertially-fixed torque components about the $\hat{x}_*$ and $\hat{y}_*$ axes

t	time
t_y	epoch, in years
t_-	time instant immediately preceding sampling time
t_+	time instant immediately following sampling time
t_1, t_2	pulse width of right and left horizon sensors
$\hat{u}$	signal proportional to $\vec{u}$
$u, u(t), \vec{u}$	system input or control vector
u_x, u_y	$\hat{x}_B$ and $\hat{y}_B$ components of $\vec{u}$
u_1, u_2	elements of $\vec{u}$
$\vec{V}$	arbitrary vector
$\vec{V}_{air}$	inertial velocity of air mass of the atmosphere
$\overset{B}{\dot{\vec{V}}}$	time derivative of $\vec{V}$ in body frame
V_B	$\vec{V}$ coordinatized in body frame
Vol	volume of material
V_g	gravitational potential of the earth
$\vec{V}_I$	inertial velocity of satellite
V_i, $\lvert\vec{V}_i\rvert$	relative speed of incoming air molecules
$V_\ell(\vec{x},t)$	Lyapunov function
V_m	magnetic potential of the earth
$\overset{R}{\dot{\vec{V}}}$	time derivative of $\vec{V}$ in reference frame
V_R	$\vec{V}$ coordinatized in reference frame
V_r, $\lvert\vec{V}_r\rvert$	relative speed of outgoing air molecules
$\vec{V}_s$	inertial velocity of satellite
$\vec{v}$, $\vec{V}_i$	normalized disturbance torque
$v_1, \ldots, v_4$	random changes to disturbance torques

$W_1(t)$, $W_2(t)$	positive definite functions
w	measurement noise
w_1	$\Gamma e^{-c_1 t}$
$\hat{X}$, $\hat{Y}$, $\hat{Z}$	inertial reference frame used to define the nutation angle
X_m, Y_m, Z_m	northward, eastward, and downward components of the earth magnetic field (Fig. A.1)
$\hat{\vec{x}}$	estimated value of $\vec{x}$
x, $x(t)$, $\vec{x}$	system state vector
$\vec{x}(0)$	the initial value of $\vec{x}(t)$
$\hat{x}_B$, $\hat{y}_B$, $\hat{z}_B$	cartesian unit vectors defining the satellite-fixed or body-fixed frame with $\hat{z}_B$ being the nominal spin axis
$\hat{x}_I$, $\hat{y}_I$, $\hat{z}_I$	cartesian unit vectors defining an inertial reference frame
$\hat{x}_L$, $\hat{y}_L$, $\hat{z}_L$	cartesian unit vectors defining a local reference frame
$\hat{x}_p$, $\hat{y}_p$, $\hat{z}_p$	cartesian unit vectors defining the non-spinning frame aligned with $\hat{z}_p$ along the nominal spin axis
$\hat{x}_R$, $\hat{y}_R$, $\hat{z}_R$	cartesian unit vectors defining a general reference frame
$\hat{x}_*$, $\hat{y}_*$, $\hat{z}_*$	cartesian unit vectors defining the star reference frame
$\hat{x}_1$, $\hat{x}_2$	subvectors of x
$\hat{x}_1$, $\hat{y}_1$	unit vectors used to define atmospheric torques
$\bar{x}_2$	state of reduced-order observer
$\hat{x}_2$	output of reduced-order observer - an estimate of x_2
$x_\odot$	function of T_∞

y, $y(t)$, $\vec{y}$	system output vector
$\hat{y}_k$	unit vector along the descending line of nodes of the orbit
$\hat{z}$, $\hat{z}(t)$	state estimator system state
$\hat{z}_e$	unit vector along the earth's spin axis

GREEK SYMBOLS

α_a	accommodation coefficient
α_d	thermal diffusion factor
α_{max}	the maximum eigenvalue of F
α_p	phase angle
α_x, α_y	body rates along $\hat{x}_p$ and $\hat{y}_p$ in the nonspinning frame
α_{xo}, α_{yo}	initial values of α_x and α_y
α_v	$90° - \delta_v$
α_l	$\alpha_x + j\alpha_y$
$\alpha 1$, $\alpha 2$	indices used to form M_l
$\alpha_\odot$	angle between vectors from the geocenter to the sun and the satellite
β	a function of eccentricity: $e/(1 + \sqrt{1-e^2})$
β_n	time constant of the Markov process η_n
β_v	$\sin^{-1}(a_e/R)$
β_{10}, $\cdots$ $\beta_{p,\alpha p}$	elements of the matrix F_l
Γ	earth albedo
Γ_l	$\phi + j\theta$
γ_m	gamma (equal to 10^{-5} gauss)
γ_v	$\dot{\psi} t_l/2$
γ_x, γ_y	star tracker variables defined in Eq. 2.25

γ_{xo}, γ_{yo}	initial values of γ_x and γ_y
γ_1, ... γ_n	coefficients of the desired observer characteristic equation
Δ_ℓ	lead angle
Δt	$(t_2 - t_1)/2$
Δt_1, Δt_2	increments of time used to estimate pulse torques
Δt_3	$\Delta t_1 + \Delta t_2$
$\Delta\dot{\psi}$	spin speed deviation
δI_x, δI_y, δI_z	variations of the moments of inertia of the satellite from the nominal values used in modeling
δ_m, δ_{k-1}	function in associated Legendre function of the Schmidt normalized earth magnetic field model
δ_n	$\cos^{-1}(a_e/R)$
δ_r	distance the satellite center of mass is from the nominal spin axis
δrj1, ... δmj4	misaligned jet average moment arms normal to nominal spin axis of satellite
δ_{ts}	Dirac delta function equal to unity at time of horizon sensor measurement
δ_v	half-vee angle of horizon sensors
δ_{x+}, δ_{x-}, δ_{y+}, δ_{y-}	delta functions equal to one when appropriate translational control jet is firing
δ_z	distance center of mass of satellite is from geometric center as projected along the nominal spin axis
δ_{zj}	misaligned jet average moment arm along spin axis
$\delta\omega_z$	$\omega_z - \dot{\psi}_o$, i.e., spin speed variation
ϵ	grey-body emissivity of earth
ϵ_o	angle traveled during one-half the off-time of the skewed-coil controller
ϵ_x, ϵ_y	small angles of misalignment of the $\hat{x}_B$ magnetometer
ϵ_1, ϵ_2	error states of reduced-order observer

ζ_r,	angle at which $\vec{R}a$ strikes the satellite wall
ζ_x, ζ_y	small angles of misalignment of the $\hat{z}_B$ magnetic coil
ζ_1	the angle nt - ξ_o used in describing the uncontrolled motion of the spinning satellite.
η_i	angle between $\vec{V}_i$ and satellite wall
η_n	variable which represents a Markov noise process
η_r	angle between $\vec{V}_r$ and satellite wall
η_x	small angle misalignment of the $\hat{y}_B$ magnetic coil
η_o	phase angle of $\eta_1(t)$
$\eta_\odot$	the angle 0.5 $\lvert\lambda_s - \lambda_\odot\rvert$ used to define the atmospheric temperature
$\eta_1(t)$	the angle nt + η_o used in describing the uncontrolled motion of the spinning satellite
Θ_o	latitude of the geomagnetic south pole
θ	roll error
θ_e	hour angle of Greenwich
θ_n	$\cos^{-1}(\hat{n} \cdot \vec{L}_\odot / \lvert\vec{L}_\odot\rvert$
θ_p	satellite's earth colatitude
$\hat{\theta}_p$	the vector $(\cos\theta_p \hat{R} - \hat{Z}_e)/\sin\theta_p$
θ_s	sampled value of θ
θ_0	initial value of θ
$\theta_\odot$	the angle 0.5 $\lvert\lambda_s + \lambda_\odot\rvert$ used to define the atmospheric temperature
θ'	geomagnetic colatitude

Λ	matrix used to solve for covariance P_2
Λ_e	general emittance
$\Lambda_{11}, \Lambda_{12}, \Lambda_{21}, \Lambda_{22}$	sub-blocks of Λ
Λ_*	right ascension of reference star
λ	an eigenvalue of a matrix
λ_m	$\cos^{-1}(\vec{B} \cdot \hat{Z}_B / B)$
$\lambda_{max}(P)$	maximum eigenvalue of covariance matrix P
λ_n	$\cos^{-1}(\hat{R}_\odot \cdot \hat{n})$
λ_s	declination of satellite position
$\lambda_\odot$	declination of the sun
λ_*	declination of reference star
μ	product of mass of the earth and the universal gravitation constant
μ_x, μ_y	small angles of misalignment of the $\hat{y}_B$ magnetometer
μ_1	a constant
ν	a constant
ν_n	angle between $\vec{R}$ and $\vec{D}_3$
ν_x, ν_y	small angles of misalignment of the $\hat{z}_B$ magnetometer
ξ, η, ζ	classical Euler angles rotating $\hat{X}$, $\hat{Y}$, and $\hat{Z}$ into $\hat{x}_B$, $\hat{y}_B$, and $\hat{z}_B$ in wobble process. The angle η is the nutation angle. These angles are defined in Fig. 2.4.
ξ_y, ξ_z	small angles of misalignment of the $\hat{x}_B$ magnetic coil
ξ_o	phase angle of $\xi_1(t)$
$\xi_1(t)$	the angle $D_s t + \xi_o$

ρ	atmospheric density in gm/cm^3
$\vec{\rho}_p$	position of each particle m_p of satellite with respect to the center of mass
ρ_r	surface reflectivity
$\Sigma(t)$	covariance matrix of $(\vec{x} - \hat{x})$
Σ_∞	steady state value of $\Sigma(t)$
σ	the angle of the satellite position with respect to the line of nodes, i.e., $f + \omega_p$
σ_c	electric conductivity of satellite wall
σ_{sb}	Stefan-Boltzmann constant
τ	time
$\tau_\odot$	angle used to express position of solar bulge
$\vec{\tau}_s$, τ_s	atmospheric or radiation shear force per unit area
Φ_b	beam width factor
Φ_o	longitude of the geomagnetic south pole
φ_e	steady-state value of the yaw angle with estimator in the control mechanization
φ_L	bound on illuminated area of earth viewed from satellite
φ_{ne}	steady-state value of the yaw angle with no estimator in the control mechanization
φ_o, θ_o	initial values of φ and θ
φ_p	satellite's earth east longitude
φ, θ, ψ	non-classical Euler angles; φ is yaw angle, θ is roll angle; ψ is angle about nominal spin axis defined in Fig. 2.1.

$\dot{\psi}$	satellite spin rate
$\psi_{\ell mpq}$	argument of $R_{\ell mpq}$
$\dot{\psi}_o$	nominal value of $\dot{\psi}$
Ω	right ascension of ascending node of orbit
Ω_r	open region about the origin
Ω_s	frequency of a harmonic oscillator
$\vec{\omega}$	$\vec{\omega}^{B-I}$
$\vec{\omega}^{B-I}$	angular velocity of satellite about its center of mass with respect to an inertial coordinate system
$\overset{\omega}{B}$	$\vec{\omega}^{B-I}$ coordinatized in the body frame
$\vec{\omega}_e$	earth spin rate
ω_p	argument of orbit perigee
ω_{vi}	frequency of the i^{th} component of $\vec{V}_l$
ω_x, ω_y, ω_z	components of $\vec{\omega}^{B-I}$ in the body frame
ω_{xo}, ω_{yo}	initial values of ω_x and ω_y

SPECIAL SYMBOLS AND NOTATION

$\frac{d}{dt}^{I}(\vec{\ })$	time rate of change of the vector in the inertial frame
diag{ }	a diagonal matrix whose diagonal elements are enclosed in the brackets
E{ }	the expected value of
Im( )	imaginary part of complex variable
Re( )	real part of complex variable
$\overline{s_{12}}$	conjugate of complex variable s_{12}
tr( )	trace of matrix

$\overset{B}{(\vec{\ })}$	time derivative of a vector in the body frame
$(_B)$	vector coordinatized in the body frame
$\overset{I}{(\vec{\ })}$	time derivative of a vector in the inertial frame
$(\ )^T$	transpose of matrix
$\nabla(\ )$	gradient
$(\ )^{-1}$	matrix inverse
$(\dot{\ })$	time derivative; i.e., $\frac{d}{dt}(\ )$
$(\hat{\ })$	a unit vector
$(\ )^*$	complex conjugate of transpose of matrix
$(\vec{\ })$	a vector quantity
$(\vec{\vec{\ }})$	a dyadic
$(\vec{\ }) \cdot (\vec{\ })$	vector inner product
$(\vec{\ }) \times (\vec{\ })$	vector cross product
$\lvert(\ )\rvert$	absolute value of a quantity
$\lVert(\ )\rVert$	the maximum eigenvalue of the enclosed matrix
$\triangleq$	defined as
$\cong$	approximately equal
∎	end of theorem, corollary, or definition
$\emptyset$	matrix block of zero elements
$\hat{\hat{1}}$	the idemfactor, a dyadic for which $\hat{\hat{1}} \cdot \vec{V} = \vec{V}$

ACKNOWLEDGMENT

I wish to thank Professor Benjamin O. Lange for his advice and guidance throughout the course of this study, and Professor Robert H. Cannon, Jr., for his thorough review and constructive criticism which greatly improved this final presentation. The enthusiasm, encouragement, and enlightening counsel of Professor John V. Breakwell and Dr. Daniel B. DeBra during the pursuit of this research are gratefully acknowledged. Special thanks go to Earl Hall and many other associates at Stanford for their time spent in the discussions so necessary for maintaining the day-to-day endeavor.

I also wish to express my appreciation to Connie Calica, Ida Lee, and Diana Shull for their conscientious effort in typing this manuscript.

Particular gratitude is expressed for the partial financial support of this research received initially from NASA's Electronics Research Center under Contract NAS 12-695, and finally through NASA Headquarters under Contract NSR 05 020 379. The work on attitude control of spinning drag-free satellites was also partially supported under Air Force Contract F33615-67-C-1245.

Finally, I must acknowledge the active support of my wife, Susan, for her part in preparing this presentation. In addition, her constant devotion was invaluable.

CHAPTER I

INTRODUCTION

PURPOSE OF THIS RESEARCH

The spacecraft which is spin-stabilized about its maximum axis of inertia is widely used for earth orbital applications because of its inherent ability to hold a fixed spin-axis orientation. The special purpose of this satellite may require that the spin axis be held to within minute tolerances of the desired attitude. For precision orientation, an active attitude control system is usually incorporated as an integral part of the vehicle. This control system also sustains the spacecraft spin speed.

The degree of accuracy to which a spin axis can be pointed is highly dependent upon the vehicle and its orbit. This research studies the design and analysis of continuous precision attitude control systems for satellites requiring that the spin axis be pointed normal to the orbit plane or toward a star. Specific examples of such spacecraft include two applications of the drag-free satellite.

In particular, magnetic actuation of the attitude control system for the above two applications is investigated. This control is achieved by producing a magnetic moment on the spacecraft which interacts with the earth's magnetic field to create a torque. Magnetic controllers have the advantages of requiring low power, having no moving parts or serious lifetime limitations, and being lightweight. A specific disadvantage is that they produce very weak torques. However, for the particular applications studied here, even a weak magnetic torque is sufficient for offsetting the effects of environmental disturbances. A more relevant disadvantage of magnetic control is that the local magnitude of the earth's magnetic field is time varying and rarely in the desired direction for achieving continuous pointing and spin control. Thus, basic questions arise concerning the achievable accuracies, dynamic response, and stability of such control systems. It is these areas with which this research is directly concerned.

In designing a control system for removal of small attitude error,

it is convenient if the spacecraft has mass symmetry about its spin axis, because this produces linear, constant-coefficient equations of motion. No foreseen difficulty precludes attempting to build the satellite this way, so it is usually assumed in the following development that axial mass symmetry or near symmetry exists. The subject of control synthesis for nonsymmetric spinning vehicles is treated in the last chapter.

PREVIOUS STUDIES OF MAGNETIC AND OTHER PRECISION ATTITUDE CONTROL SYSTEMS FOR SPINNING SPACECRAFT

Magnetic attitude control was first suggested around 1960 (see Kamm, Ref. 1, and White, *et al.*, Ref. 2) and was primarily directed toward control of nonspinning spacecraft about two axes. Several investigations have followed of applications to both spin-stabilized and three-axis attitude control requirements. Configurations studied have varied from single permanent magnets to three orthogonal coils used in conjunction with reaction wheels or control-moment gyros. References 3-8 represent studies of systems where magnetic torquing is used for control of nonspinning spacecraft, as a means of damping vehicle rates, or for unloading reaction wheels or control-moment gyros. Of particular interest is the paper by Paiken and Fleisig (Ref. 7) concerning the fine, three-axis momentum control of the Orbiting Astronautical Observatory (OAO) by use of inertia wheels which are unloaded using electromagnetic coils. This spacecraft is designed to achieve ± 0.1 arc sec. pointing accuracies and is now operational. Both Sonnabend (Ref. 9) and Arnesen (Ref. 10) studied versions of dual-spin spacecraft in which magnetic coils on the despun part were used to complement the reaction wheel function of the spinning portion.

Extensive studies have been made of using a single magnetic dipole aligned with the spin axis as a possible means of attitude control of a rigid spinning spacecraft. Both Ergin and Wheeler (Ref. 11) and Mobley (Ref. 12) discussed specific applications of this configuration for keeping the spin axis normal to the orbit plane. Wheeler (Ref. 13) and Renard (Ref. 14) investigated further applications of the single coil controller to general purpose satellites in circular orbits.

Vrablik, et al. (Ref. 15), discussed using electromagnetic coils with axes perpendicular to the spin axis of the Lincoln Experimental Satellite (LES) 4 for maintaining the spin axis nearly normal to the orbit plane. This spacecraft operates in a circular, near-synchronous equatorial orbit and controls the spin axis to point to within 2.6° of the orbit normal. Fischell (Ref. 16) recognized that magnetic control could be used for regulating the spin speed of the satellite. The performance of this method was elaborated upon by Mobley, et al. (Ref. 17) for the DME-A satellite.

Successful uses of magnetic attitude control systems for spinning spacecraft are also represented by the Tiros satellite program (Ref. 18) and several of the APL satellites (Ref. 19). In all, a wealth of information appears in the literature on simple, practical applications of magnetic control technique.

Much of the previous work could be directly applied to the design of a control system for maintaining the spin axis of a satellite normal to the orbit plane. However, basic questions remain to be answered when the orbit is highly eccentric and the only attitude error measurements considered are those from horizon sensors. The desire for a new look at the control requirements of this mission provides the motivation for Chapter III.

The high-accuracy attitude control of spacecraft for space astronomy has been previously studied with requirements for three-axes control. Both Fosth and Zimmerman (Ref. 20) and Liska (Ref. 21) investigated systems for achieving pointing accuracies as fine as 0.01 arc second (equivalent to pointing a telescope at a human hair one mile away) for periods of up to an hour. Further requirements of these systems are that the satellite be able to maneuver several degrees within a few minutes of time for application on the Manned Orbiting Telescope. Their basic conclusion, which is summarized in Figure 1.1, is that the control-moment gyro represents the logical choice for achieving such high precision.

Conspicuously missing from Figure 1.1 is the precision available from magnetic control. As will be seen, if the requirements of holding high accuracies for up to one hour are somewhat relaxed and no rapid

maneuvering is required, magnetic control compares favorably with the control-moment gyro.

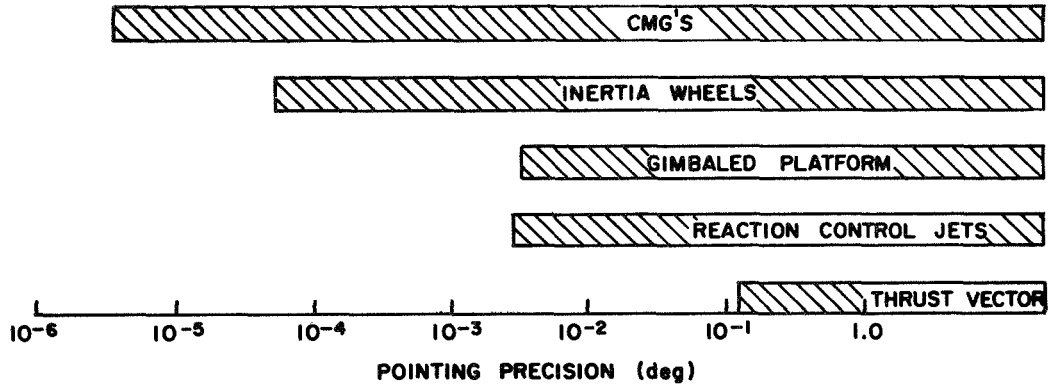

FIG. 1.1. ACHIEVABLE POINTING ACCURACIES OF NON-MAGNETIC CONTROL SYSTEMS.

OUTLINE OF NEW RESULTS AND CONTRIBUTIONS

In Chapter II, the attitude equations of motion of the rigid spinning spacecraft studied in this research are presented. Next, suitable orbits are selected for two different satellites which serve as interesting examples of systems requiring precision attitude control. From the orbit and spacecraft characteristics, the time history of various environmental disturbance torques is determined for later use in evaluating the investigated control systems.

The application of one of the satellites selected for study--the drag-free geodesy satellite--is to provide the means for measuring the unknown tesseral harmonic coefficients of the earth's gravitational potential. It is theoretically established that tracking four distinct eccentric orbits of this geodesy satellite can produce most of the unknown coefficients through degree and order 15.

In Chapter III, a technique for magnetically controlling the spin axis of a symmetric geodesy satellite to point nearly normal to the orbit plane is presented. This control method is applicable to satellites in near-earth orbits with inclinations between 20° and 70° and eccentricities of up to 0.7. The technique involves employing a Kalman filter to determine yaw error and vehicle angular rates from horizon-

sensor measurements of the roll error. Orientation and spin control are mechanized in a unique three-mode logic based upon magnitude of spin-speed variation. Computer simulations are used to demonstrate that this attitude control system outperforms magnetic controllers studied previously from the standpoints of faster transient response and ability to withstand disturbance torques. Additional contributions resulting from the development of this chapter include the following:

1. A systematic method for obtaining the algebraic solution to the quadratic matrix equations governing the optimal control of a general system possessing complex symmetry is developed. This method is utilized to determine the minimum-power optimal control gains and associated control law for the spinning spacecraft.
2. A new mechanization scheme consisting of a single coil skewed at 45° to the spin axis used in conjunction with a passive wobble damper is shown to be effective for three-degree-of-freedom attitude control.
3. Because of the time-varying magnetic field, the control system has fluctuating gains resulting in questionable attitude stability. A new method for generating Lyapunov functions is adapted to establish the bounds on the damping required for guaranteeing that the vehicle is asymptotically stable.

In Chapter IV, an all-magnetic attitude control system is investigated for precisely pointing the spin axis of a symmetric satellite at a star while maintaining spin speed. It is demonstrated that, theoretically, the pointing error can be kept within 0.01 arc second of the reference for more than 90 per cent of the period of a polar orbit. An error analysis is performed to determine the deviation of an actual system's performance from that of the ideal. Other contributions in Chapter IV include the following:

1. An extension of the Gopinath reduced-order observer for noncyclic, noncontrollable systems is made.
2. It is shown that inertially-fixed and body-fixed disturbance torques acting on the satellite are mathematically observable quantities and can thus be effectively cancelled by a propor-

tional signal being incorporated into the control law. In addition, it is demonstrated that the pulse disturbance torques due to misaligned translational control jets can be estimated and magnetically cancelled.

Finally, in Chapter V, a new method of generating a continuous control law for nonsymmetric vehicles is developed by extending a method used for symmetric vehicles. The resulting control law allows the designer to provide the system with arbitrary dynamic response. This method can be directly applied to problems of magnetically controlling the attitude of nonsymmetric spinning satellites.

CHAPTER II

EQUATIONS OF MOTION AND ORBIT-DEPENDENT DISTURBANCE TORQUES

The purpose of this chapter is to define explicitly the mathematical dynamic models of the satellite systems and their environments with which the rest of the research is concerned. These models are formulated in such a way that the characteristics of the satellite and environment (which determine the degree of accuracy obtainable and the type of magnetic attitude control required) are evident.

Attitude control is defined as maintaining the satellite in a given orientation with respect to a reference frame fixed in inertial space. In the cases studied here, the desired orientation consists of directing the spin axis of the satellite toward a fixed point on the celestial sphere or aligning it parallel to some instantaneous axis defined in space. Correct orientation is also defined to include the maintenance of the satellite spin speed within some required bounds of a nominal value.

The question of attitude control accuracy--i.e., how far and for how long does the actual vehicle orientation vary from the desired orientation--cannot be answered in general. Any meaningful answer is highly orbit dependent, and to answer the question specifically depends directly upon how much information one knows about the satellite. What types of sensors are available, what degree of electronic sophistication is acceptable, and what type of disturbance environment will be encountered--all must be considered.

With the above in mind, this research is concerned with two quite different attitude control problems. The first requires that the spacecraft spin axis be maintained almost normal to the orbit plane. Horizon sensors mounted on the spacecraft produce roll-error information for the attitude control system. The controller's function is to maintain both the pointing error and spin-speed error within the required tolerances.

The second application is one in which the spin axis of the vehicle is required to point at a star. A star tracker is the primary orientation-error sensor, and it is assumed that this device gives very accurate two-axes cartesian measurements of the spin-axis angular deviation. The at-

titude control system's job is to keep this deviation as small as possible during each orbital period while holding the spin speed within an acceptable tolerance of the nominal value.

It is assumed that both types of satellites have surfaces with the geometrical shape of a right circular cylinder for purposes of describing the atmospheric and radiation pressure torques. In addition, it is assumed that the vehicles are nominally spinning about their maximum axes of inertia and are built with near inertial symmetry about their spin axes.

The continuous attitude control of a nonsymmetric spinning vehicle is also studied, in which case it is assumed that the control axes (axes about which the control moments are applied) are the principal axes.

Having briefly described the satellites to be considered, this chapter proceeds to present the dynamic model of each satellite with respect to relevant reference frames.

A section on orbit selection is next described to enable the development of approximate models of the disturbance torques. This section contains new results in the analysis of geodetic measurements obtainable from satellites.

Finally, with the orbits defined, a description of the major attitude-perturbing torques is presented and comparisons of relative disturbance-torque sizes are given as functions of the many orbital and spacecraft parameters involved.

ATTITUDE DYNAMICS OF RIGID SPINNING SPACECRAFT

In this section, equations representing the dynamics of the spinning spacecraft with respect to relevant reference frames are described as a means of notation and coordinate system definition.

Spacecraft Kinetics

From Newton's Second Law (Ref. 22), the time rate of change of the angular momentum $\vec{H}$ of a body in inertial space is equal to the applied torque $\vec{T}$, or

$$\frac{d^I}{dt}\vec{H} = \vec{T} , \tag{2.1}$$

where

$$\vec{H} = \vec{\vec{I}}\,\vec{\omega}^{B-I} \quad . \tag{2.2}$$

$\vec{\vec{I}}$ is the inertia tensor of the body and can be represented as the matrix:

$$\underset{B}{I} = \begin{bmatrix} I_{xx} & -I_{xy} & -I_{xz} \\ -I_{xy} & I_{yy} & -I_{yz} \\ -I_{xz} & -I_{yz} & I_{zz} \end{bmatrix} . \tag{2.3}$$

Here, $\vec{\vec{I}}$ is coordinatized in a body-fixed reference frame with orthogonal unit vectors $(\hat{x}_B, \hat{y}_B, \hat{z}_B)$ and with its origin at the satellite center of mass.

The vector $\vec{\omega}^{B-I}$, or $\vec{\omega}$, is the instantaneous angular velocity of the body about its center of mass with respect to an inertial reference frame, and it is coordinatized in the same body-fixed system as

$$\underset{B}{\omega} = \begin{bmatrix} \omega_x \\ \omega_y \\ \omega_z \end{bmatrix} . \tag{2.4}$$

Applying the law of Coriolis yields

$$\frac{d^I}{dt}\vec{H} \triangleq \overset{I}{\vec{H}} = \overset{B}{\vec{H}} + \vec{\omega}^{B-I} \times \vec{H} ,$$

$$= \overset{B}{\vec{\vec{I}}}\,\vec{\omega} + \vec{\vec{I}}\,\overset{B}{\vec{\omega}} + \vec{\omega} \times \vec{\vec{I}}\,\vec{\omega} . \tag{2.5}$$

In this development, it will be assumed that the satellite is rigid so that the time rate of change of $\vec{\vec{I}}$ in the body frame is negligibly small. Solving (2.5) for $\overset{B}{\vec{\omega}}$ [with (2.1)] yields

$$\overset{B}{\vec{\omega}} = \vec{\vec{I}}^{-1} (\vec{T} - \vec{\omega} \times \vec{\vec{I}}\,\vec{\omega}) . \tag{2.6}$$

It is also assumed that the body-fixed reference axes are very close to the principal axes of inertia of the satellite, so that the cross-product-of-inertia terms I_{xy}, I_{xz}, and I_{yz} are much smaller than I_{xx}, I_{yy}, and I_{zz}. In addition, it is assumed that the $\hat{z}_B$ axis is the nominal

satellite spin axis and that ω_z is much larger than ω_x and ω_y. Then, to first order,

$$I_B^{-1} \cong \frac{1}{I_{xx} I_{yy} I_{zz}} \begin{bmatrix} I_{yy} I_{zz} & I_{xy} I_{zz} & I_{xz} I_{yy} \\ I_{xy} I_{zz} & I_{xx} I_{zz} & I_{xx} I_{yz} \\ I_{xz} I_{yy} & I_{xx} I_{yz} & I_{xx} I_{yy} \end{bmatrix} , \tag{2.7}$$

and

$$T_B - \omega_B \times I_B \omega_B \cong \begin{bmatrix} T_x + (I_{yy}-I_{zz}) \omega_y \omega_z - I_{yz} \omega_z^2 \\ T_y + (I_{zz}-I_{xx}) \omega_x \omega_z + I_{xz} \omega_z^2 \\ T_z + (I_{xx}-I_{yy}) \omega_x \omega_y + (I_{yz} \omega_x - I_{xz} \omega_y) \omega_z \end{bmatrix} . \tag{2.8}$$

If the terms due to the presence of cross-products of inertia are neglected, the Eqs. (2.6) become the familiar Euler equations:

$$\dot{\omega}_x = \frac{1}{I_{xx}} \left[T_x + (I_{yy}-I_{zz}) \omega_y \omega_z \right] , \tag{2.9a}$$

$$\dot{\omega}_y = \frac{1}{I_{yy}} \left[T_y + (I_{zz}-I_{xx}) \omega_x \omega_z \right] , \tag{2.9b}$$

$$\dot{\omega}_z = \frac{1}{I_{zz}} \left[T_z + (I_{xx}-I_{yy}) \omega_x \omega_y \right] . \tag{2.9c}$$

Equations (2.9) are used throughout this study as the basic kinetic equations of the spinning spacecraft. Perturbations to these equations due to the presence of cross-product-of-inertia terms are considered later.

Relative Coordinate Systems and Spacecraft Kinematics

It is necessary to define some additional transformations and kinematic relationships to describe the inertial orientation of the satellite. One can transform a vector $\vec{V}$ coordinatized in a reference frame (R) to coordinates in a body-fixed frame (B) by the transformation

$$V_B = C_{B/R} V_R , \tag{2.10}$$

where $C_{B/R}$ is the orthogonal matrix of direction cosines between the two frames. $C_{B/R}$ can be represented by the nonclassical Euler transfor-

mation illustrated in Fig. 2.1. Again using the law of Coriolis, it can be shown that

$$\dot{C}_{B/R} = -C_{B/R} \left(\omega_R^{B-R} \times\right) . \tag{2.11}$$

Eqs. (2.11) are the kinematic relationships which, along with Eqs. (2.9), are used to determine the time history of the attitude of the spinning spacecraft.

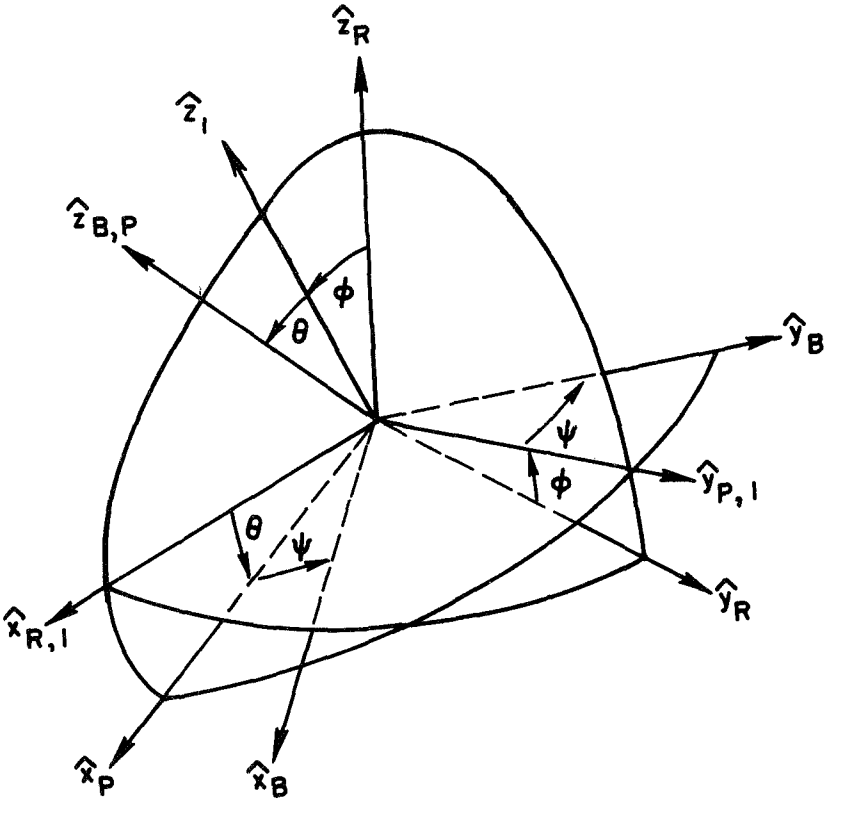

FIG. 2.1. NON-CLASSICAL EULER ANGLE TRANSFORMATION FROM A REFERENCE FRAME (R) TO A BODY-FIXED FRAME (B) BY SUCCESSIVE ROTATIONS ABOUT THE $\hat{x}_R$, $\hat{y}_P$, AND $\hat{z}_B$ AXES THROUGH ANGLES φ, θ, AND ψ.

It remains to define the coordinate systems which are used in this study. The axes of interest are shown in Figs. 2.2 and 2.3. The primary inertial reference frame is determined by the $\hat{x}_I$ axis pointing to the Vernal equinox, the $\hat{z}_I$ axis pointing along the earth's spin axis, and $\hat{y}_I$ completing the right-hand set.

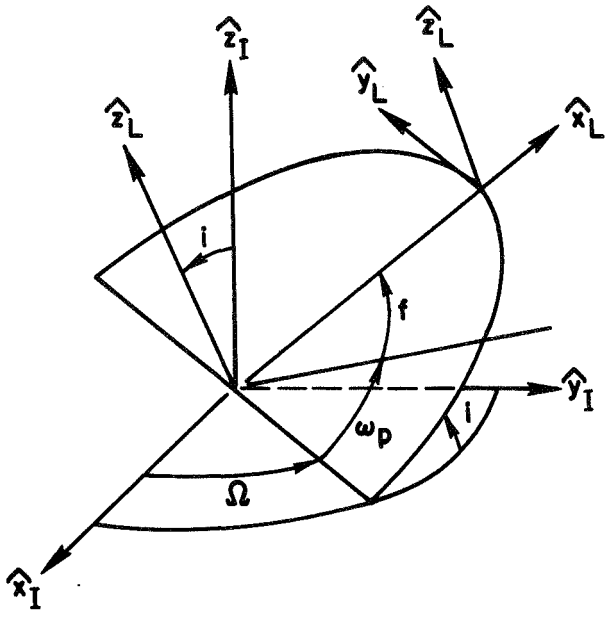

FIG. 2.2. ORIENTATION OF THE LOCAL (L) REFERENCE FRAME.

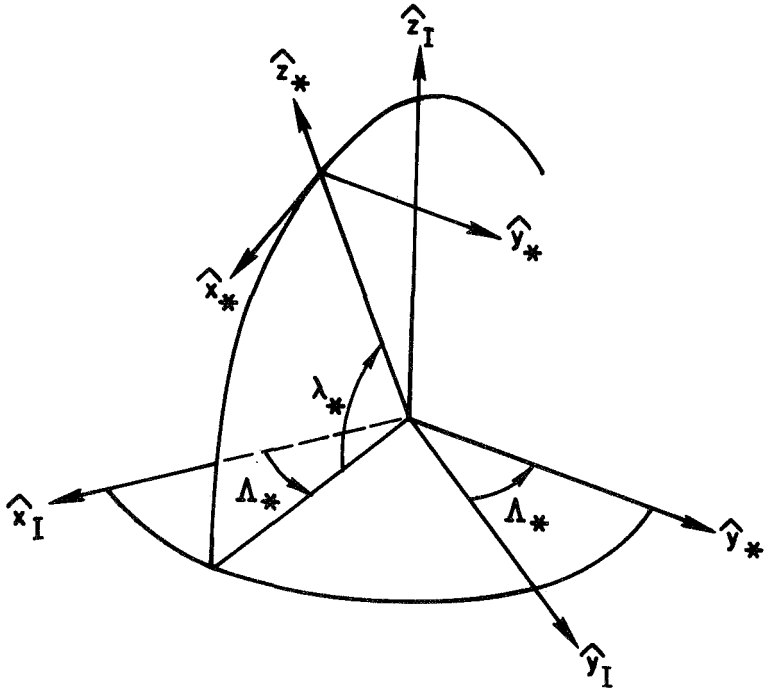

FIG. 2.3. ORIENTATION OF THE STAR (*) REFERENCE FRAME

Figure 2.2 shows the "local" reference frame with $\hat{x}_L$ along the direction of the vector $\hat{R}$ from the geocenter to the satellite. The axis $\hat{z}_L$ is normal to the orbit plane and along the orbit's angular momentum vector $\vec{R} \times \vec{V}_I$, and $\vec{y}_L$ completes the right-hand set. The angles i, Ω, ω_P, and f have the usual definitions of inclination, right ascension of ascending node, argument of perigee, and true anomaly. This system is used as the reference set (R) in the study of controlling the spin axis to be aligned normal to the orbit plane.

Figure 2.3 shows the "star" reference frame with $\hat{z}_*$ pointing toward the reference star, $\hat{y}_*$ being perpendicular to the plane containing $\hat{z}_*$ and $\hat{z}_I$, and $\hat{x}_*$ completing the right-hand set. Here, Λ_* and λ_* are the right ascension and declination of the star. These coordinates are utilized as the reference set (R) in the investigation of precision attitude control with the star tracker.

Linearized Equations of Motion

The equations of motion are next linearized so that they can be used for control law development.

First, consider the case where it is desired to point the spin axis normal to the orbit plane. The natural axes about which to apply control are the local axes labelled (L) in Fig. 2.2. These correspond to the reference axes (R) in Fig. 2.1. However, the closest possible positions of the principal axes of the satellite are the intermediate axes labeled (P) in Fig. 2.1. These axes correspond to a non-spinning set or the position of the body-fixed axes at the time when the angle ψ equals zero. Thus, control torques can be applied about the body-fixed axes (B) such that the average values correspond to those torques required about axes (P). The equations of motion are now formulated in the (P) frame.

Assume that the angles φ and θ (corresponding to yaw and roll angles about $\hat{x}_R$ and $\hat{y}_P$ respectively in Fig. 2.1) are small enough so that the small angle approximations

$$\sin \varphi \cong \varphi \ ,$$
$$\sin \theta \cong \theta \ ,$$
$$\cos \varphi \cong \cos \theta \cong 1 \ ,$$

can be made, and assume that $\psi = 0$. Then the transformation $C_{B/R}$ becomes

$$C_{P/L} \cong \begin{bmatrix} 1 & 0 & -\theta \\ 0 & 1 & \varphi \\ \theta & -\varphi & 1 \end{bmatrix} . \tag{2.12}$$

The time rate of (2.12) is

$$\dot{C}_{P/L} = -C_{P/L} \left(\omega_L^{P-L} \times\right) \tag{2.13}$$

where

$$\omega_L^{P-L} = C_{P/L}^T \left(\omega_P^{B-I} - \omega_P^{B-P}\right) - \omega_L^{L-I} .$$

If one defines the variables

$$\alpha_x = \omega_x \cos \psi - \omega_y \sin \psi ,$$

$$\alpha_y = \omega_x \sin \psi + \omega_y \cos \psi ,$$

then

$$\omega_P^{B-I} = \begin{bmatrix} \alpha_x \\ \alpha_y \\ \omega_z \end{bmatrix} .$$

With

$$\omega_P^{B-P} = \begin{bmatrix} 0 \\ 0 \\ \omega_z \end{bmatrix} ,$$

and

$$\omega_L^{L-I} = \begin{bmatrix} 0 \\ 0 \\ \dot{\sigma} \end{bmatrix} ,$$

one obtains

$$\omega_L^{P-L} = \begin{bmatrix} \alpha_x \\ \alpha_y \\ \dot{\sigma} \end{bmatrix} .$$

Here, $\dot{\sigma} = \dot{f} + \dot{\omega}_p$. Thus,

$$(\omega_L^{P-L} \times) = \begin{bmatrix} 0 & \dot{\sigma} & \alpha_y \\ -\dot{\sigma} & 0 & -\alpha_x \\ -\alpha_y & \alpha_x & 0 \end{bmatrix} . \qquad (2.14)$$

Eqs. (2.12) - (2.14) produce (assuming small angles φ and θ)

$$\dot{\varphi} = \alpha_x + \dot{\sigma}\,\theta , \qquad (2.15a)$$

$$\dot{\theta} = \alpha_y - \dot{\sigma}\,\varphi . \qquad (2.15b)$$

If the spin speed of the satellite is controlled to be nearly constant for a satellite possessing axial mass symmetry (i.e., $I_{xx} = I_{yy}$), the equations of motion in the non-spinning reference frame (P) become

$$\begin{bmatrix} \dot{\alpha}_x \\ \dot{\alpha}_y \\ \dot{\varphi} \\ \dot{\theta} \end{bmatrix} = \begin{bmatrix} 0 & -(1+a_s)\dot{\psi} & 0 & 0 \\ (1+a_s)\dot{\psi} & 0 & 0 & 0 \\ 1 & 0 & 0 & \dot{\sigma} \\ 0 & 1 & -\dot{\sigma} & 0 \end{bmatrix} \begin{bmatrix} \alpha_x \\ \alpha_y \\ \varphi \\ \theta \end{bmatrix} + \begin{bmatrix} 1 & 0 \\ 0 & 1 \\ 0 & 0 \\ 0 & 0 \end{bmatrix} \begin{bmatrix} T_{x1} \\ T_{y1} \end{bmatrix} , \qquad (2.16)$$

where

$$a_s = (I_{zz} - I_{xx})/I_{xx} ,$$

and the disturbances torques (T_{x1}, T_{y1}) are normalized by I_{xx}.

Now consider the satellite for which the attitude control system's function is to point the spin axis toward a star. A star tracker, which is assumed to be aligned with the nominal spin axis, has two outputs called "star-tracker variables" which are computed from a signal representing the star's image on a four-quadrant light-sensitive head. These variables, defined as γ_x and γ_y, are body-fixed orthogonal components of the star's

projection and for small angles are a linear measurement of the misalignment error. Physically, the variables are defined as

$$\gamma_x = \varphi \cos \psi + \theta \sin \psi, \tag{2.17a}$$

$$\gamma_y = -\varphi \sin \psi + \theta \cos \psi. \tag{2.17b}$$

Here, the angles φ and θ represent small angular rotations about the axes $\hat{x}_*$ and $\hat{y}_*$ depicted in Fig. 2.3.

For a symmetric satellite, one can write

$$\begin{bmatrix} \dot{\omega}_x \\ \dot{\omega}_y \\ \dot{\gamma}_x \\ \dot{\gamma}_y \end{bmatrix} = \begin{bmatrix} 0 & -a_s\dot{\psi} & 0 & 0 \\ a_s\dot{\psi} & 0 & 0 & 0 \\ 1 & 0 & 0 & \dot{\psi} \\ 0 & 1 & -\dot{\psi} & 0 \end{bmatrix} \begin{bmatrix} \omega_x \\ \omega_y \\ \gamma_x \\ \gamma_y \end{bmatrix} + \frac{1}{I_{xx}} \begin{bmatrix} 1 & 0 \\ 0 & 1 \\ 0 & 0 \\ 0 & 0 \end{bmatrix} \begin{bmatrix} T_x \\ T_y \end{bmatrix}, \tag{2.18}$$

where again it is assumed that the spin rate $\dot{\psi}$ is held nearly constant by control action. Equations (2.18) represent the equations of motion for the system investigated in Chapter IV.

"Wobble" Damper Analysis

The precession of a spinning body in the absence of external torque consists of a rotation about the spin axis and a conical motion of this axis about the inertially-fixed, total angular momentum vector of the body. If the body has mass symmetry about the spin axis, this axis precesses in a right circular cone with half-angle η called the nutation angle. For an unsymmetric body, the nutation angle varies periodically in a motion referred to as nutation. The combined precession and nutation motion is known as "wobble." In general, it is desirable to remove this wobble from a spinning spacecraft.

A common method of removal is by use of a mechanical damper of which several versions have been proposed in the literature and mechanized on existing satellites. Typical wobble-damper analysis is by means of the "energy-sink" method introduced by Yu (Ref. 23), which is outlined here.

A symmetric spinning spacecraft has total angular momentum

$$H = \left[I_{xx}^2 (\omega_x^2 + \omega_y^2) + I_{zz}^2 \omega_z^2 \right]^{1/2} \tag{2.19a}$$

and kinetic energy

$$E = \frac{1}{2}\left[I_{xx}(\omega_x^2 + \omega_y^2) + I_{zz}\,\omega_z^2\right] . \qquad (2.19b)$$

Figure 2.4 depicts the geometry of the angles and angular rates of the wobble process. The body axes $(\hat{x}_B, \hat{y}_B, \hat{z}_B)$ are rotated from an inertially-fixed set $(\hat{X}, \hat{Y}, \hat{Z})$ through the classical Euler angles ξ, η, and ζ. The $\hat{Z}$ axis is aligned with the total angular momentum vector $\vec{H}$. The rates $\dot{\xi}$ and $\dot{\eta}$ are the inertial precession and nutation. The

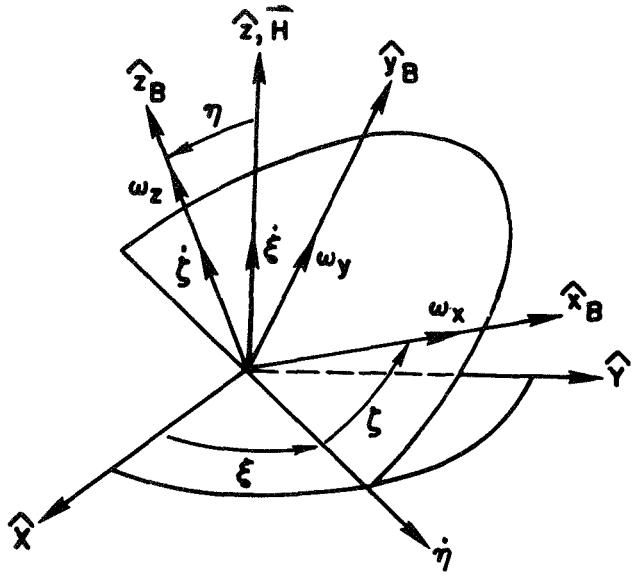

FIG. 2.4. GEOMETRY OF THE ANGLES AND ANGULAR RATES OF THE WOBBLE PROCESS.

nutation angle η is described by

$$\cos\,\eta = I_{zz}\,\omega_z/H . \qquad (2.20)$$

Combining (2.19) - (2.20) and differentiating yields, for small angles,

$$\eta\,\dot{\eta}\,\frac{(I_{zz}-I_{xx})}{I_{xx}}\,I_{zz}\,\omega_z^2 = \dot{E}\ .^{*} \tag{2.21}$$

$\dot{E}$ typically has the linearized form (See Refs. 24 and 25)

$$\dot{E} = -K_d\,\eta^2\ ,$$

where K_d is a constant dependent upon vehicle parameters. Then (2.21) can be written

$$\frac{\dot{\eta}}{\eta} = -d_p\ ,$$

and

$$\eta = \eta_o\,e^{-d_p t}\ ,$$

where d_p^{-1} is the time constant of the damper and η_o is the initial value of the nutation angle.

If $\dot{\eta}$ is small during one cycle of ξ, ω_z is the constant $\dot{\psi}$, and the nutation angle is approximately

$$\eta \cong \tan\eta = \frac{I_{xx}\,\dot{\xi}\,\eta}{I_{zz}\,\dot{\psi}}\ ,$$

then, by using Fig. 2.4, it can be shown that Eqs. (2.16) modify to

$$\begin{bmatrix}\dot{\alpha}_x\\ \dot{\alpha}_y\\ \dot{\varphi}\\ \dot{\theta}\end{bmatrix} = \begin{bmatrix}-d_p & -(1+a_s)\dot{\psi} & 0 & 0\\ (1+a_s)\dot{\psi} & -d_p & 0 & 0\\ 1 & 0 & 0 & n\\ 0 & 1 & -n & 0\end{bmatrix}\begin{bmatrix}\alpha_x\\ \alpha_y\\ \varphi\\ \theta\end{bmatrix} + \begin{bmatrix}1 & 0\\ 0 & 1\\ 0 & 0\\ 0 & 0\end{bmatrix}\begin{bmatrix}T_{x2}\\ T_{y2}\end{bmatrix}\ . \tag{2.22}$$

Equations (2.22) are the linearized equations of motion used for the control system analysis of Chapter III. For the unsymmetric vehicle, the

*Equation (2.21) shows that for decreasing kinetic energy, the vehicle spin axis must be the maximum inertia axis for the nutation angle to be decreasing. This is also true for damping due to elastic deformation of the spacecraft. Hence, for stability it is required that the nominal spin axis be the maximum axis.

wobble-damping terms have a more complicated effect on the system equations.

The exact equations of a mechanical wobble damper are generally more complex than has been indicated by the energy-sink procedure, and require evaluation of a higher order system. However, most wobble-damper references indicate that the energy-sink approximation gives reasonably close results to actual behavior. Thus, the method will be retained rather than increasing the order of the system equations which would be necessary for a closer investigation of the effect of a particular type of damper.

ORBIT SELECTION FOR APPLICATIONS OF SPINNING DRAG-FREE SPACECRAFT

Lange (Ref. 26) developed the concept of the drag-free satellite and proposed many useful experiments for this satellite. The "drag-free satellite" consists of a small, spherical proof-mass inside a completely enclosed cavity of a larger satellite. The outer satellite has a gas-jet translational control system which centers the cavity about the inner proof-mass. In the ideal case, such a satellite's orbit will be determined strictly by gravitational attractions and, thus, it is "drag-free."

Two drag-free satellite applications in which spin is desirable are the geodesy-measurement vehicle and the carrier of the unsupported gyroscope experiment. The geodesy satellite's purpose, as considered here, is to yield measurements of the unknown tesseral harmonic coefficients in the spherical harmonic expansion of the earth's gravitational potential. These coefficients are determined most easily by measuring the in-track motion perturbations of satellites which orbit at rational multiples of the earth's spin rate (resonant orbits). Because measurements of the in-track perturbations to the satellite's position produce the resonant tesseral coefficients' magnitudes, it is desirable to eliminate all non-gravitational forces acting on the vehicle by use of the drag-free system. To minimize (by cancellation) in-track perturbations caused by the gravitational attraction between the satellite and proof mass, it is important to spin the satellite with the spin axis maintained normal to the orbit plane. The degree to which this latter gravitational attraction is reduced depends directly upon the pointing accuracy achievable by the atti-

tude control system.

The unsupported gyroscope experiment consists of using a nearly spherical rotor, spinning about its maximum axis of inertia, as the proof-mass of the drag-free satellite. Because it is thereby devoid of support forces, this rotor is a gyroscope existing in a nearly torque-free environment. The small motion of the spin axis of this gryo can be monitored in the satellite by measuring the rotor spin axis deviation from a vehicle-star reference line. This experiment can produce fundamental information about achievable accuracies of spaceborne gyroscopic devices. It is desirable to spin stabilize (see Ref. 26) the satellite which houses the unsupported gyroscope experiment for improved attitude control, and to effect averaging of a number of already-small torques. The experiment requires the existence of a very accurate star tracker aligned with its optical axis along the satellite's spin axis. The attitude control system's ability to maintain this spin axis pointing toward the star for long periods of time with accuracies of better than one arc second is also required. In order to predict the disturbance torques acting on these spin-stabilized satellites (and, hence, the pointing accuracies achievable), the selection of feasible orbits for these two missions is now discussed.

The Selection of Orbits for the Determination of the Tesseral Harmonic Terms of the Gravitational Potential

From the report by Strange, et al. (Ref. 27), the tesseral harmonic coefficients of degree 7-15 and order 3-10 are at present relatively unknown. The following analysis indicates how these coefficients can be obtained by placing a series of satellites into resonant orbits.

Long-Period Perturbations

Long-period perturbations are defined as those with periods of fluctuation of several days in length. Perturbation analysis is begun by considering the gravitational potential

$$V_g = \frac{\mu}{R} + \sum_{\ell=2}^{\infty} \sum_{m=0}^{\ell} \sum_{p=0}^{\ell} \sum_{q=-\infty}^{\infty} R_{\ell mpq} , \qquad (2.23)$$

where

$$R_{\ell mpq} = \frac{\mu}{a}\left(\frac{a_e}{a}\right)^{\ell} J_{\ell m} F_{\ell mp}(i) G_{\ell pq}(e) \begin{cases} \cos \\ \sin \end{cases} \begin{matrix} (\ell-m) \text{ even} \\ (\ell-m) \text{ odd} \end{matrix} \psi_{\ell mpq} , \qquad (2.24)$$

and

$$\psi_{\ell mpq} = \left[(\ell-2p)\omega_p + (\ell-2p+q)M + m(\Omega-\theta_e-\lambda_{\ell m})\right] . \qquad (2.25)$$

The quantities a, e, i, Ω, ω_p and M are the orbital elements; μ is the product of the earth mass and the universal gravitational constant; R is the satellite radial distance from the geocenter; $J_{\ell m}$ and $\lambda_{\ell m}$ are the amplitude and phase angle associated with the tesseral coefficients of degree ℓ and order m. The angle θ_e is the hour angle of Greenwich and a_e is the earth's equatorial radius. The function $F_{\ell mp}(i)$, known as the inclination function, results from the potential being rotated into the orbit plane. It is expressed as (Kaula, Ref. 28)

$$F_{\ell mp}(i) = \sum_t \frac{(2\ell-2t)!}{t!(\ell-t)!(\ell-m-2t)!2^{2(\ell-t)}} \sin^{\ell-m-2t} i \sum_{s=0}^{m} \binom{m}{s} \cos^s i$$

$$\times \sum_c \binom{\ell-m-2t+s}{c} \binom{m-s}{p-t-c} (-1)^{c-k} , \qquad (2.26)$$

where k is the integer part of $(\ell-m)/2$, t is summed from 0 to the lesser of p or k, and c is summed over all values making the binomial coefficient nonzero. The eccentricity function $G_{\ell pq}(e)$ comes from converting radius and true anomaly into a, e, and M. For $(\ell-2p+q) \neq 0$, $G_{\ell pq}(e)$ is expressed as

$$G_{\ell pq}(e) = (-\beta)^{|q|} (1+\beta^2)^{\ell} \sum_{k=0}^{\infty} P_{\ell pqk} Q_{\ell pqk} \beta^{2k} , \qquad (2.27)$$

where

$$\beta = e/(1+\sqrt{1-e^2}) ,$$

$$P_{\ell pqk} = \sum_{r=0}^{h} \binom{2(p'-\ell)}{h-r} \frac{(-1)^r}{r!} \left(\frac{(\ell-2p'+q')e}{2\beta}\right)^r ,$$

$$h = k + q' \quad \text{for} \quad q' > 0 \ ,$$

$$= k \quad \text{for} \quad q' \leqslant 0 \ ,$$

and

$$Q_{\ell pqk} = \sum_{r=0}^{h} \binom{-2p'}{h-r} \frac{1}{r!} \left(\frac{(\ell - 2p' + q')e}{2\beta} \right)^r \ ,$$

$$h = k \quad \text{for} \quad q' > 0 \ ,$$

$$= k - q' \quad \text{for} \quad q' \leqslant 0 \ .$$

Here,

$$p' = p \ , \quad q' = q \quad \text{for} \quad p \leqslant \ell/2$$

$$p' = \ell - p \ , \quad q' = -q \quad \text{for} \quad p > \ell/2 \ .$$

The instantaneous time rate of change of the orbital elements due to any one term in the gravitational potential is found by using the Lagrange planetary equations (Ref. 28), which are

$$\frac{da}{dt} = \frac{2}{na} \frac{\partial R_\ell}{\partial M} \ , \tag{2.28}$$

$$\frac{de}{dt} = \frac{\sqrt{1-e^2}}{na^2 e} \left(\sqrt{1-e^2} \frac{\partial R_\ell}{\partial M} - \frac{\partial R_\ell}{\partial \omega_p} \right) \ ,$$

$$\frac{d\omega_p}{dt} = \frac{-\cos i}{na^2 \sqrt{1-e^2} \sin i} \frac{\partial R_\ell}{di} + \frac{\sqrt{1-e^2}}{na^2 e} \frac{\partial R_\ell}{\partial e} \ ,$$

$$\frac{di}{dt} = \frac{1}{na^2 \sqrt{1-e^2} \sin i} \left(\cos i \frac{\partial R_\ell}{\partial \omega_p} - \frac{\partial R_\ell}{\partial \Omega} \right) ,$$

$$\frac{d\Omega}{dt} = \frac{1}{na^2 \sqrt{1-e^2} \sin i} \frac{\partial R_\ell}{\partial i} \ ,$$

$$\frac{dM}{dt} = n - \frac{1-e^2}{na^2 e} \frac{\partial R_\ell}{\partial a} - \frac{2}{na} \frac{\partial R_\ell}{\partial a} \ ,$$

where $R_\ell = R_{\ell mpq}$ given in Eq. (2.24) and n is the mean orbital rate. Approximate closed-form solutions to these equations are found by treating

the angles $\psi_{\ell mpq}$ as linear functions of time (Ref. 28). These linear solutions all have the rate term

$$\dot{\psi}_{\ell mpq} = (\ell-2p)\dot{\omega}_p + (\ell-2p+q)\dot{M} + m(\dot{\Omega}-\dot{\theta}_e)$$

in the denominator. For example,

$$\Delta a = \frac{2\mu a_e^{\ell}}{n a^{\ell+2} \dot{\psi}_{\ell mpq}} F(i)\, G(e)(\ell-2p+q) \begin{Bmatrix} \cos \\ \sin \end{Bmatrix}_{\substack{(\ell-m) \text{ odd} \\ (\ell-m) \text{ even}}} \psi_{\ell mpq} \quad .$$

These solutions are valid except when this rate term is very small. A small $\dot{\psi}_{\ell mpq}$ would mean that the sine and cosine terms in the planetary equations change very slowly, allowing large amplitude buildup. Then, the assumption of small perturbations leading to the closed-form linear solution is not valid. The condition where $\dot{\psi}_{\ell mpq} \cong 0$ occurs when

$$(\ell-2p+q)\dot{M} \cong m\,\dot{\theta}_e \quad .$$

This is, of course, the condition of resonance where the satellite orbits at nearly a rational multiple of the earth's rate.

The exact solution to the perturbations of the elements can only be found by numerical integration of Eqs. (2.28). For the case where the number of revolutions per day equals the order m, $(\ell-2p+q) = 1$. Then,

$$\dot{\psi}_{\ell mpq} = (1-q)\dot{\omega}_p + \dot{M} + m(\dot{\Omega}-\dot{\theta}_e) \quad ,$$

$$\cong C_{lo} - q\,\dot{\omega}_p \quad ,$$

where C_{lo} is a constant dependent upon the mean elements of the particular orbit. Thus, for a given orbit, there is a large set of beat frequencies corresponding to each value of the index q. This, of course, implies that the orbit is not inclined in the close neighborhood of the critical inclination where $\dot{\omega}_p = 0$. For $(\ell-2p+q) = 2$,

$$\dot{\psi}_{\ell mpq} \cong 2C_{lo} - q\,\dot{\omega}_p \quad .$$

Hence, another large set of beat frequencies exists; in fact, many other sets exist for C_{lo} not equal to zero or some multiple of $\dot{\omega}_p$. The physical reason for the existence of the multiple beat frequencies is due

to the combined effect of the orbit eccentricity and the slow movement of the perigee point about the orbit. Because of the multiple beat frequencies, it is theoretically possible to detect the effect of many tesseral harmonic coefficients from a given resonant orbit.

The time rates of the mean elements are not constant, but only the acceleration of the mean anomaly, $\ddot{M}$, is significant in the resonant situation. From Ref. 29, this acceleration due to a single combination of indices of a single tesseral coefficient is

$$\ddot{M}_{\ell mpq} = -\frac{3}{2}\frac{n}{a}\dot{a}_{\ell mpq} + O(J_{\ell m}\cdot\dot{\psi}_{\ell mpq}) + O(J^2_{\ell m})$$

$$\cong -\frac{3\mu}{a^3}\left(\frac{a}{a}e\right)^{\ell}(\ell-2p+q)F_{\ell mp}(i)\,G_{\ell pq}(e)\,J_{\ell m}\begin{cases}-\sin\\ \cos\end{cases}\begin{matrix}(\ell-m)\text{ even}\\ (\ell-m)\text{ odd}\end{matrix}\psi_{\ell mpq} \quad . \quad (2.29)$$

Although Eq. (2.29) is approximate, it can be used to determine the relative magnitude of the perturbations to the in-track position of a satellite in a nearly resonant orbit. The highest possible eccentricity is desirable for such orbits because $G_{\ell pq}(e)$ is proportional to $e^{|q|}$. It is precisely this $e^{|q|}$ attenuation factor which physically prevents beat frequencies associated with higher values of $|q|$ from being detectable.

Resonant Analysis Results

A general study was made of the feasibility of measuring the 72 pairs of the coefficients of degree 3-10 and order 7-15 by computing the magnitude of Eq. (2.29) for several combinations of the indices (ℓ,m,p,q). The magnitude $|\ddot{M}|_{\ell mpq}$ was computed as a function of inclination, and the semimajor axis and eccentricity were chosen so the orbit was resonant, with the altitude of perigee being 450 km. Typical plots of $|\ddot{M}|$ vs. i are shown in Fig. 2.5. The complete set of these plots for other combinations of indices (ℓ,m,p,q) can be found in Ref. 30. The hypothetical value of $J_{\ell m}$ used in the computation of $|\ddot{M}|$ was

$$J_{\ell m} = \left[\frac{(\ell-m)!\,(4\ell+2)}{(\ell+m)!}\right]^{1/2}\bar{J}_{\ell m}\ ,$$

where $\bar{J}_{\ell m}$ is the normalized approximation given by Kaula (Ref. 28) as

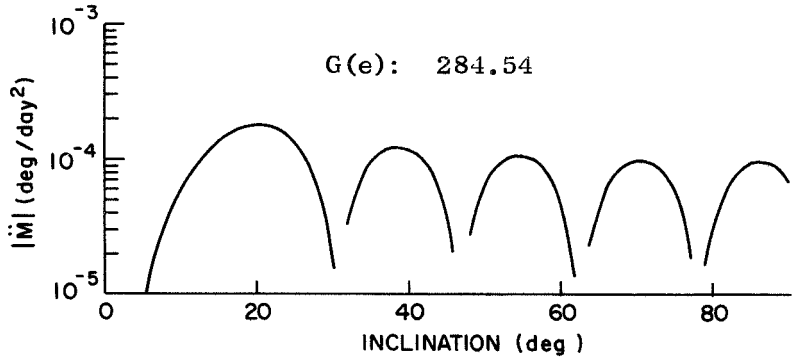

L:12
M:5
P:5
Q:-1

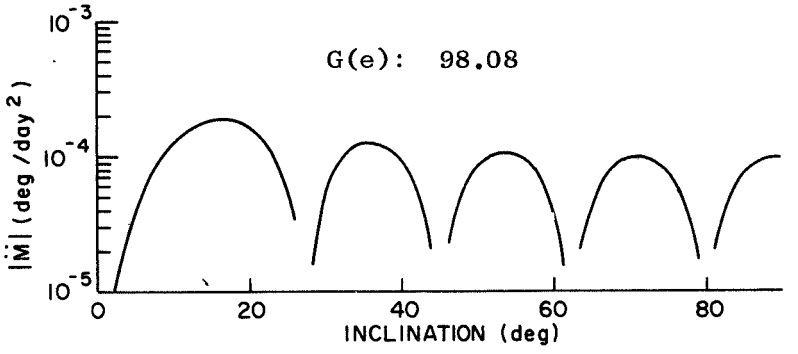

L:11
M:5
P:4
Q:-2

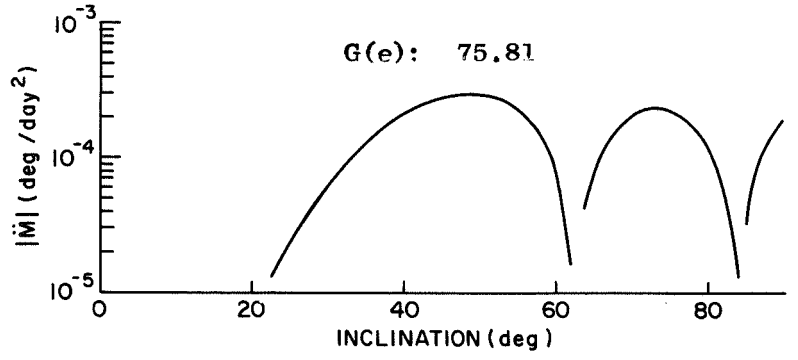

L:10
M:5
P:6
Q:3

FIG. 2.5. TYPICAL VALUES OF $|\ddot{M}|_{\ell mpq}$ AS FUNCTIONS OF INCLINATION FOR A SATELLITE ORBITING FIVE TIMES PER DAY WITH a = 14,446 km AND e = 0.5273.

Table 2.1. MAXIMUM ACCELERATIONS OF THE MEAN ANOMALY $|\ddot{M}| \times 10^5$ deg/day^2 DUE TO INDICATED TESSERAL COEFFICIENTS $J_{\ell m}$. Shown are results of four resonant orbits with perigee altitude of 450 km. Values were computed (using the inclinations shown) from Equation (2.29).

			m = 3	m = 6	m = 9	m = 4	m = 8	m = 5	m = 10	m = 7
			3 orbits per day i = 58°			4 orbits per day i = 50°		5 orbits per day i = 52°		7 orbits per day i = 50°
ℓ	p	Q1	q = Q1	q = Q1 + 1	q = Q1 + 2	q = Q1	q = Q1 + 1	q = Q1	q = Q1 + 1	q = Q1
15	7	0	.03	.10	.56	.13	1.72	1.23	3.28	10.17
14	7	1	.21	.38	.27	1.45	1.09	2.71	19.06	25.75
13	7	2	.41	1.66	3.73	1.94	9.68	10.01	17.69	30.13
12	5	-1	.55	.70	.39	3.11	.91	9.48	26.65	45.68
11	4	-2	.59	1.40	1.12	2.60	1.63	10.47	30.69	34.24
10	6	3	3.72	9.50		8.72	6.15	27.64		35.39
10	3	-3			2.74				16.40	
9	6	4								3.55
9	2	-4	.07	.50	2.26	.20	1.61	1.60		
8	2	-3	1.29	4.74		3.94	14.83	4.56		14.74
7	5	4	8.06	2.48		6.80		5.17		
7	1	-4								1.89

$$\bar{J}_{\ell m} \cong \sqrt{2} \times 10^{-5}/\ell^2 \ .$$

As a criterion for choosing acceptable orbits for tesseral harmonic measurement, the maximum value of $|\ddot{M}|$ being greater than 10^{-5} degree/day^2 was considered to represent a substantially measurable effect. Maximum $|\ddot{M}|$ between 10^{-6} and 10^{-5} degree/day^2 was considered to be marginally detectable.

Using this criterion and taking advantage of the multiple beat frequencies, orbit inclinations were found such that the effect of all but possibly three of the 72 pairs of unknown coefficients can be measurable from only four resonant orbits. In the final orbit specification, it is required that inclinations be adjusted to insure that the resulting data is well conditioned. The magnitudes of maximum $|\ddot{M}|$ for a set of four suitable orbits are presented in Table 2.1.

The general orbit selection for optimum tesseral harmonic determinations requires orbits to be as eccentric as possible and have inclinations between 20° and 70°. From the attitude control standpoint, these facts have two pertinent implications. They are:

1. Atmosphere torques can be significant because of the high eccentricity.
2. The magnetic field will be favorable (as explained later) for its utilization as the primary control torque source.

Orbit Selection for the Unsupported Gyroscope Experiment

For the unsupported gyroscope experiment, the proof-mass of the drag-free satellite becomes a spinning spherical rotor with the spin axis pointed toward a star. For rotor stability, the rotor spin axis is designed to be the maximum axis of inertia. Because the rotor does not have spherical mass symmetry, it will be subjected to gravity-gradient torques from the earth. To minimize these torques, the satellite's orbit is selected to be circular and polar with the plane of the orbit containing the reference star. Thus, the spin axes of the rotor and the surrounding spinning satellite will be nominally in the orbit plane. The polar inclination prevents the orbit plane from precessing. The gravity-gradient torque effect on the rotor is minimized by the averaging effect of this

orbit.

The altitude of such an orbit should be high enough to avoid large atmospheric drag and yet low enough to ease boost requirements. The nominal orbit altitude studied here is 700 km.

SATELLITE ATTITUDE DISTURBANCE TORQUES

In this section, analytical expressions are developed for the major perturbing torques which act upon a satellite. There are several reasons for including this section at this point. A primary goal of this study is to examine the degree of accuracy to which the spin axis of the rotating vehicle can be kept pointing to some given reference. If no disturbances are present, the answer is simple; any asymptotically stable regulator will do the job. But this is not the case. The ability to determine the actual motion taken by the vehicle and to establish the requirements for its attitude control system depend directly on a thorough knowledge of the torque environment which influences the satellite.

When proceeding to design a precision attitude control system, it is necessary to know the torque profile with which the system must be able to cope. This knowledge can be gained by developing a model for each of the more important torques which are functions of the orbit, the desired reference tracked, and the vehicle design itself. With the torque characteristics known, the designer can determine the time history of the torques acting on the satellite during its orbital lifetime. This time history can either be formulated as analytical expressions which are functions of time or orbital position, or it can be determined by computer simulation. (Computer simulation of disturbance torques as functions of orbital position can be used to develop approximate analytical expressions of the torque environment.)

With an adequate description of the disturbances torque history, one is able to determine the angular momentum and power requirements of the attitude control system. Another important motivation for this study is for the case where a satellite utilizes magnetic attitude control. Here, there are portions of the orbit (as will be seen later) in which full attitude control cannot be maintained. The amount the spin axis

drifts off the reference at these times depends directly on the disturbance torque values.

Disturbance torques considered here can be broken into three categories. Two, referred to as "inertially-fixed" and "body-fixed" torques, are those which tend to move the spin axis off the reference and are about the vehicle's lateral axes. The third type of torque is about the spin axis and tends to change the rate of spin speed. Disturbances due to misapplied attitude control torques (caused by system errors such as sensor noise, coil misalignment, and electronics delays) will not be considered here. Their effect will later be examined in the error analyses of particular systems. The discussion of torques due to nonsymmetry of the spacecraft will also be deferred until later.

Analytical models are developed here of torques (averaged over one satellite rotation) caused by the following sources:

1. The atmosphere ,
2. Radiation pressure ,
3. Misaligned and leaky translational control jets ,
4. Gravity-gradient effect ,
5. Magnetic effects,
6. Reference-frame kinematics.

Other torque sources of minor importance may be present and will be briefly mentioned. In the analysis it is generally assumed that the satellite is cylindrical in shape and spinning nominally about its maximum axis of inertia. Other assumptions will be made at the time that they are required.

Torques Due to the Atmosphere

It is generally assumed that spacecraft in earth orbit are exposed to atmospheric density low enough that free molecular flow takes place. Free molecular flow is defined as the limiting flow which exists when the Knudsen number (the ratio of the molecular mean free path to the greatest projected body length perpendicular to the flow direction) is greater than 10.

Schaaf and Chambre (Ref. 31) developed the exact expression for the pressure and shear forces acting on a surface in free molecular flow.

These expressions are complicated functions of the ratios of surface temperature to environmental temperature and vehicle speed to the mean thermal speed of the molecules. Schamberg (Ref. 32) showed that for typical values of the latter ratio existing in satellite flight, the normal and shear forces per unit wall area are approximately

$$p = \rho V_i^2 \sin^2 \eta_i \left[1 + \Phi_b \frac{V_r}{V_i} \frac{\sin \eta_r}{\sin \eta_i} \right], \tag{2.30}$$

and

$$\tau_s = \rho V_i^2 \sin \eta_i \cos \eta_i \left[1 - \Phi_b \frac{V_r}{V_i} \frac{\cos \eta_r}{\cos \eta_i} \right], \tag{2.31}$$

respectively. Here,

V_i = relative speed of incoming molecules,
V_r = relative speed of outgoing molecules,
η_i = angle between incoming velocity and the wall surface,
η_r = angle between wall and $\vec{V}_r$,
ρ = mass density,
Φ_b = beam width factor.

(See Fig. (2.6).)

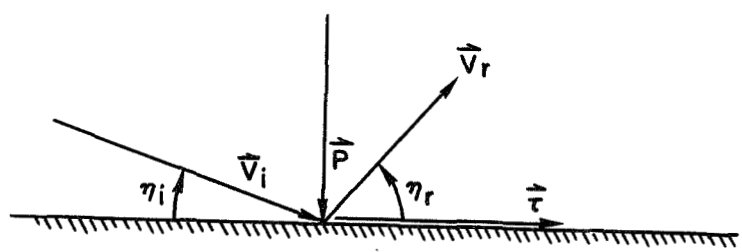

FIG. 2.6. ATMOSPHERIC SURFACE FORCE GEOMETRY.

Schamberg also shows that Φ_b ranges from 2/3 to 1 when re-emission goes from the diffuse to spectral regime. Also, $V_r/V_i \cong \sqrt{1-\alpha_a}$ where α_a is the accommodation coefficient for the particular surface defined as

$$\alpha_a = \frac{T_{mr} - T_{mi}}{T_{mw} - T_{mi}} \quad . \tag{2.32}$$

Here, T_{mi}, T_{mr}, and T_{mw} are absolute temperatures of the incident and reflected molecules and the wall. The angle η_r is related to η_i by

$$\cos \eta_r = (\cos \eta_i)^{\nu} \quad , \tag{2.33}$$

where ν ranges from 1 for spectral reflection to ∞ for diffuse re-emission.

There exists a wide range of accommodation coefficients experimentally determined for various wall materials and flight conditions. Moe (Ref. 33) presents accommodation coefficients ranging from 0.65 to 0.95 for flights of Explorer VI and Ariel II where the greatest percentage of the surface areas are coated with solar cell material. Schamberg presents data for aluminum and iron surfaces exposed to gaseous nitrogen with α_a ranging from 0.32 to 0.50.

For the case of diffuse re-emission, Eqs. (2.30) and (2.31) become

$$p = \rho V_i^2 \sin \eta_i \left[\sin \eta_i + \frac{2}{3} \frac{V_r}{V_i} \right] , \tag{2.34a}$$

$$\tau_s = \rho V_i^2 \sin \eta_i \cos \eta_i \quad . \tag{2.34b}$$

For spectral re-emission, they are

$$p = \rho V_i^2 \sin^2 \eta_i \left[1 + \frac{V_r}{V_i} \right] \quad , \tag{2.35a}$$

$$\tau_s = \rho V_i^2 \sin \eta_i \cos \eta_i \left[1 - \frac{V_r}{V_i} \right] \quad . \tag{2.35b}$$

Equations (2.34a,b) and (2.35a,b) represent the range of values of normal and shear forces acting on an incremental area of satellite surface. These expressions can be integrated (over the surface of the satellite exposed to the incoming velocity) to find the total forces acting on the vehicle for different orientations with respect to $\vec{V}_i$. Carrying out this integration over the cylindrical surface yields a shear force of

$$S_{cyl} = 2 f_\tau \ell r \rho V_i^2 \sin \eta_i \cos \eta_i \quad , \tag{2.36}$$

where it is assumed that all elements of the cylindrical shell have the same re-emission characteristics. This force acts at a distance from the centerline of $\pi r/4$. Here, f_τ ranges from 1 to $[1 - V_r/V_i]$ as indicated in (2.34b) and (2.35b) and ℓ and r are the length and radius of the cylinder. Similarly, the total normal force acting on the cylinder is found by integrating the force component on each element which is parallel to the normal force $\vec{p}$ acting on the element contained in the $\vec{V}_i, \hat{z}_B$ plane. This yields the normal pressures

$$P_{cyl_{diffuse}} = 2\ell\, r\, \rho V_i^2 \sin\eta_i \left(\sin\eta_i + \frac{\pi}{6}\frac{V_r}{V_i}\right), \tag{2.37}$$

and

$$P_{cyl_{spectral}} = \frac{2}{3}\ell\, r\, \rho V_i^2 \sin^2\eta_i \left(3 + \frac{V_r}{V_i}\right). \tag{2.38}$$

Noting that the angle which the relative velocity vector makes with the end plate is $(\pi/2 - \eta_i)$, the normal and shear forces acting on the end are:

Diffuse:

$$P_{end} = \pi r^2\, \rho V_i^2 \cos\eta_i \left(\cos\eta_i + \frac{2}{3}\frac{V_r}{V_i}\right), \tag{2.39}$$

$$S_{end} = \pi r^2\, \rho V_i^2 \sin\eta_i \cos\eta_i, \tag{2.40}$$

Spectral:

$$P_{end} = \left(1 + \frac{V_r}{V_i}\right)\pi r^2\, \rho V_i^2 \cos^2\eta_i, \tag{2.41}$$

$$S_{end} = \left(1 - \frac{V_r}{V_i}\right)\pi r^2\, \rho V_i^2 \sin\eta_i \cos\eta_i, \tag{2.42}$$

where again constant re-emission characteristics are assumed.

If the vehicle's center of mass is removed from the center of pressure by an amount δz along the spin axis and δr away from the centerline, then the average inertially fixed torque acting on the satellite due

to the above components is (See Fig. 2.7)

$$\vec{T}_{Iaero} = \left[S_{end} \cdot (\ell/2 + \delta z) + P_{cyl} \cdot \delta z - \frac{\pi r}{4} S_{cyl} \right] \hat{e} \qquad (2.43a)$$

for $\hat{z}_B \cdot \vec{V}_{is} < 0$ with vector $\vec{V}_{is}$ the relative velocity of the satellite and

$$\vec{T}_{Iaero} = -\left[S_{end} (\ell/2 - \delta z) - P_{cyl} \cdot \delta z - \frac{\pi r}{4} S_{cyl} \right] \hat{e} \qquad (2.43b)$$

for $\hat{z}_B \cdot \vec{V}_{is} \geq 0$, where $\hat{e} = \hat{z}_B \times \vec{V}_{is} / (V_{is} \sin \eta_i)$. The resulting body-fixed torque magnitude is

$$T_{Baero} = P_{end} \cdot \delta r \, . \qquad (2.44)$$

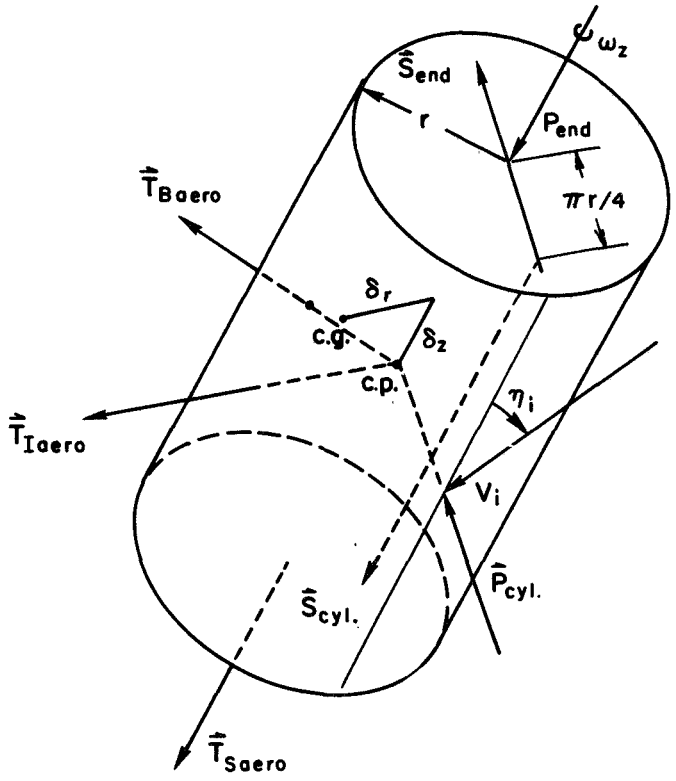

FIG. 2.7. AERODYNAMIC FORCES AND TORQUES ACTING UPON THE CYLINDRICAL SATELLITE.

It can be seen that with $\delta z = \delta r = 0$, and with all surfaces of the satellite having the same reflective properties, these torques disappear.

There is also a disturbance torque from the atmosphere because the satellite is rotating. As developed by Johnson (Ref. 34), this torque can be written as

$$\vec{T} = -\rho\vec{\omega}\cdot\int_s(\vec{d}\vec{d} - \hat{\vec{1}}\vec{d}\cdot\vec{d})d\vec{s}\cdot\vec{V}_{is} - \rho\vec{V}_{is}\times\int_s\vec{d}(\vec{d}\times d\vec{s})\cdot\vec{\omega}\,, \qquad (2.45)$$

where $\vec{d}$ is a vector from some origin to the incremental area of the satellite surface $d\vec{s}$. Integrating this expression over one end of the cylinder and over one-half the cylindrical surface yields the disturbance torque

$$\vec{T} = -\left[\rho V_{is}^2\ r\ \ell\ \sin\eta_i\left(\frac{1}{6}\frac{\omega_x}{V_{is}}\left\{4r^2+\ell^2\right\}\hat{x}_1 + \frac{1}{3}\frac{\omega_y}{V_{is}}\left\{4r^2+\ell^2\right\}\hat{y}_1 + 2r^2\frac{\omega_z}{V_{is}}\hat{z}_B\right)\right]$$

$$-\left[\rho V_{is}^2\ \frac{\pi}{2}\ r^2\ \cos\eta_i\left(\frac{\omega_x}{V_{is}}\left\{r^2+\frac{\ell^2}{2}\right\}\hat{x}_1 + \frac{\omega_y}{V_{is}}\left\{r^2+\frac{\ell^2}{2}\right\}\hat{y}_1 + r^2\left\{\frac{\omega_z}{V_{is}} - \tan\eta_i\frac{\omega_x}{V_{is}}\right\}\hat{z}_B\right)\right]\,, \qquad (2.46)$$

where the expression in the first set of brackets is that torque due to the cylindrical shell, and the expression in the second set is that torque due to the end plate. The unit vector $\hat{x}_1$ is normal to $\hat{z}_B$ and lies in the plane of $\hat{z}_B$ and $\vec{V}_{is}$. The vector $\hat{y}_1 = \hat{z}_B\times\hat{x}_i$. For a vehicle with $\omega_z \gg \omega_x$ and ω_y, this torque simplifies to

$$\vec{T}_{Saero} = -\rho V_{is}\ r\ \omega_z\left(2\ell\ r^2\ \sin\eta_i + \frac{\pi r^3}{2}\cos\eta_i\right)\hat{z}_B\,, \qquad (2.47)$$

which is a despinning disturbance torque.

The relative velocity $\vec{V}_{is}$ of the incoming atmosphere is found by adding the inertial velocity of the atmosphere to the negative inertial velocity of the satellite or

$$\vec{V}_{is} = -\vec{V}_I + \vec{V}_{air} , \tag{2.48}$$

with

$$\vec{V}_{air} = K_w \vec{\omega}_e \times \vec{R} , \tag{2.49}$$

where $\vec{\omega}_e$ = earth spin rate,

$\vec{R}$ = radius vector from the geocenter, and

K_w = wind constant.

The angular velocity of the upper atmosphere has been determined by examining changes in inclinations of various satellites by King-Hele (Ref. 35). He found $K_w = 1.46$ for nine satellites at heights of 200-300 km.

The literature abounds with atmospheric density models used for various research projects. The model used here is a modified version of the Jacchia model which has been approximated by a set of polynomials for numerical use. Its development, which is presented in Appendix B, accounts for the day-night effect, the 27-day solar effect, the 11-year solar cycle, the semiannual effect, and the magnetic storm effect for altitudes above 120 km.

Radiation Pressure Torques

The four sources of radiation which cause force and torques on satellites are direct solar radiation, solar radiation reflected by the earth and its atmosphere, direct radiation from the earth, and radiation emitted by the satellite. If one assumes geometric symmetry of the satellite surface material and even temperature distribution over the cylindrical wall due to the satellite's rotation, no inertially-fixed torque will result due to the last effect. Any body-fixed torque from end-plate emitted radiation can be lumped in with the body-fixed torque due to atmospheric effects.

Vector approximations to the incremental pressure caused by the first three sources have been developed in Appendix C and are summarized here. For direct solar radiation,

$$\vec{Ra}_1 = -4.66 \times 10^{-5} R_\odot \text{ dyne/cm}^2 \text{ for } \cos^{-1}(\hat{R}_\odot \cdot \hat{R}) < \frac{\pi}{2} + \cos^{-1}(a_e/R) \ , \quad (2.50)$$

$$= 0 \qquad \text{for } \cos^{-1}(\hat{R}_\odot \cdot \hat{R}) \geq \frac{\pi}{2} + \cos^{-1}(a_e/R) \ ,$$

where $\vec{Ra}_1$ is the incremental solar radiation pressure, $\hat{R}_\odot$ is a unit vector in the sun direction, and a_e is the earth radius. For earth emitted radiation, the pressure $\vec{Ra}_2$ is

$$\vec{Ra}_2 = 7.53 \times 10^{-6} (a_e/R)^2 \hat{R} \text{ dyne/cm}^2 \ . \quad (2.51)$$

The pressure due to the earth-reflected radiation has magnitude

$$Ra_3 = 1.80 \times 10^{-5} \exp(-3. \times 10^{-4} h_a) \cos \alpha_\odot \text{ dyne/cm}^2 \quad (2.52a)$$

(where h_a is the altitude in km, and $\alpha_\odot = \cos^{-1}(\hat{R}_\odot \cdot \hat{R})$) for $\alpha_\odot < \pi/2$, and zero elsewhere. This magnitude is about 37 per cent of the direct solar radiation, for example, at an altitude of 100 km above the subsolar point. This radiation vector acts in the $\hat{R}, \hat{R}_\odot$ plane at an angle $(\alpha_\odot + \nu_n)$ radians away from $\hat{R}_\odot$, where

$$\nu_n = f_1 (\alpha_\odot / f_1)^{2.4} \text{ rad} \ , \quad (2.52b)$$

and

$$f_1 = 4.89 - h_a(5.82 \times 10^{-4}) \text{ rad} \ . \quad (2.52c)$$

Eqs. (2.72 a,b,c) were found empirically from numerical integration of reflected radiation visible by the satellite at varying positions with respect to the $\hat{R}_\odot$ direction.

According to Evans (Ref. 36), the pressure and shear stress components due to a radiation source vector $\vec{Ra}$ striking a wall at an angle ζ_r range from

$$p = (Ra) \sin \zeta_r (\sin \zeta_r + \frac{2}{3} \rho_r) \ , \quad (2.53a)$$

$$\tau_s = (Ra) \sin \zeta_r \cos \zeta_r \ , \quad (2.53b)$$

for diffuse reflection, to

$$\rho = (Ra)(1 + \rho_r) \sin^2 \zeta_r \ , \tag{2.54a}$$

$$\tau_s = (Ra)(1 - \rho_r) \sin \zeta_r \cos \zeta_r \ . \tag{2.54b}$$

for spectral reflection. Here, ρ_r is the surface reflectivity.

It can be seen that Eqs. (2.53) and (2.54) have exactly the same form as Eqs. (2.34) and (2.35) in the previous section on aerodynamic disturbances. Because the radiation pressures have been formulated as vectors, the radiation disturbance torque evaluation can be done in exactly the same fashion as the aerodynamic analysis.

Translation Control Torques (Average Effect)

If the satellite is drag-free, translational control gas jets are provided to keep the outer spacecraft structure following the translational motion of the shielded proof mass. Assume that for a rotating cylindrical satellite, there would be six gas jets arranged with one centered on each end and four laterally spaced every 90° about the central perimeter of the cylinder. The two jets on each end would fire intermittently to counteract the total cylindrical shear force S_{cyl} and end-plate normal force P_{end} caused by aerodynamic and radiation effects discussed previously, and to keep the proof mass centered along the $\hat{z}_B$ direction. Likewise, the four jets located symmetrically about the cylinder would fire to counteract the total normal pressure forces P_{cyl} on the cylindrical wall and the end-plate shear force S_{end} and to maintain lateral centering of the proof mass.

There are two apparent ways in which translation control jets could produce disturbance torques on the satellite. One torque would occur due to any misalignment in the structural mounting of the jet (i.e., the line of force of the jet not passing through the center of mass of the outer structure). A lateral jet skewed or misaligned toward an end-plate would tend to produce an average inertial torque about an axis normal to the plane containing the net aerodynamic and radiation pressure force acting on the vehicle. The same jet skewed to one side would cause a spin-speed changing torque. If a lateral jet were mounted so that the equivalent moment arms' lengths with respect to the center of mass were

δz_j and δr_{j1}, the resulting torque magnitudes would be

$$T_{Ij} = \frac{1}{4} (S_{end} + P_{cyl}) \delta z_j, \tag{2.55a}$$

$$T_{sj1} = \frac{1}{4} K_{\ell 1} (S_{end} + P_{cyl}) \delta r_{j1} . \tag{2.55b}$$

T_{Ij} is an inertially-fixed torque in the average sense but can also be modeled as a discontinuous body-fixed torque. T_{sj1} is the spin torque. The term $K_{\ell 1}$ in T_{sj1} accounts for limit-cycling of the translational control system. This occurs when control jet force is strong enough to accelerate the vehicle across its deadband before drag force turns it around.

An intermittently firing end-jet will not cause an average inertially fixed torque but can cause a spin torque equal to

$$T_{sj2} = K_{\ell 2} (S_{cyl} + P_{end}) \delta r_{j2} . \tag{2.56}$$

Here, $K_{\ell 2}$ is the limit cycle effect and δr_{j2} is the effective lever arm. The limit cycle terms $K_{\ell 1}$ and $K_{\ell 2}$ are drag-force dependent and with careful design can probably be treated as equal to unity.

The other torque source exists when a jet is leaky and misaligned. A lateral jet with effective leak force P_c will cause a body-fixed torque

$$T_{Bj1} = P_c \delta z_j , \tag{2.57a}$$

and a spin torque

$$T_{sj3} = P_c \delta r_{j1} . \tag{2.57b}$$

Similarly, a leaky end-nozzle with force P_e will cause a body-fixed torque

$$T_{Bj2} = P_e \delta r_{j3} , \tag{2.58a}$$

and a spin torque

$$T_{sj4} = P_e \, \delta r_{j2} \ , \tag{2.58b}$$

where δr_{j1}, δr_{j2}, δr_{j3}, and δz_j are appropriately defined lever arms with respect to the vehicle center of mass. Direction of torque vectors depend on satellite and nozzle geometry.

The actual effect of torques due to translational control being discontinuous rather than continuous will be discussed in more detail later.

Gravity Gradient Torque

For gravity gradient torque effects (See DeBra, Ref. 37), one can assume the earth is a body with axial symmetry about its spin axis. Thus its gravitational potential can be written as

$$V_g(R,\theta_p) = \frac{\mu}{R}\left[1 - \sum_{k=2}^{\infty} J_k (a_e/R)^k \, P_k(\cos\,\theta_p)\right] \ , \tag{2.59}$$

where $P_k(\cos\,\theta_p)$ are the Legendre polynomials;

$$P_0(\cos\,\theta_p) = 1 \ ,$$

$$P_1(\cos\,\theta_p) = \cos\,\theta_p \ ,$$

$$\vdots$$

$$P_k(\cos\,\theta_p) = \frac{1}{k}\left[(2k-1)\cos\,\theta_p \, P_{k-1}(\cos\,\theta_p) - (k-1)P_{k-2}(\cos\,\theta_p)\right] \ .$$

(2.60)

θ_p is the colatitude $\cos^{-1} \hat{R} \cdot \hat{z}_e$, where $\hat{R}$ and $\hat{z}_e$ are unit vectors along the geocenter-satellite radius and earth spin-axis respectively. The constant μ is the mass of the earth times the universal gravitation constant. The coefficients J_k are empirically determined by experiment for the earth, and typical values are (Kaula, Ref. 38)

$$J_2 = 1082.3 \times 10^{-6} ,$$

$$J_3 = -2.56 \times 10^{-6} ,$$

and

$$J_4 = -2.04 \times 10^{-6} .$$

Neglecting terms higher than J_2, the potential (2.59) becomes

$$V_g(R, \theta_p) = \frac{\mu}{R}\left[1 - \frac{J_2}{2} (a_e/R)^2 (3 \cos^2 \theta_p - 1)\right] . \qquad (2.61)$$

The force attraction of a particle of mass m_p at a point p is the gradient of (2.81) or

$$\vec{f}_p = m_p \nabla V_g ,$$

$$= m_p\left[\frac{\partial V_g}{\partial r} \hat{R} + \frac{1}{R} \frac{\partial V_g}{\partial \theta_p} \hat{\theta}_p\right] , \qquad (2.62)$$

where

$$\hat{\theta}_p = \frac{(\hat{z}_e \times \hat{R}) \times \hat{R}}{|\hat{z}_e \times \hat{R}|} = \frac{\cos \theta_p \hat{R} - \hat{z}_e}{\sin \theta_p} , \qquad (2.63)$$

the unit vector in the direction of increasing θ_p. Thus (2.62) becomes

$$\bar{f}_p = m_p\left\{\left[\frac{\partial V_g}{\partial R} + \frac{1}{R} \frac{\partial V_g}{\partial \theta_p} \cot \theta_p\right]\hat{R} - \frac{1}{R} \frac{\partial V_e}{\partial \theta_p} \csc \theta_p \hat{z}_e\right\}$$

$$= \mu m_p\left\{\left[-\frac{1}{R_p^2} - \frac{3}{2} \frac{J_2 a_e^2}{R_p^4} (1 - 5 \cos^2 \theta_p)\right]\hat{R} - \frac{3J_2 a_e^2}{R_p^4} \cos \theta_p \hat{z}_e\right\} . \qquad (2.64)$$

The position $\vec{R}_p$ of each point mass in the satellite can be written

$$\vec{R}_p = \vec{R} + \vec{\rho}_p , \qquad (2.65)$$

where $\vec{R}$ is to the satellite center of mass and $\vec{\rho}_p$ is the vector from the mass center to p. The torque about the center of mass is

$$\vec{T}_{gg} = \sum_{m_p} \vec{\rho}_p \times \vec{f}_p \ . \tag{2.66}$$

R_p^2 can be expanded to

$$R_p^2 = \vec{R}_p \cdot \vec{R}_p \cong R^2(1 + 2\vec{\rho}_p \cdot \vec{R}/R^2) \ . \tag{2.67}$$

Using (2.67) and (2.64) in (2.66) yields the torque equation in invariant form,

$$\vec{T}_{gg} = \frac{3\mu}{R^3} \hat{R} \times \vec{\vec{I}} \cdot \hat{R} + 15 \frac{\mu J_2 R_e^2}{R^5} \left[\frac{(1-7\cos^2\theta_p)}{2} \hat{R} \times \vec{\vec{I}} \cdot \hat{R} \right.$$

$$\left. + \cos\theta_p (\hat{R} \times \vec{\vec{I}} \cdot \hat{z}_e + \hat{z}_e \times \vec{\vec{I}} \cdot \hat{R}) - \frac{1}{5} \hat{z}_e \times \vec{\vec{I}} \cdot \hat{z}_e \right] \ . \tag{2.68}$$

Here, $\vec{\vec{I}}$ is the moment-of-inertia dyadic of the satellite.

Magnetic Torques

Magnetic disturbance torques are primarily caused by current loops in the spacecraft and materials subject to permanent or induced magnetism. The instantaneous torque is the vector cross product of the spacecraft's effective dipole moment M_s and the magnetic induction of the local field $\vec{B}$, or

$$\vec{T}_{mag} = \vec{M}_s \times \vec{B} \ . \tag{2.69}$$

This is the same type of torque which is to be used for control purposes in this research, but here $\vec{M}_s$ is considered to include all but the dipole generated by the control coils. Generally, for a spacecraft which employs magnetic attitude control, care is taken to minimize the spacecraft-fixed dipole and magnetic characteristics in order to not influence

on-board magnetometer readings. However, shielding can hide a certain portion of the dipole, and spacecraft magnetic characteristics can change between the laboratory and the orbit. Reference 39 gives an account of spacecraft whose attitudes have been measurably affected by the dipole. For a spinning satellite with dipole component M_z along the spin axis and M_L along a lateral axis, the resulting inertially fixed torque magnitude T_{IM} will be

$$T_{IM} = M_z B_L \quad , \tag{2.70}$$

where B_L is the lateral component of the magnetic field. For B_z equal to the component of $\vec{B}$ along the spin axis, the body-fixed torque will be

$$T_{BM} = M_L B_z \quad .$$

Because the satellite spins with respect to the magnetic field vector, torques due to the induced currents (eddy currents) and the irreversible magnetism of permeable materials (hysteresis effects) must also be considered. Smith (Ref. 40) developed the theoretical expressions for determining the eddy current torques due to rotating shells. For the cylinder, the $\hat{x}_e$-axis is defined so $\vec{B}$ lies in the $\hat{x}_e, \hat{z}_B$ plane and forms the angle λ_m with the $\hat{z}_B$-axis. The total torque, in vector form, is

$$\vec{T}_e = \pi \sigma_c c_\ell^{-2} B^2 \omega_z \sin \lambda_m r^3 \ell d_w \left(1 - \frac{2r}{\ell} \tanh \frac{\ell}{2r}\right)(\cos \lambda_m \hat{x}_e - \sin \lambda_m \hat{z}_B) \quad , \tag{2.72}$$

where σ_c is the electric conductivity of the shell material, c_ℓ is the speed of light, and d_w is the wall thickness. This torque will be assumed to approximately represent that torque due to eddy currents induced into the vehicle structural components. It can be seen to have both an inertially-fixed component and a spin component.

The energy loss per cycle due to permeable material being rotated in a magnetic field is

$$\Delta E = \text{Vol}\int (B\ dB_i) \ , \tag{2.73}$$

where Vol is the volume of material and B_i is the induced magnetic flux in the material. This expression can be directly converted to a spin torque.

Kinematics of the Reference Frame

If the spin axis reference is moving, a control torque is required to precess the spin axis to follow this reference. For the spin axis to point normal to the orbit plane, for instance, control torque must be provided to precess the spin axis at a rate which matches the precessional rate of the orbit plane. This change in inertial orientation of the reference can be thought of as an inertial disturbance torque precessing the spin axis away from an inertially fixed reference. For a satellite in an earth orbit with inclination i, the instantaneous orbit precession rate is, to first order,

$$\dot{\Omega} = \frac{-3\mu\ J_2 a_e^2\ \cos\ i\ \sin^2\ \sigma}{H_o R^3} \tag{2.74}$$

where μ is the product of the universal gravitation constant and the earth mass, σ is the sum of the orbit's argument of perigee and the true anomaly, H_o is the orbit's angular momentum with respect to the earth, and J_2 is the first harmonic term in the expansion of the earth's potential [see Eq. (2.79)]. This rate is about the earth spin axis $\hat{z}_e$. When averaged over one orbit, this rate is approximately

$$\dot{\Omega}_{ave} = -\frac{3}{2}\ J_2 (a_e/p)^2 n\ \cos\ i\ \hat{z}_e \ , \tag{2.75}$$

where n is the mean motion and p the semilatus rectum.

For the case where the spin axis of the satellite is required to be kept normal to the orbit plane, the geometry can be described as in Figure 2.8. Here $\hat{x}_k = \hat{z}_B \times (\hat{z}_e \times \hat{z}_B)/\sin i$. The rate of change $\vec{\omega}^{B-R}$ of the spin axis position with respect to the moving reference is

$$\vec{\omega}^{B-R} = -\dot{\Omega}(\cos i\, \hat{z}_B + \sin i\, \hat{x}_k) \ . \qquad (2.76)$$

The nominal angular momentum of the satellite is

$$\vec{H} = I_{zz}\omega_z\, \hat{z}_B \ , \qquad (2.76)$$

so the "kinematic disturbance torque" is

$$\vec{T}_k = \dot{\Omega} \sin i\, I_z \omega_z\, \hat{y}_k \ , \qquad (2.77)$$

where $\hat{y}_k = \hat{z}_B \times \hat{x}_k$ is along the descending line of nodes.

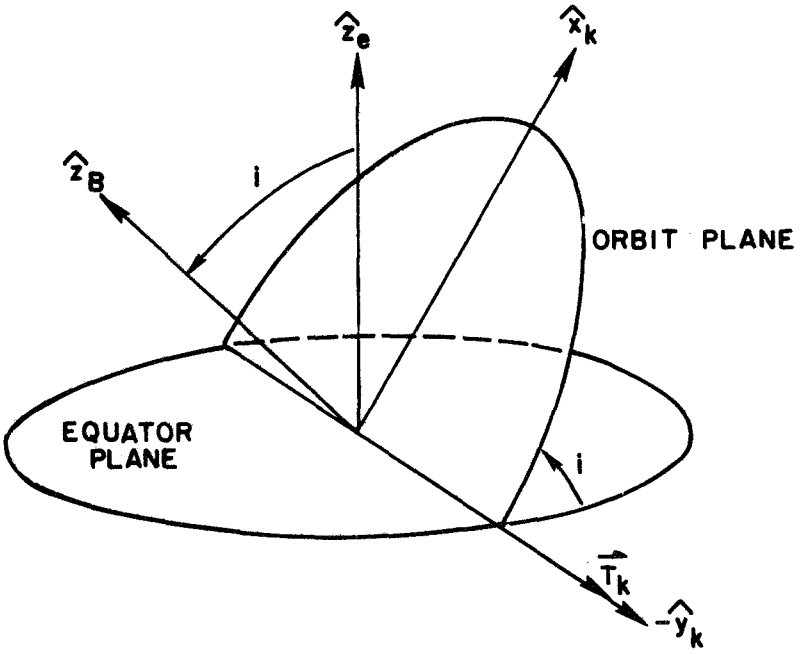

FIG. 2.8. GEOMETRY OF "KINEMATIC" DISTURBANCE TORQUE.

Other Torque Sources

There are a multitude of other sources of torques which tend to change the attitude of the satellite. Models of these torques are not developed here because these torques can be included with torque sources already discussed, or their effect is relatively small.

Torques similar in nature to aerodynamic and radiation torques are those due to dust clouds and electric drag on a charged satellite. Torques which resemble translational control jet torques are those caused by meteorite impact (in the impulsive sense), and the venting, outgassing, and leakage of system parts (in the average sense).

Additional gravitational torques are caused by higher order terms of the earth potential, the tidal bulge, and the moon and sun although these are definitely second order. Any moving parts which may exist on the satellite must be considered as possible torque sources. Finally, because no satellite is perfectly rigid, satellite wobble causes small elastic damping forces which act to decrease the satellite energy. How-
from these inertially-fixed torque plots. Also, the effect of any parameter changes on the satellite (such as increased c.p. offset from the mass center) can be directly determined.

Disturbance Torque Magnitudes

As a means of determining the total disturbance torque acting on a cylindrical spinning satellite, a digital computer program was written using the torque expressions developed in this section. This program computes the torques as a function of the parameters which change with orbital position of the satellite. Typical "inertially-fixed" torques acting on the orbits described in the previous section are presented in Figures 2.9-2.12. In both cases it is assumed that the ends and cylindrical wall have the same diffuse reflection properties. The body-fixed and spin torques also acting on the satellite can directly be estimated from these inertially-fixed torque plots. Also, the effect of any parameter changes on the satellite (such as increased c.p. offset from the mass center) can be directly determined.

The orbits selected for these plots are representative of typical ones for the drag-free satellite applications considered. Figures 2.9-2.10 are the yaw and roll torques acting on a spinning satellite in a resonant orbit of 15 revs/day. Here, the spin axis is controlled to point normal to the orbit plane. Perigee altitude is 300 km at the

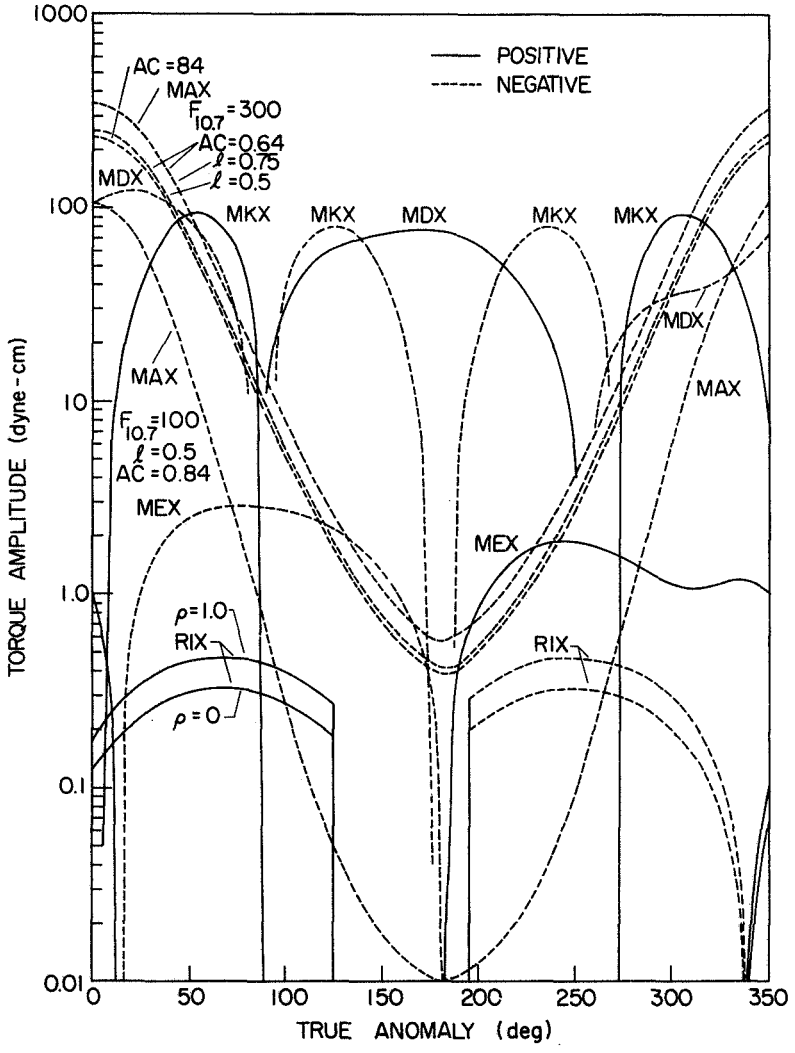

Key: MAX - aerodynamic
R1X - solar radiation
MEX - eddy current
MDX - satellite dipole
MKX - kinematic

ℓ - length of vehicle, m
ρ - reflectivity
A.C. - accommodation coefficient
$F_{10.7}$ - 10.7 cm decimetric flux

FIG. 2.9. TYPICAL YAW-TORQUE COMPONENTS ACTING UPON A CYLINDRICAL GEODESY SATELLITE. Here, h_p = 300 km; e = 0.0394; i = 45°.

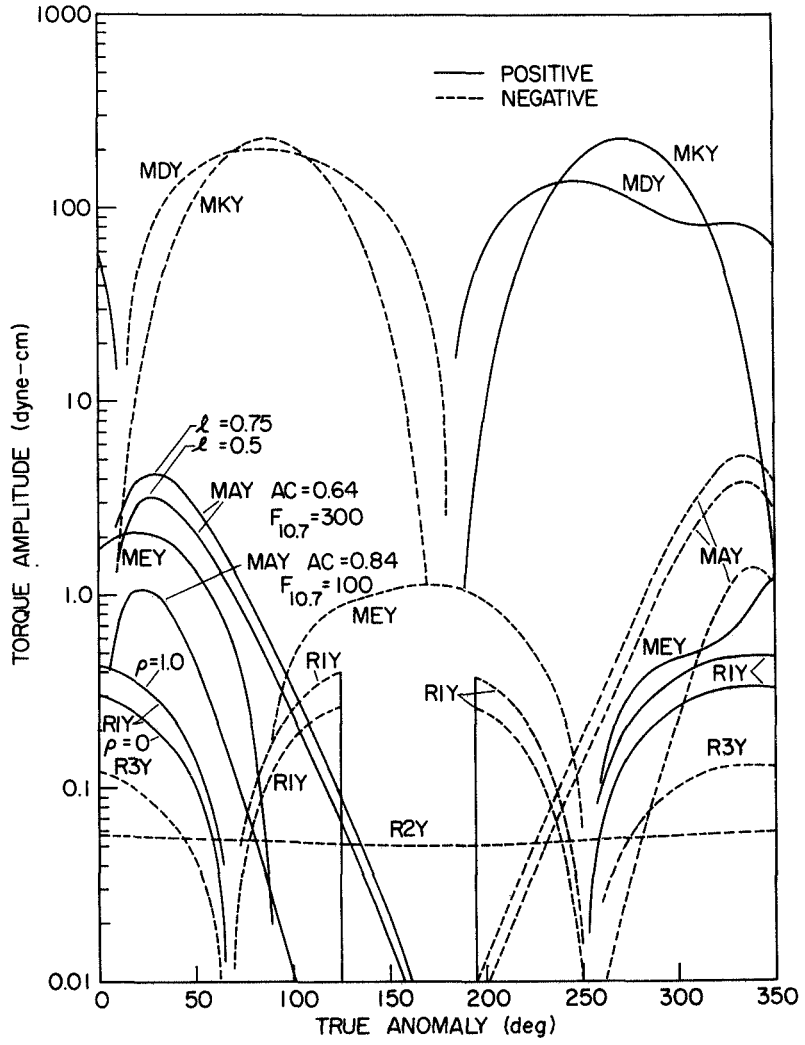

Key: MAY - aerodynamic
R1Y - solar radiation
R2Y - reflected radiation
R3Y - earth radiation
MEY - eddy current
MDY - satellite dipole
MKY - kinematic
ℓ - length of vehicle, m
ρ - reflectivity
A.C. - accommodation coefficient
$F_{10.7}$ - 10.7 cm decimetric flux

FIG. 2.10. TYPICAL ROLL-TORQUE COMPONENTS ACTING UPON A CYLINDRICAL GEODESY SATELLITE. Here, h_p = 300 km; e = 0.0394; i = 45°.

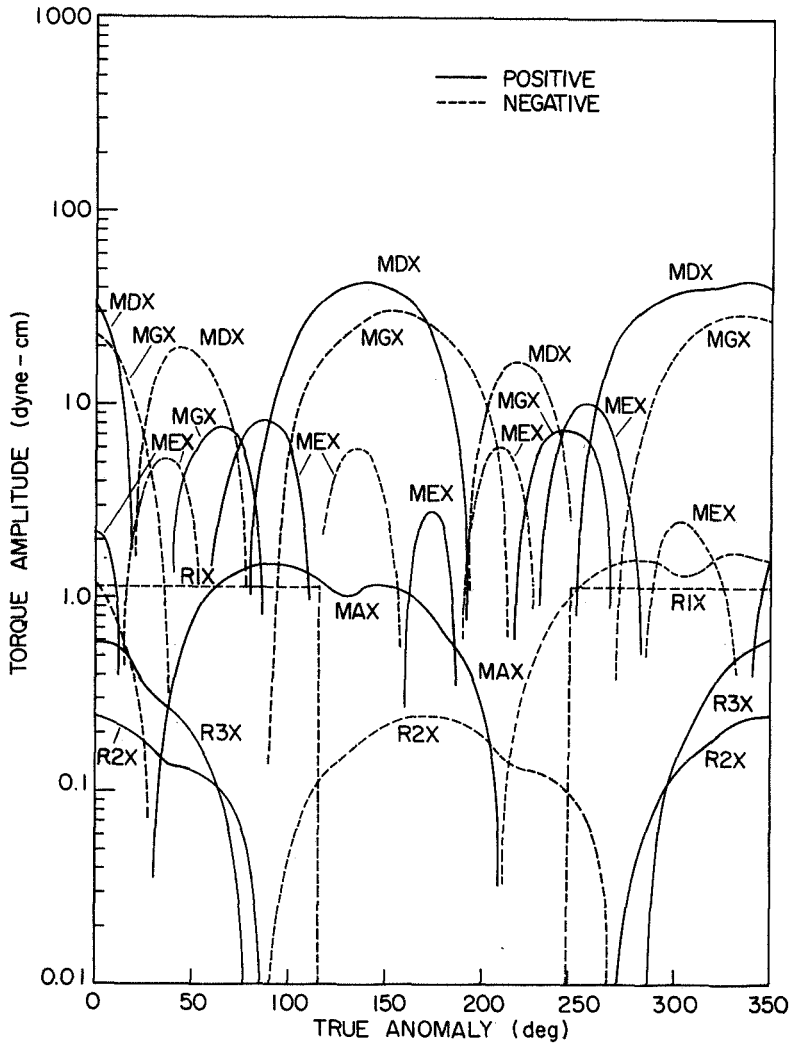

Key: MAX - aerodynamic
R1X - solar radiation
R2X - earth radiation
R3X - reflected radiation
MDX - satellite dipole
MEX - eddy current
MGX - gravity gradient

FIG. 2.11. TYPICAL $\hat{x}_*$-AXIS INERTIALLY-FIXED DISTURBANCE TORQUES ACTING UPON A STAR-TRACKING SATELLITE IN A CIRCULAR, POLAR ORBIT.

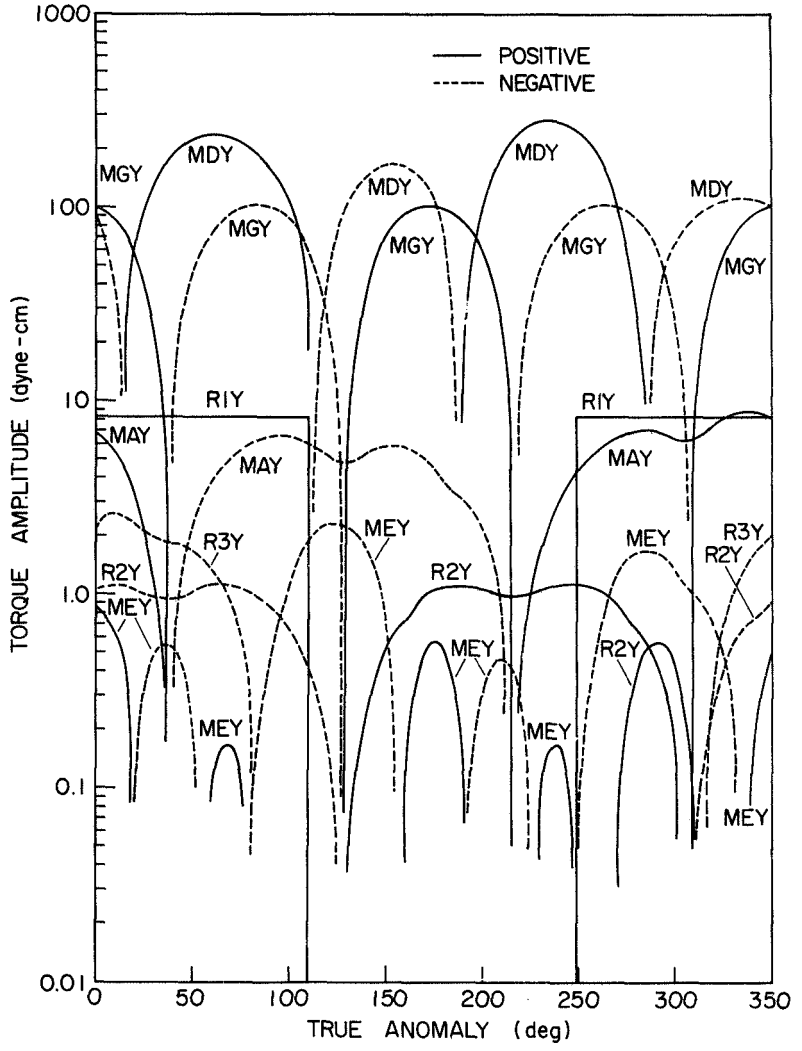

Key: MAY - aerodynamic
R1Y - solar radiation
R2Y - earth radiation
R3Y - reflected radiation
MDY - satellite dipole
MEY - eddy current
MGY - gravity gradient

FIG. 2.12. TYPICAL $\hat{y}_*$-AXIS INERTIALLY-FIXED DISTURBANCE TORQUES ACTING UPON A STAR-TRACKING SATELLITE IN A CIRCULAR, POLAR ORBIT.

subsolar point and inclination is 45°. These torques are not inertially fixed literally, but instead are fixed in the local frame of reference.

Figures 2.11 - 2.12 represent the inertially fixed torques about a spinning satellite in a circular, polar orbit with the spin axis controlled to point at the star Canopis. It is assumed that the orbit plane has precessed 10° to the left of the right ascension of Canopis.

The basic parameters used for these plots are

	Geodesy Satellite	Star Tracking Satellite
Length (m)	0.5/0.75	0.5
Radius (m)	0.5	0.5
Spin moment of inertia ($kg-m^2$)	15.	18.75
Transverse moment of inertia ($kg-m^2$)	10.	12.5
Spin speed (rad/sec)	1.	1.
Skin thickness (cm)	0.1	0.2
Mass center displacement from center of pressure (cm)	0.5	-1.0
Average moment arm from jet misalignment (cm)	-0.5	1.0
Average skin reflectivity	0.0/1.0	1.0
Accommodation coefficients	0.64/0.84	0.89
Decimetric flux index	100/300	300
Spin axis magnetic dipole ($Amp-m^2$)	0.6	0.6
Magnetic activity index	7	7

It is noted from Figures 2.9 - 2.10 that aerodynamic torques are significant at perigee, and kinematic and dipole torques are the chief disturbances throughout the rest of the orbit. From Figures 2.11 - 2.12, it is noted that the gravity gradient and dipole torques are the largest. Careful vehicle design can, of course, substantially reduce the disturbance torque levels except for the kinematic and gravity gradient torques where they are pertinent.

CHAPTER III

A MAGNETIC THREE-DEGREE-OF-FREEDOM ATTITUDE CONTROL SYSTEM FOR AN AXISYMMETRIC SPINNING SPACECRAFT WITH HORIZON SENSOR ERROR MEASUREMENT

This chapter is a study of a continuous magnetic attitude control system which points the spin axis of a symmetric satellite normal to the orbit plane of a highly eccentric orbit. This control system also maintains nearly constant vehicle spin speed. The attitude error measurement comes solely from a pair, or several pairs, of infrared horizon sensors placed upon the vehicle.

Horizon sensors mounted with their sensitive axes in "vee" shaped pairs as shown in Figure 3.1 are able to produce a sampled measurement of the roll error of the satellite. Because the variables in the vehicle's attitude motion are mathematically observable, it is feasible to build a state observer which estimates the yaw error and body rates from the horizon sensor measurements. The sensor signals are noisy, so a Kalman filter is utilized for the observer. Techniques are studied for processing the sampled input with the continuous filter.

With the satellite attitude-error state known, a minimum-power optimal control law, utilizing a quadratic function of the state elements and control effort as the performance index, is developed to drive

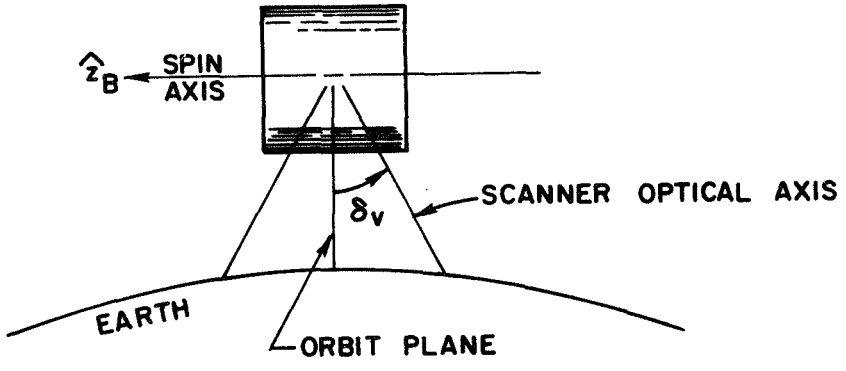

FIG. 3.1. HORIZON SENSOR "VEE" CONFIGURATION THAT PRODUCES TWO PULSE SIGNALS WHOSE DIFFERENCE IS PROPORTIONAL TO THE ROLL ERROR.

the state to zero. This control law takes into account the possible existence of a passive nutation damper as part of the attitude control system. Gains for the control law are obtained from the general solution of the optimum regulator for a fourth-order system possessing complex symmetry. This general solution is derived in this chapter.

Next, a study of magnetically mechanizing the desired control torques is presented. The resulting controller has three logic modes making possible both pointing control and spin speed control. This investigation also demonstrates that a single electromagnetic coil skewed to the spin axis can provide both types of control.

To simplify the onboard computational requirements, the control gains are implemented as constants. Because of the fluctuating magnetic field, constant gains produce time-varying control torques. This variation poses the question of how large the fluctuations can be and still insure attitude stability. Bounds on the control gains which guarantee stability are explicitly established by the generation of suitable Lyapunov functions and the use of averaging techniques. System stability bounds are established for satellites with and without the nutation damper. The Lyapunov functions are obtained from a generating procedure which is derived for systems possessing complex symmetry.

The last section summarizes the results of the analog and digital simulations used to verify and extend the preceeding analyses. The general performance capabilities of the control system during transient response and in the presence of disturbance torques and system nonlinearities are explored.

STATE ESTIMATION BY FILTERING HORIZON SENSOR DATA

By proper placement of a pair of infrared horizon sensors (bolometers), it is possible to measure directly the spinning satellite's roll error θ. (See Fig. 2.1.) Because of the structure of the satellite's state equations, the system is observable. Therefore, a filter can be constructed which will produce estimates of the other state variables from the roll-error measurements. To account for random disturbance torques and measurement noise, a steady-state Kalman (Wiener)

filter is developed which gives best estimates of these states. This system is developed in this section.

Horizon Sensor Determination of Roll Angle, Spin Speed, and Orbital Rate

Roll-error measurement can be provided by using the output of two infrared bolometers arranged with their optical axes in a "Vee" configuration, as shown in Figure 3.1. The optical axes lie in a plane containing the vehicle spin axis. As the satellite spins, the optical axes sweep out two cones in space. Each sensor periodically responds to the radiance change existing between cold outer space and the warmer infrared earth.

The intersection of these sensor paths with the earth, and the corresponding sensor output are shown in Figure 3.2. When the spin axis is normal to the earth-satellite radius vector, the sensor pulse outputs will have the same width and occur at the same time for an ideal spherical earth. If a roll error exists, pulse duration will be different, as

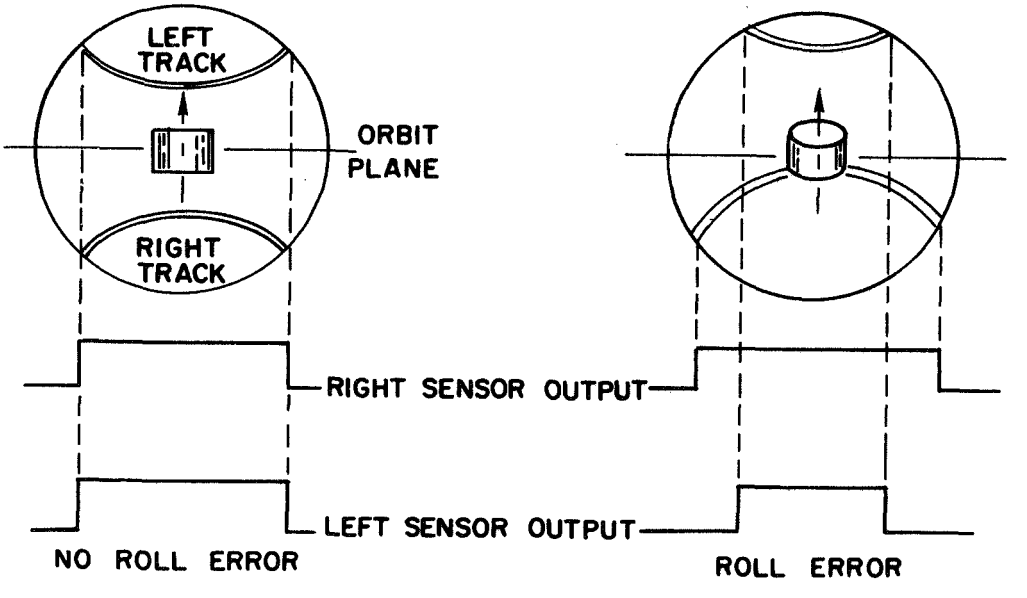

FIG. 3.2. HORIZON SENSOR OUTPUT WITH AND WITHOUT ROLL ERROR. This representation illustrates looking at the spacecraft with the earth behind it.

illustrated. A yaw error will not be fully detected by such a sensor until 90° later in the orbit when it becomes the roll error.

The geometry of the horizon sensor scheme is depicted in Figure 3.3 where

θ = roll error,

δ_v = half-vee angle,

$\alpha_v = 90° - \delta_v$,

$\beta_v = \sin^{-1}(a_e/R)$,

t_1 = pulse width of the right sensor,

$\dot{\psi}$ = local spin rate $\cong \omega_z - \dot{\sigma}$,

$\gamma_v = \dot{\psi}\, t_1/2$.

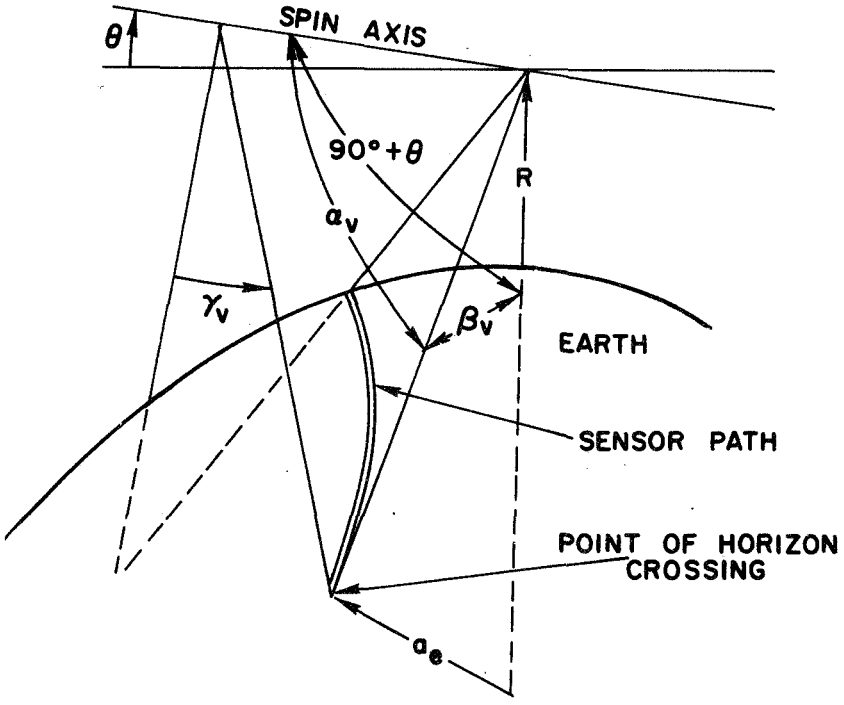

FIG. 3.3. GEOMETRY OF THE HORIZON SENSOR SCHEME. The angles illustrated are:

θ - the roll error,

β_v - the angle between the geocenter-satellite line and the line joining the satellite and the point where the sensor optical axis crosses the horizon,

α_v - the angle between the spin axis and the horizon crossing point.

The pulse width t_1 for an ideal spherical earth can be computed as

$$t_1 = \frac{2}{\dot{\psi}} \cos^{-1}\left[\frac{\cos \beta_v + \sin \theta \sin \delta_v}{\cos \theta \cos \delta_v}\right] . \qquad (3.1)$$

Equation (3.1) was used to compute the output characteristics of sensors with half-vee angles of 3°, 6°, and 9° for an elliptic orbit with an altitude ranging from 300 km at perigee to 27559 km at apogee. Orbital rate was three revs/day. The roll-angle error as a function of two 9° sensor pulse-width differences is shown in Figure 3.4 for various values of the orbit radius between the indicated apogee and perigee.

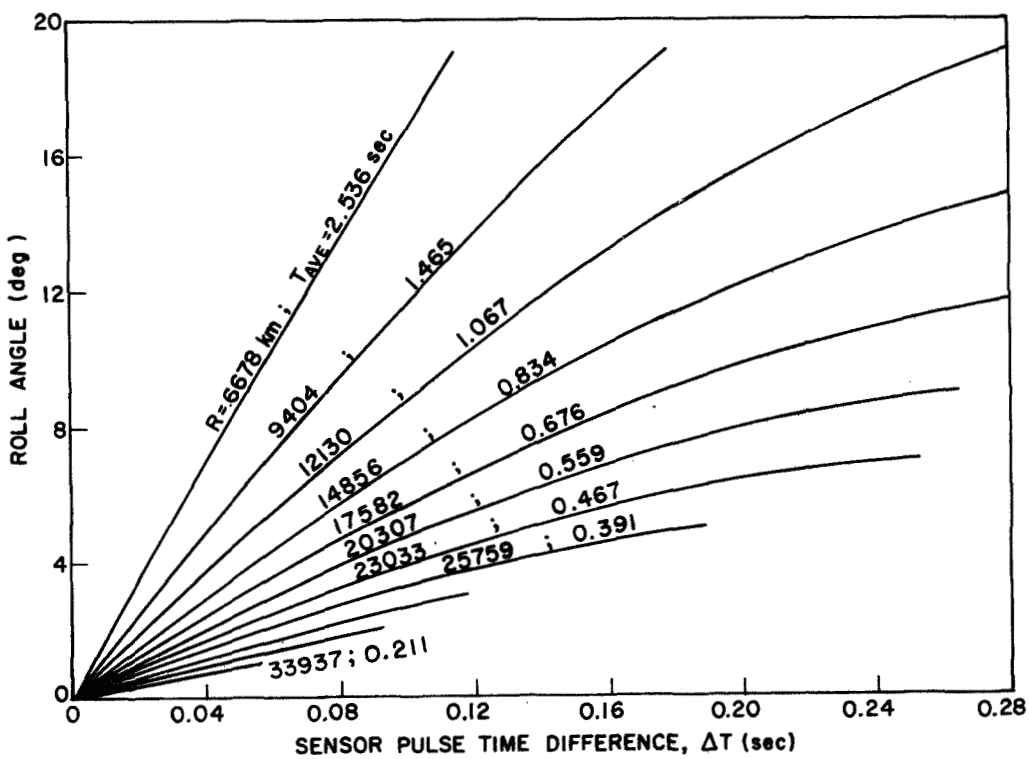

FIG. 3.4. ROLL ERROR VS SENSOR SIGNAL PULSE DIFFERENCE FOR 9° HALF-VEE ANGLE IN A 3 REVS/DAY ORBIT. Here, h_p = 300 km and e = 0.6711. Parameters of this plot are values of the geocentric radius from perigee (6678 km) to apogee (33937 km). Also indicated is the average sensor pulse width.

Here

$$\Delta t = (t_2 - t_1)/2 \ ,$$

where t_2 is the pulse width of the left sensor. The roll error is found by multiplying the pulse difference by a gain (slope of curves such as those in Figure 3.4) which is altitude dependent. This gain, as a function of average pulse width, is shown in Figure 3.5 for the three sensor angles investigated here. (The pulse width average remains fairly constant at a given altitude for small values of roll error.) As can be seen from Eq. (3.1), the error signal is less sensitive with a larger half-vee angle. However, a trade-off must be made because larger sensor angles will cause the sensor to miss the earth at high altitudes of the highly eccentric orbits.

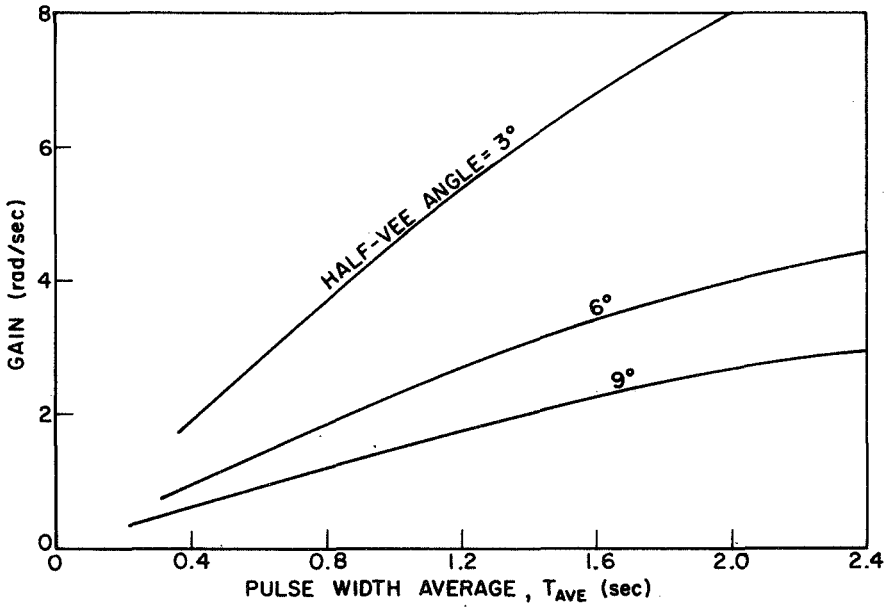

FIG. 3.5. ERROR GAIN VS PULSE WIDTH FOR DIFFERENT HALF-VEE ANGLES IN A 3 REVS/DAY ORBIT. These gains are the slopes of the curves similar to Figure 3.4.

Because the horizon sensors produce a pulse train (where the pulse width varies with satellite altitude), this output can also be used to

give a direct measurement of the vehicle's spin speed and the current orbital rate $\dot{\sigma}$ of the vehicle.

Kalman Filtering for State Estimation

The linearized state equations of the symmetric spinning satellite in an elliptic orbit, as presented in Chapter 2, are

$$\begin{bmatrix} \dot{\alpha}_x \\ \dot{\alpha}_y \\ \dot{\varphi} \\ \dot{\theta} \end{bmatrix} = \begin{bmatrix} -d_p & -D & 0 & 0 \\ D & -d_p & 0 & 0 \\ 1 & 0 & 0 & \dot{\sigma} \\ 0 & 1 & -\dot{\sigma} & 0 \end{bmatrix} \begin{bmatrix} \alpha_x \\ \alpha_y \\ \varphi \\ \theta \end{bmatrix} + \begin{bmatrix} 1 & 0 \\ 0 & 1 \\ 0 & 0 \\ 0 & 0 \end{bmatrix} \begin{bmatrix} T_{x_1} \\ T_{y_1} \end{bmatrix} . \tag{3.2}$$

Here, $D = (I_{zz}/I_{xx})\,\dot{\psi}$ and the torque components (T_{x_1}, T_{y_1}) are normalized by dividing by I_{xx}. The state vector of this system, as coordinatized in the unspinning reference frame (R), is

$$x_R^T \triangleq \begin{bmatrix} \alpha_x & \alpha_y & \varphi & \theta \end{bmatrix} . \tag{3.3}$$

The driving torque consists of a control component and a disturbance component designated as

$$\begin{aligned} T_R^T &= \begin{bmatrix} T_{x_1} & T_{y_1} \end{bmatrix} = \begin{bmatrix} u_x & u_y \end{bmatrix} + \begin{bmatrix} v_x & v_y \end{bmatrix} , \\ &= u_R^T + v_{1R}^T . \end{aligned} \tag{3.4}$$

The vectors $\vec{x}$, $\vec{u}$ and $\vec{v}_1$ are all functions of time where $\vec{u}$ and $\vec{v}_1$ are the control and disturbance torques respectively.

To build an efficient attitude controller for this spacecraft, it is necessary to estimate the yaw angle error φ. If active damping is to be provided, the values of the vehicle rates α_x and α_y must also

be provided. The state estimator synthesis is begun by putting the differential Eqs. (3.2) in the form

$$\dot{\vec{x}} = F\vec{x} + G\vec{u} + L_1\vec{v}_1 ,$$

$$y = H\vec{x} + w . \qquad (3.5)$$

Here, y is the electronic signal representing the scalar measurement of the roll error θ; it is corrupted by various noise sources such as earth oblateness effect, cloud cover, and system nonlinearities which cause the horizon sensor signal to deviate from the ideal of Eq. (3.1). This measurement noise is designated by the scalar w.* The matrix H is

$$H = \begin{bmatrix} 0 & 0 & 0 & \delta_{ts} \end{bmatrix} . \qquad (3.6)$$

The δ_{ts} term in H is equal to one when a measurement is made and zero otherwise. The measurement noise w is also multiplied by the δ_{ts} function. Hence, the measurement y must be treated as a discrete signal.

If the control $\vec{u}$, the disturbance $\vec{v}_1$, and noise w are known, the entire state $\vec{x}$ of the system (3.5) can be exactly reconstructed because (F,H) form an observable pair. The control $\vec{u}$ is known because it is generated as a function of the state.

As seen in Figures 2.9 - 2.10 of Chapter 2, the major part of the "inertially-fixed" torques acting on the spacecraft are oscillatory in

---

*The measurement errors from the horizon sensor pairs can be modeled as biases plus white noise for a simple approximation, in which case the order of the system is increased. This is done by adding the state equations

$$\dot{b}_i = 0$$

for every pair of horizon sensors. (Here, b_i represents the bias error of the i^{th} sensor pair.) The H matrix must be modified to add this bias to the actual roll angle θ. Further sophistication can be incorporated into the measurement error model by recognizing the existence of orbital position dependent correlation characteristics. (See Fitzgerald, Ref. 41). For the sake of system mechanization simplicity, however, the measurement error is assumed to consist of strictly white noise.

nature, with periods which are small integer multiples of the orbital period. The "body-fixed" torque also affects the vehicle attitude error, and it too is a sinusoidal disturbance as projected into the Reference (R) frame. These oscillatory disturbances can be modeled as states with differential equations

$$\dot{v}_{xi} = -\omega_{vi}\, v_{yi} \ ,$$

$$\dot{v}_{yi} = \omega_{vi}\, v_{xi} \ . \qquad (3.7)$$

Here, ω_{vi} is the frequency of change of the i^{th} component of the total oscillating disturbance with respect to the (R) frame. Each pair of the components of oscillating disturbances $\vec{v}_1$ with unique frequency ω_{vi} can be incorporated into the system matrix F of Eq. (3.5). The resulting pair (F,H) will still be observable in the mathematical sense. However, simulation has shown that poor results are obtained when attempting to build a filter to obtain these disturbances is addition to the unknown attitude components. (This is true because the observability of the system is dependent upon the presence of the orbital cross-coupling term n (or $\dot{\sigma}$) which is quite small compared to the speed of dynamic change governed by the parameter D.) The inclusion of disturbance torques in the state equations also increases the complexity of the resulting filter.

With the foregoing in mind, it is assumed that the disturbance torques $\vec{v}_1$ to the system and the measurement noise w are stationary white noise with statistics

$$E[\vec{v}_1(t)] = 0 \ ,$$

$$E[w(t)] = 0 \ ,$$

$$E[\vec{v}_1(t)\, w(t)] = 0 \ ,$$

$$E[\vec{v}_1(t)\, \vec{v}_1^{T}(\tau)] = Q_1 \delta(t - \tau) \ ,$$

$$E[w^2(t)] = R_1 \ . \qquad (3.8)$$

Again, the expected value of $w^2(t)$ is a discrete function. Q_1 is a constant positive definite matrix and R_1 is a positive scalar constant. The initial state $\vec{x}(0)$ is assumed to be independent of the stochastic processes $\vec{v}_1(t)$ and $w(t)$.

It is desired that a filter be mechanized which will produce a continuous estimate of the unknown attitude errors so that these quantities can be utilized in a continuous control law. Some form of the Kalman filter (Ref. 42) which will minimize the square of the difference between the actual $\vec{x}$ and the estimated $\hat{x}$ seems to be a logical choice for the state estimator.

For power optimal control it will be seen that some active damping is always required. Hence, the mechanization of the complete filter which estimates vehicle rates in addition to altitude errors is considered with the assumption that an adequate sampling rate is available. One method which can be used to process the sampled input for the filter is to hold this input between samples and use the regular continuous filter

$$\dot{\hat{x}} = F\hat{x} + G\hat{u} + \Sigma(t)\, H^T R_1^{-1}(\theta_s - \hat{\theta}) \,. \tag{3.9}$$

Here, the θ_s is the sampled-and-held measurement of θ and the δ_{ts} is replaced by 1.0 in H. The matrix $\Sigma(t)$ is the covariance matrix of the error $(\vec{x} - \hat{x})$ and satisfies the matrix Riccati equation

$$\dot{\Sigma}(t) = F\,\Sigma(t) + \Sigma(t)F^T + L_1 Q_1 L_1^T - \Sigma(t)H^T R_1^{-1} H\,\Sigma(t) \,,$$

$$\Sigma(0) = \Sigma_0 \,. \tag{3.10}$$

For convenience in the immediate discussion, it is assumed that the orbital rate $\dot{\sigma}$ in Eqs. (3.2) can be replaced by the constant n so the synthesis can be applied to a constant system. The effect of the time-varying $\dot{\sigma}$ will be discussed shortly. With a constant system, the limit Σ_∞ exists, where

$$\Sigma_\infty = \lim_{t \to \infty} \Sigma(t) \ ,$$

and is found by setting $\dot{\Sigma}(t) = 0$ and solving (3.10). The resulting constant coefficient filter (which is equivalent to the Wiener filter of Ref. 43) is

$$\dot{\hat{x}} = F\hat{x} + G\hat{u} + \Sigma_\infty H^T R_1^{-1}(\theta_s - \hat{\theta}) \ . \qquad (3.11)$$

Because the satellite attitude control problem of concern here is a long-life regulator problem, the initial transient performance difference of employing a constant coefficient filter [Eq. (3.11)] as opposed to a time-varying filter governed by Eqs. (3.9) and (3.10) is of little concern. The mechanization advantages of the constant coefficient filter are obvious.

By dividing Eq. (3.10) by R_1, it can be seen that the solution $\Sigma(t)$ depends solely upon the matrix Q_1/R_1. The control vector $\hat{u}$ of (3.9) and (3.11) is the ideal value of the control torque which will differ from the actual $\vec{u}$ by unknown mechanization errors. In this application, the matrices G and L_1 are identical.

It was assumed that Q_1/R_1 was of the form

$$\frac{Q_1}{R_1} = \begin{bmatrix} q_1 & 0 \\ 0 & q_1 \end{bmatrix} .$$

Equations (3.10) were solved by numerical integration for a wide range of the ratio of variances q_1 for an example satellite. This example used the parameters $D = 1.5 \text{ sec}^{-1}$ and $n = 1.09 \times 10^{-3} \text{ sec}^{-1}$ which corresponds to the mean orbital rate of fifteen revs/day. The steady-state results are presented in Figure 3.6a with

$$[K_1 \ K_2 \ K_3 \ K_4] = \left[\Sigma_\infty H^T/R_1\right]^T$$

being the gain matrix of the continuous filter.

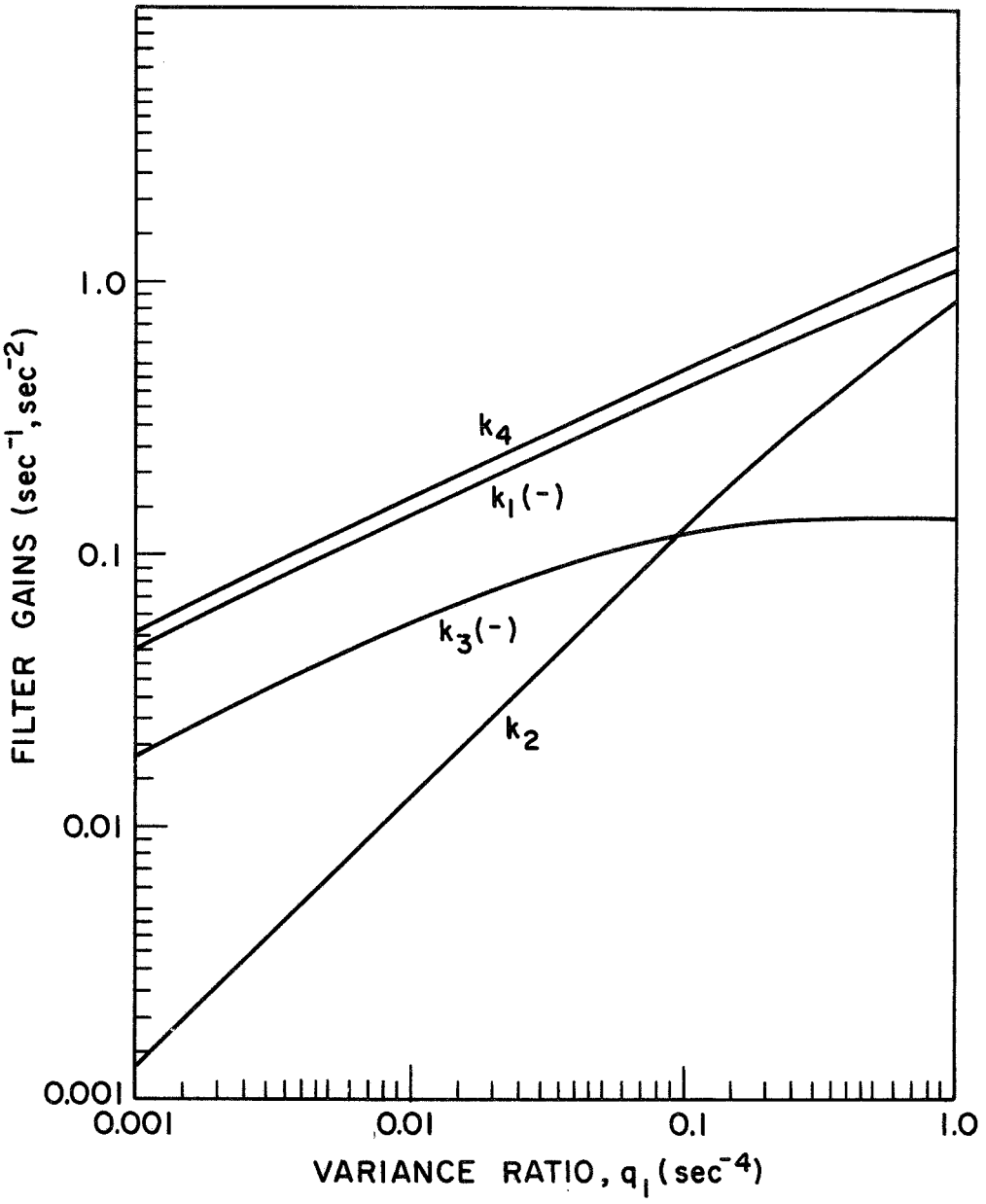

FIG. 3.6a. KALMAN FILTER GAINS VS NOISE VARIANCE RATIO FOR SPINNING SATELLITE WITH APPROXIMATION OF CONTINUOUS ROLL ERROR MEASUREMENT OF THE SPINNING SATELLITE. The parameters D and n of the state equations have values of 1.5 sec^{-1} and 1.09×10^{-3} sec^{-1}.

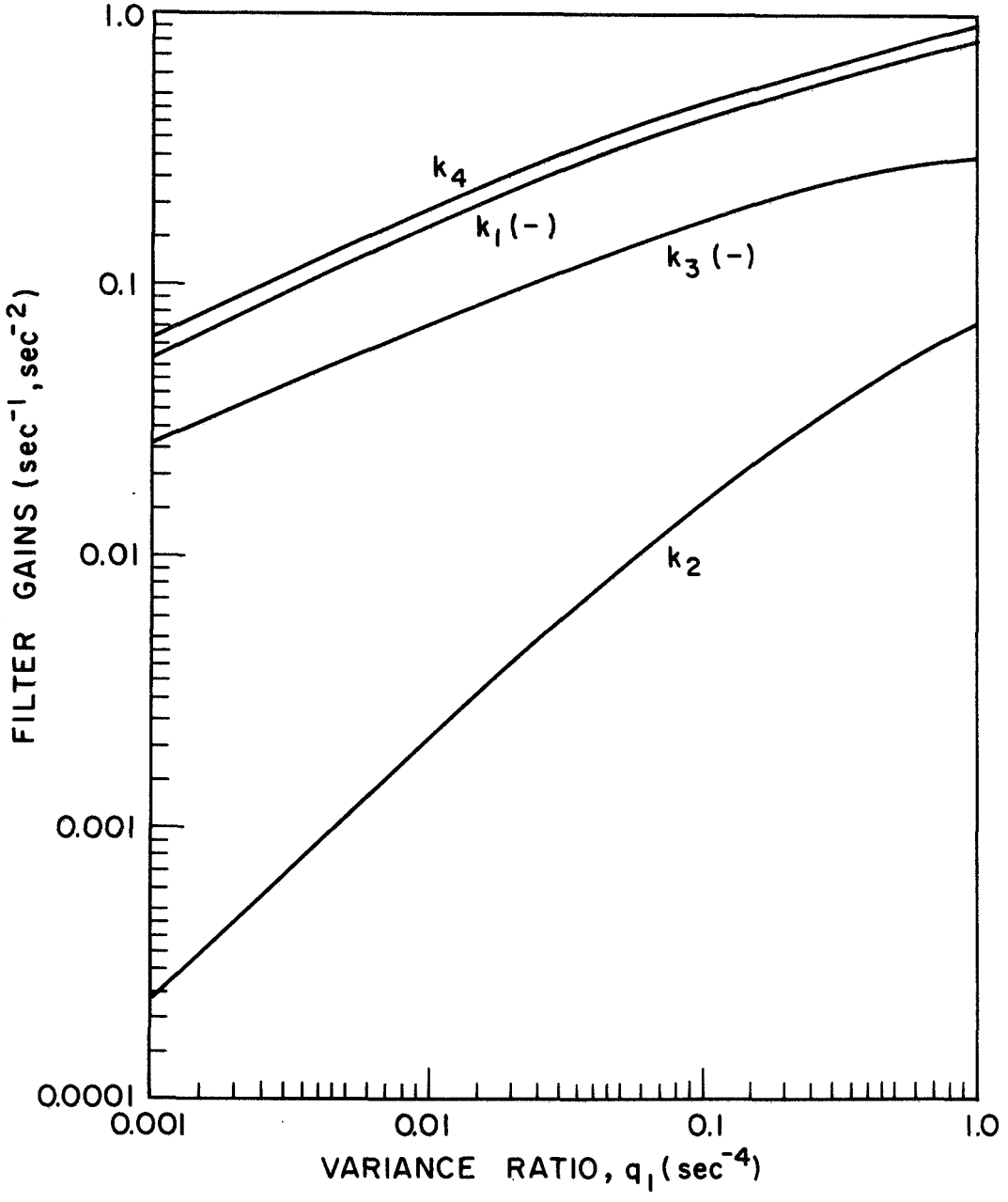

FIG. 3.6b. DISCRETE KALMAN FILTER GAINS VS NOISE VARIANCE RATIO FOR SPINNING SATELLITE WITH ROLL ERROR MEASUREMENTS TAKEN FOUR TIMES PER SATELLITE ROTATION. Vehicle parameters are the same as in Fig. 3.6a.

Changing the parameter n to 2.10×10^{-4} sec^{-1}, corresponding to an orbital rate of 3 revs/day, changed the steady-state gains by less than 2%. Thus, replacing the time-varying orbital rate term $\dot{\sigma}$ by the constant n is a justifiable simplification from the filter design standpoint.

If θ_s is a piecewise constant input and $\hat{\theta}$ is continuously varying in Eq. (3.12), the estimated rates $\hat{\alpha}_x$ and $\hat{\alpha}_y$ lag the actual rates α_x and α_y. This must be compensated for in the control law mechanization because of system efficiency and stability reasons, and is discussed in the last section of this chapter on simulation results. If the estimated roll error $\hat{\theta}$ is synchronously sampled with θ_s, and this sampled value is used in (3.12), no lag problem arises.

It was determined by analog and digital simulation that the sampling rate required by the continuous filter (3.9) to obtain accurate estimates of vehicle rates seemed to be the Nyquist rate dictated by the sampling theorem (Ref. 44). The filter must reconstruct motion which in its uncontrolled form is

$$\alpha_x = \alpha_{xo} \cos Dt - \alpha_{yo} \sin Dt,$$

$$\alpha_y = \alpha_{xo} \sin Dt + \alpha_{yo} \cos Dt ,$$

$$\varphi = \varphi_o \cos \dot{\sigma}t + \theta_o \sin \dot{\sigma}t + \frac{\alpha_{xo}}{D + \dot{\sigma}} (\sin \dot{\sigma}t + \sin Dt)$$

$$- \frac{\alpha_{yo}}{D + \dot{\sigma}} (\cos \dot{\sigma}t - \cos Dt) ,$$

$$\theta = \varphi_o \sin \dot{\sigma}t + \theta_o \cos \dot{\sigma}t + \frac{\alpha_{xo}}{D + \dot{\sigma}} (\cos \dot{\sigma}t - \cos Dt)$$

$$+ \frac{\alpha_{yo}}{D + \dot{\sigma}} (\sin \dot{\sigma}t + \sin Dt) .$$

Here, α_{xo}, α_{yo}, φ_o, and θ_o are arbitrary initial conditions. Thus, it is necessary that the roll angle θ be sampled at least 2D times per satellite rotation because the rate terms α_x and α_y oscillate with the rate D. For a spacecraft spinning about its maximum axis, one pair of horizon sensors can provide ample sampling speed for spin rates

up to 0.5 rad/sec. For D greater than 0.5 $\sec^{-1}$, the horizon sensor head must either be spun at least at the rate 2D $\sec^{-1}$, or the number of horizon-sensor pairs used must be greater than or equal to 2D.

A simple way to alleviate having to provide more than one horizon sensor pair for the spacecraft is to provide an active control torque based upon roll and yaw errors only (i.e. provide only active "position" control). The attitude error estimates $\hat{\varphi}$ and $\hat{\theta}$ from the Kalman filter would be correct in the average sense after the rate terms have been dampened away by a passive nutation damper.

With a small amount of circuit logic, a statistically superior means of implementing the Kalman filter exists. This consists of modeling a continuous filter between sampling intervals and a discrete filter at the time of horizon sensor input. That is, between samples, the equations

$$\dot{\hat{x}} = F\hat{x} + G\hat{u} \ , \tag{3.12a}$$

$$\dot{\Sigma} = F\,\Sigma \ + \ \Sigma F^T + L_1 Q L_1^T \tag{3.12b}$$

are integrated to produce the estimate $\hat{x}$. At the time of measuring the roll error θ_s, the state is updated by the equation

$$\hat{x}(t_+) = \hat{x}(t_-) + K(\theta_s - \hat{\theta}) \ , \tag{3.12c}$$

where the gain matrix K is

$$K = \Sigma(t_-)H^T \left(H\ \Sigma\ (t_-)H^T + R_1\right)^{-1} \ . \tag{3.12d}$$

The covariance is updated by

$$\Sigma(t_+) = (I - KH)\ \ \Sigma(t_-) \ . \tag{3.12e}$$

Here, (t_-) and (t_+) indicate the instances before and after the sampling point.

For the symmetric spinning spacecraft with a constant sampling interval, the gain K also achieves a steady-state value so that only Eqs. (3.12a) and (3.12c) require mechanization. The values of the gain elements of the same satellite studied in Figure 3.6a were found from Eqs. (3.12b,d, and e) with the sampling rate set at four times per satellite rotation. The driving noise variance used was 0.25×10^{-6} sec^{-4}. Values of the measurement noise variance were varied with the results presented in Figure 3.6b in terms of the variance ratios.

A remarkable similarity exists between the plots in Figures 3.6a-b in that the gains of Figure 3.6b are about the same as those of Figure 3.6a at approximately two orders of magnitude lower variance ratio. In fact, computer results showed that increasing the sampling rate moved the resulting filter gains closer to those of the continuous filter of Figure 3.6a. This is expected because in the limit (as the sampling interval becomes very small) the discrete Kalman filter becomes the continuous filter. It can be hypothesized that the steady state gain curves associated with any sampling rate can be approximated by those of the continuous filter shifted to some lower variance ratio.

The additional advantage of the hybrid mechanization of the filter [Eqs. (3.12)] is that only one sample of the roll error needs to be taken per satellite rotation in order to provide an adequate estimate of the four elements of the error state. The only restriction is that the product of the spin period $(2\pi/\dot{\psi})$ and the parameter D not be close to an integer multiple of π.

THE MINIMUM POWER CONTROLLER

Magnetic control torque is created by passing current through coils of wire fixed on the spacecraft. It is desirable that attitude control gains be provided which minimize the power used by such a system, in addition to providing the required response characteristics. If more than one coil of wire is used for control actuation, minimum power is obtained by minimizing the time integral of the sum of the power used by each coil with some constraint placed upon the attitude error. Time extends over the period required to drive the attitude to the required orientation.

Such a power optimum controller, which maintains the spin axis normal to the orbit plane, is now developed.

The Optimal Regulator Problem

As defined in Ref. 45, a regulator is a feedback controller designed to keep a stationary system within an acceptable deviation from a reference condition using acceptable amounts of control. This control can be provided by choosing a control law which minimizes the performance index

$$J_f = \frac{1}{2} \int_{t_o}^{t_f} (\vec{x}^T \, Q_2 \vec{x} + \vec{u}^T R_2 \vec{u}) \, dt \, . \tag{3.13}$$

Here, Q_2 is a positive semidefinite matrix, R_2 is positive definite, and $\vec{u}$ represents the control effort.

For the case of magnetic control, the magnetic moment m of a wire coil, in Weber-m^2, is

$$m = NA_c i_c \, ,$$

where N is the number of turns of wire, A_c is the coil area, and i_c is the current. Thus, the control effort is proportional to the current in the wire; minimization of the performance index J_f in (3.13) represents a power minimization because it is quadratic in $\vec{u}$ (and therefore i_c).

Reference 45 shows that the optimal solution of control for the regulator is found by setting $t_f - t_o = -\infty$ and finding the steady-state solution to the Riccati equation

$$\dot{P} = -PF - F^T P + PGR_2^{-1} G^T P - Q_2 \, , \tag{3.14}$$

with $P(t_f) = 0$. The optimal control law is

$$\bar{u}(t) = -C_o \vec{x}(t) \, , \tag{3.15}$$

where

$$C_o = R_2^{-1} G^T P_\infty ,$$

and

$$P_\infty = P(-\infty) .$$

The cost of driving an initial state $\vec{x}(0)$ to the origin is

$$J_{fmin} = \frac{1}{2} \vec{x}^T(0) \; P_\infty \vec{x}(0) . \tag{3.16}$$

Because the pair $(F, Q_2^{1/2})$ is completely observable, the symmetric matrix P_∞ is positive definite, and the resulting system is stable.

One method of solving the matrix Riccati Eq. (3.14) is by numerically integrating backwards in time until a steady-state solution is achieved. This method is perfectly acceptable and results in the correct solution for P_∞, if one exists. However, it is a time consuming procedure on the computer, and must be repeated for changes to the system parameters. Because the spinning satellite studied here has the property of complex symmetry,* an algebraic method is available which can be used to solve the steady-state solution of Eq. (3.14). This method is now presented.

The Algebraic Solution to the Quadratic Matrix Equation Governing the Optimal Regulator of a General System Possessing Complex Symmetry

This analysis will be directed to fourth order systems because of the immediate application and simplification of presentation. It is, however, applicable to all higher order complex symmetric systems and the extension to these cases is obvious.

---

*Complex symmetry is defined as the property in which a system of order $2n$ real state elements can be reduced to one of order n complex state elements. This should not be confused with the idea of the symmetric matrix in which a matrix $A = A^T$.

The general equations of motion of a fourth order system possessing complex symmetry are

$$\ddot{x}_1 + a_{1s}\dot{x}_1 - b_{1s}\dot{x}_2 + a_{0s}x_1 - b_{0s}x_2 = u_1 ,$$

$$\ddot{x}_2 + a_{1s}\dot{x}_2 + b_{1s}\dot{x}_1 + a_{0s}x_2 + b_{0s}x_1 = u_2 . \qquad (3.17)$$

In matrix form, Eqs. (3.17) are

$$\begin{bmatrix} \ddot{x}_1 \\ \ddot{x}_2 \\ \dot{x}_1 \\ \dot{x}_2 \end{bmatrix} = \begin{bmatrix} -a_{1s} & b_{1s} & a_{0s} & b_{0s} \\ -b_{1s} & -a_{1s} & -b_{0s} & -a_{0s} \\ 1 & 0 & 0 & 0 \\ 0 & 1 & 0 & 0 \end{bmatrix} \begin{bmatrix} \dot{x}_1 \\ \dot{x}_2 \\ x_1 \\ x_2 \end{bmatrix} + \begin{bmatrix} 1 & 0 \\ 0 & 1 \\ 0 & 0 \\ 0 & 0 \end{bmatrix} \begin{bmatrix} u_1 \\ u_2 \end{bmatrix} \qquad (3.18)$$

Define

$$x \triangleq x_1 + jx_2 , \qquad (3.19a)$$

$$u \triangleq u_1 + ju_2 , \qquad (3.19b)$$

$$A_{1s} \triangleq a_{1s} + jb_{1s} , \qquad (3.19c)$$

$$B_{1s} \triangleq a_{0s} + jb_{0s} . \qquad (3.19d)$$

Then (3.18) becomes

$$\begin{bmatrix} \ddot{x} \\ \dot{x} \end{bmatrix} = \begin{bmatrix} -A_{1s} & -B_{1s} \\ 1 & 0 \end{bmatrix} \begin{bmatrix} \dot{x} \\ x \end{bmatrix} + \begin{bmatrix} 1 \\ 0 \end{bmatrix} [u] , \qquad (3.20)$$

or

$$\dot{\vec{x}} = F\vec{x} + G\vec{u} \qquad (3.21)$$

which are complex state equations.

The optimal control gains for a regulator system in which the desired final state $x(t_f) = 0$ are found from the steady state solution (at time $t_o = -\infty$) to Eqs. (3.14).

For the complex state equations, the matrix Riccati equation (3.14) must be formulated in Hermitian form

$$\dot{S} = SF - F^*S - Q + SGR^{-1}G^*S \ , \tag{3.22}$$

where the notation F^* refers to the complex conjugate of the transpose of F. The matrix S has the property that $S^* = S$.

The steady-state solution to (3.22) is defined as

$$S(-\infty) \triangleq S_\infty \ , \tag{3.23}$$

and the states are defined as

$$\begin{bmatrix} \dot{x}_1 \\ \dot{x}_2 \\ x_1 \\ x_2 \end{bmatrix} \triangleq \vec{z} \ , \tag{3.24a}$$

$$\begin{bmatrix} \dot{x} \\ x \end{bmatrix} \triangleq \vec{x} \ . \tag{3.24b}$$

The cost to bring the initial complex state $\vec{x}(t_o)$ to zero is

$$J_f = \frac{1}{2} \vec{x}(t_o)^* \, S_\infty \vec{x}(t_o) \ . \tag{3.25}$$

Noting that

$$\vec{x} = \begin{bmatrix} 1 & j & 0 & 0 \\ 0 & 0 & 1 & j \end{bmatrix} \begin{bmatrix} \dot{x}_1 \\ \dot{x}_2 \\ x_1 \\ x_2 \end{bmatrix} \triangleq T\vec{z} \ ,$$

where T is the indicated transformation, Eq. (3.25) becomes

$$J_f = \frac{1}{2} \vec{z}^T(t_o) \ T^* S_\infty T \vec{z}(t_o) \ ,$$

$$= \frac{1}{2} \vec{z}^T(t_o) \ P \tag{3.26}$$

Define

$$P_1 \triangleq T^* \ S_\infty T \ . \tag{3.27}$$

With

$$S_\infty = \begin{bmatrix} s_{11} & s_{12} \\ \bar{s}_{12} & s_{22} \end{bmatrix} , \tag{3.28}$$

(where $\bar{s}_{12}$ is the complex conjugate of s_{12}) P_1 becomes

$$P_1 = \begin{bmatrix} s_{11} & js_{11} & s_{12} & js_{12} \\ -js_{11} & s_{11} & -js_{12} & s_{12} \\ \bar{s}_{12} & j\bar{s}_{12} & s_{22} & js_{22} \\ -j\bar{s}_{12} & \bar{s}_{12} & -js_{22} & s_{22} \end{bmatrix} . \tag{3.29}$$

Because the cost J_f is a quadratic form, (3.26) becomes

$$J_f = \frac{1}{2} \vec{z}_o^T P_\infty \vec{z}_o = \frac{1}{2} \vec{z}_o^T \ P_1 \vec{z}_o = \frac{1}{4} \vec{z}_o^T \ (P_1 + P_1^T) \vec{z}_o \ ,$$

so

$$P_\infty = \frac{1}{2}\,(P_1 + P_1^T)\ ,$$

$$= \begin{bmatrix} s_{11} & 0 & \mathrm{Re}(s_{12}) & -\mathrm{Im}(s_{12}) \\ 0 & s_{11} & \mathrm{Im}(s_{12}) & \mathrm{Re}(s_{12}) \\ \mathrm{Re}(s_{12}) & \mathrm{Im}(s_{12}) & s_{22} & 0 \\ -\mathrm{Im}(s_{12}) & \mathrm{Re}(s_{12}) & 0 & s_{22} \end{bmatrix} . \qquad (3.30)$$

which has the required real symmetric form. Instead of solving for ten unknowns by integrating the ten equations of (3.14), only four unknowns exist. The equations of (3.14) can be manipulated, so algebraic solutions of these four unknowns are obvious. Because of the control law (3.15), the variable s_{22} can be eliminated from consideration. Define

$$K_v \triangleq s_{11}$$

$$K_{p1} + jK_{p2} \triangleq s_{12}$$

Using the system and distribution matrices F and G defined by Eqs. (3.19)-(3.21), Eq. (3.22) can be formulated. For optimizing the performance index

$$J_f = \frac{1}{2}\int_{-\infty}^{t_f} \left(\left[\dot{x}_1^2 + \dot{x}_2^2\right]q_1 + \left[x_1^2 + x_2^2\right]q_2 + \left[u_1^2 + u_2^2\right]\right) dt\ , \qquad (3.31)$$

the matrices Q_2 and R_2 become

$$Q_2 = \begin{bmatrix} q_1 & 0 \\ 0 & q_2 \end{bmatrix}$$

$$R_2 = [1]\ .$$

Employing (3.22) and setting $\dot{S} = 0$ results in the equations

$$2(K_{p1} - a_1 K_v) - K_v^2 + q_1 = 0 ,$$

$$- a_o K_v - a_1 K_{p1} - b_1 K_{p2} + s_{22} - K_v K_{p1} = 0$$

$$- b_o K_v + b_1 K_{p1} - a_1 K_{p2} - K_v K_{p2} = 0 ,$$

$$- 2(a_o K_{p1} + b_o K_{p2}) - K_{p1}^2 - K_{p2}^2 + q_2 = 0$$

Algebraic manipulations of these equations result in

$$2K_{p1}^3 + (b_1^2 + a_1^2 + 4a_o + q_1)K_{p1}^2$$

$$+ 2(a_1 b_1 b_o + a_1^2 a_o - b_o^2 - q_2 + a_o q_1)K_{p1}$$

$$- a_1^2 q_2 + b_o^2 q_1 + q_1 q_2) = 0 , \qquad (3.32)$$

$$K_v = -a_1 + \sqrt{a_1^2 + q_1 + 2K_{p1}} , \qquad (3.33)$$

$$K_{p2} = -b_o - \sqrt{b_o^2 + q_2 - K_{p1}^2 - 2a_o K_{p1}} . \qquad (3.34)$$

The cubic Eq. (3.32) has a closed form solution of which the correct root is chosen on the basis that all elements of S_∞ are real. With K_{p1} known, Eqs. (3.33), (3.34) can be solved for K_v and K_p and the optimal control law will be

$$u_1 = -K_v \dot{x}_1 - K_{p1} x_1 - K_{p2} x_2 , \qquad (3.35a)$$

$$u_2 = -K_v \dot{x}_2 + K_{p2} x_1 - K_{p1} x_2 . \qquad (3.35b)$$

Control of the Spining Satellite

As an immediate application of the foregoing method, consider Eqs. (3.2) which are the equations of motion of a symmetric spinning satellite

$$\begin{bmatrix} \ddot{\varphi} \\ \ddot{\theta} \\ \dot{\varphi} \\ \dot{\theta} \end{bmatrix} = \begin{bmatrix} -d_p & -D+n & -Dn & d_p n \\ D-n & -d_p & -d_p n & -Dn \\ 1 & 0 & 0 & 0 \\ 0 & 1 & 0 & 0 \end{bmatrix} \begin{bmatrix} \dot{\varphi} \\ \dot{\theta} \\ \varphi \\ \theta \end{bmatrix} + \begin{bmatrix} 1 & 0 \\ 0 & 1 \\ 0 & 0 \\ 0 & 0 \end{bmatrix} \begin{bmatrix} u_x \\ u_y \end{bmatrix} , \tag{3.36}$$

where constant n is substituted for $\dot{\sigma}$. Comparing (3.36) with (3.18) the following analogies are apparent:

$$a_0 = Dn$$

$$b_0 = d_p n$$

$$a_1 = d_p$$

$$b_1 = -D+n$$

Thus, Eq. (3.32) becomes

$$2K_{p1}^3 + (D^2 + 2Dn + n^2 + d_p^2 + q_1)K_{p1}^2 + 2(Dnq_1 - q_2)K_{p1}$$

$$- (d_p^2 q_2 + d_p^2 n^2 q_1 + q_1 q_2) = 0 , \tag{3.37}$$

and (3.33) and (3.34) are

$$K_v = -d_p + \sqrt{d_p^2 + q_1 + 2K_{p1}} , \tag{3.38}$$

$$K_{p2} = -d_p n - \sqrt{(d_p n)^2 + q_2 - K_{p1}^2 - 2DnK_{p1}} . \tag{3.39}$$

Solutions to (3.37) - (3.39) as utilized in Eqs. (3.35a-b) represent the optimum power control law from the standpoint of minimizing the index (3.31).

As an example of this method, solutions to (3.37) - (3.39) were found for a spacecraft with the product of the moment-of-inertia ratio and spin rate $D = 1.5$. Values of the damping coefficient d_p ranged from 10^{-4} to 10^{-1} sec^{-1}. The mean orbital rate n was set to values of 1.09×10^{-3} sec^{-1} and 2.18×10^{-4} sec^{-1}. The results are delineated in Figure 3.7. Here the parameter q_1 was set to zero and q_2 was given the five values shown. The differences in the optimal gains due to variation of the mean orbital rate n were undistinguishable.

Using this algebraic solution to obtain all the data required to produce Figure 3.7 required about 2 percent of the computer time required to find solutions to the matrix Riccati equation by numerical integration for one set of values of the parameters d_p and q_1. The cubic equation (3.27) was easily solved by synthetic division.

The choice of which particular set of gains to use from Figure 3.7 depends upon the designer's choice of the nutation damper. To obtain the response desired involves the choice of the damping coefficient d_p and the parameter q_2. As can be seen from Figure 3.7, the position gain K_{p1} is relatively small compared to K_{p2}. Also, the increase of the mechanical damping term d_p does not cause K_v to markedly decrease.

The control gains obtained above are based on state variables $(\dot{\varphi}, \dot{\theta}, \varphi, \theta)$. Replacing $(\dot{\varphi}, \dot{\theta})$ by (α_x, α_y), the control law (3.35) becomes

$$u_x = -K_v \alpha_x - K_{p1} - (K_{p2} - nK_v)\theta \ , \tag{3.40a}$$

$$u_y = -K_v \alpha_y + (K_{p2} - nK_v)\varphi - K_{p1} \theta \ . \tag{3.40b}$$

It is essential to realize that mechanization of this optimum control assumes the presence of a filter for estimating values of the system state. The combined system is optimal by the certainty equivalence principle.

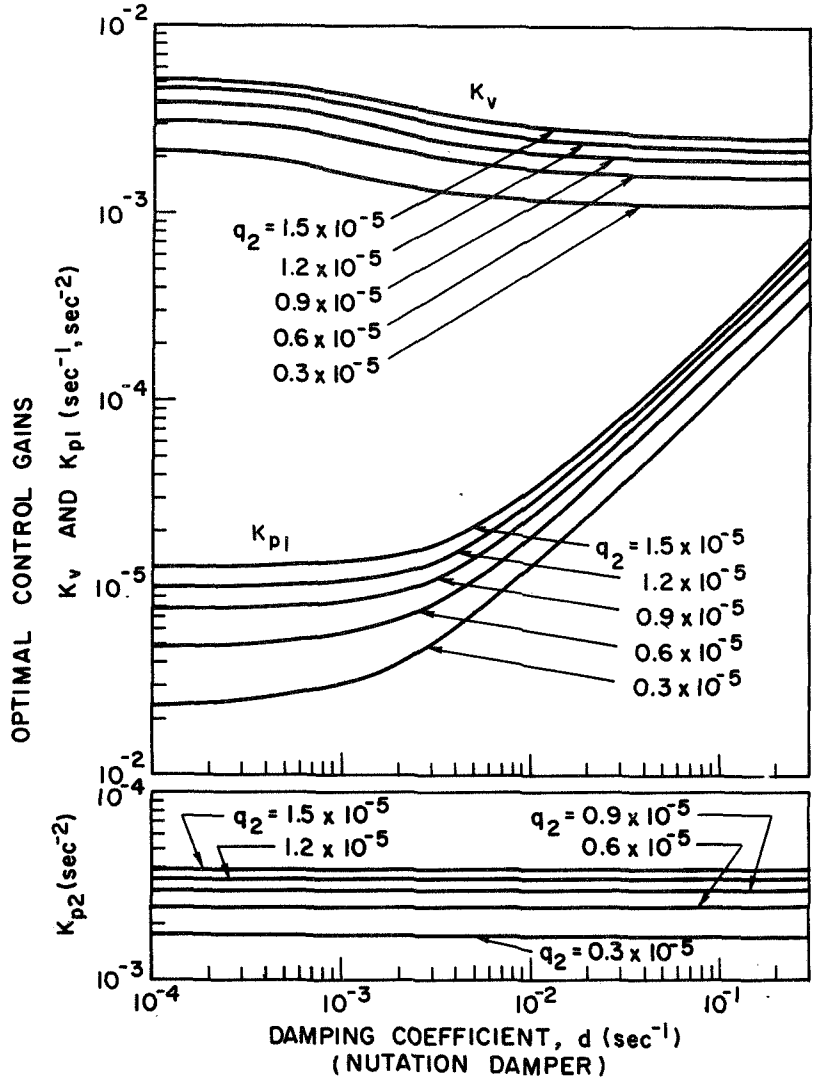

FIG. 3.7. OPTIMUM GAINS OF THE CONTROL LAW (3.40) FOR POWER MINIMIZATION OF A MAGNETICALLY CONTROLLED SPINNING SATELLITE AS A FUNCTION OF DAMPING. The parameter q_2 is chosen to achieve the desired response.

In the following development, Eqs. (3.40) are not mechanized exactly. However, these equations do serve as a basis for choosing control gains which optimize a magnetic control system's power requirements as averaged over an orbital period.

MAGNETIC IMPLEMENTATION OF THE CONTROL LAW

So far, the discussion has been mainly concerned with the continuous application of an optimum control law based upon a quadratic performance index and upon input from a Kalman filter. This controller could be mechanized by any continuous method and provides only the pointing control signal required by the attitude control system. It is now necessary to consider how this control will be implemented magnetically, and to be cognizant of the spin control requirement.

Magnetic torquing is made possible by applying a voltage to a coil of wire fixed in the spacecraft. The current in the wire causes a Lorentz force to exist between each element of moving charge and the local magnetic field of the earth $\vec{B}$. (This phenomenon is discussed in Ref. 46). The effect of the total force results in a torque $\vec{T}$ being applied upon the spacecraft which can be expressed as

$$\vec{T} = \vec{m} \times \vec{B} \, . \tag{3.41}$$

Here, $\vec{m}$ is the generated magnetic dipole moment of the vehicle-fixed coil; it is directed normal to the plane of the coil and obeys the right-hand rule with respect to current flow direction. The magnitude of $\vec{m}$ is

$$|\vec{m}| = NA_c \, i_c \, , \tag{3.42}$$

where N is the number of turns of wire in the coil, A_c is the planar area of the coil, and i_c is the coil current. By having three orthogonal coils on the satellite, the magnetic moment $\vec{m}$ may be directed in any orientation (except that, of course, no resulting torque can be produced parallel to $\vec{B}$).

In the previous section on minimum-power optimal control, two idealized expressions [Eqs. (3.40)] were derived for applying control torque components about the vehicle yaw $(\hat{x}_p)$ and roll $(\hat{y}_p)$ axes. For full attitude control, the capability of applying another torque component about the spin axis $(\hat{z}_B)$ also needs to be implemented. However, for this study, the active control applied is restricted to be magnetic. Thus, a means must be provided for using Eq. (3.41) to achieve the full torque $\vec{T}$ required (at least in an average sense). But, it is only a rare occasion during any orbit when the local value $\vec{B}$ of the magnetic field is so oriented that a magnetic moment $\vec{m}$ can be generated which will produce all three components of the required $\vec{T}$.

It is usually not necessary to maintain the exact control on the spin speed as that required for pointing the spin axis of the satellite. The spin-speed tolerance must be maintained only to the extent that the mechanized pointing control (based upon nominal spin speed) works correctly. Therefore, in this section, concentration is first directed toward achieving magnetic pointing control, and the spin component of the desired control is ignored. It is assumed that the spin speed is nearly at its nominal value.

A pointing control scheme is defined which uses only two orthogonal coils with axes perpendicular to the spin axis. This scheme is referred to as Mode 1 control. During this mode of control, a spin component of magnetic torque exists which may not be in the desired direction.

It is necessary to have the ability to apply control which maintains the spin speed within some tolerance, so logic is developed for using another mode (Mode 2) of magnetic control which removes the spin-speed error. This mode simply reverts back to Mode 1 control if Mode 1's spin component of torque is correctly directed. If the Mode 1 direction is incorrect, pointing control is supplied by the Z-axis coil which does not produce a spin component of torque.

A third mode of control (Mode 3) is provided to correctly initialize the spin speed and to serve as a backup in case spin speed continues to deviate beyond some bounding tolerance. The mechanization logic for combining these modes is specified.

Finally, in this section, it is shown that the three coils required to mechanize the full three-mode control can be replaced by a single coil (with its axis skewed to the spin axis) and a nutation damper.

Pointing Control

Equations (3.40) express the optimum control torque required along the $\hat{x}_p$ and $\hat{y}_p$ axes of the body's nonspinning reference frame. These components are used to define the desired pointing control torque $\vec{T}_D$ which is

$$\vec{T}_D = T_{Dx}\hat{x}_p + T_{Dy}\hat{y}_p \ .$$

From (3.40) the resulting torque $\vec{T}$ due to an applied $\vec{m}$ must lie in a plane which is perpendicular to the field vector $\vec{B}$. For power efficiency, it is also desirable that the magnetic moment $\vec{m}$ lies in this plane. The vector geometry involved here is delineated in Figure 3.8. The direction of $\vec{m}$ is chosen such that the lateral component of $\vec{T}$ coincides with the desired $\vec{T}_D$. This is accomplished by solving the equations

$$\begin{aligned} T_{Dx} &= m_y B_z - m_z B_y \ , \\ T_{Dy} &= m_z B_x - m_x B_z \ , \\ \vec{m} \cdot \vec{B} &= 0 \ , \end{aligned} \tag{3.43}$$

for the components of $\vec{m}$. The solutions to (3.43) are

$$\begin{aligned} m_z &= (T_{Dy}B_x - T_{Dx}B_y)/B^2 \ , \\ m_x &= (m_z B_x - T_{Dy})/B_z \ , \\ m_y &= (m_z B_y + T_{Dx})/B_z \ . \end{aligned} \tag{3.44}$$

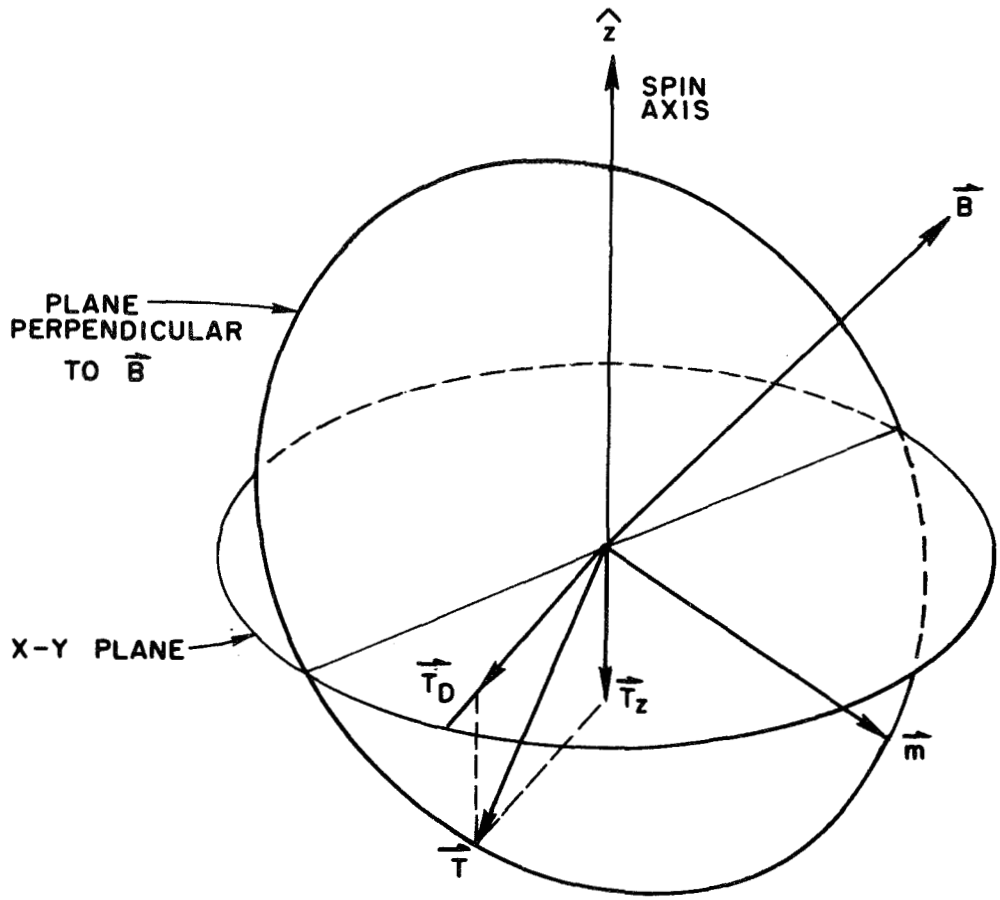

FIG. 3.8. VECTOR GEOMETRY OF MAGNETIC TORQUING WHERE $\vec{B}$ IS THE MAGNETIC FIELD, $\vec{m}$ IS THE GENERATED MAGNETIC MOMENT, AND $\vec{T}_D$ IS THE DESIRED TORQUE.

Equations (3.44) are fundamental to the mechanization of magnetic attitude control and have been used in many versions since appearing in Ref. 2 (White, et. al.)

Mechanization of Eqs. (3.44) will result in a torque which has a component along the spin axis, which is apparent from Figure 3.8. This spin component's magnitude will be

$$T_z = m_x B_y - m_y B_x \quad . \tag{3.45}$$

Because of the random nature of the desired control torques and the change in direction of the magnetic field component in the satellite's lateral plane, the orbital average of (3.45) should be zero.

Notice that Eqs. (3.44) require the division of terms by B^2 and B_z. The magnetic field of the earth is roughly an earth-centered dipole (See Appendix A) and for conceptual purposes can be approximated as a simple dipole with axis antiparallel to the earth's spin axis in the time-average sense. (See Figure 3.9.) In this study, the orbit inclinations considered are between 20° and 70° and the satellite spin axis points toward the northern side of the orbit plane. As a consequence, the satellite's spin-axis component B_z of the magnetic field will always be positive. Thus, there is no problem of sign reversal and the divisor going to zero in (3.44).

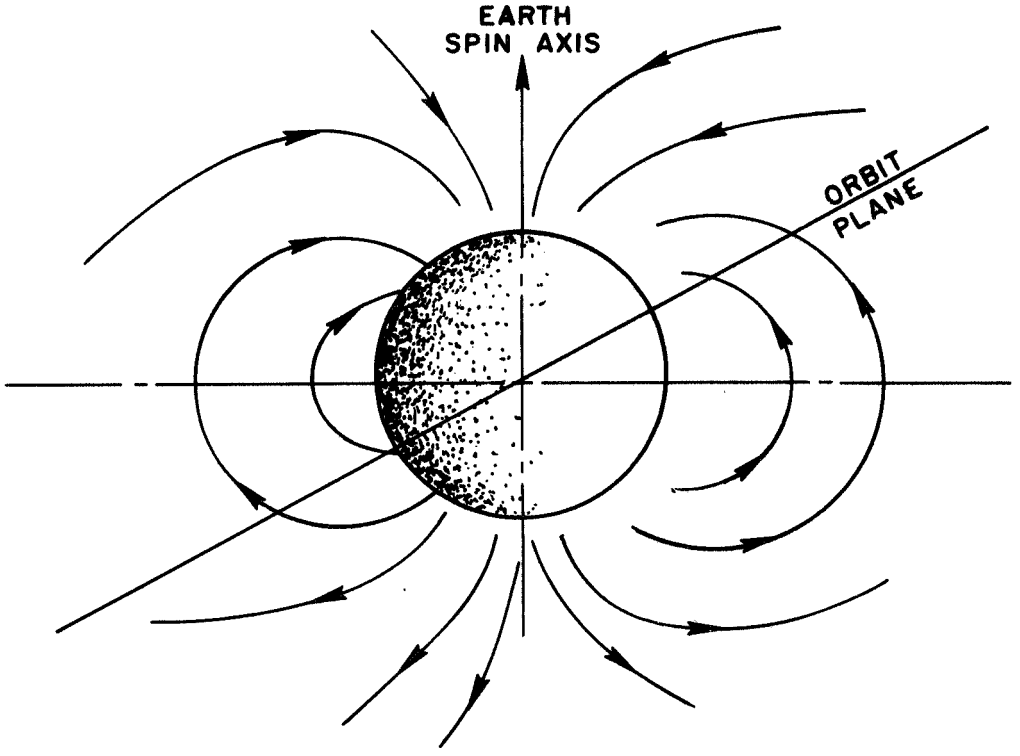

FIG. 3.9. ORBIT PASSAGE THROUGH THE EARTH MAGNETIC DIPOLE FIELD.

On the other hand, the actual division process required by Eqs. (3.44) is not in itself desirable. Figure 3.10 indicates the variation of the reference axis (R) components of $\vec{B}$ over three orbits of typical

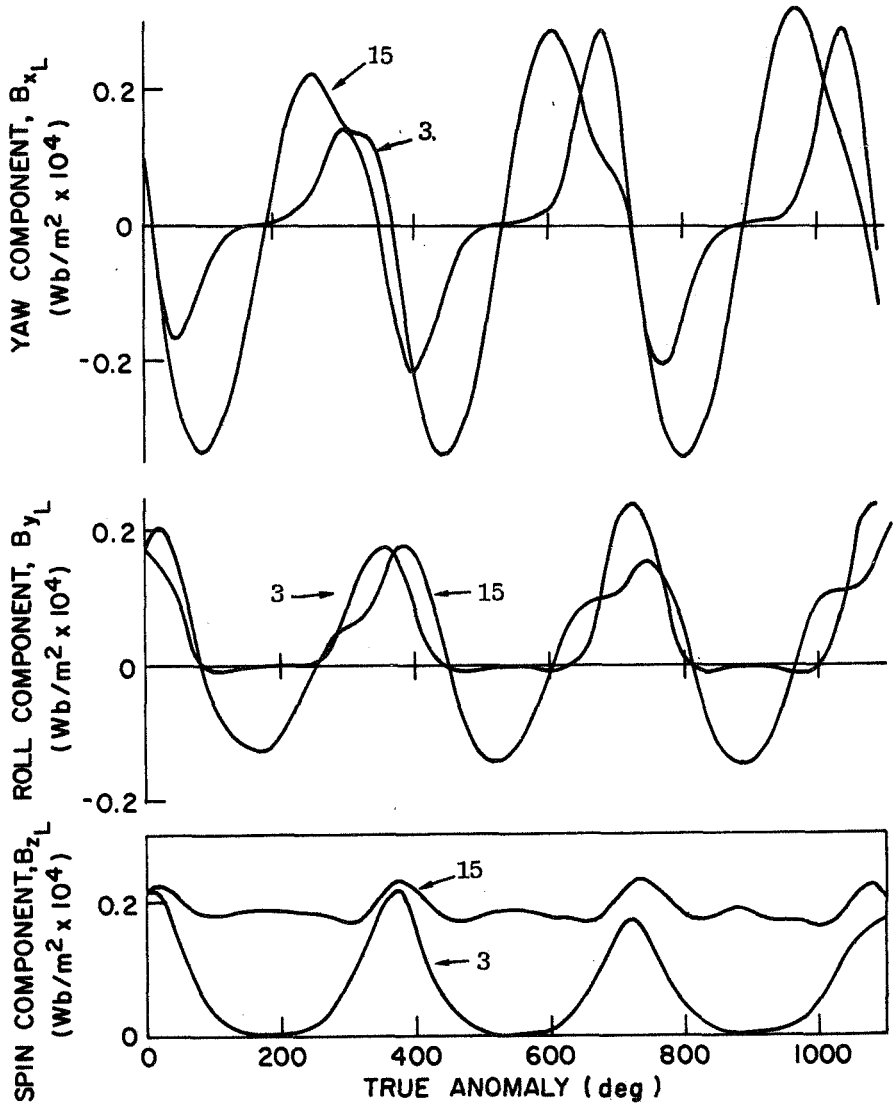

FIG. 3.10. EARTH'S MAGNETIC FIELD COMPONENT VARIATION FOR 3 REVS/DAY AND 15 REVS/DAY ORBITS INCLINED AT 45° WITH 300 km ALTITUDE OF PERIGEE.

resonant satellites. The magntidue of B_z fluctuates over two orders of magnitude for the 3 revs/day orbit.

One method previously employed (See Refs. 13 and 14) to simplify Eqs. (3.44) (which generate the magnetic moment) for satellites in circular orbits has been to use just a single spin-axis coil. Over the circular orbit, $|\vec{B}|$ varies by about, at most, a factor of two; so $(1/B^2)$ was replaced by a constant K_{0B}, which resulted in adequate control torque.

The magnetic signal for this single-coil controller is

$$m_z = K_{0B}(B_x T_{Dy} - B_y T_{Dx}) \tag{3.45}$$

from the first of Eqs. (3.44). Equation (3.45) also results from crossing $\vec{B}$ into $\vec{T}_D$ which is a permutation of (3.41). This equation represents the most common mechanization of magnetic attitude control of spinning spacecraft studied and applied to date.

Use is made of Eq. (3.45) later, as a part of the overall attitude control mechanization. The effect of using the constant K_{0B} over a highly eccentric orbit is also explored.

The advantage of using (3.45) for the control law mechanization is that no unwanted spin component to the torque exists, and spin modulation of the applied voltages is not required. The chief disadvantages are that such a control mechanization offers no means of controlling spin speed and that the actual resultant torque is not in the direction of $\vec{T}_D$ specified by (3.40). Because the goal of this research is to find a system which provides both precision control and spin-speed correction, use of a single spin-axis coil alone is not satisfactory.

The Z coil used the lateral component (normal to the spin axis) of magnetic field to produce torque. This component is seldom aligned in the proper direction to produce a torque parallel to the desired $\vec{T}_D$. For precision control, the alternative is to use two orthogonal coils (X and Y coils) with dipole axes in the lateral plane. This allows producing two magnetic moments which react with the spin component of the magnetic field (B_z) such that the pointing torque is parallel to $\vec{T}_D$. This is the primary mode of spin-axis orientation considered in this chapter. The ideal magnetic moments along the $\hat{x}_L$ and $\hat{y}_L$ axis for such control are found by setting m_z to zero in Eqs. (3.44).

The ideal control required to produce $\vec{T}_D$ still necessitates dividing by B_z. For mechanization simplicity, it is assumed that this division process can be eliminated by replacing $(1/B_z)$ by the constant K_{Bz} which is the orbital average value. (An approximation to this average value can be obtained from Figure A.2 in Appendix A). The resulting torque components found from Eqs. (3.44) and (3.41) are

$$T_x = K_{Bz} B_z T_{Dx} , \tag{3.46a}$$

$$T_y = K_{Bz} B_z T_{Dy} , \tag{3.46b}$$

$$T_z = -K_{Bz}(B_y T_{Dy} + B_x T_{Dx}) . \tag{3.46c}$$

Again, under such a scheme, the spin-torque component T_z should average to zero over several orbits if no disturbance torques are present.

Replacing the factor $(1/B_z)$ by the constant K_{Bz} raises two questions. First of all, the actual pointing control torque components under such a scheme are directly proportional but seldom equal to the desired components because they have the time-varying factor B_z in them. As is seen, this applied torque is no longer always optimal (in the minimum-power sense). Thus, there is no longer a reason to conclude that the control system is always stable.

The second question is whether control torque of such time-varying magnitude can drive the attitude error to zero and maintain it there in the presence of disturbances. These two questions are investigated after the overall magnetic mechanization of the control system is completely defined.

The magnetic moments required for implementing (3.46) are

$$m_x = -K_{Bz} T_{Dy} ,$$

$$m_y = K_{Bz} T_{Dx} ,$$

$$m_z = 0 , \tag{3.47}$$

where T_{Dx} and T_{Dy} are specified along the nonspinning reference axes. Because of vehicle spin, the actual voltages applied to the orthogonal X and Y coils must be proportional to

$$m'_x = m_x \cos \dot{\psi} t + m_y \sin \dot{\psi} t ,$$

$$m'_y = -m_x \sin \dot{\psi} t + m_y \cos \dot{\psi} t , \tag{3.48}$$

where m_x and m_y are as given in (3.47). Equations (3.47) to (3.48) represent Mode 1 (primary) control.

No measurements of the magnetic field are necessary to actuate the controller as is seen from equations (3.47) because only those orbits are considered which always have a positive value of B_z. However, it is necessary to have a Z-axis sensitive magnetometer for such a system in order that correct control estimates be put into the Kalman filter.

The primary mode of magnetic spin-axis orientation defined by Eqs. (3.47) seems to provide better pointing accuracy than many other all-magnetic control systems studied previously. This point is discussed later in the section on system performance. In addition, the X-Y coil system provides a means for spin control which is now developed.

Spin Control

If the spin speed deviates away from the nominal value, this will be detected by variations in the periodic signal coming from the horizon sensors. The desired control torque to correct such a deviation $\Delta\dot{\psi}$ might be either

$$T_{Dz} = -K_z \Delta\dot{\psi} \tag{3.49a}$$

or

$$T_{Dz} = -K_z \operatorname{sgn}(\Delta\dot{\psi}) , \tag{3.49b}$$

when $|\Delta\dot{\psi}|$ exceeds some deadband value. There are two ways in which a similar spin control can be actuated.

The first type of spin control occurs due to the pointing control Eqs. (3.46). One can see from (3.46c) that a spin torque will usually exist from application of this primary pointing control. Thus, one can incorporate logic into the control system such that pointing control by Eqs. (3.46) is actuated only when the resulting spin torque is in the desired direction. This is done here when the spin-speed deviation $|\Delta\dot{\psi}|$ exceeds some threshold; this mechanization is considered as the primary means of spin control and is labeled Mode 2.

The other way that spin control can be enacted is by applying voltage to the X and Y coils in such a way that the resulting magnetic moment is normal to the component of the magnetic field in the X-Y plane. That is

$$m_x = K_z B_y \operatorname{sgn} \Delta\dot{\psi} , \tag{3.50a}$$

$$m_y = -K_z B_x \operatorname{sgn} \Delta\dot{\psi} . \tag{3.50b}$$

Applying (3.50a-b) will result in a pointing disturbance. It is therefore desirable to use the second method of spin control only in the event that spin-speed deviation approaches the point where serious degradation to pointing control will occur. Use of this spin control is implemented by logic known as Mode 3.

Partial pointing control can be maintained during spin-speed control by use of a spin-axis coil and the control law (3.45). A philosophy is taken in which the X and Y coils are used for position control during normal operations, (i.e. portions of the orbits where the spin speed is adequately close to the nominal value.) During those periods when the X and Y coils cannot be used for pointing control, the Z coil is used for partial control.

During operation of the Z coil for pointing control and during an X-Y spin control phase, the system must measure both the yaw and roll components (B_x and B_y) of the magnetic field. Measurements can be taken by a magnetometer with a single sensitive axis lying in the plane of the Z coil (perpendicular to both coil and spin axes). The magnetometer output needs to be sampled and held twice per spin revolution for obtaining both B_x and B_y. During spin control using (3.50a-b) or (3.46c), the magnetic moment which is aligned with the sensitive magnetometer axis needs to be zeroed during sampling periods to prevent interference from the generated magnetic moment.

Because application of spin control by (3.50a-b) results in pointing deviation, it is necessary to investigate how this deviation can be minimized. For control efficiency, it is desirable that this control action

be centered around the perigee position of the orbit where the average lateral magnetic-field component will be largest.

The magnetic-field vector $\vec{B}$ can be thought of as roughly describing a cone around the $\hat{x}_L$ axis of the local frame once per orbit. Thus, if the magnetic moment $\vec{m}$ is constrained to be 90° out of phase with lateral component of $\vec{B}$ for spin control, the resulting lateral torques due to the presence of B_z will be of the form

$$T_x = T \cos(nt + \alpha_p),$$

$$T_y = T \sin(nt + \alpha_p), \tag{3.51}$$

Here,

$$T = \sqrt{m_x^2 + m_y^2}\, B_z .$$

For no further control-induced disturbance torques or damping, and for the phase angle α_p equal to zero and T a constant, the resulting values of roll and yaw error are found by solving Eqs. (3.2) with (3.51) substituted for T_x and T_y. This results in the yaw and roll angles

$$\varphi = \frac{T}{D^2 - n^2} [\cos nt - \cos Dt] ,$$

$$\theta = \frac{DT}{D^2 - n^2} \left[\frac{\sin nt}{n} - \frac{\sin DT}{D}\right] . \tag{3.52}$$

Here, the fluctuation of θ is substantial because of the small divisor n. Therefore, to minimize the general pointing deviations (in the average sense), the applied spin control torque should be applied over a 180° segment of the orbit centered about the perigee point. The point in the orbit where this control is enacted can be based upon the value of orbital rate $\dot{\sigma}$ obtained from the horizon sensors.

Combined Control with System Logic

It is now necessary to formulate a means of combining the previously developed pointing and spin control laws into a single controller that can be mechanized with appropriate logic. This can be done by defining two constants C_{d1} and C_{d2} which represent boundaries of deadbands associated with the spin speed $\dot{\psi}$. Let C_{d1} be the value of spin speed deviation $|\Delta\dot{\psi}|$ beyond one should provide some sort of spin control. Let C_{d2} be the value of $|\Delta\dot{\psi}|$, beyond which it is mandatory that spin control action be taken. Let C_p be the value of orbital rate $\dot{\sigma}$ which indicates the spacecraft is within 90° of the perigee point. Then, suitable logic governing the voltages applied to three orthogonal coils would be:

Mode 1 $(-C_{d1} \leq \Delta\dot{\psi} \leq Cd_1)$:

$$m_x = -K_{Bz}\, T_{Dy} ,$$

$$m_y = K_{Bz}\, T_{Dx}$$

$$m_z = 0 . \qquad (3.47)$$

Mode 2 $(C_{d1} < |\Delta\dot{\psi}| \leq C_{d2})$:

a. If $\text{sgn}(T_z) \equiv \text{sgn}\,(B_x T_{Dy} - B_y T_{Dx}) = -\text{sgn}(\Delta\dot{\psi})$,

use Mode 1.

b. If $\text{sgn}(T_z) = \text{sgn}(\Delta\dot{\psi})$,

$$m_x = 0 ,$$

$$m_y = 0 ,$$

$$m_z = K_{OB}(B_x T_{Dy} - B_y T_{Dx}) . \qquad (3.45)$$

Mode 3 ($|\Delta\dot{\psi}| > C_{d2}$):

a. If $\dot{\sigma} < C_p$, use Mode 2.

b. If $\dot{\sigma} \geq C_p$,

$$m_x = K_z B_y \operatorname{sgn}(\Delta\dot{\psi}) ,$$

$$m_y = -K_z B_x \operatorname{sgn}(\Delta\dot{\psi}) , \tag{3.50}$$

$$m_z = K_{OB}(B_x T_{Dy} - B_y T_{Dx}) . \tag{3.45}$$

Once Mode 3b is entered, the control is constrained to remain in this mode until the point where $\dot{\sigma} = C_p$ is again reached. The constant K_z is chosen so that application of Mode 3b drives the spin speed well within the Mode 2 range. Large angle error buildup is prevented by simultaneous use of the Z coil.

If the gains are set properly and care is exercised during design and construction of the satellites, Mode 3 will not be required during normal operation. However, it should be mechanized for use during initial spin-up or for the case where spin speed changes but no pointing error accumulates.

Measurement of the three magnetic field components during Mode 3 can be made with a three-axes fluxgate magnetometer described in Ref. 47. The magnetometer's sensitive axes must be mounted so that no interference is created from the magnetic field produced by the control coil. When the magnetic components m_x and m_y are both being generated, this interference can best be prevented by a time-sharing procedure. Here, the coil currents are cut off momentarily once or twice each cycle of space craft spin. At this time the magnetic field measurements are sampled and held during the controlled portion of the cycle. Care in vehicle design must be taken to insure that errors due to ferromagnetic materials on the vehicle are acceptably small.

A New Method of Magnetic Control Application - the Skewed Coil

It is possible to simplify to a great extent the mechanization of the control system suggested in the previous section. This can be done by replacing the three coils with a single coil skewed at 45° (for example) to the spin axis as shown in Figure 3.11a. A further simplification is

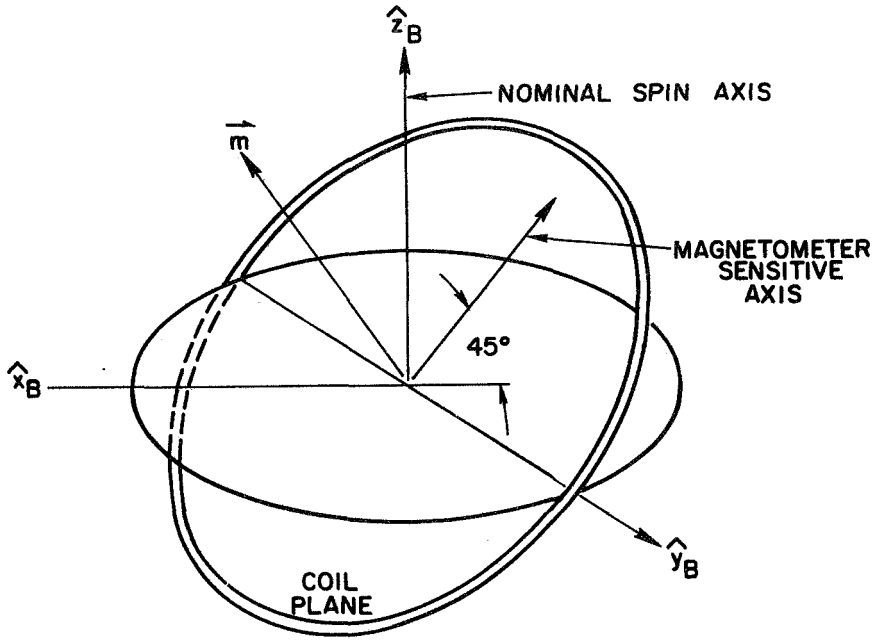

FIG. 3.11a. GEOMETRY OF SKEWED COIL IN A SPINNING SPACECRAFT. The magnetometer sensitive axis lies in the plane of the coil.

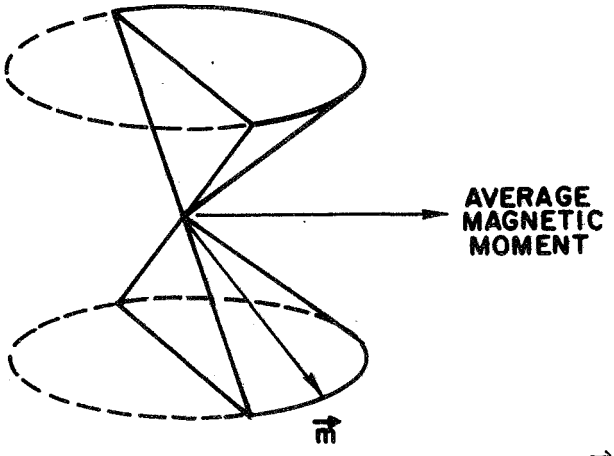

FIG. 3.11b. PATH OF MAGNETIC MOMENT VECTOR $\vec{m}$ FOR ROTATING SKEWED COIL WITH CURRENT DIRECTION SWITCHED EVERY 180°.

to use only one magnetometer with its sensitive axis in the plane of the coil as indicated. For such a system, if the coil current magnitude and direction are constant, an average magnetic dipole moment is generated along the spin axis. If a constant current has its direction reversed every 180°, the average magnetic moment is in the X-Y plane pointing in the direction 90° from the switch points, as is delineated in Figure 3.11b. Thus, one has the ability to generate all three components of the desired magnetic dipole $\vec{m}$ averaged over a spin cycle of the satellite.

For minimum power in the skewed coil during Mode 1 control, it is necessary to apply a voltage signal which is not a full square wave, but a pulse train. The total current in the coil for generating the dipoles m_x and m_y is the sum of two pulse trains shown in Figure 3.12. The value of current i_x in the coil to produce a magnetic moment m_x along the yaw axis is

$$i_x = m_x \pi / [\, 2\, NA_c \cos(\epsilon_o \dot{\psi})]$$

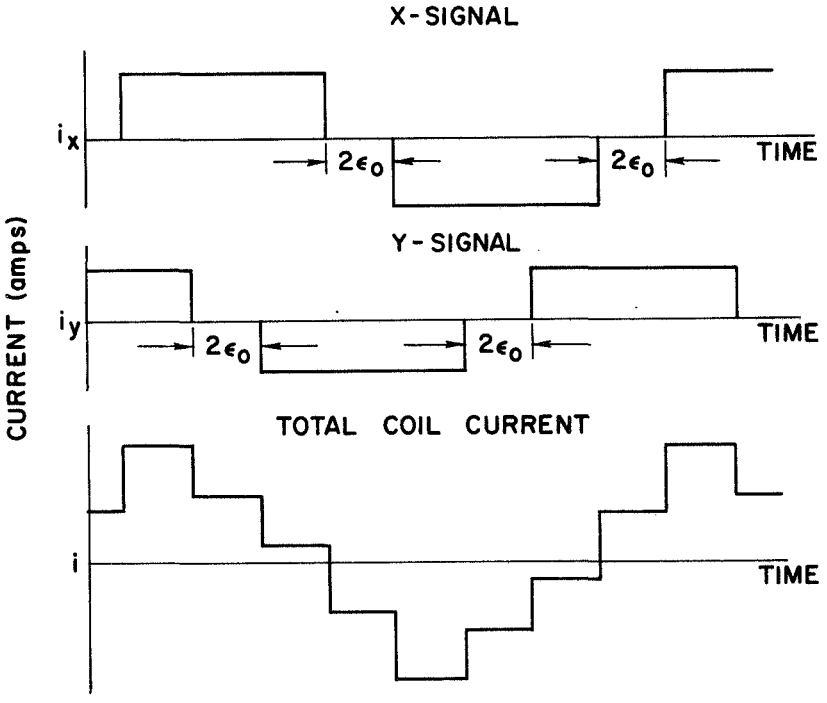

FIG. 3.12. TOTAL SKEWED-COIL CURRENT TO ACHIEVE AN AVERAGE m_x AND AN AVERAGE m_y DURING SPIN.

for the coil skewed at 45°. Here the angle $\epsilon_o\dot{\psi}$ corresponds to the product of one-half the off period of the pulse train and the spin rate. Other skew-angles can, of course, be used depending upon the amount of use which is made of the Z-component capability. To minimize i_x^2 requires that

$$\epsilon_o\dot{\psi} = \tan^{-1}[1/(\pi - 2\epsilon_o\dot{\psi})]$$

which has a solution of $\epsilon_o\dot{\psi} \cong 23°$. It can be shown that minimization of the total power of the applied voltage indicated in Fig. 3.12 again requires minimization of $i_x^2 + i_y^2$, where i_x and i_y are the two currents passed through the same coil. Thus, the previous analysis of the minimum-power optimal controller for the orthogonal coils is also valid for the skewed coil.

It is illustrative to compare the power requirements of three orthogonal coils and one skewed coil. Assume that the total weights of the coil systems are the same, that the areas (A_c) of each are equal, and that each coil of the three-coil system has one-third the number of turns N and electrical resistance (r_c) as that of the skewed coil. Then the power P_w required by the two lateral coils to generate a constant lateral moment m is

$$P_w = 6\, m^2 r_c/(NA_c)^2 \text{ Watts.}$$

The power required by the skewed coil averaged over a spin period is

$$P_w = \frac{(\pi - 2\epsilon_o\dot{\psi})\pi}{2\cos^2(\epsilon_o\dot{\psi})} \cdot \frac{m^2 r_c}{(NA_c)^2} \text{ Watts.}$$

For $\epsilon_o\dot{\psi}$ of 23°, this last expression is about

$$P_w \cong 6.9\, m^2 r_c/(NA_c)^2 \text{ Watts.}$$

Hence, the skewed coil requires about 15 percent more power when in Mode 1 operation.

On the other hand, if the moment is desired along the $\hat{z}_B$ axis, the skewed coil's power is

$$p_w = 2m^2 r_c / (NA_c)^2 \text{ Watts.}$$

The power consumed by the smaller Z coil is

$$p_w = 3m^2 r_c / (NA_c)^2 \text{ Watts,}$$

or 50 percent greater for Mode 2.b operation.

A disadvantage of the skewed-coil arrangement is that it tends to generate the required magnetic components in the X and Y directions *averaged over one spin cycle*. *It has poor ability to generate control* torques which fluctuate faster than spin rate such as the wobble-damping terms. Therefore, the skewed-coil probably requires a mechanical nutation damper. (Typically, magnetic controllers are so supplemented anyway.) However, the packaging advantages of a single coil and single-axis magnetometer seem to make this a system worthy of consideration.

CONTROL SYSTEM STABILITY

In the previous two sections, a control system has been described which removes the spinning satellite's error state, with the resulting applied torque being optimal (minimum power usage) in a time average sense. It remains to determine what conditions guarantee that this control system will be asymptotically stable for all time over the entire magnetic field environment of the orbit.

It is known from the theory of optimal control that if the gains are chosen so that the applied torque is always optimal, the resulting system is asymptotically stable. However, for the simplified magnetic implementation considered here, the applied torques vary directly with the magnitude of the magnetic field. This magnitude varies by more than two orders of magnitude for the highly eccentric orbits considered in this thesis. (Refer again to Figure 3.10.) Thus, one cannot conclude stability over the entire orbit.

Three control torque configurations require consideration here. One might classify these as satellites with pure active damping (i.e., no mechanical damper), pure passive damping, or a combination of damping methods. The pure passive damping case includes the skewed-coil controller where the applied magnetic torque is for angular position control only.

There are also two methods of applying pointing control which have been developed in the previous section. These methods include using the X and Y magnetic moments as in Mode 1 control, and using the Z magnetic moment as in Modes 2b and 3b. If stability can be established for each of these control modes individually, then stability of the entire system can be concluded.

The following section provides the analytical means for obtaining at least the necessary conditions required for system stability. The stability analysis methods of Lyapunov and Kryloff-Bogoliuboff are employed for this task. The two control modes are investigated individually.

X-Y Coil Control

The limits on the allowable gain variations in the mechanization of the X-Y control mode can be established by the use of the Lyapunov "second method". Before this theory is applied, however, some of its theorems are presented which are of direct use.

Lyapunov Stability

A scalar energy-like function $V_\ell(\vec{x},t)$ is a Lyapunov function if it satisfies the following conditions in an open region Ω_r about the origin:

1) $V_\ell(\vec{x},t)$ is defined in Ω_r for all $t \geq 0$;
2) $V_\ell(0,t) = 0$, for $t \geq 0$;
3) $V_\ell(\vec{x},t)$ dominates a certain positive definite $W_1(\vec{x})$; that is, $W_1(\vec{x}) \leq V_\ell(\vec{x},t)$ for all $\vec{x}$ in Ω_r and all $t \geq 0$;
4) $\dot{V}_\ell(\vec{x},t) \leq 0$ in Ω_r. For $\dot{\vec{x}} = F(\vec{x},t)$, $\dot{V}_\ell(\vec{x},t) = \partial V/\partial t + \text{grad } V \cdot F$.

The following theorems (Ref. 48) are associated with the Lyapunov function.

Theorem 3.1. If there exists in some neighborhood Ω_r of the origin a Lyapunov function $V(\vec{x},t)$, then the system is stable at the origin.

Theorem 3.2. If $\dot{V}_\ell(\vec{x},t) < 0$ in Ω_r for all $t \geq 0$, then the stability is asymptotic provided that $V_\ell(\vec{x},t) \leq W_2(\vec{x})$ where $W_2(\vec{x})$ is another positive definite function. If $W_1(\vec{x})$ approaches infinity as $|\vec{x}|$ approaches infinity, then the system is said to be asymptotically stable in the large (ASIL).

Theorem 3.3. If $V_\ell(\vec{x},t)$ with $V_\ell(0,t)$ have continuous first partials with respect to each element of $\vec{x}$ in Ω_r, $\dot{V}_\ell(\vec{x},t)$ is positive definite, and $V_\ell(\vec{x},t)$ is able to assume positive values arbitrarily near the origin, then the system is unstable at the origin.

This theory can be applied to linear systems as is stated in the following theorem (Ref. 49).

Theorem 3.4. The equilibrium state $\vec{x} = 0$ of a continuous-time, free, linear, stationary dynamic system $\dot{\vec{x}} = F\vec{x}$ is asymptotically stable and the eigenvalues of the matrix F are less than some constant μ_1, if, and only if, given any symmetric, positive-definite matrix Q_r, there exists a symmetric, positive-definite matrix M_r which is the unique solution of

$$(F^T - \mu_1 I)M_r + M_r(F - \mu_1 I) = -Q_r$$

and $\mu_1 \leq 0$. Moreover, $\vec{x}^T M_r \vec{x}$ is a Lyapunov function for this dynamic system.

This theorem has recently been extended by Moore and Anderson (Ref. 50) and used to generalize the "circle criterion" for establishing

the stability of linear systems with time-varying feedback elements. An adaptation of this new method (presented here for the first time) begins by stating the following theorem.

Theorem 3.5. Consider the system with state equations

$$\dot{\vec{x}} = F\vec{x} + G\vec{u} = (F - GK_g(t)H)\,\vec{x}\,,$$

$$\vec{y} = H\vec{x}\,, \tag{3.53}$$

where $\vec{\mu}$ is the input vector governed by the time-varying gain matrix $K_g(t)$ and is expressed as

$$\vec{u}(t) = -K_g(t)\,\vec{y}(t)\,.$$

The matrices (F,G,H) are constant.
The matrix $K_g(t) = \text{diag.}\,\{k_1(t), k_2(t), \ldots, k_p(t)\}$ satisfies the condition $K_1 \leq K_g(t) \leq K_2$ for all $t > 0$ where $K_1 = \text{diag}\,\{k_{11}, k_{12}, \ldots, k_{1p}\}$ and $K_2 = \text{diag}\,\{k_{21}, k_{22}, \ldots, k_{2p}\}$ are constant and $K_2 - K_1 > 0$, i.e. positive definite. Now, if a bounded, symmetric, positive definite matrix M_r can be found which satisfies the equations

$$M_r(F-\mu_1 I-GK_1H) + (F^T-\mu_1 I-H^TK_1G^T)M_r = -N_rN_r^T \tag{3.54a}$$

$$M_rG = H^T/2 - N_rP_r \tag{3.54b}$$

$$P_r^TP_r = (K_2 - K_1)^{-1} \tag{3.54c}$$

where $\mu_1 \leq 0$, then the system is stable in the large. If $\mu_1 < 0$, the system is asymptotically stable in the large.

Proof.

Consider the Lyapunov function

$$V_\ell(\vec{x}) = \vec{x}^T M_r \vec{x} \tag{3.55}$$

which is bounded and positive definite. Its time derivative is

$$\dot{V}_\ell = \dot{\vec{x}}^T M_r \vec{x} + \vec{x}^T M_r \dot{\vec{x}}$$

$$= \vec{x}^T (F^T - H^T K_g(t) G^T) M_r \vec{x} + \vec{x}^T M_r (F - G K_g(t) H) \vec{x}$$

From (3.54a),

$$\dot{V}_\ell = \vec{x}^T (-N_r N_r^T + 2\mu_1 M_r + M_r G K_1 H + H^T K_1 G^T M_r) \vec{x}$$

$$-\vec{x}^T (H^T K_g(t) G^T M_r + M_r G K_g(t) H) \vec{x} .$$

Substituting (3.54b),

$$\dot{V}_\ell = \vec{x}^T (-N_r N_r^T + 2\mu_1 M_r - H^T (K_g(t) - K_1)(H/2 - P_r^T N_r^T)$$

$$- (H^T/2 - N_r P_r)(K_g(t) - K_1) H) \vec{x} .$$

Completing the square, this becomes

$$\dot{V}_\ell = -\vec{x}^T (N_r^T - P_r (K_g(t) - K_1) H)^T (N_r^T - P_r (K_g(t) - K_1) H) \vec{x}$$

$$-\vec{x}^T H^T (K_g(t) - K_1) H \vec{x} + 2\mu_1 \vec{x}^T M_r \vec{x}$$

$$+ \vec{x}^T H^T (K_g(t) - K_1) P_r^T P_r (K_g(t) - K_1) H \vec{x} .$$

Substituting (3.54c) into the last term produces

$$\dot{V}_\ell = -\vec{x}^T (N_r^T - P_r (K_g(t) - K_1) H)^T (N_r^T - P_r (K_g(t) - K_1) H) \vec{x}$$

$$-\vec{x}^T H^T [K_2 - K_g(t)] (K_2 - K_1)^{-1} (K_g(t) - K_1) H \vec{x} + 2\mu_1 V_\ell .$$

This expression is always at least negative semidefinite for $\mu_1 \leq 0$. For $\mu_1 < 0$, it is always negative definite. Thus, the function $V(\vec{x})$ of (3.55) satisfies the requirements for a Lyapunov function and the solution

for a suitable M_r satisfying Eqs. (3.54) insures that the system is stable.∎

Corollary 3.6. Let it be given that a system is descibed by Eq. (3.54) and that Eq.(3.54) can be solved for a positive definite M_r with the constant $\mu_1 > 0$. Then the system is unstable by Theorem 3.3.∎

This powerful theorem provides a means by which the stability of a linear constant system with time varying gains may be investigated. The establishment of system stability requires the solution of Eqs. (3.54) for a bounded symmetric positive definite M_r. Equations (3.54) can be combined to yield

$$M_r(F-\mu_1 I-0.5G(K_2+K_1)H) + (F^T-\mu_1 I-0.5H^T(K_2+K_1)G^T)M_r + M_rG(K_2-K_1)G^TM_r + 0.25H^T(K_2-K_1)H = 0 \quad , \tag{3.56}$$

which is a matrix quadratic equation.

The use of Theorem 3.5 and the solution to Eq. (3.56) can be applied rigorously to determine stability of a system in which the matrices (F, G,H) are constant. However, if elements of the system matrix F are time varying, the system can still be correctly analyzed using the above theory under certain circumstances. These conditions are that the time-varying elements may be removed from the F matrix and be included in the $GK_g(t)H$ matrix; i.e., these dynamic elements can be treated as time-varying control gains adhering to the form given in Theorem 3.5. This is true in particular for time-varying elements in a system possessing complex symmetry. For the axisymmetric satellite in elliptic orbit studied here, this technique may be used to handle the time-varying orbital rate $\dot{\sigma}$ appearing in the F matrix.

Range of Time-Variable Gain for Mode 1 Stability

Consider the skewed-coil controller with passive damping. Here, the damping terms of Eq. (3.40) are lumped in with the nutation damper

so that the desired magnetic torques are

$$T_{Dx} = -K_{p1}\varphi - K_{p2}\theta \ ,$$

$$T_{Dy} = K_{p2}\varphi - K_{p1}\theta \ . \qquad (3.57)$$

From (3.46) the actual position control gains are

$$T_x = -K_{Bz}(K_{p1}\varphi + K_{p2}\theta)B_z(t) \ ,$$

$$= -k_1(t)(K_{p1}\varphi + K_{p2}\theta) \ , \qquad (3.58a)$$

$$T_y = -K_{Bz}(-K_{p2}\varphi + K_{p1}\theta)\ B_z(t) \ ,$$

$$= -k_1(t)(-K_{p2}\varphi + K_{p1}\theta) \ , \qquad (3.58b)$$

where $k_1(t) = K_{Bz}B_z(t)$. Let the orbital rate be defined as

$$\dot{\sigma} = n_1 + k_2(t)\ n_2 \ . \qquad (3.59)$$

If n_1 is the apogee value of $\dot{\sigma}$ and $(n_1 + n_2)$ is the perigee value, then $k_2(t)$ varies between 0 and 1 in value. Thus, the matrix, $(F-GK_g(t)H)$ may be written from Eq. (3.2) as (with $G = I$)

$$F-GK_g(t)H = \begin{bmatrix} -d_p & -D & 0 & 0 \\ D & -d_p & 0 & 0 \\ 1 & 0 & 0 & n_1 \\ 0 & 1 & -n_1 & 0 \end{bmatrix} - \begin{bmatrix} k_1(t) & 0 & 0 & 0 \\ 0 & k_1(t) & 0 & 0 \\ 0 & 0 & k_2(t) & 0 \\ 0 & 0 & 0 & k_2(t) \end{bmatrix} \begin{bmatrix} 0 & 0 & K_{p1} & K_{p2} \\ 0 & 0 & -K_{p2} & K_{p1} \\ 0 & 0 & 0 & -n_2 \\ 0 & 0 & n_2 & 0 \end{bmatrix} \qquad (3.60)$$

Therefore,

$$\begin{bmatrix} \dot{\alpha}_x \\ \dot{\alpha}_y \\ \dot{\varphi} \\ \dot{\theta} \end{bmatrix} = \begin{bmatrix} -d_p & -D & -k_1(t)K_{p1} & -k_1(t)K_{p2} \\ D & -d_p & k_1(t)K_{p1} & -k_1(t)K_{p1} \\ 1 & 0 & 0 & n_1+k_2(t)n_2 \\ 0 & 1 & -n_1-k_2(t)n_2 & 0 \end{bmatrix} \begin{bmatrix} \alpha_x \\ \alpha_y \\ \varphi \\ \theta \end{bmatrix} . \quad (3.61)$$

The time varying gains $k_1(t)$ and $k_2(t)$ are bounded by

$$0 \leq k_1(t) \leq k_m , \quad (3.62a)$$

$$0 \leq k_2(t) \leq 1 . \quad (3.62b)$$

The problem then is to determine the maximum value of the constant k_m in Eq.(3.62a) for which a positive definite M_r exists which satisfies (3.56). If such an M_r can be found, then the system (3.61) is stable for all time and for any time histories of $k_1(t)$ and $k_2(t)$ as bounded by (3.62).

The solution of (3.56) for M_r can be found by using the method of Potter (Ref. 11). Consider the matrix quadratic equation

$$M_r C_r M_r + B_r M_r + M_r B_r^* + A_r = 0 , \quad (3.63)$$

where A_r and C_r are symmetric and B_r is a square matrix. Define the matrix

$$P_3 = \begin{bmatrix} B_r^* & A_r \\ -C_r & -B_r \end{bmatrix} . \quad (3.64)$$

Assume T_r is a matrix which produces $T_r^{-1} P_3 T_r$ in Jordan canonical form. Then one can write

$$\begin{bmatrix} B_r^* & A_r \\ -C_r & -B_r \end{bmatrix} \begin{bmatrix} T_1 & T_2 \\ T_3 & T_4 \end{bmatrix} = \begin{bmatrix} T_1 & T_2 \\ T_3 & T_4 \end{bmatrix} \begin{bmatrix} J_a & J_b \\ 0 & J_c \end{bmatrix} \tag{3.65}$$

If T_3 is nonsingular, a solution to (3.63) is

$$M_r = T_1 T_3^{-1} \tag{3.66}$$

The condition which guarantees that T_3^{-1} exists is that J_a be associated with the eigenvalues of P_3 with positive real parts.

As can be envisioned, this method of solution as applied to (3.56) is somewhat involved. Some effort is saved by realizing that the matrices of (3.56) come from a system with complex symmetry so that (3.56) may be reduced to a 2×2 Hermite form.

As a practical matter, the problem of solving for an M_r which satisfies (3.56) can be greatly reduced because it can be shown that the time-varying element $\dot{\sigma}$ of (3.59) has an insignificant effect upon the stability of the system (3.61). This is demonstrated by presuming it, tentatively, and then performing numerical checks. If $\dot{\sigma}$ is set to a constant n, then the matrix product GK_2H becomes

$$GK_2H = \begin{bmatrix} 1 & 0 \\ 0 & 1 \\ 0 & 0 \\ 0 & 0 \end{bmatrix} \begin{bmatrix} k_m & 0 \\ 0 & k_m \end{bmatrix} \begin{bmatrix} 0 & 0 & K_{p1} & K_{p2} \\ 0 & 0 & -K_{p2} & K_{p1} \end{bmatrix} . \tag{3.67}$$

By setting $\mu_1 = 0$ and using the matrices defined by (3.67) in (3.56), the property of complex symmetry provides the solution of M_r from the following algebraic expressions:

$$2(-m_1 d_p + m_2) + k_m m_1^2 = 0 ,$$

$$- 0.5\, k_m K_{p1} m_1 - d_p m_2 - (D+n) m_3 + m_4 + k_m m_1 m_2 = 0 ,$$

$$- 0.5\, k_m K_{p2} m_1 + (D+n) m_2 - d_p m_3 + k_m m_1 m_3 = 0 ,$$

$$- K_{p1}m_2 - K_{p2}m_3 + 0.25(K_{p1}^2 + K_{p2}^2) + m_2^2 + m_3^2 = 0 \ . \tag{3.68}$$

Here, M_r has the form

$$M_r \triangleq \begin{bmatrix} m_1 & 0 & m_2 & m_3 \\ 0 & m_1 & -m_3 & m_2 \\ m_2 & -m_3 & m_4 & 0 \\ m_3 & m_2 & 0 & m_4 \end{bmatrix} \ .$$

M_r is positive definite if

$$\begin{aligned} m_1 &> 0 \ , \\ m_1 m_4 &> m_2^2 + m_3^2 \end{aligned} \tag{3.69}$$

A systematic way is thus established for determining the limit of position gain variation that assures stability of the spinning satellite due to time variations of the magnetic field. The constant k_m is raised in magnitude in Eqs. (3.86) until a solution can no longer be found which satisfies Eqs. (3.69).

As an example of this method, the maximum value of k_m allowable for a satellite with parameters

$$\begin{aligned} D &= 1.5 \text{ sec}^{-1} \ , \\ d_p &= 1.26 \times 10^{-2} \text{ sec}^{-1} \ , \\ n &= 1.09 \times 10^{-3} \text{ sec}^{-1}, \text{ (a typical perigee value)} \\ K_{p1} &= 2.85 \times 10^{-5} \text{ sec}^{-2} \ , \\ K_{p2} &= 3.5 \times 10^{-3} \text{ sec}^{-2} \ , \end{aligned}$$

was determined to be 5.398. If the orbital rate n is set to 2.18×10^{-4} sec^{-1} (a typical apogee value), the limit on k_m becomes 5.392. These values of k_m are so close that the slow variation of $\dot{\sigma}$ between perigee and apogee values can be seen to be unconsequential. The assumption of constant $\dot{\sigma}$ is thus a valid one.

The limit on k_m for this system can be approximated by use of Routh's criterion. Referring to Figure 3.7 it can be seen that K_{p2} is more than an order of magnitude larger than K_{p1} for most values of the damping term d_p. Thus, if K_{p1} is set to zero, $k_1(t)K_{p2}$ is set to K, and $n_1 + k_2(t)n_2$ is set to n in (3.61), the conditions for stability are

$$2d_p > 0 \ ,$$

$$(D^2 + d_p^2)d_p/(D-n) > K \ ,$$

and

$$\left[(D-n)d_p(D^2 + d_p^2 - n^2) + 2nd_p^3\right] \Big/ \left[(D-n)^2 + d_p^2\right] > K \ .$$

From these, the bound on K is approximately

$$Dd_p > K = k_m K_{p2} \ , \tag{3.70}$$

which agrees very closely with the results of the Lyapunov test in the example. This is quite remarkable when considering that B_z can vary over a large range in any manner. Stability can be assured in such a system by maintaining K_{p2} small enough with respect to the variable B_z or by increasing the nutation damper coefficient d_p for highly eccentric orbits.*

*It is interesting to note that the fourth order system studied here (with $\dot{\sigma} = n$) can be reduced to two second order coupled Hill's equations which have been extensively discussed in the literature (see Ref. 52). Defining the complex variables $\alpha_1 = \alpha_x + j\alpha_y$ and $\Gamma_1 = \varphi + j\theta$ produces the complex equation

$$\ddot{\Gamma}_1 + \left[d_p + j(n-D)\right]\dot{\Gamma}_1 + \left[nD + jnD + K(t)(K_{p1} - jK_{p2})\right]\Gamma_1 = 0 \ .$$

This method can also be applied to the satellite which is actively dampened.

In this case, the matrix H is

$$H = \begin{bmatrix} K_v & 0 & K_{p1} & K_{p2} \\ 0 & K_v & -K_{p2} & K_{p1} \end{bmatrix} ,$$

and no nutation damper term d_p is present. The resulting four algebraic equations [which are modifications of (3.68)] are

$$2(-3K_3K_v m_1 + m_2) + K_4 m_1^2 + 0.25\, K_4 K_v^2 = 0 ,$$

$$- K_3K_{p1}m_1 - K_3K_v m_2 - (D+n)m_3 + m_4 + K_4 m_1 m_2 + 0.25\, K_4 K_v K_{p1} = 0 ,$$

$$- K_3K_{p2}m_1 + (D+n) - K_3K_v m_3 + K_4 m_1 m_3 + K_4 m_1 m_3 + 0.25\, K_4 K_v K_{p2} = 0,$$

$$- 2K_3(K_{p1}m_2 + K_{p2}m_3) + K_4(m_2^2 + m_3^2) + 0.25\, K_4(K_{p1}^2 + K_{p2}^2) = 0,$$

with

$$K_3 = (k_1 + k_2)/2 ,$$

and

$$K_4 = k_2 - k_1 .$$

Examples using these equations with gains K_v, K_{p1}, and K_{p2} extrapolated from Figure 3.9 indicate that the system is always stable for the lower bound k_1 nonnegative. Thus, the upper bound can approach an

---

Then with $w_1 = \Gamma_1 e^{-c_1 t}$ and $c_1 = -[d_p + j(n-D)]/2$, this becomes

$$\ddot{w}_1 + \left[\left(\frac{D + n + jd_p}{2}\right)^2 + K(t)(K_{p1} - jK_{p2})\right] w_1 = 0 .$$

Further, by letting $w_1 = x + jy$, this equation results in the two coupled Hill's equations with $K(t)$ periodic. Modeling the variation of the magnetic field as a sinusoid results in two coupled Mathieu equations.

infinite magnitude with the system remaining stable. This seems reasonable because the actual damping torque increases proportionally with the increase in the position torques.

One can conjecture from the above investigation that a satellite which utilizes a combination of passive and active damping will be stable over the same regime of magnetic fields as a satellite which is totally actively dampened.

Z-Coil Control

During Mode 2 and 3 control, the magnetic moment applied to the Z coil (or in the average Z direction) is

$$m_z = K_{OB}(B_x T_{Dy} - B_y T_{Dx}) \ . \tag{3.45}$$

For the satellite with active damping, the resulting kinetic equations of the vehicle rates are

$$\begin{aligned}\dot{\alpha}_x &= -D\alpha_y - m_z B_y \ , \\ &= -D\alpha_y - K_{OB}B_y\Big[B_x(-K_v\alpha_y + K_{p2}\varphi - K_{p1}\theta) \\ &\qquad - B_y(-K_v\alpha_x - K_{p1}\varphi - K_{p2}\theta)\Big] \ .\end{aligned} \tag{3.71a}$$

$$\begin{aligned}\alpha_y &= D\alpha_x + m_z B_x \ , \\ &= D\alpha_x + K_{OB}B_x\Big[B_x(-K_v\alpha_y + K_{p2}\varphi - K_{p1}\theta) \\ &\qquad - B_y(-K_v\alpha_x - K_{p1}\varphi - K_{p2}\theta)\Big] \ .\end{aligned} \tag{3.71b}$$

These are obtained from (3.40) and (3.41) with K_{p2} used for $(K_{p2}-nK_v)$. As can be readily seen, Eqs. (3.71) do not possess complex symmetry on which the Lyapunov function generating procedure used in the preceding section relied for a straightforward algebraic solution.

Kryloff-Bogoliuboff Method of Averaging

The main difficulty, of course, with using the Lyapunov technique is the problem of finding a suitable function. For the Z-coil control law, this problem was indeed the situation (except for a special case which will be indicated shortly). For this control mode, a different approach is used which establishes the necessary conditions for system stability. This approach, known as the method of averaging, was used by Wheeler (Ref. 13) to predict the response characteristics of his Z-coil controller and control law. The method is formulated as a modification of the procedure established by Kryloff and Bogoliuboff (Ref. 53) and consists essentially of the following steps:

1. Find the solution to the uncontrolled equations of motion.
2. Take the time derivative of these equations. From these derivative equations, solve for the time derivatives of the amplitudes (or parameters) which appear in the uncontrolled equations. These derivatives will be functions of the first time derivative of the system states.
3. Substitute the actual controlled state equations (the first order differential equations) into the above equations.
4. Determine the time average of the resulting equations by integrating them over the shortest periodic function's time period. This is especially valid if the control torques are relatively weak and are long-period functions so that over the short period investigated they can be treated as constants. For magnetic control, this is the case.
5. By inspection, determine if the resulting average time rate of change of the parameters investigated are decreasing for stability.

The analogy between this procedure and the Kryloff-Bogoliuboff averaging technique for investigating stability of an equation of the type

$$\ddot{x} + \omega^2 x + \epsilon f(x,\dot{x},t,\epsilon) = 0$$

is evident.

Necessary Conditions for Stability

The method is now applied to the system with rate Eqs. (3.71a-b). Define the angles

$$\xi_1 = Dt + \xi_o \ ,$$

$$\eta_1 = nt + \eta_o \ ,$$

$$\zeta_1 = nt - \xi_o \ ,$$

where ξ_o and η_o are phase angles based on initial conditions. Then the uncontrolled motion of the spinning satellite described by Eqs. (3.2) (with $d_p = 0$) is described by

$$\alpha_x = A_\alpha \cos \xi_1 \tag{3.72a}$$

$$\alpha_y = A_\alpha \sin \xi_1 \ , \tag{3.72b}$$

$$\varphi = B_\alpha \cos \eta_1 + \frac{A_\alpha}{D+n} [\sin \xi_1 + \sin \zeta_1] \ , \tag{3.72c}$$

$$\theta = B_\alpha \sin \eta_1 + \frac{A_\alpha}{D+n} [-\cos \xi_1 + \cos \zeta_1] \ . \tag{3.72d}$$

It is desired to determine the time response of the amplitude parameters A_α and B_α for the controlled situation. Taking the time derivative of (3.72a-b) and solving for $\dot{A}_\alpha$ yields

$$\dot{A}_\alpha = \dot{\alpha}_x \cos \xi_1 + \dot{\alpha}_y \sin \xi_1 \ ,$$

$$= (-D\alpha_y + T_x) \cos \xi_1 + (D\alpha_x + T_y) \sin \xi_1 \ ,$$

$$= m_z (B_x \sin \xi_1 - B_y \cos \xi_1) \ . \tag{3.73}$$

The value of m_z from (3.45) [with values of T_{xD} and T_{yD} from (3.40)] and values of α_x, α_y, φ, and θ from (3.72) are all substituted into

(3.73). The resulting equation is averaged over the short period $2\pi/D$ holding η_1 and ζ_1 as constants. This procedure results in the average time rate change of the amplitude $\dot{A}_\alpha$ which is

$$\dot{A}_{\alpha ave} = -\frac{K_{OB}}{2}\left(K_v - \frac{K_{p2}}{D+n}\right)(B_x^2 + B_y^2)\, A_{\alpha ave} \,. \tag{3.74}$$

This equation is stable for $K_{OB} > 0$ and $K_v > K_{p2}/(D+n)$.

Now attention is turned to determining the time rate of change of the parameter B_α. Repeating the procedure above, the time rate of change of B_α is

$$\dot{B}_\alpha = \dot{\varphi}\cos\eta_1 - \frac{1}{D+n}(\dot{\alpha}_y + \dot{A}_\alpha \sin\zeta_1 + A_\alpha n\cos\zeta_1)\cos\eta_1$$

$$+ \dot{\theta}\sin\eta_1 - \frac{1}{D+n}(-\dot{\alpha}_x + \dot{A}_\alpha\cos\zeta_1 - A_\alpha n\sin\zeta_1)\sin\eta_1 . \tag{3.75}$$

Substitutions are made for the controlled $(\alpha_x, \alpha_y, \varphi, \theta)$ as before, and again the resulting expression is averaged over the short period $2\pi/D$. The resulting time average rate of $B_{\alpha ave}$ is

$$\dot{B}_{\alpha ave} = -\frac{K_{OB}}{D+n} B_{\alpha ave}\Big[K_{p2}(B_x\cos\eta_1 + B_y\sin\eta_1)^2 - K_{p1}\Big\{B_x B_y(\sin^2\eta_1 - \cos^2\eta_1)$$

$$+ (B_x^2 - B_y^2)\sin\eta_1\cos\eta_1\Big\}\Big] + f(A_\alpha, \dot{A}_\alpha) \,. \tag{3.76}$$

Here, $f(A_\alpha, \dot{A}_\alpha)$ is linear in A_α and $\dot{A}_\alpha$, and it disappears. As can be seen in (3.76) the quantity in braces multiplied by K_{p1} does not consistently contribute to the stability of B_α; in fact, it may produce instability for certain trajectories through the magnetic field. Thus, during Z-coil control one should set $K_{p1} = 0$. Therefore, the necessary conditions for stable Z-coil control with active damping are

$$K_v > K_{p2}/(D+n) \tag{3.77}$$

$$K_{p1} = 0 \ . \tag{3.78}$$

The resulting control law (3.45) is

$$m_z = K_{OB}(B_x[-K_v\alpha_y + K_{p2}\varphi) + B_y(K_v\alpha_x + K_{p2}\theta)] \tag{3.79}$$

which is essentially the control law used by Wheeler.

With this hindsight, a Lyapunov function can be formulated for the resulting system. This is

$$V_\ell = \frac{1}{2}\frac{K_{OB}}{K_v}\left\{(K_{p2}\theta + K_v\alpha_x)^2 + (K_{p2}\varphi - K_v\alpha_y)^2 + K_{p2}(K_v(D+n) - K_{p2})(\varphi^2 + \theta^2)\right\} \tag{3.80}$$

with $\dot{V}_\ell = -m_z^2$. V_ℓ is always positive definite by the constraint (3.77). This function is a simple modification of the one used by Wheeler to establish stability of his control law for a satellite in a circular orbit. Thus, with the gain constant $K_{p1} = 0$, sufficiency conditions are produced which insure stability of the actively dampened system. Although asymptotic stability cannot be concluded because there may be trajectories for which m_z is identically zero, it seems rather doubtful that such a condition could exist for any length of time because of the complexity of the actual magnetic field. (See Appendix A).

Using the averaging method on the passively dampened system leads to the condition that

$$\dot{A}_{\alpha ave} = -\left[d_p - \frac{K_{OB}K_{p2}}{2(D+n)}(B_x^2 + B_y^2)\right] A_{\alpha ave}. \tag{3.81}$$

There can be noted a marked similarity between the stability constraint which is inherent in this equation (3.81) and the constraint (3.70) placed upon the gain variation for the passively dampened case of Mode 1. The actual constraint is formalized as

$$d_p(D+n) > K_{OB}K_{p2}B_o^2/2 \tag{3.82}$$

for system stability, where $B_o^2 = \max(B_x^2 + B_y^2)$ encountered during the orbit.

The response of the parameter B_α for the passively dampened case is the same as that for the actively dampened case (3.76).

In summary, the special case in which damping is done entirely actively has a legitimate Lyapunov function for guaranteeing stability. Necessary conditions are provided for the stability of passively dampened satellites by averaging. Sufficiency conditions must rely upon adequate computer simulation.

GENERAL SYSTEM PERFORMANCE

Having now defined a magnetic attitude control system and having specified the limits of stability for that system, it remains to evaluate the general satellite control performance for a variety of situations which would be encountered in the actual environment. The satellite controller-estimator and dynamics have eight states, are subject to a time-varying magnetic field, control torque, and disturbance torque, and have a sampled roll error measurement. Because of the complexity involved then, this performance evaluation generally has to be conducted by use of both analog and digital computer simulations. The results of these simulations and the accompanying analysis are described in this section.

In the digital simulation, the full ninth-order spherical harmonic model of the earth's magnetic field described in Appendix A was utilized. The nonlinear effects of orbit eccentricity and time-varying spin rate were also included. The simulated disturbances were those environmental torques described in Chapter 2. All three modes of magnetic control previously discussed were investigated.

The analog simulation concentrated upon performance studies of the system in Mode 1 control. Here, the $\hat{z}_B$ component of the magnetic field was assumed to be constant. The time-varying $\dot{\sigma}$ due to orbital eccentricity was approximated as a constant-plus-sinusoidal term. Disturbance

torques were also approximated as constants and sinusoidal terms. The Z-coil portion of the controller used in Modes 2 and 3 were not simulated on the analog computer because it is essentially the same as the system studied by Wheeler (Ref. 13). This reference contains a complete analog evaluation of the Z-coil controller used for a satellite in a circular orbit.

Transient Response With and Without the State Estimator

The attitude control system which has been considered has been based upon the presence of an optimum state estimator from which the vehicle rates and the yaw error are determined. An alternate controller could be one in which the magnetic control law is based upon the roll error measurements θ_s only, i.e.

$$T_x = -K_{p2}\,\theta_s \,. \tag{3.83}$$

The body rates would be controlled by the passive nutation damper. Such a control is described and evaluated by Sonnebend in Reference 9.

The Mode 1 control law (3.40) developed here was compared directly with that of (3.83) in the transient situation with no disturbance torques. The comparison was made on an analog computer by measuring the response time required to drive the spin axis to within 0.1° of the nominal from various sets of initial conditions. The trajectories in the φ-θ plane for such comparisons are shown in Figures 3.13 and 3.14.

As was mentioned before, a roll disturbance torque is mathematically observable for the satellite using horizon sensor error measurements. Therefore, an evaluation of the system trying to estimate roll torque was also made at this point. This involved mechanizing a five-state estimator (Kalman filter).

Figure 3.13 indicates the transient response trajectories of systems with a five-state estimator, a four-state estimator, and no estimator for initial conditions of $\varphi = \theta = 0.15$ radians, $\alpha_x = .05$ rad/sec, and $\alpha_y = 0$. It can be seen that the trajectories resulting from state estimation go more directly to the origin than one without the estimator.

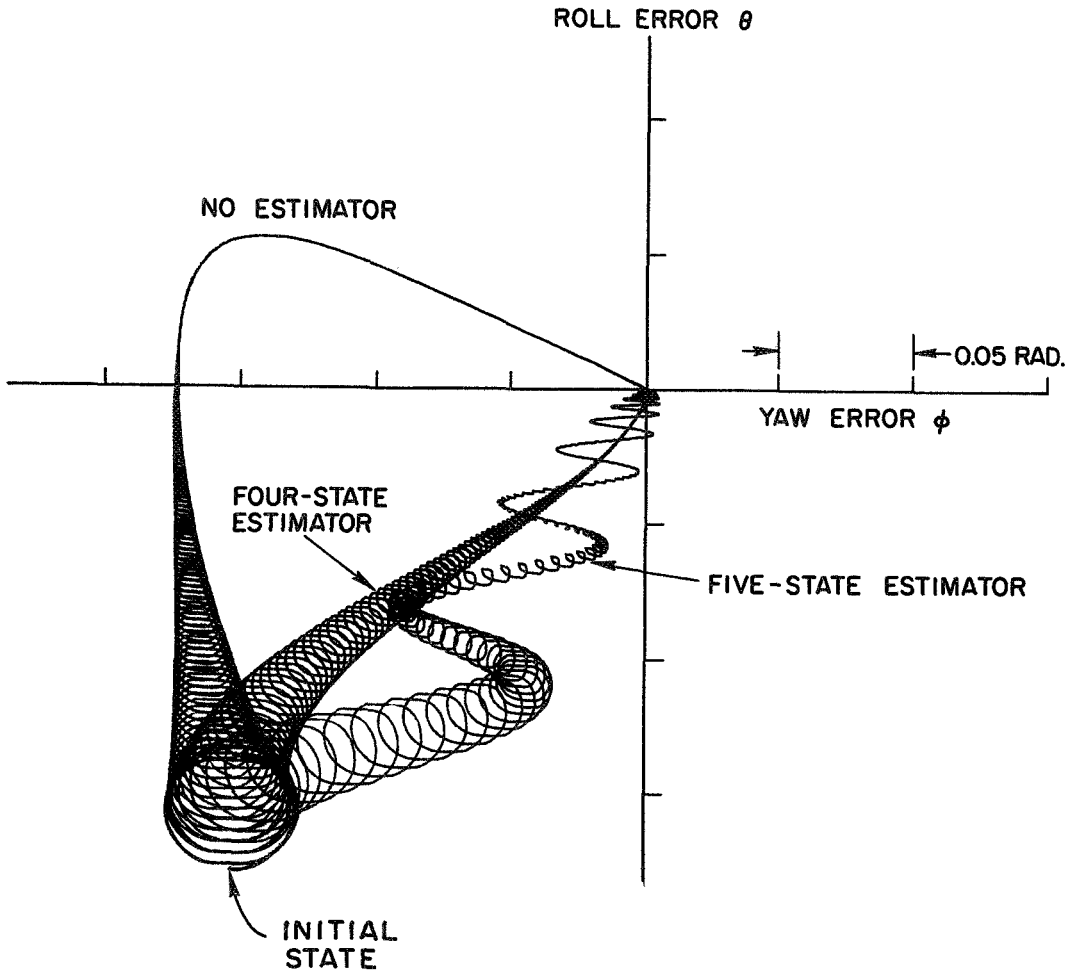

FIG. 3.13. TRANSIENT RESPONSE OF THE POINTING ERROR FOR THE SATELLITE WITH AND WITHOUT A STATE ESTIMATOR AS PART OF THE CONTROL SYSTEM. The five-state estimator also determines the roll disturbance torque.

It can also be seen that the trajectory of the five-state estimator has a large amount of fluctuation as compared to the four-state estimator. This erratic behavior was generally the case for arbitrary sets of initial conditions. It was observed from monitoring the outputs of the five-state estimator that this mechanization is extremely sensitive to gain setting deviations. Small deviations caused large fluctuations in the transient response of the estimate of the roll disturbance. This affected the response of the rest of the state variables as seen in Fig. 3.13. This degree of sensitivity is, of course, undesirable. The constant roll torque estimation is not that important to the

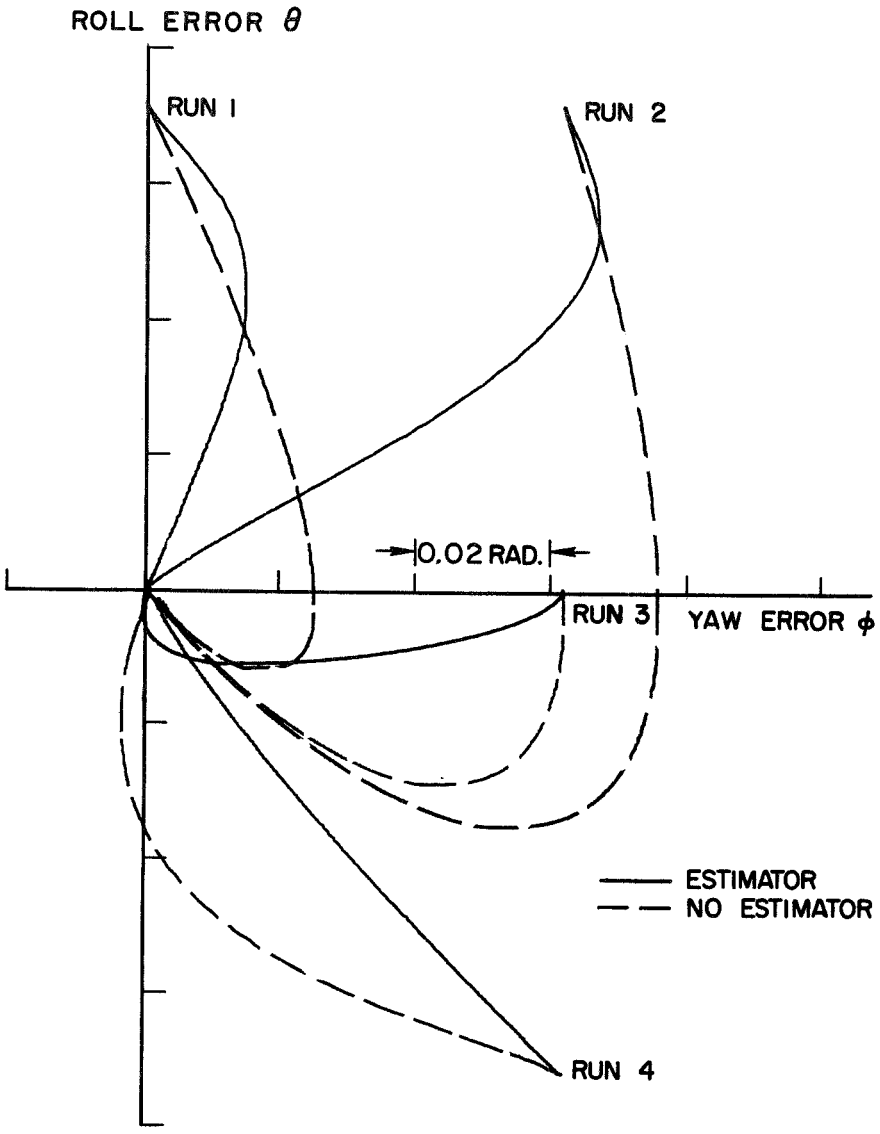

FIG. 3.14. TRANSIENT RESPONSE OF THE SATELLITE POINTING ERROR TO VARIOUS INITIAL CONDITIONS. Response with and without the state estimator in the control system is compared.

type of satellite studied here. It is also desirable to be able to mechanize the control system and its associated filter using mostly analog circuitry with components which may have some deviation from nominal values. Therefore, the rest of the study is concerned with only the four-state estimator.

The sensitivity of the five-state estimator is partially due to the weak orbital cross coupling which exists between the roll and yaw

channels of the Kalman filter. The noisy horizon sensor measurements could also compound the problem.

As would be suspected, the transient response time of the system with the state estimator was significantly superior to that of the system with no estimator. The transient times of a satellite with parameters

$$D = I_{zz}\dot{\psi}/I_{xx} = 1.6 \text{ sec}^{-1} ,$$

$$n = 1.16 \times 10^{-3} \text{ sec}^{-1} ,$$

$$I_{xx} = 10 \text{ kg - m}^2 ,$$

and the nonoptimal gains

$$K_{p2} = 0.03 - 0.1 \text{ sec}^{-2} ,$$

$$K_v = 0.1 \text{ sec}^{-1} ,$$

were simulated. A comparison of response times for four sets of initial conditions with and without the estimator is presented in Table 3.1. The improvement from estimator application is evident. Response trajectories from Runs 1 through 4 are shown in Figure 3.14.

Rapid response is important for two reasons. Because disturbance torques are going to move the satellite spin axis away from normal to the orbit plane, fast response means that the average deviation is less. Also, because the control torque depends upon the magnetic field available (which fluctuates considerably in eccentric orbits), it is desirable to apply full control whenever the magnetic field strength is sufficiently high. However, without an estimator, detection of the full error (i.e., at that region of the orbit where the error is mostly in roll) might conceivably occur only when the magnetic field strength is low. Thus, without an estimator (which serves as a memory of the error), it could take much longer to drive the system to the null position, and the average steady state error could be larger.

Table 3.1. COMPARISON OF TRANSIENT RESPONSE TIMES FOR DRIVING THE POINTING ERROR OF THE SATELLITE TO ZERO. Directly compared are times of a system with and without a state estimator (Kalman filter). Different initial conditions are used. Magnitude of the position gain in the control law is also varied.

Run Number	Initial Conditions (rad)		Position Gain K_{p2} (sec^{-2})	Time-to-Origin (sec)	
	φ_o	θ_o		With Estimator	Without Estimator
1	0.18	0	0.03	1700	6300
2	0.18	0.15	0.03	1100	7300
3	0	0.15	0.03	700	6400
4	-0.18	0.15	0.03	1200	3200
5	0.18	0	0.1	800	700
6	0.18	0.15	0.1	1100	>18000
7	0	0.15	0.1	1100	>18000
8	-0.18	0.15	0.1	900	>18000

Steady Performance in the Presence of Disturbance Torques

Probably the most important criterion upon which to judge the merits of an attitude control system such as the one studied here is its steady-state or average performance in the presence of environmental and vehicle attitude disturbance torques. By performance is meant the average pointing accuracy achievable, or the spacecraft's ability to stand off these disturbance torques. Unfortunately, this performance measurement is difficult to assess properly in the presence of the complex environment of the satellite in the highly eccentric orbit. The only way valid prediction of precise performance can be made is by use of extensive digital computer simulations covering a wide spectrum of orbits and satellite parameters. The cost of such an undertaking is prohibitively high for a study such as this, so a different tactic was pursued.

It was felt that if worst-case environmental torques could be defined, then an upper bound on the pointing accuracies achievable from this satellite attitude control system could be made directly. Because the spin component of the magnetic field (B_z) is time-varying, a natural

question arises as to where the ratio of the disturbance torque magnitudes to the available control torque is worst.

Figures 3.15a-b are plots of the worst yaw and roll components of disturbance torques acting upon the satellite. Also plotted on these

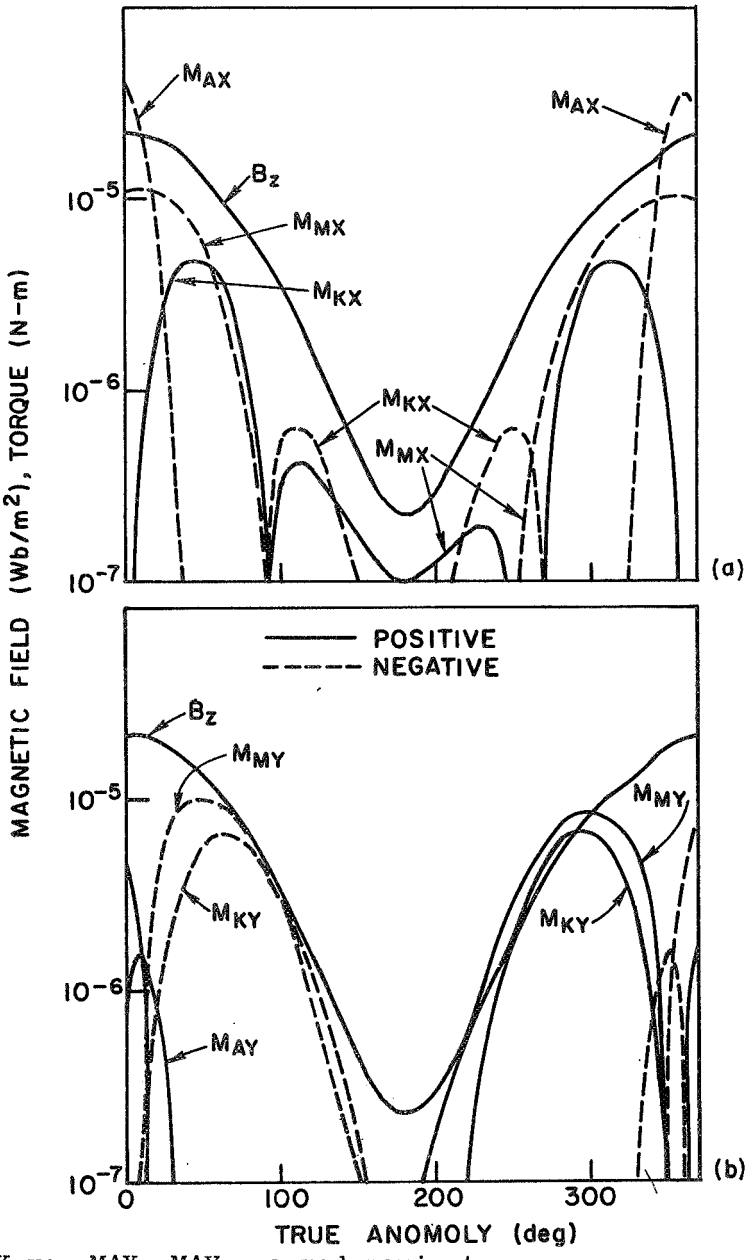

Key: MAX, MAY - aerodynamic torque
MKX, MKY - kinematic torque
MMX, MMY - satellite dipole torque
B_z - spin component of magnetic field

FIG. 3.15. PRIMARY TORQUES ACTING ON A SPINNING SATELLITE IN AN ECCENTRIC 3 REVS/DAY RESONANT ORBIT WITH PERIGEE ALTITUDE OF 300 km. Also shown is the spin component of the magnetic field. (a) Yaw torques; (b) Roll torques.

curves is the magnetic field component B_z. Parameters of the satellite and environment are the same as those used to generate Figures 2.9 - 2.10 of Chapter 2, except that the orbit has an eccentricity of 0.6367 corresponding to a resonant orbit of three revolutions per day. As can be readily seen, (and is not unexpected) the disturbance torques seem to decrease in magnitude proportionally to the decrease in magnitude of B_z. Thus, it seems as valid to check the performance with respect to perigee torques (or for that matter, torques of a circular orbit at perigee altitude) as to any other point on the orbit. The approach taken is to assume that the satellite is in a 16 rev/day orbit with each individual torque component at its worst value in relationship to the B_z magnitude.

The torques which are of most concern are the aerodynamic torques, the torques due to a magnetic dipole fixed along the spin axis, and the kinematic torque due to the reference axis moving because of orbit plane precession. These torques can be modeled as

$$\text{Aerodynamic:} \quad M_{AX} = C_1 + C_2 \cos nt.$$

$$\text{Magnetic dipole:} \quad M_{MX} = C_3 \cos nt \ ,$$

$$M_{MY} = C_4 \sin nt \ .$$

$$\text{Kinematic:} \quad M_{KX} = C_5 \cos nt \ ,$$

$$M_{KY} = -C_5 \sin nt \ .$$

Values of the constants used for simulation were

$$C_1 = -10^{-4} \text{ N-m} \ ,$$

$$C_2 = -10^{-4} \text{ N-m} \ ,$$

$$C_3 = -4 \times 10^{-5} \text{ N-m} \ ,$$

$$C_4 = -8 \times 10^{-5} \text{ N-m} \ ,$$

$$C_5 = 2 \times 10^{-5} \text{ N-m} \ ,$$

The constants C_1 to C_4 represent a center-of-mass offset of about 5 cm (at 300 km) and a magnetic dipole of about 2.5 AMp-m^2, which are both quite conservative.

Again runs were made with and without an estimator. Gains used were $K_{p2} = 0.003$ and $d_p = 0.01$. The largest fluctuations were in the

Table 3.2 YAW FLUCTUATIONS FOR DIFFERENT TORQUE INPUTS TO THE SATELLITE WITH AND WITHOUT THE STATE ESTIMATOR.

Type Torque	Torque Magnitude (N - m)		Yaw Fluctuations (deg)	
	Yaw (x)	Roll (y)	No Estimator	Estimator
Total	-10^{-4} $-0.8 \times 10^{-4} \cos nt$	$-10^{-4} \sin nt$	0. to 0.70	-0.20 to 0.93
No aerodynamic	$-0.2 \times 10^{-4} \cos nt$	$-10^{-4} \sin nt$	-0.38 to 0.30	-0.06 to 0.07
Dipole only	$-0.4 \times 10^{-4} \cos nt$	$-0.8 \times 10^{-4} \sin nt$	-0.31 to 0.25	-0.14 to 0.16
Kinematic only	$0.2 \times 10^{-4} \cos nt$	$-0.2 \times 10^{-4} \sin nt$	-0.10 to 0.08	-0.07 to 0.09

yaw error φ, and are presented in Table 3.2 (with $I_{xx} = 10$ kg-m^2 and $D = 1.6$ sec^{-1}).

The four types of disturbance torques simulated were:

1. The total aerodynamic, magnetic, dipole, and kinematic torques;
2. Magnetic dipole plus kinematic torques;
3. Dipole torque only; and
4. Kinematic torque only.

Results are presented in that order.

As would be expected, a large steady yaw torque tends to produce the largest yaw error. Because this type of torque is mathematically unobservable, it seems reasonable that the control system would be less adapted to cope with the yaw torque's presence than some other torque source.

Also seen in Table 3.2 is the fact that large steady yaw torques tend to produce larger yaw fluctuations for the system with the state estimator. However, if constant yaw torques are reduced by better vehicle construction, the yaw fluctuations are decreased by using the state estimator.

The steady-state value of a yaw error due to a constant yaw torque can be found by applying the Final Value Theorem to the transfer function between yaw torque input and yaw angle output. With no state estimator, the steady-state value of the yaw error is

$$\varphi_{ne} = \frac{DnT_x}{n^2(d_p^2 + D^2) - d_p n K_{p2}} .$$

With the four-state estimator this becomes

$$\varphi_e = \frac{T_x}{n^2(d_p^2 + D^2) + K_{p2}^2 - 2d_p n K_{p2}}$$

$$\times \left[D_n + K_{p2} \frac{(-K_1 Dn - K_2 d_p n + K_2 K_{p2} - K_3 K_{p2} D - K_4 d_p^2 n - K_4 D^2 n + K_4 d_p K_{p2})}{(d_p^2 n^2 - d_p^2 K_3 n + D^2 n^2 - K_3 D^2 n + K_2 Dn - K_1 d_p n)} \right] .$$

Here K_1, K_2, K_3, and K_4 are the estimator gains and the gain K_{p1} is set to zero. T_x is the magnitude of the disturbance torque. These steady-state values are approximately

$$\varphi_{ne} \cong T_x \frac{1}{Dn} ,$$

$$\varphi_e \cong \frac{T_x}{K_{p2}^2} \left(Dn + \frac{K_{p2}^2}{Dn} \right) .$$

For typical values of gain K_{p2} [that is, $Dn \ll K_{p2}^2/(Dn)$] these two are essentially equal. To reduce the steady-state yaw error due to constant yaw torques requires either reducing the yaw torque itself by better vehicle design or increasing the vehicle angular momentum.

Performance During Mode 3 Control

It was desired to determine if a pointing angle error is decreased by using a magnetic moment along the spin axis during Mode 3 spin control. Recall that during Mode 3, the lateral magnetic moment is constrained to be normal to the lateral component of the magnetic field for spin speed adjustment. This gives rise to a pointing disturbance torque.

To study performance during Mode 3 control, a digital computer program was developed which contained the Euler equations of motion, the estimator, and the complete control logic. Also included were the ninth order magnetic field model developed in Appendix A and the entire disturbance torque program as developed in Chapter II.

Several simulations were made with this program with different initial conditions and the control law

$$m_x = -10^5 B_y \, \mathrm{sgn}(\Delta\dot{\psi}) ,$$
$$m_y = 10^5 B_x \, \mathrm{sgn}(\Delta\dot{\psi}) ,$$
$$m_z = 3.5 \times 10^6 (B_x \varphi + B_y \theta) ,$$

during Mode 3. Here, the magnetic moments are measured in Amp-m^2 and the magnetic field components are measured in Wb/m^2. The parameters d_p and D were 0.0126 sec^{-1} and 1.5 sec^{-1}. Mode boundaries were C_{d1} = 0.01 rad/sec and C_{d2} = 0.02 rad/sec. A typical response plot is shown in Figure 3.16 where the control goes from Mode 2 to Mode 3 to Mode 1.

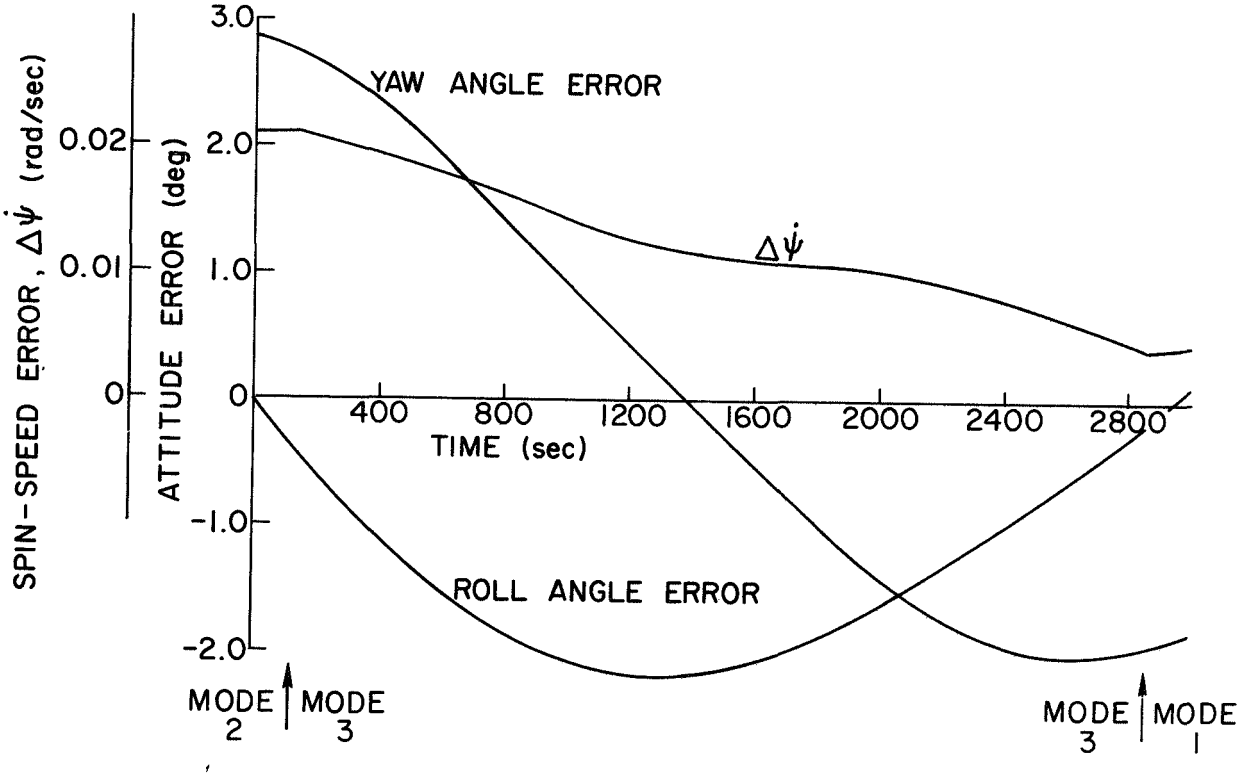

FIG. 3.16. TYPICAL RESPONSE OF SPIN SPEED, ROLL, AND YAW ERRORS DURING MODE 3 CONTROL.

In all cases run, the total pointing error never grew larger during Mode 3 control. It appeared that the spin speed could be controlled within 0.03 rad/sec. of the nominal value, or 3 percent. This spin control was dependent, of course, upon the ability of the horizon sensor to measure spin speed that accurately.

Miscellaneous Simulation Studies

Some other points were also studied on the analog computer involving the stability of the control system. A determination was made of the

effect of a sampled roll error being used as the input to a continuous filter. Some studies were made of the stability effects due to the control torques of Mode 1 being subject to saturation and deadband nonlinearities. Finally, an investigation was conducted concerning the effect of modeling the orbital rate $\dot{\sigma}$ as a constant in the filter. Each of these studies will be discussed in turn.

The Estimate Lag Problem Due to Roll Error Sampling

If the sampled roll error is fed into the continuous estimator (filter), then the estimated vehicle rates $\hat{\alpha}_x$ and $\hat{\alpha}_y$ lag the actual rates α_x and α_y. If the damping portion of the control law has components

$$T_{Dx} = -K_v \hat{\alpha}_x ,$$

$$T_{Dy} = -K_v \hat{\alpha}_y , \tag{3.84}$$

poor damping characteristics result. In the case where the parameter D was equal to 1.5 sec^{-1} with three samples per vehicle rotation, instability actually occurred. This lag problem could be corrected by either sampling the estimated roll error $\hat{\theta}$ before comparing it with the sampled measurement θ_s or by introducing a lead angle Δ_ℓ into the damping control law, i.e.

$$T_{Dx} = -K_v(\hat{\alpha}_x \cos \Delta_\ell - \hat{\alpha}_y \sin \Delta_\ell) ,$$

$$T_{Dy} = -K_v(\hat{\alpha}_x \sin \Delta_\ell + \hat{\alpha}_y \cos \Delta_\ell) . \tag{3.85}$$

Figure 3.17 shows the results of damping on α_x using Eqs. (3.85) instead of (3.84) in the control law for a system which samples the roll rate four times per rotation. Here the lead angle Δ_ℓ is 60°. The improvement is obvious.

The Inclusion of Saturation and Deadband in the Control Feedback

During Mode 1 control, it may be desirable to place a deadband about the nominal spin axis attitude so that power requirements might

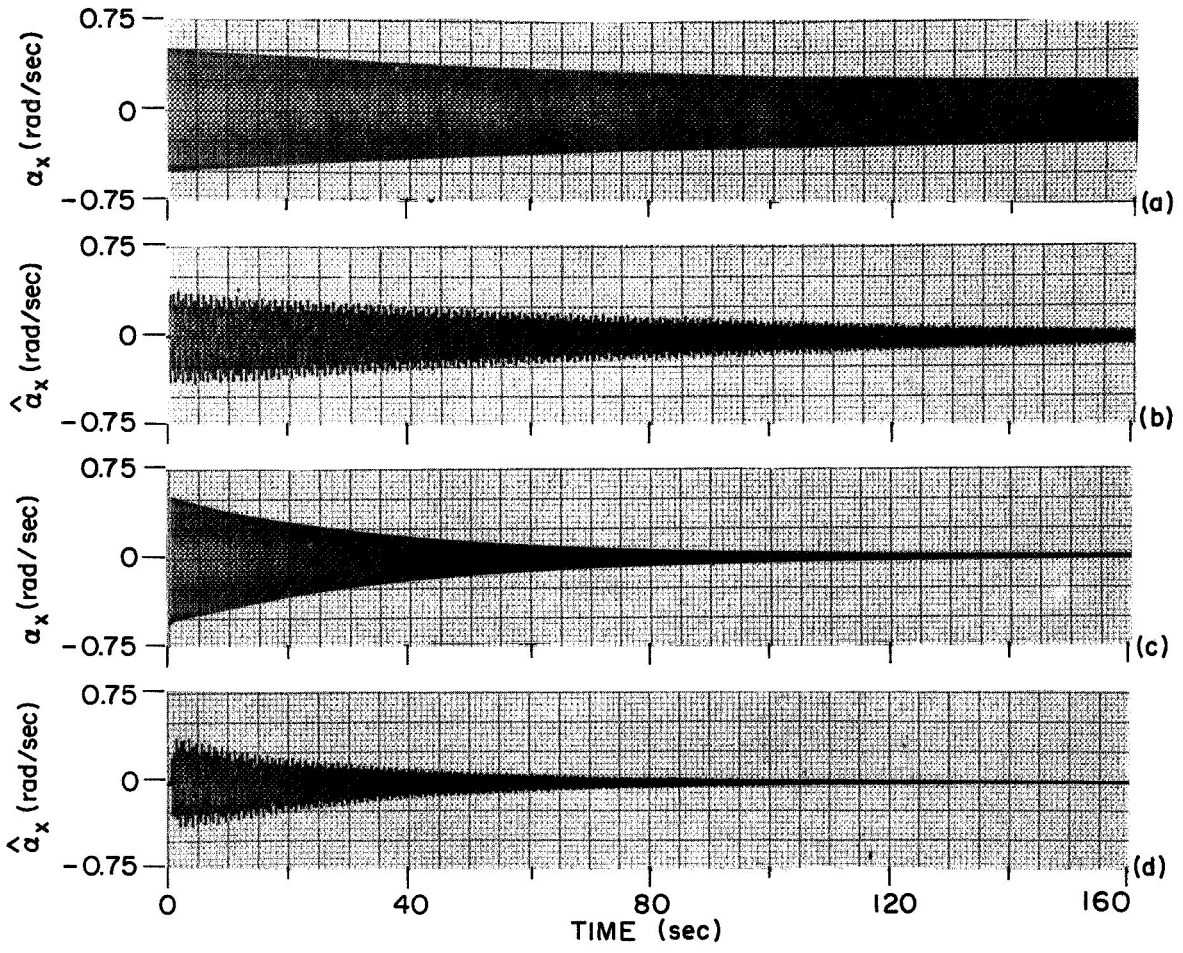

a. Actual rate α_x with no lead in control. Rate only partially dampens.

b. Estimated rate $\hat{\alpha}_x$ with no lead in control.

c. Actual rate α_x with 60° lead in control.

d. Estimated rate $\hat{\alpha}_x$ with 60° lead in control.

FIG. 3.17. TIME PLOTS SHOWING THE SAMPLING EFFECT ON ACTIVE RATE DAMPING. Here, the sample rate is 4 times per satellite spin period. With no lead angle in the active control, the rates are only partially dampened.

be further lowered. Also, because there will always be power limitations upon each coil of wire of the control system, each feedback channel of control is subject to saturation. The question arises as to what effect these nonlinearities would have upon the stability of the system.

It has been shown (Ref. 54) that any linear system which has a normal optimal feedback control law based upon a quadratic loss function can have a great deal of nonlinearity in the control mechanization. Using a multivariable Popov criterion, it has been shown that the actual mechanized control of each channel can be anywhere within the shaded portion of Figure 3.18a and still result in a stable system. Thus, types of linearities which automatically result in systems that are still stable include those containing saturation or relay control with deadband as shown in Figures 3.1b-c.

Portions of the saturation-plus-deadband nonlinearity considered here (Figure 3.18d) do not lie above the line with slope $\frac{1}{2}$. Therefore, computer investigations were made of the satellite system with different values of the parameters d_b and s_a of Figure 3.18d. The deadband d_b on the applied control ranged from 0 to 0.025 K_{p2} sec^{-2}. The saturation level s_a was varied from 0.05 K_{p2} to 0.1 K_{p2} sec^{-2}. The nonlinear system was always stable (or achieved a stable limit cycle about the origin) when the linear system was stable.

The Modeling of Orbital Rate as a Constant

Because the satellite is in an eccentric orbit, the time rate of change of the truly anomaly $\dot{\sigma}$ is time varying. This rate was considered before in deriving the Kalman filter gains and the optimal control gains. The variation was shown to have a negligible effect on the results. It also had little effect upon the development of a Lyapunov function for providing the range of damping to insure Mode 1 stability. One might suspect from these previous conclusions, then, that this orbital rate $\dot{\sigma}$ could be adequately modeled as a constant in the estimator. In other words, one might use a constant n in the estimator equations instead of updating a variable $\dot{\sigma}$ based upon readings from the horizon sensors. The advantage from such a conclusion would, of course, be that

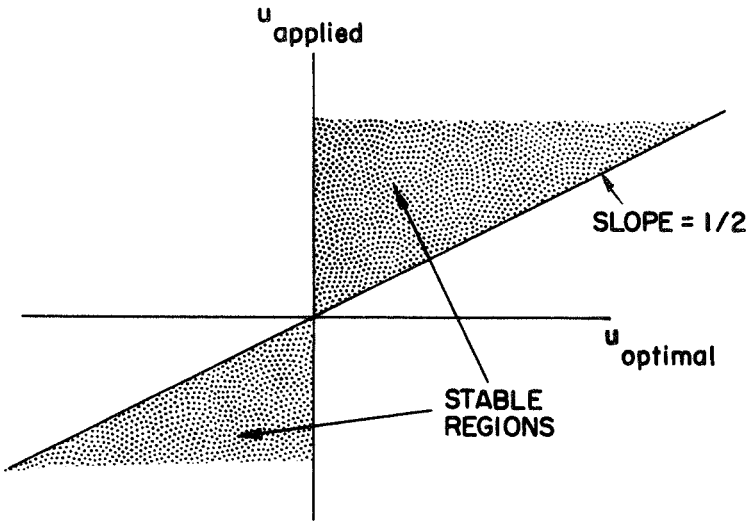

FIG. 3.18a. STABILITY REGION OF NONLINEARITIES AFFECTING THE OPTIMAL CONTROL DERIVED FROM A QUADRATIC LOSS FUNCTION.

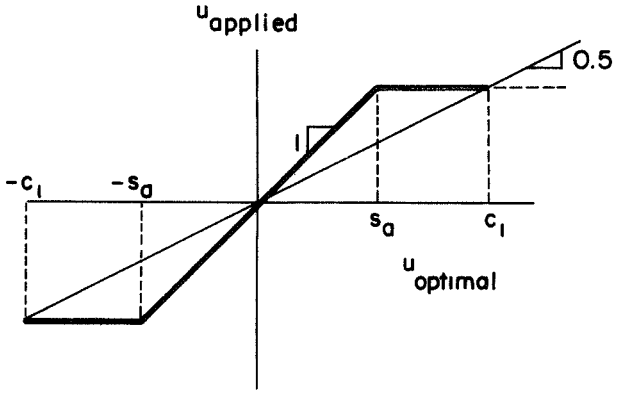

FIG. 3.18b. OPTIMAL CONTROL WITH SATURATION. Stability guaranteed to $|u_{opt}| = C_1$.

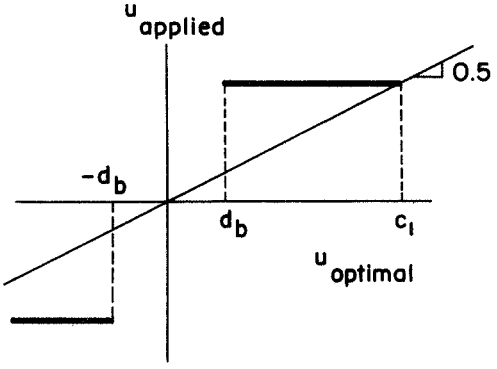

FIG. 3.18c. OPTIMAL CONTROL WITH RELAY ACTUATION AND DEADBAND. Stability guaranteed to $|u_{opt}| = C_1$.

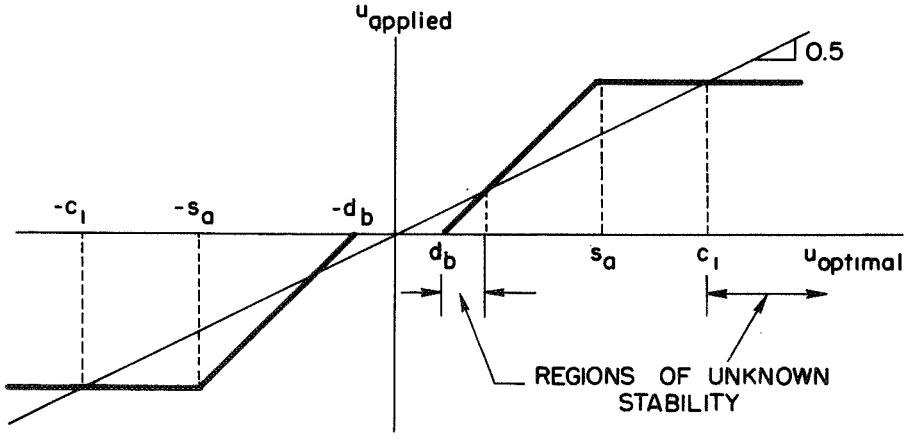

FIG. 3.18d. OPTIMAL CONTROL WITH DEADBAND AND SATURATION. Regions of unknown stability are indicated.

great simplification could be realized in mechanizing the estimator (replacement of multipliers by constant gain potentiometers).

Such a conclusion cannot be made, however. Figure 3.19 shows the analog computer response of a model plant similar to the satellite with mean rate n equal to 8×10^{-4} rad/sec and actual rate $\dot{\sigma}$ equal to 8×10^{-4} rad/sec + 7×10^{-4} cos $(8 \times 10^{-4}\ t)$ rad/sec. Modeling of $\dot{\sigma}$ as a constant-plus-sinusoid is crude, but the results indicate what could happen from the actual effect.

Figure 3.19a shows the response of a system starting at apogee ($\dot{\sigma} = 10^{-4}$ sec^{-1}) and initial conditions of $\varphi = -0.075$ rad with both linear and nonlinear (saturation-plus-deadband) feedback controls. The linear case goes directly to the origin and the nonlinear case achieves an irregular limit cycle about that point. Figure 3.19b has the same initial conditions but starts at perigee ($\dot{\sigma} = 15 \times 10^{-4}$ sec^{-1}). Here, it can be seen that the linear feedback system achieves a small limit cycle which is not centered about the origin and the nonlinear system goes through an erratic motion before finally achieving an irregular limit cycle about the origin.

Other initial conditions produced equally confusing results, although in all cases, the trajectories ended up in the vicinity of the origin. Stability in such a situation cannot be concluded, however. It would seem advisable to take advantage of the horizon sensor's ability to determine $\dot{\sigma}$, especially for the nonlinear feedback mechanizations.

SUMMARY

This chapter studies a new theoretical design of a magnetic three-degree-of-freedom attitude control system which maintains the spin axis of an axisymmetric satellite to within less than 1° of normal to the orbit plane in the presence of worst-case disturbance torques. The spin speed of the satellite is kept within 0.03 rad/sec or 3 percent of the nominal value by the same control system. The control system is capable of operating at orbit inclinations between 20° and 70° and eccentricities of from 0 to 0.7, with perigee between 300-500 km altitude.

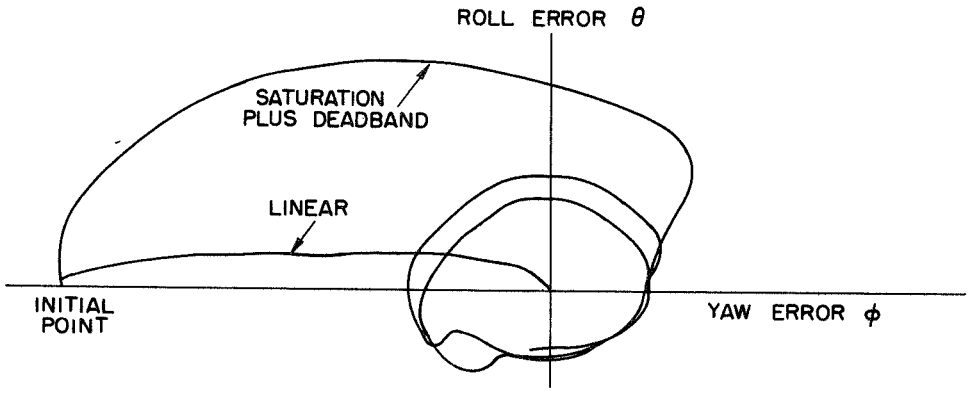

FIG. 3.19a. THE RESPONSE OF THE POINTING ERROR OF A SPINNING SATELLITE IN AN ECCENTRIC ORBIT WHEN THE ORBITAL RATE IS MODELED AS A CONSTANT IN THE CONTROL SYSTEM'S KALMAN FILTER. Indicated here is the response when starting at the apogee for both a linear controller and one with saturation and deadband.

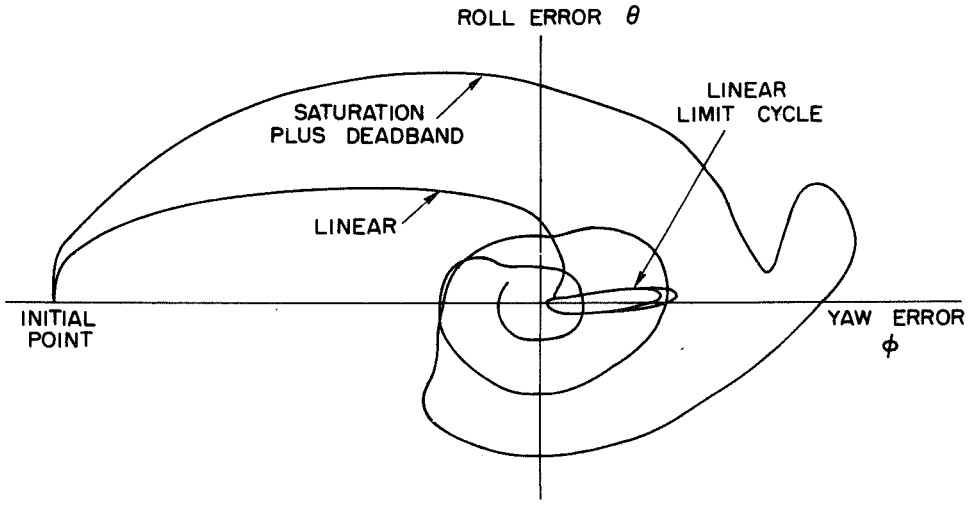

FIG. 3.19b. THE RESPONSE OF THE SAME SYSTEM ILLUSTRATED IN FIGURE 3.10a EXCEPT THAT THE INITIAL POINT IS AT PERIGEE.

A Kalman filter is utilized to estimate yaw error and vehicle rates from horizon sensor roll error measurements. Analog computation demonstrated a significantly improved performance of the system with the filter.

The control law was chosen to minimize the power requirements of the magnetic controller. The determination of the control law gains was made utilizing a new method of algebraic solution of a quadratic matrix equation. This general method can be applied to any system of equations with complex symmetry.

The control law is implemented with magnetic coils and possibly a nutation damper. Control can be actuated via either three orthogonal coils or a single coil whose plane is skewed 45° with respect to the spin axis. The unique skewed-coil concept requires only a single magnetometer and has certain packaging advantages. The magnetic control is applied by a logic system broken into three modes. These modes enable the system to achieve and maintain correct spin speed in addition to correct pointing attitude with minimum constraints placed upon the magnetic field vector. These constraints are that the spin component (B_Z) always be positive and that a lateral component be present for spin control.

For simplicity, the actual magnetic mechanization of the control law is based upon using the average value of the magnetic field. This mechanization results in a time-varying controller that provides questionable stability. A new method of generating a Lypunov function which establishes the stability bounds on the magnetic field variation during Mode 1 control is utilized. Constraints of Mode 2 (Z-coil) stability are specified by use of the Kryloff-Bogoliuboff averaging procedure.

Analog and digital simulations are used to verify the stability of the control system, to evaluate its performance, and to determine control accuracy in the presence of environmental disturbance torques. The overall control system concept, while simple in design, is capable of achieving greater control accuracies for longer periods of time than previously studied all-magnetic designs utilizing the horizon sensor. The only added electronics sophistication is the Kalman filter and mode

logic which can be easily mechanized with present-day technology. Of course, the reliability of the added electronics must be carefully evaluated.

The fundamental limitation on the achievable pointing accuracy of the controller studied in this chapter is its inherent ability to withstand a constant yaw torque. This type of disturbance torque is unobservable from the horizon-sensor scheme. The ability of the control system to reduce steady-state errors is also limited to some extent by the noisy character of the horizon-sensor measurements and the weak cross coupling that exists between the roll and yaw channels of the Kalman filter.

In Chapter IV, a satellite example is studied whose error sensor has the ability to measure simultaneously the equivalent of both the roll and yaw errors. These measurements are assumed to be extremely accurate and a strong cross-coupling term exists between channels. For this set of circumstances, it will be seen that very good estimates of the disturbance torques can be made. These estimates enable the construction of a control system with vastly improved performance.

CHAPTER IV

PRECISION MAGNETIC ATTITUDE CONTROL OF A SPINNING SYMMETRIC STAR TRACKER

In this chapter, a magnetic attitude control system is studied for precisely pointing (at a star) the spin axis of an axisymmetric satellite in a polar orbit. The limitations of this control system are explored to the extent that a direct comparison of its performance can be made with other types of precision attitude control mechanizations. Particular points investigated in this chapter include the following:

1. A continuous control law is derived which keeps the spin axis aligned accurately in the presence of normal disturbance torques associated with this particular orientation of the satellite. The key to this control law is that the major portion of the disturbance torque acting upon the satellite is observable.
2. A magnetic actuation system is devised which mechanizes the pointing control law while maintaining satellite spin speed.
3. Physical limitations of the magnetic control system for providing the pointing accuracy desired for the ideally constructed satellite are determined.
4. A qualitative analysis is made of further limitations to the pointing accuracy caused by deviations from the ideal construction of the satellite and control system equipment.

The control system studied can generally be utilized on any spinning symmetric satellite. It is specifically applicable to a drag-free satellite housing an unsupported gyroscope experiment (Ref. 26). This satellite has two basic differences from other satellites with respect to attitude control considerations. First, the drag-free feature implies that the spinning satellite is translationally controlled by means of gas jets to keep the spinning proof mass (the gyroscope) centered within its central cavity. The jet forces give rise to the existence of pulse torques (which would not normally be present) acting upon the satellite.

The second unique feature of this drag-free satellite is that it has two optical instruments which can be used to determine attitude error. A precision stellar monitor is mounted on the end of the satellite so that the monitor's optically sensitive axis is nominally aligned with the satellite spin axis. An autocollimator is similarly located on the interior wall of the satellite to monitor the rotor spin axis. The autocollimator's optically sensitive axis is also nominally aligned with the satellite spin axis and thus detects the angular position of an optical flat ground on the rotor's maximum axis. (This requires that the rotor spin axis be nearly aligned with the satellite spin axis.) Both the stellar monitor and autocollimator have four-quadrant sensitive optical heads so that cartesian measurements of the angular positions of the star image and rotor spin axis can be made.

The reference star is nominally in the plane of the polar orbit so the nominal position of the spacecraft spin axis lies in the orbit plane. It is initially assumed that perfect measurement of the position of a reference point on the celestial sphere (either from the stellar monitor or autocollimator) is constantly available for providing pointing error measurements to the satellite. The attitude error measurement device will be known as the "star tracker."

As in Chapter III, it is desired that the satellite's spin speed remain nearly constant. Spin speed can be monitored from the oscillating readings of a magnetometer measuring the lateral component of the magnetic field.

THE OBSERVABILITY OF DISTURBANCE TORQUES

With the assumption that the spacecraft has a constant spin speed $\dot{\psi}$, the rotational equations of motion are described as in Eqs. (2.27), repeated here:

$$\begin{bmatrix} \dot{\omega}_x \\ \dot{\omega}_y \\ \dot{\gamma}_x \\ \dot{\gamma}_y \end{bmatrix} = \begin{bmatrix} 0 & -a_s\psi & 0 & 0 \\ a_s\dot{\psi} & 0 & 0 & 0 \\ 1 & 0 & 0 & \dot{\psi} \\ 0 & 1 & -\dot{\psi} & 0 \end{bmatrix} \begin{bmatrix} \omega_x \\ \omega_y \\ \gamma_x \\ \gamma_y \end{bmatrix} + \frac{I}{I_{xx}} \begin{bmatrix} 1 & 0 \\ 0 & 1 \\ 0 & 0 \\ 0 & 0 \end{bmatrix} \begin{bmatrix} T_x \\ T_y \end{bmatrix}, \tag{4.1}$$

where again

ω_x, ω_y = lateral axes x and y components of the angular velocity of the spacecraft about its center of mass,

γ_x, γ_y = body-fixed orthogonal components of the star image's (or gyro optical axis) misalignment error,

a_s = moment of inertia ratio $(I_{zz} - I_{xx})/I_{xx}$,

T_x, T_y = torque acting upon the spacecraft about its $\hat{x}_B$ and $\hat{y}_B$ axes.

In this ideal situation, if the applied torque $(T_x \hat{x}_B + T_y \hat{y}_B)$ is strictly a control torque which is a function of the states, then the pointing error can be made arbitrarily small. However, it is known that the spacecraft will be exposed to disturbance torques which are dependent upon the environment. These disturbances will cause deviation from the nominal attitude if they are not taken into account.

The disturbance torques which are of immediate concern include those classified as inertially-fixed, body-fixed, and spin torque, and those due to misaligned thrusters used for translational control purposes. The development of models for the first three torques was the subject of the final section of Chapter 2. The latter torque can be thought of as an inertially-fixed and spin torque in the average sense, as explained in Chapter 2. However, thruster torques can more correctly be classified as short-period, body-fixed, and spin disturbances. Exactly how these pulse torques can be treated will be investigated in this section.

The inertially-fixed and body-fixed torques acting on the spacecraft do not have constant magnitude as is evident from Figures 2.11 - 2.12. Rather, they can be characterized by their derivatives being random forcing functions which tend to change the magnitudes. In the body-fixed frame the derivatives of the body fixed torques are

$$\dot{T}_{Bx} = v_1 \ , \tag{4.2a}$$

$$\dot{T}_{By} = v_2 \ . \tag{4.2b}$$

Here, v_1 and v_2 represent random changes. For the inertially-fixed torque having components T_{*x} and T_{*y}, the transformation to the body frame produces components

$$T_{Ix} = T_{*x} \cos \psi + T_{*y} \sin \psi \ , \tag{4.3a}$$

$$T_{Iy} = -T_{*x} \cos \psi + T_{*y} \cos \psi \ . \tag{4.3b}$$

Taking the derivative of Equations (4.3) produces

$$\dot{T}_{Ix} = \dot{\psi} \, T_{Iy} + v_3 \ , \tag{4.4a}$$

$$\dot{T}_{Iy} = -\dot{\psi} \, T_{Ix} + v_4 \ , \tag{4.4b}$$

where v_3 and v_4 represent further random change.

It is desirable to be able to measure the disturbances T_{Bx}, T_{By}, T_{Ix}, and T_{Iy}. If their magnitude is known, corrective control torque can be applied to cancel them. Incorporating Eqs. (4.2) and (4.4) into (4.1) produces the state equations

$$\begin{bmatrix} \dot{T}_{Bx} \\ \dot{T}_{By} \\ \dot{T}_{Ix} \\ \dot{T}_{Iy} \\ \dot{\omega}_x \\ \dot{\omega}_y \\ \dot{\gamma}_x \\ \dot{\gamma}_y \end{bmatrix} = \begin{bmatrix} 0 & 0 & 0 & 0 & 0 & 0 & 0 & 0 \\ 0 & 0 & 0 & 0 & 0 & 0 & 0 & 0 \\ 0 & 0 & 0 & \dot{\psi} & 0 & 0 & 0 & 0 \\ 0 & 0 & -\dot{\psi} & 0 & 0 & 0 & 0 & 0 \\ 1 & 0 & 1 & 0 & 0 & 0 & -a_s\psi & 0 \\ 0 & 1 & 0 & 1 & a_s\dot{\psi} & 0 & 0 & 0 \\ 0 & 0 & 0 & 0 & 1 & 0 & 0 & \dot{\psi} \\ 0 & 0 & 0 & 0 & 0 & -\dot{\psi} & 1 & 0 \end{bmatrix} \begin{bmatrix} T_{Bx} \\ T_{By} \\ T_{Ix} \\ T_{Iy} \\ \omega_x \\ \omega_y \\ \gamma_x \\ \gamma_y \end{bmatrix} + \begin{bmatrix} v_1 \\ v_2 \\ v_3 \\ v_4 \\ T_{cx} \\ T_{cy} \\ 0 \\ 0 \end{bmatrix} . \tag{4.5}$$

Here, T_{cx} and T_{cy} represent the applied control torque components which are functions of the states. In compact notation, Eq. (4.5) can be expressed as

$$\dot{\vec{x}} = F\vec{x} + G\vec{u} + D\vec{v}, \tag{4.6}$$

where $\vec{u}$ is the applied control torque and $\vec{v}$ the random change to the disturbance torque magnitude.

The distribution matrix G has the form

$$G \triangleq \begin{bmatrix} 0 & 0 \\ 0 & 0 \\ 0 & 0 \\ 0 & 0 \\ 1 & 0 \\ 0 & 1 \\ 0 & 0 \\ 0 & 0 \end{bmatrix}.$$

The quantities measured by the star tracker and available to base the control law upon are γ_x and γ_y. The observation equation is

$$\vec{y} = H\vec{x} + \vec{w}$$

where $\vec{w}$ represents measurement noise, $\vec{y}^T = [\gamma_x, \gamma_y]$ and

$$H \triangleq \begin{bmatrix} 0 & 0 & 0 & 0 & 0 & 0 & 1 & 0 \\ 0 & 0 & 0 & 0 & 0 & 0 & 0 & 1 \end{bmatrix}.$$

It can be shown that (H,F) form an observable set. Thus, a Wiener filter or an observer with arbitrary dynamics can be built which will give estimates of the eight state components. The pair (F,G) does not form a controllable set, however. This is obvious because there is no physical way of removing disturbance torques.

Although disturbance torques cannot be removed (at least not completely), their effect can be cancelled by the proper application of control torque. Thus, it is desirable to form estimates of the disturbance torque magnitudes. This torque estimation is a logical extension of an observer which is required for measuring rates ω_x and ω_y needed in the control law.

The Gopinath Reduced-Order Observer for Noncyclic Systems

As mentioned above, estimates of the unknown elements of the state vector can be produced by either a Wiener filter or an observer. The Wiener filter is identically the steady-state solution to the Kalman filter described in Chapter 3, and is useful in the presence of Gaussian driving and measurement noise. It is initially assumed here that the noise vectors $\vec{v}$ and $\vec{w}$ are negligible, so that this filter mechanization represents undue complication. The effect of this assumption will be considered later in the error-analysis section.

With the star-tracker variables representing very clean measurements of the attitude error, it becomes feasible to employ a reduced-order observer to estimate the rates ω_x and ω_y and the disturbance torque magnitudes. A recently developed mechanization of such an observer was formulated by Gopinath and is outlined in Appendix D. Gopinath's formulation requires that the system's equations be cyclic (or controllable so that they can be made cyclic). Equations (4.5) are neither controllable nor cyclic so an extension of Gopinath's method is required to handle this case.

The general state equations

$$\dot{\vec{x}} = F\vec{x} + G\vec{u} ,$$
$$\vec{y} = H\vec{x} , \tag{4.7}$$

are considered. Here, the dimensions of x, u, y, F, G, and H are $n \times 1$, $r \times 1$, $m \times 1$, $n \times n$, $n \times r$ and $m \times n$ respectively. As is seen in Appendix D, Gopinath's method for producing an observer with arbitrary dynamics for Eqs. (4.6) is a specialization of the general method using

canonical forms. Thus, for F noncyclic and the pair (F,G) not controllable, it is necessary to follow a procedure similar to the one required to produce the canonical-form observer. This procedure is dependent upon the following corollary which is derived from the theorems presented in Appendix D.

Corollary 4.1. Let F be similar to an $n \times n$ Jordan matrix J and let p be the maximum number of Jordon chains in which each one of the individual eigenvalues of F appears. Then if (F,H) is observable, the pair (F,CH) is almost surely observable where C is a $p \times m$ matrix $(p \leq m)$ made up of arbitrary elements.

Proof.

The Jordan matrix J can be rearranged by a simple transformation into p diagonal subblocks so that the Jordan chains making up each subblock have no individual eigenvalue appearing in more than one chain. By the definition of cyclicity, each of these subblocks defines a cyclic subspace. At least one scalar output must emanate from each of the subblocks because the overall system (F,H) is observable. Multiple outputs come from some of the subblocks when $m > p$. These multiple outputs can be combined into a single output which renders the associated subblock observable by Theorem D.1. Thus, the original $m \times 1$ system output vector can be transformed into a $p \times 1$ output vector which also produces observability. The p individual components of the output vector can be transformed into p independent combinations which again yields an observable system. Thus, any $p \times m$ matrix C which combines with H to produce a $p \times 1$ output vector whose elements are independent combinations of the outputs from the p cyclic subblocks renders (F,CH) observable. The basic requirement is that C have rank p. This will almost surely occur if the elements of C are arbitrarily chosen. ∎

This corollary suggests a systematic way for creating a state estimator with arbitrary dynamics for an observable, noncyclic, noncontrollable system. The method consists of following the general procedure

outlined in Appendix D which utilizes canonical forms except when forming the M_1 matrix. Instead of using individual rows of H successively with F to create M_1, one can generate p arbitrary $m \times 1$ matrices c_i. Then, each of the p row vectors $c_i^T H$ (which make up CH) is sequentially used to generate the n independent rows of M_1.

Because the index p is usually unknown without transforming to Jordan form (which is to be avoided), the process actually consists of generating random vectors c_i and using them until a satisfactory matrix M_1 is formed. This procedure can be repeated twice with different sets of c_i's to insure that the minimum index p has been found.

This procedure can be utilized for constructing the Gopinath reduced-order observer to insure that the minimum number of output combinations are used to generate estimates of the unknown elements of the state vector. The modified Gopinath reduced-order observer is now demonstrated.

Application to the Star Tracker Satellite

In this subsection, the Gopinath procedure is applied in two ways to generate a state observer with arbitrary dynamics. The first application employs the modification suggested previously for handling the noncyclicity of the F matrix. The second approach utilizes the fact that the system equations possess complex symmetry. The resulting complex system is cyclic so that the process of generating the reduced-order observer can be applied directly in its original form. The modified observer is now discussed.

Following the procedure outlined in Appendix D, the state vector $\vec{x}$ is partitioned as

$$x = \begin{bmatrix} x_1 \\ --- \\ x_2 \end{bmatrix},$$

where x_1 represents the directly observable p elements of x. Then F and G are partitioned as

$$F = \left[\begin{array}{c|c} F_{11} & F_{12} \\ \hline F_{21} & F_{22} \end{array}\right] \begin{matrix} p \\ n-p \end{matrix} ,$$

$$G = \left[\begin{array}{c} G_1 \\ \hline G_2 \end{array}\right] \begin{matrix} p \\ n-p \end{matrix} .$$

Rearranging and partitioning Eqs. (4.4) in this way and exclusing the noise, yields

$$\left[\begin{array}{c} \dot{\gamma}_y \\ \dot{\gamma}_x \\ \hline \dot{\omega}_y \\ \dot{\omega}_x \\ \dot{T}_{Iy} \\ \dot{T}_{Ix} \\ \dot{T}_{By} \\ \dot{T}_{Bx} \end{array}\right] = \left[\begin{array}{cc|cccccc} 0 & -\dot{\psi} & 1 & 0 & 0 & 0 & 0 & 0 \\ \dot{\psi} & 0 & 0 & 1 & 0 & 0 & 0 & 0 \\ \hline 0 & 0 & 0 & a_s\dot{\psi} & 1 & 0 & 1 & 0 \\ 0 & 0 & -a_s\psi & 0 & 0 & 1 & 0 & 1 \\ 0 & 0 & 0 & 0 & 0 & -\dot{\psi} & 0 & 0 \\ 0 & 0 & 0 & 0 & \dot{\psi} & 0 & 0 & 0 \\ 0 & 0 & 0 & 0 & 0 & 0 & 0 & 0 \\ 0 & 0 & 0 & 0 & 0 & 0 & 0 & 0 \end{array}\right] \left[\begin{array}{c} \gamma_y \\ \gamma_x \\ \hline \omega_y \\ \omega_x \\ T_{Iy} \\ T_{Ix} \\ T_{By} \\ T_{Bx} \end{array}\right] + \left[\begin{array}{cc} 0 & 0 \\ 0 & 0 \\ \hline 0 & 1 \\ 1 & 0 \\ 0 & 0 \\ 0 & 0 \\ 0 & 0 \\ 0 & 0 \end{array}\right] \left[\begin{array}{c} T_{cy} \\ T_{cx} \end{array}\right] , \tag{4.8}$$

$$\left[\begin{array}{c} \gamma_y \\ \gamma_x \end{array}\right]_{\text{observed}} = \left[\begin{array}{cccccccc} 1 & 0 & 0 & 0 & 0 & 0 & 0 & 0 \\ 0 & 1 & 0 & 0 & 0 & 0 & 0 & 0 \end{array}\right] [x] .$$

Because (F,H) is observable, (F_{22},F_{12}) is observable by Theorem D.5. The submatrix F_{22} is not cyclic, however, because of the last two rows of zeroes. Thus, two independent output combinations of γ_x, γ_y are necessary to form an observable set.

The simplest matrix C that can be used to form the reduced-order observer in this case is the 2×2 identity matrix. Thus, the M_1 matrix (of Appendix D) is formulated by using both rows of the H matrix.*

As an example, use $\dot{\psi} = 1$ and $a_s = 0.5$ in Eqs. (4.8). This produces

$$M_1 = \begin{bmatrix} 1. & 0 & 0 & 0 & 0 & 0 \\ 0 & .5 & 1. & 0 & 1. & 0 \\ -.25 & 0 & 0 & -.5 & 0 & .5 \\ 0 & -.125 & -.75 & 0 & -.25 & 0 \\ .0625 & 0 & 0 & .625 & 0 & -.125 \\ 0 & 1. & 0 & 0 & 0 & 0 \end{bmatrix} \begin{matrix} \leftarrow \text{1st row of } H \\ \\ \\ \\ \\ \leftarrow \text{2nd row of } H. \end{matrix}$$

The characteristic equation of F_{22} can be found by transforming the matrix to canonical form as is indicated in Appendix D. This is

$$F_1 = M_1 F_{22} M_1^{-1} = \left[\begin{array}{ccccc:c} 0 & 1. & 0 & 0 & 0 & 0 \\ 0 & 0 & 1. & 0 & 0 & 0 \\ 0 & 0 & 0 & 1. & 0 & 0 \\ 0 & 0 & 0 & 0 & 1. & 0 \\ 0 & -.25 & 0 & -1.25 & 0 & 0 \\ \hdashline 0 & 0 & 3. & 0 & 4. & 0 \end{array}\right].$$

Thus, F_{22} has the characteristic equation

$$(s^5 + 1.25\, s^3 + 0.25\, s)(s) = 0$$

If the gain matrix K of Appendix D is of the form

*The satellite example used here does not illustrate the full potential available from the extension of the Gopinath observer stated in Corollary 4.1. No more illustrative example was contrived, however, for the sake of maintaining subject unity.

$$K = \begin{bmatrix} k_1 & 0 \\ k_2 & 0 \\ k_3 & 0 \\ k_4 & 0 \\ k_5 & 0 \\ 0 & k_6 \end{bmatrix},$$

the observer will have the characteristic equation

$$\left[s^5 + k_1 s^4 + (k_2 + 1.25)s^3 + k_3 s^2 + (k_4 + 0.25)s + k_5\right](s + k_6) = 0 .$$

For a desired characteristic equation $(s + 1)^6 = 0$, K becomes

$$K = \begin{bmatrix} 5. & 0 \\ 8.75 & 0 \\ 10. & 0 \\ 4.75 & 0 \\ 1.0 & 0 \\ 0 & 1.0 \end{bmatrix},$$

and the matrix L of (F-LH) is equal to

$$L = M_1^{-1} A^{-1} K = \begin{bmatrix} 5. & 0 \\ 0 & 1. \\ 8. & 0 \\ -8. & 0 \\ 0.75 & -0.5 \\ 2. & 0 \end{bmatrix}.$$

Here, A is formed by inspection from F_1 and is

$$A = \left[\begin{array}{cccccc:c} 1. & 0 & 0 & 0 & 0 & 0 \\ 0 & 1 & 0 & 0 & 0 & 0 \\ 1.25 & 0 & 1. & 0 & 0 & 0 \\ 0 & 1.25 & 0 & 1. & 0 & 0 \\ 0.25 & 0 & 1.25 & 0 & 1 & 0 \\ \hdashline 0 & 0 & 0 & 0 & 0 & 1. \end{array}\right] .$$

The matrix A^{-1} can be formed by inspection from the A matrix.

The second method of forming the reduced-order observer is now discussed. The problem that F_{22} is noncyclic can be circumvented by recognizing that the system equations have complex symmetry. Thus, Eqs. (4.5) can be reformulated in complex form as

$$\left[\begin{array}{c} \dot{\gamma} \\ \hdashline \dot{\omega} \\ \dot{T}_I \\ \dot{T}_B \end{array}\right] = \left[\begin{array}{c:ccc} -j\dot{\psi} & 1. & 0 & 0 \\ \hdashline 0 & ja_s\dot{\psi} & 1. & 1. \\ 0 & 0 & -j\dot{\psi} & 0 \\ 0 & 0 & 0 & 0 \end{array}\right] \left[\begin{array}{c} \gamma \\ \hdashline \omega \\ T_I \\ T_B \end{array}\right] + \left[\begin{array}{c} 0 \\ \hdashline 1. \\ 0 \\ 0 \end{array}\right] [T] ,$$

$$\left[\gamma_{observed}\right] = \left[1. \quad 0 \quad 0 \quad 0\right] [x] .$$

Here, the matrix M_1 becomes

$$M_1 = \left[\begin{array}{ccc} 1. & 0 & 0 \\ ja_s\dot{\psi} & 1. & 1. \\ -(a_s\dot{\psi})^2 & j\dot{\psi}(a_s-1) & ja_s\dot{\psi} \end{array}\right] .$$

The characteristic equation of F_{22} is

$$s^3 + j\dot{\psi}(1-a_s)s^2 + a_s\dot{\psi}^2 s = 0 .$$

The A matrix is therefore

$$A = \begin{bmatrix} 1 & 0 & 0 \\ j\dot{\psi}(1-a_s) & 1. & 0 \\ a_s\dot{\psi}^2 & j\dot{\psi}(1-a_s) & 1. \end{bmatrix} .$$

If the desired characteristic equation of $F_{22} - LF_{12}$ is

$$s^3 + b_1 s^2 + b_2 s + b_3 = 0 ,$$

L is found by

$$L = M_1^{-1} A^{-1} K ,$$

$$= \begin{bmatrix} 1. & 0 & 0 \\ 0 & a_s & j/\dot{\psi} \\ -ja_s\dot{\psi} & 1.-a_s & -j/\dot{\psi} \end{bmatrix} \begin{bmatrix} 1. & 0 & 0 \\ -j\dot{\psi}(1.-a_s) & 1. & 0 \\ -\dot{\psi}^2(1.-a_s+a_s^2) & -j\dot{\psi}(1.-a_s) & 1. \end{bmatrix} \begin{bmatrix} b_1 - j\dot{\psi}(1.-a_s) \\ b_2 - a_s\dot{\psi}^2 \\ b_3 \end{bmatrix} .$$

With $L^T = [\ell_1, \ell_2, \ell_3]$, the complex reduced-order observer for the star-tracking spacecraft studied here is depicted in Figure 4.1. Either this complex reduced-order observer or the modified observer discussed previously will produce estimates of the vehicle rates and disturbance torques with arbitrary dynamics.

The reduced-order observer generally yields a system which is simpler to mechanize than one of full order. The modified Gopinath observer developed above reduces the total number of outputs utilized from a multi-dimensional output system to that minimum number which still produces an observer for obtaining the unmeasurable states.

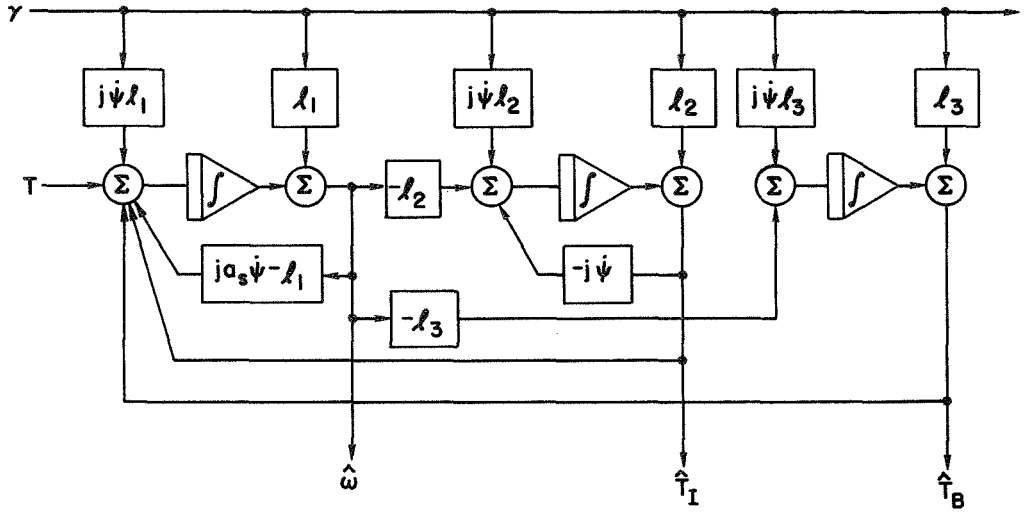

FIG. 4.1. COMPLEX REDUCED-ORDER OBSERVER FOR A SATELLITE EMPLOYING A STAR TRACKER FOR ATTITUDE ERROR MEASUREMENT.

The Observation of Misaligned Thruster Torques

The previous subsection demonstrated two ways in which a reduced order observer could be used to generate estimates of the unknown body-fixed and inertially-fixed disturbance torques acting upon the satellite. Inherent in the observer construction was the fact that the magnitudes of these torques were slowly changing with respect to time. For the case of the drag free satellite with gas jet translational control, the existence of pulse torques associated with each jet firing must be taken into account.

Assume that the spinning satellite is cylindrical in shape and has six jets to control its translational motion. Assume that four of these jets are on the perimeter of the cylindrical surface, 90° apart, and in the plane containing the nominal center of mass. The other two jets are on each end. These jets are considered to be mounted on the body axes $\hat{x}_B$, $\hat{y}_B$, and $\hat{z}_B$ defined before.

Misalignment of the four jets on the cylinders produces pulse torques that have both a body-fixed portion and spin portion. The jet on the end of the $\hat{y}_B$ axis produces a torque about the $\hat{x}_B$ axis. The two jets mounted on the satellite ends can produce torque components about both the $\hat{x}_B$ and $\hat{y}_B$ axes. The magnitude of these jet-produced torques

will vary slowly with time if the center of mass of the satellite shifts due to gas usage.

The pulse torques cannot be followed by the observer as developed to this point because of the short length of time (less than 0.1 second) a typical jet firing lasts. What actually occurs is that the average torque produced by these jets tends to be in a constant orientation with respect to the translational motion of the satellite in its orbit. Thus, as discussed in Chapter II, these pulse torques are observed in the average sense as an inertially-fixed torque.

A natural question at this time is whether the observer utilized can be modified to produce a more precise estimate of the pulse torques when they occur. An electric signal is available when each gas jet is fired and can be utilized by the observer as additional information.

To answer the question, consider an analogous system consisting of a double integrator plant driven by an input with two levels of magnitude. If one observes the output and knows at what times the magnitude-changes to the input occur, it is certainly possible to determine these magnitudes precisely. It therefore seems reasonable that one could predict the individual pulse magnitudes--i.e., the total inpulse--caused by each of the six gas jets.

Consider now the short term response of the satellites acted upon only by an occasional pulse torque. From Eqs. (4.1) the response of the variable γ_x to a body-fixed torque T_{xo} is

$$\gamma_x(t) = \gamma_{xo} \cos \dot{\psi}t + \gamma_{yo} \sin \dot{\psi}t + \frac{(\omega_{xo} + T_{xo}/I_{xx})}{\dot{\psi}(a_s + 1)} (\sin a_s \dot{\psi}t + \sin \dot{\psi}t)$$

$$+ \frac{\omega_{yo}}{\dot{\psi}(a_s + 1)} (\cos a_s \dot{\psi}t - \cos \dot{\psi}t) , \qquad (4.9)$$

where ω_{xo}, ω_{yo}, γ_{xo}, and γ_{yo} are initial conditions. Thus for the jet responsible for T_{xo} on for Δt_1 seconds, the new value of γ_x from (4.9) at the end of the pulse is approximately

$$\gamma_{x1} \cong \gamma_{xo} + \gamma_{yo}\dot{\psi}\Delta t_1 + (\omega_{xo} + T_{xo}/I_{xx})\,\Delta t_1 \ . \qquad (4.10a)$$

Similarly,

$$\omega_{x1} \cong \omega_{xo} - (a_s\dot{\psi}\omega_{yo} - T_{xo}/I_{xx})\,\Delta t_1 \ , \qquad (4.10b)$$

$$\gamma_{y1} \cong \gamma_{yo} - \gamma_{xo}\dot{\psi}\Delta t_1 + \omega_{yo}\,\Delta t_1 \ . \qquad (4.10c)$$

The value of γ_x at a time Δt_2 seconds later (where Δt_2 is again small) with no torque T_{xo} is

$$\gamma_{x2} \cong \gamma_{x1} + \gamma_{y1}\dot{\psi}\,\Delta t_2 + \omega_{x1}\,\Delta t_2 \ ,$$

or from Eqs. (4.10)

$$\gamma_{x2} \cong \gamma_{xo} + \gamma_{yo}\dot{\psi}(\Delta t_1 + \Delta t_2) + \omega_{xo}(\Delta t_1 + \Delta t_2) + \frac{T_{xo}}{I_{xx}}\Delta t_1 \ . \qquad (4.11)$$

Thus, the magnitude of the pulse T_{xo} is approximately

$$T_{xo} \cong I_{xx}\left[\gamma_{x2} - \gamma_{xo} - (\gamma_{yo}\dot{\psi} + \omega_{xo})\Delta t_3\right]\Big/\Delta t_1 \ . \qquad (4.12)$$

Similarly,

$$T_{yo} \cong I_{xx}\left[\gamma_{y2} - \gamma_{yo} + (\gamma_{xo}\dot{\psi} - \omega_{yo})\Delta t_3\right]\Big/\Delta t_1 \ , \qquad (4.13)$$

where $\Delta t_3 = (\Delta t_1 + \Delta t_2)$.

Equations (4.12, 4.13) suggest that the observer utilized to estimate the other states may be adapted to estimate pulse torques recursively. By sampling the values of γ_x, γ_y, $\hat{\omega}_x$, and $\hat{\omega}_y$ at the beginning of a pulse and at some increment of time Δt_2 after the pulse, pulse torque estimates can be updated from the equations

$$\hat{T}_{xo} = \hat{T}_{xo} + K_{pu}\left[\gamma_x - \gamma_{xo} - \Delta t_3(\dot{\psi}\gamma_{yo} + \hat{\omega}_{xo})\right] ,$$

$$\hat{T}_{yo} = \hat{T}_{yo} + K_{pu}\left[\gamma_y - \gamma_{yo} + \Delta t_3(\dot{\psi}\gamma_{xo} - \hat{\omega}_{yo})\right] . \qquad (4.14)$$

Here, variations in the pulse length Δt_1 are neglected. The gain K_{pu} is chosen so that the pulse estimates converge at a convenient rate. This mechanization requires some circuit logic on the spacecraft which should pose no special problem. The validity of using Eqs. (4.14) for pulse torque estimation is demonstrated in the next section.

THE ATTITUDE AND SPIN SPEED CONTROL OF THE SATELLITE

In Reference 61, a general technique utilizing frequency and complex symmetry properties is developed and demonstrated for synthesizing the attitude control law for spinning symmetric vehicles. This technique enables the designer to give a spinning satellite without disturbance torques arbitrary dynamic response. When the sensor that detects pointing error consists of a star tracker aligned with the spin axis, an observer is used to obtain estimates of the vehicle body rates $\hat{\omega}_x$ and $\hat{\omega}_y$. Then, the continuous control law applied to the body-fixed axes is (in complex notation)

$$T_c = -K_v\hat{\omega} - (K_p - j0.5(I_{zz}/I_{xx})\dot{\psi}K_v)\ \gamma , \qquad (4.15)$$

or in real form

$$T_{cx} = -K_v\hat{\omega}_x - K_p\gamma_x - 0.5(I_{zz}/I_{xx})\dot{\psi}K_v\gamma_y ,$$

$$T_{cy} = -K_v\hat{\omega}_y - K_p\gamma_y + 0.5(I_{zz}/I_{xx})\dot{\psi}K_v\gamma_x . \qquad (4.16)$$

The gains K_v and K_p are chosen to produce arbitrary response from the harmonic oscillator equation (which represents the fourth-order plant uncoupled into two second-order equations),

$$\ddot{\mu}_1 + K_v\dot{\mu}_1 + \left[K_p + 0.25(I_{zz}\dot{\psi}/I_{xx})^2\right]\mu_1 = 0 \ .$$

They can also be chosen to minimize the control system power as was done in Chapter III.

The attitude error angle $\Gamma_1 \triangleq \gamma e^{j\dot{\psi}t}$ is driven to zero by application of Eqs. (4.16) when no disturbance torques are present. However, in the presence of inertially-fixed and body-fixed torques T_I and T_B, the steady state value of Γ_1 becomes

$$\Gamma_1(t) = \frac{T_B\, e^{j\dot{\psi}t}}{\left[\omega_n + j\dot{\psi}(1-0.5R_s)\right]^2} + \frac{T_I}{\left[-\omega_n + j0.5R_s\dot{\psi}\right]^2} \ ,$$

where

$$\omega_n^2 \triangleq K_p + (R_s\dot{\psi})^2/4$$

$$K_v = 2\omega_n \ ,$$

$$R_s = I_{zz}/I_{xx} \ .$$

The complex error angle $\Gamma_1(t)$ can be made quite small for large K_p but this is not always practical.

A modification of the control law is to estimate directly by means of observer mechanization, the disturbance torques. Because the rate terms ω_x and ω_y probably will be estimated anyway (rather than using some rate detection device like a gyro), the addition of necessary electronics for disturbance-torque estimation seems to be a reasonable supplementary requirement. Then, the complex control law of Eq. (4.15) is modified to

$$\boxed{T_c = -K_v\hat{\omega} - (K_p - j0.5R_s\dot{\psi}K_v)\gamma - \hat{T}_I - \hat{T}_B \ ,} \qquad (4.17)$$

where $\hat{T}_I$ and $\hat{T}_B$ are the complex estimates of the inertially-fixed and body-fixed disturbances. In addition, the estimated pulse torque also can be cancelled by an opposite control-torque pulse at the appropriate time. Equation (4.17) constitutes a new control law.

An alternate modification to the control law which is discussed in Ref. 61 is to introduce an integral feedback term that would offset the undesired torques without steady-state error. The integral control modifies Eq. (4.15) to

$$T_c(s) = -K_v\hat{\omega}(s) - (K_p - j0.5R_s\dot{\psi}K_v + \frac{K_{IB}}{s} + \frac{K_{II}}{s + j\dot{\psi}}\gamma(s) \quad (4.18)$$

in the complex frequency domain. Here, the gains K_{IB} and K_{II} are chosen to produce the desired error-removal rate. The constant K_{II} is complex, so this portion of the controller must be mechanized as two constants. In addition, if continuous control torque is not always fully available (as in the case of magnetic control), a means must be provided for limiting the integral portion of the controller to prevent amplifier saturation.

The controller based upon Eq. (4.17) seems to have two advantages over the integral-type controller. They are:

1. No choice of gains K_{IB} and K_{II} need be made by the designer. The response for providing the control torque to cancel the disturbance torques is established with the choice of observer dynamics.
2. If full control T_c cannot be provided, this is accounted for in the observer mechanization. Thus, values of disturbance-torque estimates are not affected.

The equations of motion for the system under consideration, the development of a state observer, and the provision of a continuous controller governed by Eq. (4.17) are all based upon the assumption that the spin speed $\dot{\psi}$ is a constant. Both environmental torques and those due to translation and attitude control of the satellite will cause the spin speed to deviate from the nominal value $\dot{\psi}_o$. If one applies the control torque

$$T_{cz} = -K_z \operatorname{sgn}(\dot{\psi} - \dot{\psi}_o) \quad (4.19)$$

about the spin axis for $|\dot{\psi} - \dot{\psi}_o|$ exceeding some deadband value, the spin speed can be kept within the desired accuracy limits. The limit is chosen so that the observer and controller mechanizations are not affected adversely by spin-speed deviation.

As a means of determining the performance capabilities of the reduced-order observer, the pulse estimator, and the modified control law, a digital simulation was used. This simulation assumed perfect measurements of the star-tracker variables. It was also assumed at this point that the magnitude of the spin speed was nominal and the magnitudes of the disturbance torque components were constant.

A two-dimensional model of the translational controller was used to create a time history of the pulse torques. In other words, it was assumed that the satellite was moving in the plane of the $\hat{x}_*$, $\hat{y}_*$ axes so that only the four jets on the cylinder were firing regularly.

The equations of motion and translational control synthesis for the spinning drag-free satellite were derived by Lange (Ref. 26). In the body-fixed frame, the two dimensional translation equations are

$$\ddot{x} - \dot{\psi}^2 x - 2\dot{\psi}\dot{y} = D_r \cos \dot{\psi}t + F_{cx} ,$$

$$\ddot{y} - \dot{\psi}^2 y + 2\dot{\psi}\dot{x} = -D_r \sin \dot{\psi}t + F_{cy} ,$$

where D_r is the drag magnitude, $\dot{\psi}$ is the spin rate, F_{cx} and F_{cy} are the control forces, and x and y are body-fixed measurements of the distance from the satellite reference point to the proof mass (gyro rotor). The control law used to regulate the satellite's translational motion to follow the proof mass is

$$F_{cx} = -K_{v1}\left[\dot{x} - \dot{\psi}y + k_2 x\right] ,$$

$$F_{cy} = -K_{v1}\left[\dot{y} + \dot{\psi}x + k_2 y\right] . \qquad (4.20)$$

This stable linear control can be approximated by a pulse-width, pulse-frequency gas jet control preceded by a deadband. A schematic representation of this controller is illustrated in Figure 3.2 and was included as part of the simulation.

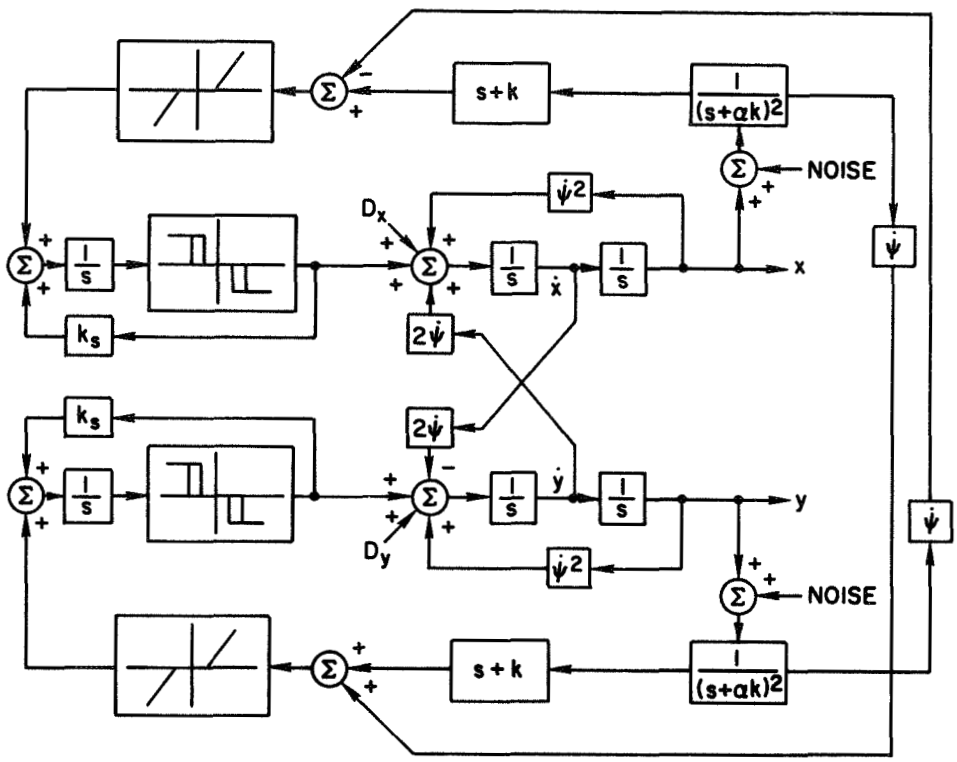

FIG. 4.2. SCHEMATIC OF THE TRANSLATIONAL CONTROL OF A SPINNING SATELLITE EMPLOYING THE PULSE-WIDTH, PULSE-FREQUENCY CONTROLLER.

When the positive x threshold is crossed, the jet at the end of the positive $\hat{x}_B$ axis of the vehicle fires. Similarly, when the minus x threshold is crossed, the negative $\hat{x}_B$ axis jet fires. These both produce pulse torque about the $\hat{y}_B$ axis.

Example results of using this simulation are shown in Figures 4.3 and 4.4. Figure 4.3 illustrates the steady state response of the attitude control system with the reduced-order observer but no pulse estimator. Figure 4.4 has the same pulse torques with the pulse estimator

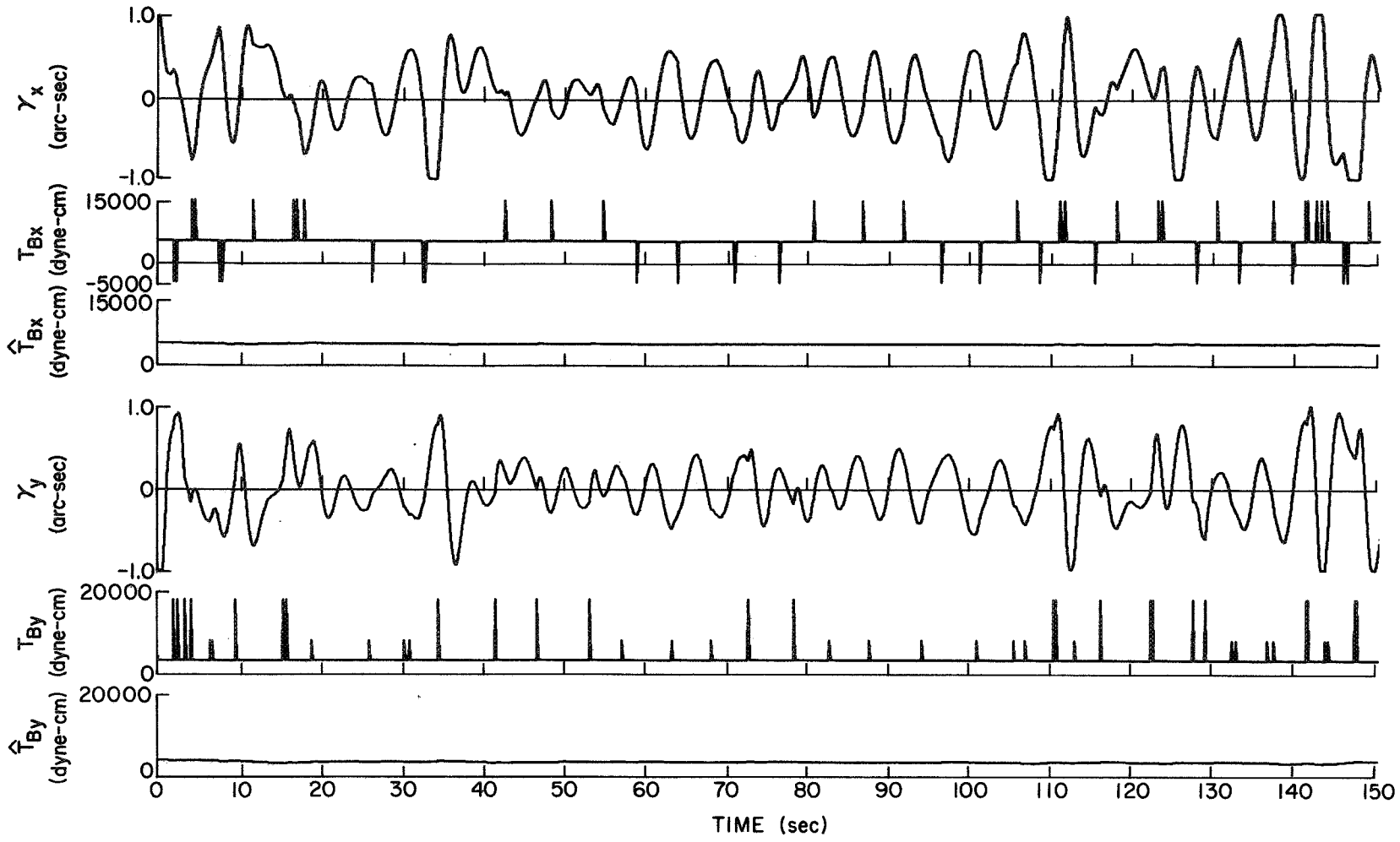

FIG. 4.3. RESPONSE OF STAR-TRACKER VARIABLES WITH NO PULSE-TORQUE ESTIMATION. Also shown are the body-fixed torques and their estimates.

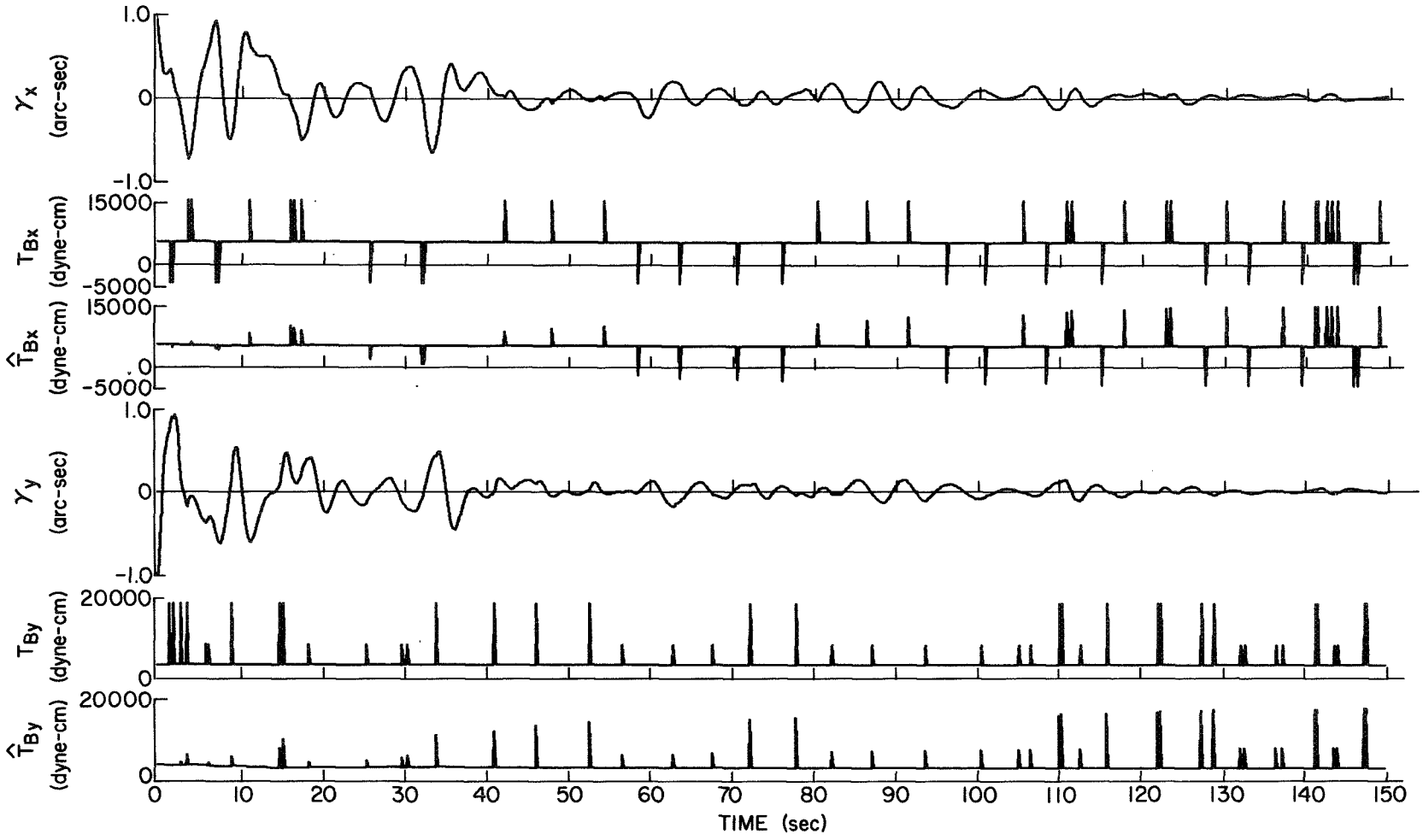

FIG. 4.4. RESPONSE OF STAR-TRACKER VARIABLES WITH PULSE-TORQUE ESTIMATION. Again, the body-fixed torques and their estimation are illustrated.

in operation. Gains used by the observer gave it the characteristic equation $(s + 1)^6 = 0$. The attitude control law [Eq. (4.18)] used with no pulse estimator was

$$T_{cx} = -\hat{\omega}_x - \gamma_x - 0.75\ \gamma_y - \hat{T}_{Bx} - \hat{T}_{Ix}\ \sec^{-2}\ ,$$

$$T_{cy} = -\hat{\omega}_y - \gamma_y + 0.75\ \gamma_x - \hat{T}_{By} - \hat{T}_{Iy}\ \sec^{-2}\ , \qquad (4.21)$$

with $\dot{\psi} = 1$ rad/sec and $(I_{zz}/I_{xx}) = 1.5$. When using the pulse estimator, the gain K_{pu} and time lag Δt_3 of Eq. (4.14) were

$$K_{pu} = 300\ \text{kg-m}\ ,$$

$$\Delta t_3 = 0.2\ \text{sec.}$$

The values of the disturbance torques used were

$$T_{Bx} = 5. \times 10^{-4}\ \text{N-m}\ ,$$

$$T_{By} = 3. \times 10^{-4}\ \text{N-m}\ ,$$

$$T_{*x} = 2.2 \times 10^{-5}\ \text{N-m}\ ,$$

$$T_{*y} = -0.3 \times 10^{-5}\ \text{N-m.}$$

The pulse torques were

$$T_{x+} = -10^{-3}\ \text{N-m}\ ,$$

$$T_{x-} = 10^{-3}\ \text{N-m}\ ,$$

$$T_{y+} = 1.5 \times 10^{-3}\ \text{N-m}\ ,$$

$$T_{y-} = 0.5 \times 10^{-3}\ \text{N-m.}$$

Figure 4.3 delineates the response of γ_x, γ_y, $\hat{T}_{Bx}$, and $\hat{T}_{By}$ the total body-fixed torques,

$$T_x = T_{Bx} + \delta_{x+} T_{x+} + \delta_{x-} T_{x-} ,$$

$$T_y = T_{By} + \delta_{y+} T_{y+} + \delta_{y-} T_{y-} , \qquad (4.22)$$

also shown. Here δ_{x+}, δ_{x-}, δ_{y+}, and δ_{y-} are each zero except when the appropriate jet is firing, at which time they become unity. Note, that γ_x and γ_y vary between ± 1.0 arc second.

Figure 4.4 indicates that using the pulse estimator enables the control system to keep γ_x and γ_y below ± 0.01 arc second. In this figure, the convergence of the estimate of the total body-fixed torques defined in (4.22) can readily be seen. The control law here is

$$\boxed{\begin{aligned} T_{cx1} &= T_{cx} - \delta_{x+} \hat{T}_{x+} - \delta_{x-} \hat{T}_{x-} , \\ T_{cy1} &= T_{cy} - \delta_{y+} \hat{T}_{y+} - \delta_{y-} \hat{T}_{y-} , \end{aligned}} \qquad (4.23)$$

where T_{cx} and T_{cy} are defined in (4.21) and $\hat{T}_{x+}$, $\hat{T}_{y+}$, $\hat{T}_{x-}$, and $\hat{T}_{y-}$ are estimates of the pulse torques. The actual applied control torque must also be modified to include estimates of torques caused by the jets on the satellite ends.

MAGNETIC IMPLEMENTATION OF THE CONTROL LAW

Equations (4.12) and (4.23) combine to form the continuous pointing control law with pulse discontinuities for the spinning satellite. Equation (4.19) represents the ideal spin control. In this section, the mechanization equations are developed which allow actuation of the desired control magnetically.

Pointing Control

As stated in Chapter III, the torque due to generating a magnetic moment $\vec{m}$ in the magnetic field $\vec{B}$ is

$$\vec{T} = \vec{m} \times \vec{B} \, . \tag{4.24}$$

If $\vec{T}$ is the desired pointing control torque $\vec{T}_D = T_{Dx}\hat{x}_B + T_{Dy}\hat{y}_B$, then (4.24) results in

$$T_{Dx} = m_y B_z - m_z B_y \, ,$$

$$T_{Dy} = m_z B_x - m_x B_z \, .$$

If for power efficiency reasons, the magnetic moment $\vec{m}$ is generated so that $\vec{m}$ is perpendicular to $\vec{B}$ (or $\vec{m} \cdot \vec{B} = 0$), the three components of $\vec{m}$ must be

$$m_z = (T_{Dy}B_x - T_{Dx}B_y)/(B_x^2 + B_y^2 + B_z^2) \, ,$$

$$m_x = (m_z B_x - T_{Dy})/B_z \, ,$$

$$m_y = (m_z B_y + T_{Dx})/B_z \, . \tag{4.25}$$

These are identically Eqs. (3.44) of Chapter III. As in Chapter III, these equations can be simplified at the cost of mechanization power by setting $m_z = 0$, resulting in

$$m_x = -T_{Dy}/B_z \, ,$$

$$m_y = T_{Dx}/B_z \, . \tag{4.26}$$

Mechanization of either Eqs. (4.25) or (4.26) will result in the desired pointing control torque. The only time when they can't be utilized is when the component of the magnetic field along the spin axis

B_z becomes very small. As can be visualized for a satellite in a circular polar orbit passing through a magnetic dipole field, B_z crosses through zero four times during an orbital period. Thus, at each of these points during the orbit, perfect pointing control by magnetic means is not possible. However, partial control is available when B_z is very small by making use of only the component m_z. This is done by using the first of Eqs. (4.25). Therefore, for pointing control of the spinning satellite studied in this chapter, the control mechanization is broken into two phases. During the precision control phase (when B_z is not near zero), Eqs. (4.25) or (4.25) are used. During Mode 2, only m_z from Eqs. (4.25) is utilized.

Implementation of this controller requires that three orthogonal coils be present on the spacecraft. Also, a three-axis magnetometer must be mounted so that all components of the magnetic field $\vec{B}$ can be measured. If Eqs. (4.25) are used during the precision-control phase, the magnetic field must be sampled at points of time with the coils turned off to prevent interference to the magnetometers. From these held samples, the continuous values of the components of $\vec{B}$ can be computed.

Utilization of Eqs. (4.26) during the precision phase eliminates the need for sampling of $\vec{B}$. During this phase, only B_z (which is perpendicular to m_x and m_y) needs to be measured. From this considsration and the simplicity of Eqs. (4.26), they seem to be more logical choice than Eqs. (4.25). The cutoff point (value of B_z) which should be used to switch from one phase logic to the other is arbitrary. Use of three components of $\vec{m}$ as in (4.25) will be known as the three-coil controller. The employment of (4.26) will be referred to as the two-coil controller.

Spin Control

It is impossible to actuate spin control simultaneously with precision pointing control due to the arbitrary direction of $\vec{B}$. However, during Mode 2 control, spin correction can be implemented by generating

$$m_x = K_z B_y \operatorname{sgn} (\dot{\psi} - \dot{\psi}_o) ,$$

$$m_y = -K_z B_x \operatorname{sgn} (\dot{\psi} - \dot{\psi}_o) , \qquad (4.27)$$

where $\dot{\psi}_o$ is the nominal spin speed. These create a component of $\vec{m}$ perpendicular to the lateral component of $\vec{B}$. The resulting spin control torque is analogous to the principle of the induction motor. Application of the spin control Eqs. (4.27) results in a disturbance to the spin axis direction due to the presence of B_z. But, B_z monotonically changes during this phase and crosses the zero point. Therefore, the effect of the pointing disturbance due to spin control after the zero point should essentially cancel the effect of the disturbance before crossover.

IDEAL PERFORMANCE OF THE MAGNETIC CONTROL SYSTEM

Based on the fact that precise pointing control of the spacecraft's spin axis cannot be maintained at four distinct instances during the orbital period, the following questions arise concerning the available magnetic precision control.

1. What percentage of the time during the orbit is precision magnetic control available?
2. How large a deviation does the spin axis of the spacecraft travel from the nominal position during periods of only partial pointing control?
3. What deviations of the spin speed take place on the spacecraft?

In answering these questions, it still is assumed that an ideal system exists; that is, the star tracker variables are precisely measured, the model of the vehicle used by the observer is correct, and the magnetometer readings and control torques are exact. Performance of the non-ideal system is investigated in the next section.

To answer the above questions, a highly accurate digital simulation of the rotational motion of the satellite in its orbital environment was made. The disturbance torque program developed in Chapter II was used as a driver for the satellite so that performance in the presence of realistic environmental conditions could be more correctly ascertained. The magnetic field model used was the ninth order spherical harmonic expansion model described in Appendix A. The satellite and environment

characteristic parameters of the torque generating portion of the program were the same as those which generated Figures 2.11 - 2.12.

The pointing control and observer gains employed were the same as those used to demonstrate the pulse estimator operation in a previous section. The value of spin control gain K_z used was 1.875×10^5 Amp-m^4/Wb. The crossover values of B_z were chosen to be the points where $B_z = 0.1 |\vec{B}|$. The amounts of time spent during a typical orbit in the precision pointing phase, the spin control phase (Mode 2), and the recovery of precision control following a spin-control period are tabulated in Table 4.1.

Table 4.1. PRECISION CONTROL TIMES FOR FOUR PORTIONS OF A TYPICAL POLAR ORBIT

Portion of Orbit	Precision Pointing Time (sec)	Spin Control Time (sec)	Recovery Time Following Spin Control (sec)
1	1165.	123.	18.
2	1575.	72.	22.
3	1025.	117.	10.
4	1665.	98.	56.

Recovery time is the time required by the control system to drive both γ_x and γ_y below 0.02 arc seconds following a spin-control period. From these results it can be seen that more than 90 percent of the orbit period is spent in precision pointing control. Several runs were made with this simulation using both the two-coil and three-coil pointing control laws.

The maximum observed deviation of the spin axis from the reference during a spin control phase of a typical orbit was 4.12 arc seconds. Maximum deviation of the spin speed was 0.0024 rad/sec under worst case spin torques. This number was obtained with a deadband on the spin speed, set at 0.001 rad/sec. The maximum value of the magnetic moment of each coil was usually fixed at 20 Amp-m^2.

If the value of the maximum magnetic moment which can be generated in each coil is too small, the control system is not capable of obtaining

the precision periods indicated above. Figure 4.5 indicates the response of the star tracker variable γ_x during a recovery phase under three sets of torque and control conditions. The body-fixed torques were $T_{Bx} = 1.25 \times 10^{-3}$ N-m and $T_{By} = 6.25 \times 10^{-4}$ N-m. With the magnetic moments limited to 20 Amp-m^2, pointing accuracy was limited to 0.5 arc second using control-mechanization Eqs. (4.26) following the spin control mode.

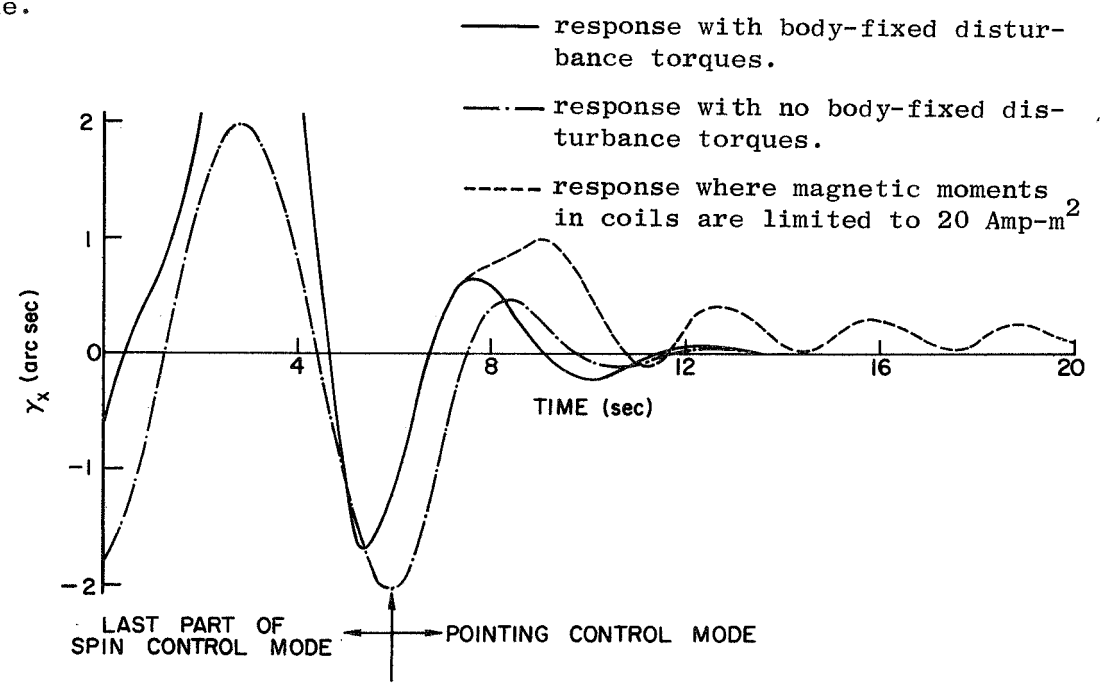

FIG. 4.5. RESPONSE OF STAR TRACKER VARIABLE γ_x VS TIME FOR DIFFERENT CONTROL SITUATIONS NEAR THE END OF A SPIN CONTROL PHASE.

SYSTEM ERROR ANALYSIS

In this section, a qualitative analysis is made to determine what effect the inaccuracies in building and modeling the spinning satellite have upon the attitude control system's performance. Specific error sources studied include:

1. The incorrect applied control torque due to misaligned magnetic coils or misaligned magnetic moments caused by the nonuniformity of the coil core,
2. Magnetometer and magnetic measurement processing errors,

3. Nonsymmetry of the spacecraft and the incorrect modeling of the spacecraft parameters in the observer, and
4. Noisy star tracker measurements.

Analytical expressions for the resulting disturbances will be derived and indications of how the resulting attitude errors can be reduced will be indicated where appropriate.

Error sources which are not investigated include those which are specifically a function of the manner in which the state observer is physically constructed. These include errors such as digital roundoff or biased integrators, gain deviations, and noise sources internal to the observer.

Misaligned Magnetic Coils

In constructing the satellite, the wire coils used to generate the magnetic moment will be mounted with some degree of misalignment with respect to the desired control axes. Also, the magnetic moment created by these coils may be deflected because of the nonuniformity of the satellite material in the core. Figure 4.6 illustrates the general misalignment of three orthogonal coils nominally aligned with the vehicle axes $\hat{x}_B$, $\hat{y}_B$, and $\hat{z}_B$. Because the satellite is symmetric, the projection of the Y coil's axis upon the lateral plane is arbitrarily defined as the $\hat{y}_B$ axis.

The actual magnetic moments created by the three coils are

$$m_x = m'_x \cos \xi_y \cos \xi_z + m'_z \sin \zeta_y ,$$

$$m_y = m'_x \cos \xi_y \sin \xi_z + m'_y \cos \eta_x - m'_z \cos \zeta_y \sin \zeta_x ,$$

$$m_z = -m'_x \sin \xi_y + m'_y \sin \eta_x + m'_z \zeta_y \cos \zeta_x ,$$

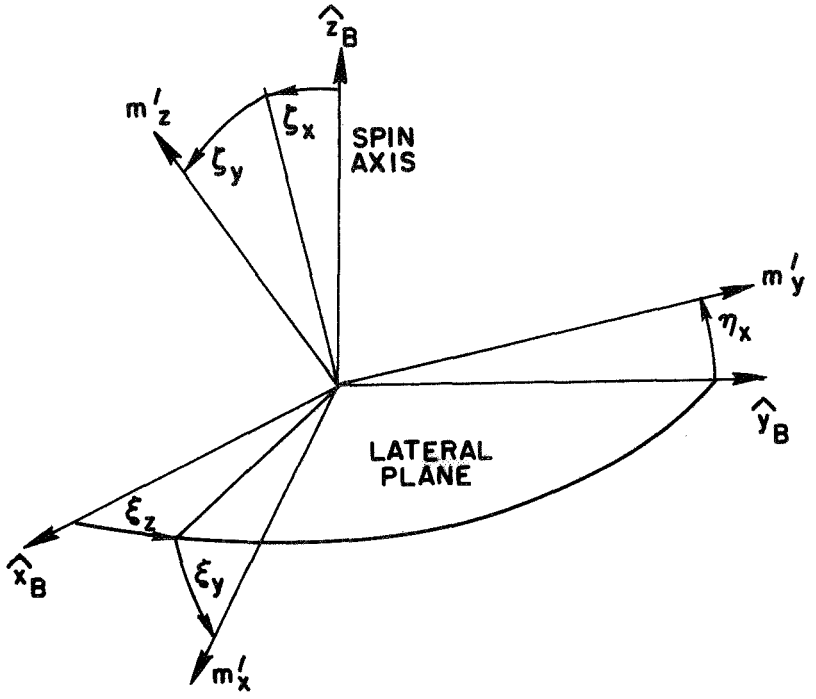

FIG. 4.6. GEOMETRY OF MAGNETIC COIL MISALIGNMENT.

where m'_x, m'_y and m'_z are the actual magnetic moments of each coil. For small angles this is approximately

$$\begin{bmatrix} m_x \\ m_y \\ m_z \end{bmatrix} = \begin{bmatrix} 1 & 0 & \zeta_y \\ \xi_z & 1 & -\zeta_x \\ -\xi_y & \eta_x & 1 \end{bmatrix} \begin{bmatrix} m'_x \\ m'_y \\ m'_z \end{bmatrix} . \tag{4.28}$$

For simplicity, it is assumed now that only the X coil is misaligned, or $\eta_x = \zeta_x = \zeta_y = 0$. Then, for the three-coil control [Eqs. (4.25)], the applied torque components are

$$T_x = m_y B_z - m_z B_y ,$$

$$= T_{cx} + m'_x(\xi_y B_y + \xi_z B_z) ,$$

$$T_y = m_z B_x - m_x B_z ,$$

$$= T_{cy} - m'_x \xi_y B_x \quad . \tag{4.29}$$

Also,

$$m'_x = (m'_z B_x - T_{cy})/B_z \quad ,$$

$$= \frac{(B_x^2 - B^2)}{B^2 B_z} T_{cy} - \frac{B_x B_y T_{cx}}{B^2 B_z} \quad . \tag{4.30}$$

In the steady state operation, the states γ_x, γ_y, ω_x and ω_y are driven to zero and the applied control just cancels the disturbance torques, or

$$T_{cx} = -(T_{Bx} + T_{Ix} \cos \psi + T_{Iy} \sin \psi) \quad ,$$

$$T_{cy} = -(T_{By} - T_{Ix} \sin \psi + T_{Iy} \cos \psi) \quad , \tag{4.31}$$

where $\psi = \dot{\psi}(t - t_o)$. Because the initial time t_o is arbitrary, one can define an arbitrary X direction such that

$$B_x = B_{xo} \cos \psi \quad ,$$

$$B_y = -B_{xo} \sin \psi \quad ,$$

$$B_z = k_c B_{xo} \quad , \tag{4.32}$$

where B_{xo} and k_c are assumed constant for a slowly changing magnetic field. It is also assumed that T_{Bx}, T_{By}, T_{*x} and T_{*y} are slowly changing so that they can be treated as constants.

Equations (4.29) - (4.32) can be combined to yield the actual applied torques

$$T_x = T_{cx} - \frac{\xi_y}{(1+k_c^2)k_c}\left[-\frac{(1+k_c^2)T_{Ix}}{2} + \left(\frac{3}{4}+k_c^2\right)T_{By}\sin\psi - \frac{1}{4}T_{Bx}\cos\psi\right.$$

$$\left. + \frac{k_c^2}{2}T_{Iy}\sin 2\psi + \frac{(1+k_c^2)T_{Ix}}{2}\cos 2\psi - \frac{1}{4}T_{By}\sin 3\psi + \frac{1}{4}T_{Bx}\cos 3\psi\right]$$

$$- \frac{\xi_z}{(1+k_c^2)}\left[-\frac{1}{2}T_{By} - k_c^2 T_{Bx} + (1+k_c^2)T_{Ix}\sin\psi - k_c^2 T_{Iy}\cos\psi\right.$$

$$\left. + \frac{1}{2}T_{Bx}\sin 2\psi + \frac{1}{2}T_{By}\cos 2\psi\right] ,$$

$$T_y = T_{cy} + \frac{\xi_y}{(1+k_c^2)k_c}\left[-\frac{k_c^2}{c}T_{Iy} + \frac{1}{4}T_{Bx}\sin\psi - \left(\frac{1}{4}+k_c^2\right)T_{By}\cos\psi\right.$$

$$\left. + \frac{(1+k_c^2)}{2}T_{Ix}\sin 2\psi - \frac{k_c^2}{2}T_{Iy}\cos 2\psi + \frac{1}{4}T_{Bx}\sin 3\psi + \frac{1}{4}T_{By}\cos 3\psi\right] .$$

For the two-coil control, the X-coil magnetic moment is

$$m_x' = -T_{cy}/B_z , \tag{4.34}$$

so that the applied torque components become

$$T_x = T_{cx} - \frac{\xi_y}{k_c}\left[\frac{T_{Iy}}{2} + T_{Bx}\sin\psi + \frac{T_{Ix}}{2}\sin 2\psi - \frac{T_{Iy}}{2}\cos 2\psi\right]$$

$$+ \xi_z\left[T_{By} - T_{Ix}\sin\psi + T_{Iy}\cos\psi\right] ,$$

$$T_y = T_{cy} - \frac{\xi_y}{k_c}\left[\frac{T_{Iy}}{2} + T_{By}\cos\psi - \frac{T_{Ix}}{2}\sin 2\psi + \frac{T_{Iy}}{2}\cos 2\psi\right] .$$

(4.35)

Thus, the error torque includes terms similar to body-fixed and inertially-fixed components which will be detected by the observer and automatically cancelled. Other torque terms include those which rotate in inertial space at one and two times the negative spin rate. Other terms act as sinusoidal inputs to one or both axes. It can be seen that these error torque magnitudes will be largest when B_z, and consequently the constant k_c, are smallest. Similar disturbance torque expressions can be found for misaligned Y and Z coils.

In general, the effect of these sinusoidal disturbance inputs can, of course, be reduced by lowering the values of the inertially-fixed and body-fixed torques through better design, by keeping the misalignments small, and by reducing the amplitude of the frequency response of the control system to sinusoidal inputs. The latter correction can be made by adjusting the characteristic equation of the state observer and by changing the gains in the control law.

Figure 4.7 shows the amplitude of the frequency response of the star tracker variables γ_x and γ_y to a sinusoidal disturbance torque

$$T_y = 10^{-5} \sin \omega t \text{ N-m.}$$

In Case 1, the observer has the characteristic equation $(s + 0.5)^6 = 0$ and the control law [Eq. (4.16)] has the gains $K_p = 1.\ \text{sec}^{-2}$ and $K_v = 1.\ \text{sec}^{-1}$. In Case 2, the control gains have been increased to $K_p = 10.\ \text{sec}^{-2}$ and $K_v = 4.\ \text{sec}^{-1}$. In Case 3, the characteristic equation of the observer has been changed to $(s + 1.0)^6 = 0$. It is apparent that increased control gains and faster observer response both tend to minimize the effects of sinusoidal disturbances.

Figure 4.8 shows the same responses when the sinusoidal disturbance is applied about the $\hat{x}_B$ axis. Here, the control system is the same as that of Case 2 in Figure 4.7.

Magnetometer Errors

The error in the signal to the controller from the magnetometer can be caused by several factors. Imperfections in magnetometer outputs can

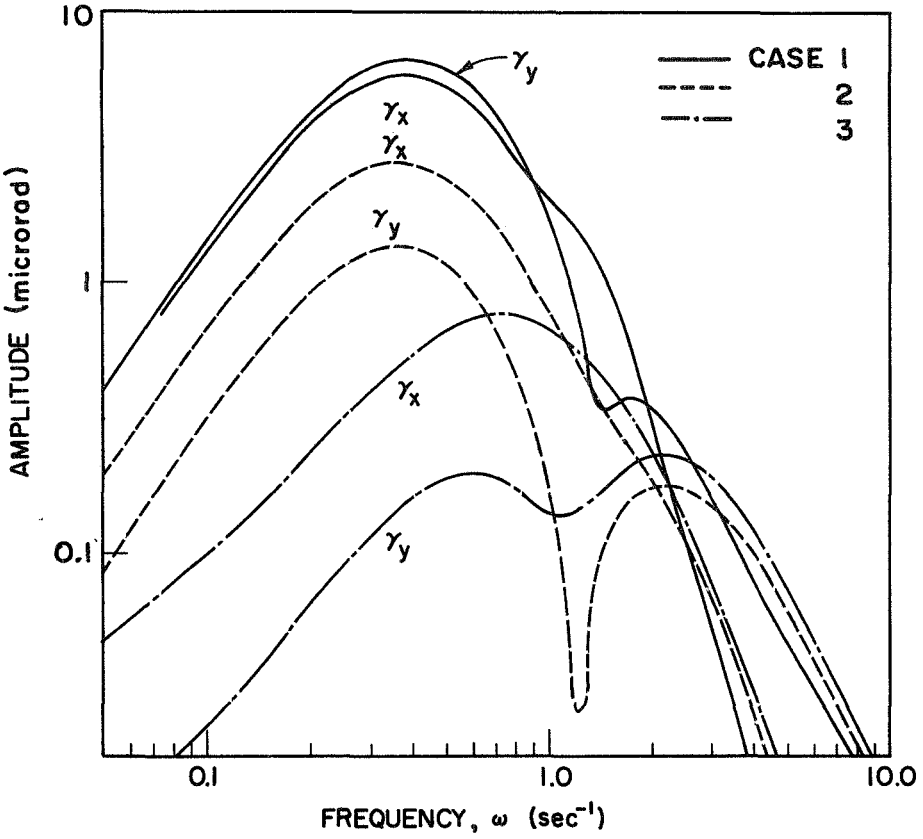

Case	Observer Characteristic Equation	Position Gain K_p (sec^{-2})	Speed Gain K_v (sec^{-1})
1	$(s + 0.5)^6 = 0$	1.0	1.0
2	$(s + 0.5)^6 = 0$	10.0	4.0
3	$(s + 1.0)^6 = 0$	10.0	4.0

FIG. 4.7. FREQUENCY RESPONSE OF STAR TRACKER VARIABLES FOR DISTURBANCE INPUT $T_y = 10^{-5}$ sin ωt N-m, AS FROM A MISALIGNED X TORQUING COIL.

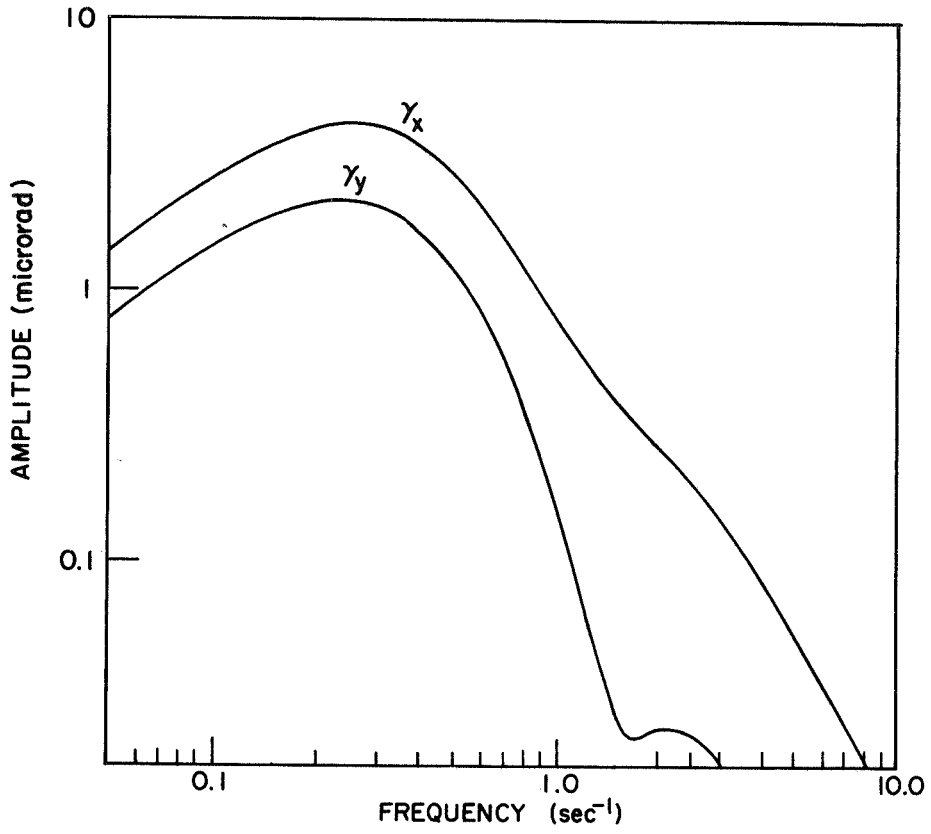

FIG. 4.8. FREQUENCY RESPONSE OF STAR TRACKER VARIABLES FOR DISTURBANCE INPUT $T_x = 10^{-5}$ sin ωt N-m AS FROM A MISALIGNED Y TORQUING COIL. The characteristic equation of the reduced-order observer is $(s + 0.5)^6 = 0$ and the control law gains are $K_p = 10$ sec^{-2} and $K_v = 4$ sec^{-1}.

result from misalignment of the sensitive axes, bias, scalefactor errors, output nonlinearities, and random fluctuations of the field not detected by sampling. Additional error is caused by a time lag in the division process to obtain $1/B^2$ and $1/B_z$. Figure 4.9 indicates the general misalignment angles. The following terms are defined as error coefficients:

$b_{x,y,z}$ - bias terms of each magnetometer,

$k_{fx,y,z}$ - scale factor errors of each,

$k_{nx,y,z}$ - quadratic nonlinearities of each,

$N_{x,y,z}$ - fluctuations in the magnetic field components.

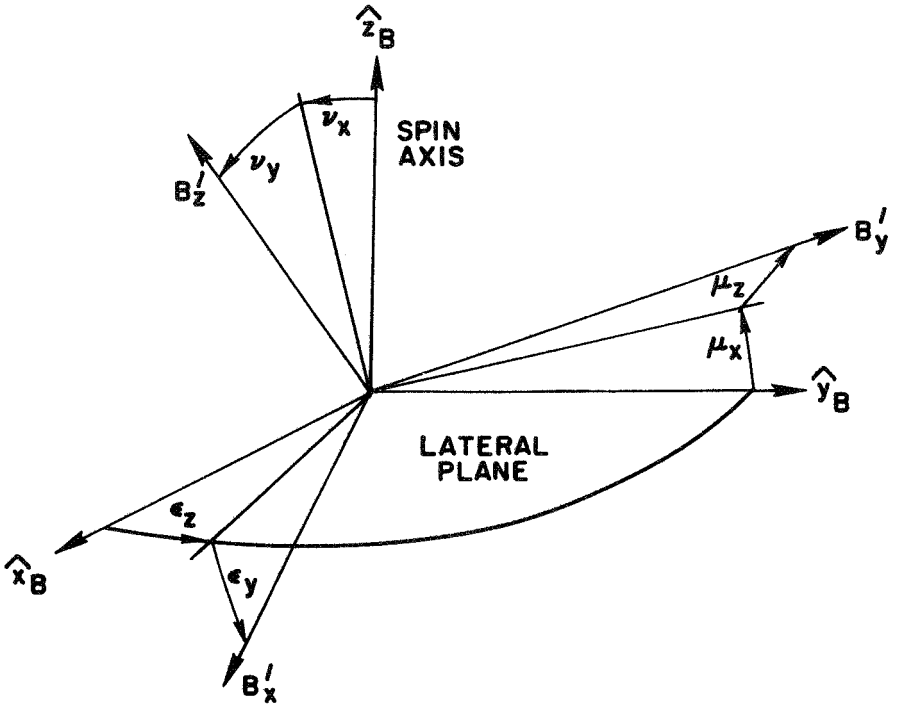

FIG. 4.9. GEOMETRY OF A MISALIGNED MAGNETOMETER.

From Figure 4.9 and these definitions, the measured signal from the X magnetometer would be

$$B'_x = \left[1 + k_{fx}\right]\left[B_x + \epsilon_z B_y - \epsilon_y B_z\right] + k_{nx}\left[B_x + \epsilon_z B_y - \epsilon_y B_z\right]^2 + b_x + N_x$$

$$\cong B_x + k_{fx}B_x + \epsilon_z B_y - \epsilon_y B_z + k_{nx}B_x^2 + b_x + N_x \; . \qquad (4.36a)$$

Similarly, for the Y and Z signals,

$$B'_y \cong B_y + k_{fy}B_y - \mu_z B_x + \mu_x B_z + k_{ny}B_y^2 + b_y + N_y \; . \qquad (4.36b)$$

$$B'_z \cong B_z + k_{fz}B_z + \nu_y B_x - \nu_x B_y + k_{nz}B_z^2 + b_z + N_z \; . \qquad (4.36c)$$

From Eqs. (4.36), one can compute the resulting error in the applied magnetic moments and the resulting error torque.

In general, the magnetometer is a fairly accurate instrument. References 55 and 56 report magnetometers with capabilities of measuring field components with a range of greater than 100 times the minimum value. Measurable frequency range is from 0 to 100 Hertz. Accuracies of measurement are on the order of 0.1 to 1 percent of the full scale readings. These devices are adjustable up to ± 50000 gamma which is well above orbital requirements.

The magnetic field during the main phase of a magnetic storm tends to be noisy with excursions having amplitudes of several hundred gamma (Ref. 57). The fluctuations occur slowly enough that they pose no problem to their measurement. A description of other smaller fluctuations is presented in Appendix A.

For the two-coil controller, the resulting applied magnetic moments due to the slightly incorrect B_z' are

$$m_x' = -\frac{T_{cy}}{B_z'} \cong -\frac{T_{cy}}{B_z}\left(1 - k_{fz} - \nu_y \frac{B_x}{B_z} + \nu_x \frac{B_y}{B_z} - k_{nz}B_z - \frac{b_z + N_z}{B_z}\right),$$

$$m_y' = \frac{T_{cx}}{B_z'} \cong \frac{T_{cx}}{Bz}\left(1 - k_{fz} - \nu_y \frac{B_x}{B_z} + \nu_x \frac{B_y}{B_z} - k_{nz}B_z - \frac{b_z + N_z}{B_z}\right). \tag{4.37}$$

Similar but more complicated expressions result for the three-coil controller. The effect of the scale factor, nonlinear, and bias terms are taken out by the observation of body-fixed and inertially-fixed torques for a slowly changing field. The noise terms pose no problem if sampling is done often enough or measurements are taken continuously. The misalignment terms due to (ν_x, ν_y), produce sinusoidal inputs into the X and Y channels as in the case of the misaligned coils. Again, the frequency-response analysis can be applied, and the plots of Figs. 4.7 and 4.8, for example, are pertinent.

Nonsymmetry of the Spacecraft

Here, the facts that the spacecraft is not perfectly symmetric about the spin axis, that the moment of inertia ratios are not perfectly known, and that the spin speed is not always nominal are considered. From Eqs. (2.6) - (2.8) of Chapter II, the equations of motion of ω_x and ω_y are

$$\dot{\omega}_x = \frac{1}{I_{xx}}\left[T_x + (I_{yy} - I_{zz})\,\omega_y\omega_z - I_{yz}\omega_z^2\right]$$

$$+ \frac{I_{xy}}{I_{xx}\,I_{yy}}\left[T_y + (I_{zz} - I_{xx})\omega_x\omega_z + I_{xz}\omega_z^2\right]$$

$$+ \frac{I_{xz}}{I_{xx}\,I_{zz}}\left[T_z + (I_{xx} - I_{yy})\omega_x\omega_y + (I_{yz}\omega_x - I_{xz}\omega_y)\omega_z\right], \tag{4.38a}$$

$$\dot{\omega}_y = \frac{I_{xy}}{I_{xx}\,I_{yy}}\left[T_x + (I_{yy} - I_{zz})\omega_y\omega_z - I_{yz}\omega_z^2\right]$$

$$+ \frac{1}{I_{yy}}\left[T_y + (I_{zz} - I_{xx})\omega_x\omega_z + I_{xz}\omega_z^2\right]$$

$$+ \frac{I_{yz}}{I_{yy}\,I_{zz}}\left[T_z + (I_{xx} - I_{yy})\omega_x\omega_y + (I_{yz}\omega_x - I_{xz}\omega_y)\omega_z\right]. \tag{4.38b}$$

If one defines

$$I_{xx} = I_{xo} + \delta I_x\,,$$

$$I_{yy} = I_{xo} + \delta I_y\,,$$

$$I_{zz} = I_{zo} + \delta I_z\,,$$

$$(I_{zo} - I_{xo})/I_{xo} = a_s \ ,$$

$$\omega_z = \dot{\psi}_o + \delta\omega_z \ ,$$

and assumes that ω_x, ω_y, I_{xy}, I_{yz}, and I_{xz} are small quantities, then Eqs. (4.38) can be written as

$$\dot{\omega}_x \cong - a_s\dot{\psi}_o\omega_y + \frac{1}{I_{xo}}(a_s\delta I_x + \delta I_y - \delta I_z)\dot{\psi}_o\omega_y - a_s\delta\omega_z\omega_y$$

$$+ \frac{T_x}{I_{xx}} - \frac{I_{yz}}{I_{xx}}\dot{\psi}_o^2 + \frac{I_{xy}}{I_{xx}I_{yy}}T_y + \frac{I_{xy}}{I_{xx}I_{yy}}(I_{zz} - I_{xx})\dot{\psi}_o\omega_x$$

$$+ \frac{I_{xy}I_{xz}}{I_{xx}I_{yy}}\dot{\psi}_o^2 + \frac{I_{xz}T_z}{I_{xx}I_{zz}} \ , \qquad (4.39a)$$

$$\dot{\omega}_y = a_s\dot{\psi}_o\omega_x + \frac{1}{I_{xo}}(-a_s\delta I_y + \delta I_z - \delta I_z)\dot{\psi}_o\omega_x + a_s\delta\omega_z\omega_x$$

$$+ \frac{T_y}{I_{yy}} + \frac{I_{xz}}{I_{yy}}\dot{\psi}_o^2 - \frac{I_{xy}I_{yz}}{I_{xx}I_{yy}}\dot{\psi}_o^2 + \frac{I_{xy}T_x}{I_{xx}I_{yy}}$$

$$+ \frac{I_{xy}(I_{yy} - I_{zz})}{I_{xx}I_{yy}}\dot{\psi}_o\omega_y + \frac{I_{yz}T_z}{I_{yy}I_{zz}} \ . \qquad (4.39b)$$

The terms in Eqs. (4.39) which are products of constants and ω_x or ω_y cause torques of frequency $a_s\dot{\psi}_o$ about each axis. The constant terms are cancelled as body-fixed torques. The multiples of T_x and T_y produce constants plus sinusoidal terms of frequency $\dot{\psi}_o$. The torque T_z due to the applied control is

$$T_z = m'_x B_y - m'_y B_x$$

$$= - \frac{1}{k_c}\left[- T_{By}\sin\psi + T_{Bx}\cos\psi + T_{Ix}\right]$$

for the two-coil controller. Hence, multiples of this term also cause constant inputs and sinusoidal inputs of frequency $\dot{\psi}_o$. Therefore, the frequency response analysis again is applicable here.

Noisy Star Tracker

The problem of noisy star-tracker measurements of γ_x and γ_y is now analyzed. In particular, the equations which define the covariances of the estimates of the other system states are derived for the Gopinath reduced-order observer. It is assumed that the noise η_n of each star-tracker readout can be described as independent Markov processes with equations

$$\dot{\eta}_n = -\beta_n \eta_n + v \tag{4.40}$$

where v is white, stationary, and Gaussian, and β_n is a positive constant. Such a noise process describes the speed of a free particle under Brownian motion, or the voltage across a capacitor in parallel with a resistor producing a white noise voltage (Johnson noise), which is typical in many instruments.

From Figure D.1 of Appendix D, if the input to the observer is $\vec{x}_1 + \vec{\eta}_n$, the output is

$$\vec{y} = \hat{x}_2 + L\vec{\eta}_n ,$$

where

$$\hat{x}_2 = \vec{z} + L\vec{x}_1$$

and $\vec{z}$ has the state equations

$$\dot{\vec{z}} = (F_{21} - LF_{11})(\vec{x}_1 + \vec{\eta}_n) + (F_{22} - LF_{12})(\vec{z} + L\vec{x}_1 + L\vec{\eta}_n) + (G_2 - LG_1)\vec{u} .$$

Also recall that the actual system equations are

$$\dot{\vec{x}}_1 = F_{11}\vec{x}_1 + F_{12}\vec{x}_2 + G_1\vec{u} \ ,$$

$$\dot{\vec{x}}_2 = F_{21}\vec{x}_1 + F_{22}\vec{x}_2 + G_2\vec{u} \ .$$

If the output error is defined as

$$\vec{\epsilon}_1 = \vec{x}_2 - \vec{y} \ ,$$

then its time rate of change can be shown to be

$$\dot{\vec{\epsilon}}_1 = (F_{22} - LF_{12})\vec{\epsilon}_1 - (F_{21} - LF_{11})\vec{\eta}_n - L\dot{\vec{\eta}}_n \qquad (4.41)$$

using the previous equations. If one defines $\vec{\epsilon}_2 = \vec{n}$, then Eqs. (4.40), (4.41) can be combined into the matrix form

$$\begin{bmatrix} \dot{\vec{\epsilon}}_1 \\ \dot{\vec{\epsilon}}_2 \end{bmatrix} = \begin{bmatrix} (F_{22}-LF_{12}) & -(F_{21}-LF_{11}) \\ 0 & D_n \end{bmatrix} \begin{bmatrix} \vec{\epsilon}_1 \\ \vec{\epsilon}_2 \end{bmatrix} + \begin{bmatrix} L \\ I_2 \end{bmatrix} [\vec{V}] \qquad (4.42)$$

where

$$D_n = \begin{bmatrix} -\beta_n & 0 \\ 0 & -\beta_n \end{bmatrix} .$$

In simpler notation, (4.42) becomes

$$\dot{\vec{\epsilon}} = F\vec{\epsilon} + G\vec{v} \ . \qquad (4.43)$$

If P_2 is defined as the covariance of the error, i.e.,

$$P_2 = E\left\{\vec{\epsilon}\ \vec{\epsilon}^T\right\} ,$$

and Q is the covariance of v, that is

$$E\left\{\vec{v}(t)\ \vec{v}^{T}(\tau)\right\} = Q\delta(t - \tau) ,$$

then the covariance P_2 has the well-known time derivative

$$\dot{P}_2 = FP_2 + P_2F^T + GQG^T . \tag{4.44}$$

$P(t)$ has a closed form solution (Ref. 58) found by defining the matrix

$$\Lambda = \begin{bmatrix} \Lambda_{11} & \Lambda_{12} \\ \Lambda_{21} & \Lambda_{22} \end{bmatrix}$$

which has the equation

$$\dot{\Lambda} = A_1\Lambda, \qquad \Lambda(0) = I .$$

If the matrix A_1 has the form

$$A_1 = \begin{bmatrix} -F^T & 0 \\ GQG^T & F \end{bmatrix} ,$$

then

$$P_2(t) = \Lambda_{21}\Lambda_{22}^T + \Lambda_{22}P_2(0)\ \Lambda_{22}^T . \tag{4.45}$$

$\Lambda(t)$ has the solution

$$\Lambda(t) = \mathcal{L}^{-1}\left[\begin{array}{c|c} (sI + F^T)^{-1} & 0 \\ \hline (sI-F)^{-1}GQG^T(sI+F^T) & (sI-F)^{-1} \end{array}\right] . \tag{4.46}$$

The steady state solution can be found for zero initial conditions by examining

$$P_2 = \Lambda_{21}\Lambda_{22}^T \quad . \tag{4.47}$$

A steady state solution exists because the characteristic equation of (4.42),

$$(s + \beta_n)^2(sI - F_{22} + LF_{12}) = 0 \ ,$$

has eigenvalues with positive real parts by correct choice of the matrix L. If P_2 is defined as

$$P_2 = E\left\{\vec{\epsilon}_1 \vec{\epsilon}_1^T\right\} \ ,$$

then from Eq. (4.44), its time derivation can be shown to be

$$\begin{aligned}\dot{P}_2 = {} & (F_{22} - LF_{12})P_2 + P_2(F_{22} - LF_{12})^T + LQL^T \\ & - \frac{q_1}{2\beta_n}\left\{(\dot{\psi}^2 LL^T + 2\beta_n LF_{11}L^T)\left[(F_{22} - LF_{12} - \beta_n I_6)^{-1}\right]^T\right. \\ & \left. + (F_{22} - LF_{12} - \beta_n I_6)^{-1}(\dot{\psi}^2 LL^T + 2\beta_n LF_{11}^T L^T)\right\} \ ,\end{aligned} \tag{4.48}$$

where

$$Q \triangleq \begin{bmatrix} q_1 & 0 \\ 0 & q_1 \end{bmatrix} \ ,$$

and $\dot{\psi}$ is the spin speed. Equation (4.48) also is in the form of Eq. (4.44), so its solution may be found from Eqs. (4.46) - (4.47). Because (4.48) is linear in P_2, the steady state solution may be found by solving the resulting 15 algebraic equations resulting from setting $\dot{P}_2 = 0$ and using a particular choice of the observer gain L.

To minimize the effect of the noise inputs for a reduced-order observer, the matrix L should be chosen so that the maximum eigenvalue of P_2 is minimized. Denoting the maximum eigenvalue of covariance P as

$$\lambda_{max}(P) \triangleq \|P\| ,$$

it was shown by Singer (Ref. 76) that this has the upper bound

$$\|P\| \leq \frac{\|U\|^2 \, \|U^{-1}\|^2 \, \|GQG^T\|}{2|\alpha_{max}|} \tag{4.49}$$

for an equation such as (4.44) at steady state. Here U is the matrix which diagonalizes F and α_{max} is the maximum real part of the eigenvalues of F. This laborious process can also be applied to (4.48). There doesn't seem to be a tractible solution useful for making a direct choice of the matrix L to minimize $\|P_2\|$. Thus, its selection will have to be based upon a cut-and-try procedure.

The alternative method for evaluating the effect of noisy star tracker data is to perform simulations of the system with noisy measurements. If the measurements are too noisy, of course, improvement can always be obtained by using a Kalman filter in place of the reduced-order observer, as was done in Chapter III.

SUMMARY

It has been shown that it is theoretically feasible to magnetically control the spin axis of a spinning satellite to point at a star with an extreme degree of accuracy. In particular, for a star tracking satellite in a circular polar orbit, the spin axis can be maintained within 0.01 arc second for greater than 90 percent of the period of the orbit. This accuracy can be achieved during normal mode operation by either using a three-coil or two-coil mechanization. The results were based, of course, upon the assumption of perfect noiseless startracking capability, magnetic-field measurement, and control actuation.

During the spin control mode of this satellite, the pointing accuracy never deviates beyond 5 arc second under worst-case disturbance torques. The spin speed deviation during the entire orbit can be kept below 0.003 rad/sec.

The key to providing the extreme accuracy capabilities is the fact that inertially-fixed torques, body-fixed torques, and pulse torques from translational jets are observable quantities. A modified version of the Gopinath reduced-order observer for noncyclic, non-controllable systems was developed and used to estimate these disturbance torques in addition to the vehicle rates. A new control law based upon the disturbance torque estimates was used to cancel their effect and to drive the satellite state to zero.

A qualitative error analysis was performed to determine the effects upon the controller's performance of misaligned magnetic coils, magnetometer errors, deviations of the satellite inertial properties from those modeled in the observer, and a noisy tracker. Actual quantitative error evaluation depends upon having a more complete description of actual satellite and control system parameters.

Although a relatively precise control system was studied in Chapter III, the vast improvement in the pointing-accuracy capability of the system studied in this chapter must be noted. Again, the improvement is due to the assumed presence of an accurate star tracker which can simultaneously measure pointing errors about two orthogonal axes.

In conclusion, it can be stated that magnetically controlling a spinning satellite to precisely point at a star compares very favorably with other types of precision control for periods of up to thirty minutes during an orbital period. The chief limitation to this and any other precision controller for the satellite considered here seems to be the accuracy limitations of the star tracker.

CHAPTER 5

THE CONTINUOUS ATTITUDE CONTROL OF RIGID NONSYMMETRIC SPINNING VEHICLES

In this chapter, the general orientation control of the spin axis of a nonsymmetric spinning vehicle will be investigated. The following general assumptions about this vehicle are made:

1. The nominal spin axis is the maximum or minimum axis of inertia.
2. The other two principal axes of inertia are also the vehicle control axes. Control torque is applied continuously to these axes.
3. The nominal spin speed is much greater than rates about the lateral axes of the vehicle. This allows the linearization of Euler's equations from which derivation of the control law follows.

This control method can be used for any spinning vehicle and is particularly relevant to magnetic control of spinning satellites. It is applicable to both the satellites which served as examples for Chapters III and IV.

The particular advantage of relaxing the requirements of satellite symmetry is that of ease in design and manufacturing. The disadvantage, from a control designer's standpoint, is that the system parameters no longer can be treated as time invariant. The method developed here essentially transforms the system equations to a set which is time invariant and, thus, greatly simplifies the choice of control law.

THE LINEARIZED EQUATIONS OF MOTION AND THEIR OBSERVABILITY

From Chapter II, the rotational equations of motion of a rigid body as coordinatized along the body-fixed principal axes are the Euler equations:

$$\dot{\omega}_x = \frac{1}{I_{xx}} \left[T_x + (I_{yy} - I_{zz}) \omega_y \omega_z \right] , \qquad (5.1a)$$

$$\dot{\omega}_y = \frac{1}{I_{yy}} \left[T_y + (I_{zz} - I_{xx})\omega_x \omega_z \right] , \tag{5.1b}$$

$$\dot{\omega}_z = \frac{1}{I_{zz}} \left[T_z + (I_{xx} - I_{yy})\omega_x \omega_y \right] . \tag{5.1c}$$

With the assumption that the rate about the spin axis $\omega_z \gg \omega_x$ or ω_y and $T_z = 0$, Eqs. (5.1a-b) can be linearized to

$$\dot{\omega}_x = T_{x1} - B_s \omega_y , \tag{5.2a}$$

$$\dot{\omega}_y = T_{y1} + A_s \omega_x . \tag{5.2b}$$

Here,

$$T_{x1} = T_x / I_{xx} ,$$

$$T_{y1} = T_y / I_{yy} ,$$

$$A_s = (I_{zz} - I_{xx})\dot{\psi}/I_{yy} ,$$

$$B_s = (I_{zz} - I_{yy})\dot{\psi}/I_{xx} ,$$

where $\dot{\psi}$ is the nominal spin rate ω_z. For small angular displacements φ and θ about the inertially-fixed $\hat{x}_I$ and $\hat{y}_I$ axes, the two additional kinematic equations of motion are

$$\dot{\varphi} = \omega_x \cos \psi - \omega_y \sin \psi , \tag{5.3a}$$

$$\dot{\theta} = \omega_x \sin \psi + \omega_y \cos \psi , \tag{5.3b}$$

where ψ is the angle $\dot{\psi}(t-t_o)$.

Equations (5.2) - (5.3) are somewhat general. Little effort is required to transform them to the equations used in the local frame employed in Chapter III or the body frame employed in Chapter IV.

This is basically a time-varying fourth order system which is to be analyzed. It is assumed that the four states (ω_x, ω_y, φ, and θ) are available from which to generate the control torque. Their availability is dependent upon the vehicle system state being completely observable.

The following definitions and theorems from Silverman (Refs. 59, 60) provide the information necessary to determine the degree of observability of a system with time-varying coefficients.

Definition 5.1. Complete observability - (Ref. 59). The class of systems described by a finite set of first order differential equations of the form

$$\dot{x}(t) = F(t)\, x(t) + G(t)\, u(t) \,, \tag{5.4a}$$

$$y(t) = H(t)\, x(t) \,, \tag{5.4b}$$

is completely observable on an interval (t_o, t_1) if any initial state x_o at t_o can be determined from the knowledge of the system output $y(t)$ and input $u(t)$ over (t_o, t_1).

A system is further said to be uniformly completely observable if it is completely observable over every subinterval of all time of system operation.

Definition 5.2. Observability matrix - (Ref. 59). The observability matrix $Q_o(t)$ is

$$Q_o(t) = \left[S_o(t) \,\vdots\, S_1(t) \;\text{---}\; \vdots\, S_{n-1}(t) \right] \,, \tag{5.5}$$

where

$$S_o(t) = H^T(t) \,,$$

and

$$S_{k+1}(t) = F^T(t) S_k(t) + \frac{d}{dt} S_k(t) \,.$$

These definitions are used to prove the theorems:

Theorem 5.1. - (Ref. 59). The system with Eqs. (5.4a-b) is completely observable on the interval (t_o, t_1) if $Q_o(t)$ has full rank for some t contained in (t_o, t_1).∎

Theorem 5.2. - (Ref. 60). If the system (5.4a-b) is periodic, then it is uniformly completely observable if and only if it is completely observable.∎

This last theorem demonstrates that it is only necessary to show that a periodic system is observable at one point in time to conclude that it is observable for all time. It has immediate application to the equations of motion of the spinning vehicle.

It is interesting to note at this time that special conditions arise when there exists an observability advantage of a nonsymmetric vehicle over one with mass symmetry about the spin axis as considered in the previous two chapters. Recall that it was mentioned in Chapter III that if a symmetric satellite had roll error ($\hat{y}_L$-axis) measurement only, a constant torque about the yaw axis was unobservable. For the nonsymmetric vehicle, the state equations of the system with constant moments of torque about the reference axes associated with the local (L) reference frame are

$$\begin{bmatrix} T_{Lx} \\ T_{Ly} \\ \dot{\omega}_x \\ \dot{\omega}_y \\ \dot{\varphi} \\ \dot{\theta} \end{bmatrix} = \begin{bmatrix} 0 & \dot{\psi} & 0 & 0 & 0 & 0 \\ -\dot{\psi} & 0 & 0 & 0 & 0 & 0 \\ 1/I_{xx} & 0 & 0 & -B_s & 0 & 0 \\ 0 & 1/I_{yy} & A_s & 0 & 0 & 0 \\ 0 & 0 & \cos\psi & -\sin\psi & 0 & n \\ 0 & 0 & \sin\psi & \cos\psi & -n & 0 \end{bmatrix} \begin{bmatrix} T_{Lx} \\ T_{Ly} \\ \omega_x \\ \omega_y \\ \theta \\ \varphi \end{bmatrix} + \begin{bmatrix} 0 & 0 \\ 0 & 0 \\ 1 & 0 \\ 0 & 1 \\ 0 & 0 \\ 0 & 0 \end{bmatrix} \begin{bmatrix} T_{x1} \\ T_{y1} \end{bmatrix},$$

$$[\theta] = [0 \quad 0 \quad 0 \quad 0 \quad 0 \quad 1] [x] . \tag{5.6}$$

Here, T_{Lx} and T_{Ly} are the constant disturbance torques. The observability matrix (5.5) has full rank at all time for Eqs. (5.6) when $I_{xx} \neq I_{yy}$ (and $A_s \neq B_s$). Thus, in this instance the system is mathematically observable, whereas a similar system with equal lateral moments of inertia $(I_{xx} = I_{yy})$ is not.

From the practical standpoint, the usefulness of the above results applied to the satellite system of Chapter III seems to be limited by the accuracy of the initial conditions provided to the state estimator. If the initial values of $(\omega_x, \omega_y, \varphi, \theta)$ are well known, computer simulation demonstrates that the estimator works well from roll error θ input only. Conversely, with initial values of $(\omega_x, \omega_y, \varphi, \theta)$ poorly known, erroneous estimates of the disturbance torque components T_{Lx} and T_{Ly} result. This seems to be a case of ill conditioning on the part of the system matrices of (5.6) because of the smallness of the parameter n.

CONTROL LAW SYNTHESIS

The method of control synthesis for spinning nonsymmetric vehicles which follows is basically an extension of the method developed by Lange (Refs. 26, 61) for symmetric vehicles or systems with equations possessing frequency symmetry. Define

$$D_s \triangleq (B_s/A_s)^{1/2} ,$$

$$q_n \triangleq \omega_x + jD_s\omega_y ,$$

$$T_n \triangleq T_{x1} + jD_sT_{y1} ,$$

$$N_s \triangleq (B_sA_s)^{1/2}/\dot{\psi} .$$

Then Eqs. (5.2a-b) can be combined into the complex equation,

$$\dot{q}_n - jN_s\dot{\psi}q_n = T , \tag{5.7}$$

by multiplying (5.2a) by jD and adding it to (5.2a). Also, from Eqs. (5.3)

$$q_n = \frac{(D_s + 1)}{2} (\dot{\varphi} + j\dot{\theta})e^{-j\psi} - \frac{(D_s - 1)}{2} (\dot{\varphi} - j\dot{\theta})e^{j\psi} . \qquad (5.8)$$

Let

$$p_s \triangleq \frac{(D_s + 1)}{2} (\varphi + j\theta)$$

$$m_s \triangleq \frac{(D_s - 1)}{2} (\varphi - j\theta).$$

Then, Eq. (5.8) becomes

$$q_n = \dot{p}_s e^{-j\psi} - \dot{m}_s e^{j\psi} . \qquad (5.9)$$

Thus,

$$\dot{p}_s = q_n e^{j\psi} + \dot{m}_s e^{j2\psi} . \qquad (5.10)$$

Taking the derivative of (5.10) and using (5.7) and (5.9) yields

$$\left[\ddot{p}_s - j(N_s+1)\dot{\psi}\dot{p}_s - \ddot{m}_s - j(N_s-1)\dot{\psi}\dot{m}_s\right]e^{j2\psi} = T_n e^{j\psi}. \qquad (5.11)$$

Now, letting

$$r_s \triangleq p_s e^{-j(N_s+1)\psi/2} ,$$

and

$$s_s \triangleq m_s e^{-j(N_s-1)\psi/2} ,$$

Eq. (5.11) becomes

$$\left[\ddot{r}_s + \frac{(N_s+1)^2}{4} \dot{\psi}^2 r_s\right] e^{j(N_s+1)\psi/2} - \left[\ddot{s}_s + \frac{(N_s-1)^2}{4} \dot{\psi}^2 s_s\right] e^{j(N_s+3)\psi/2} = T_n e^{j\psi} .$$

(5.12)

The quantity $T_n e^{j\psi}$ represents the control torque. Let this be set to

$$T_n e^{j\psi} = (-K_1\dot{r}_s - K_2 r_s)e^{j(N_s+1)\psi/2} + (K_3\dot{s}_s + K_4 s_s)e^{j(N_s+3)\psi/2} .$$

Then (5.12) becomes

$$\left[\ddot{r}_s + K_1\dot{r}_s + \left(K_2 + \frac{(N_s+1)^2\dot{\psi}^2}{4}\right) r_s\right] e^{j(N_s+1)\psi/2}$$

$$-\left[\ddot{s}_s + K_3\dot{s}_s + \left(K_4 + \frac{(N_s-1)^2\dot{\psi}^2}{4}\right) s_s\right] e^{j(N_s+3)\psi/2} = 0 , \qquad (5.13)$$

when no disturbance torques act upon the system. For (5.13) to equal zero for all time,

$$\ddot{r}_s + K_1\dot{r}_s + \left(K_2 + \frac{(N_s+1)^2\dot{\psi}^2}{4}\right) r_s = 0 , \qquad (5.14a)$$

$$\ddot{s}_s + K_3\dot{s}_s + \left(K_4 + \frac{(N_s-1)^2\dot{\psi}^2}{4}\right) s_s = 0 . \qquad (5.14b)$$

Thus, the selection of a control law for the nonsymmetric system consists of choosing four gains (K_1, K_2, K_3, K_4) to give the desired response to two uncoupled harmonic oscillators [Eqs. (5.14)] in a transformed coordinate frame. That the transformation to this coordinate frame exists is known from the theory of matrices (Ref. 62). Any linear system

$$\dot{\vec{x}} = F\vec{x}$$

where F has periodic coefficients is always reducible to one with constant coefficients.

With the choice of gains being made, the applied control in the φ-θ coordinate system becomes

$$T_n = \left[-K_1 \frac{(D_s+1)}{2} (\dot{\varphi} + j\dot{\theta}) - \left(K_2 - jK_1 \frac{(N_s+1)}{2} \dot{\psi}\right) \frac{(D_s+1)}{2} (\varphi + j\theta)\right] e^{-j\psi}$$

$$+ \left[K_3 \frac{(D_s-1)}{2} (\dot{\varphi} - j\dot{\theta}) + \left(K_4 - jK_3 \frac{(N_s-1)}{2} \dot{\psi}\right) \frac{(D_s-1)}{2} (\varphi - j\theta)\right] e^{j\psi} , \tag{5.15}$$

which is the complex control law. In real form, this becomes

(5.16)

where γ_x and γ_y (the star-tracker variables) are defined as

$$\gamma_x = \varphi \cos \psi + \theta \sin \psi ,$$

$$\gamma_y = -\varphi \sin \psi + \theta \cos \psi .$$

With the choice $K_1 = K_3$ and $K_2 = K_4$, the real control law is

$$\boxed{\begin{aligned} T_{x1} &= -K_1\omega_x - K_2\gamma_x - K_1 \frac{(N_s D_s+1)}{2} \dot{\psi}\gamma_y , \\ T_{y1} &= -K_1\omega_y - K_2\gamma_y + K_1 \frac{(N_s+D_s)}{2D_s} \dot{\psi}\gamma_x . \end{aligned}} \tag{5.17}$$

When $I_{xx} = I_{yy}$, $D_s = 1$ and (5.17) reduces to the results of (Ref. 61).

An example serves to illustrate the utility of this control synthesis. Consider a vehicle with moments of inertia

$$I_{xx} = 3.08 \text{ kg-m}^2 ,$$

$$I_{yy} = 9.24 \text{ kg-m}^2 ,$$

$$I_{zz} = 10.0 \text{ kg-m}^2 ,$$

nominally spinning about its Z axis at one rad/sec. Without Eqs. (5.16) one might attempt to control the spin-axis orientation by using a control law for an axisymmetric spinning body. An average value of the lateral moments of inertia could be assumed.

In (Ref. 61), the power optimal control for a symmetric spinning vehicle with no nutation damper was shown to be

$$T_{x1} = -K_{v1}\omega_x - K_{p1}\gamma_x - \frac{R_s\dot{\psi}K_{v1}}{2}\gamma_y ,$$

$$T_{y1} = -K_{v1}\omega_y - K_{p1}\gamma_y + \frac{R_s\dot{\psi}K_{v1}}{2}\gamma_x , \qquad (5.18)$$

where R_s is the moment-of-inertia ratio

$$R_s = I_{zz}/I_{xx} .$$

The choice of gains for power optimal control (see Ref. 61) is

$$K_{p1} = -\left(\frac{R_s\dot{\psi}}{2}\right)^2 + \sqrt{\left(\frac{R_s\dot{\psi}}{2}\right)^4 + q} ,$$

$$K_{v1} = \sqrt{2K_{p1}} .$$

These come from optimizing the cost function

$$J_f = \frac{1}{2} \int_{-\infty}^{t_f} (qx^2 + T^2)\, dt$$

This function applies to the harmonic oscillator equation

$$\ddot{x} + \Omega_s^2 x = T$$

that governs the dynamics of a symmetric spinning vehicle. In this example, it is assumed that

$$R_s = \frac{1}{2}\left(\frac{I_{zz}}{I_{xx}} + \frac{I_{zz}}{I_{yy}}\right).$$

The optimization analysis can also be applied to Eq. (5.12) (which represents two uncoupled harmonic oscillators) for determining the gains K_1, K_2, K_3, and K_4 in Eq. (5.13), but the resulting control law [Eqs. (5.16)] is strictly suboptimal.

A simulation was made of a vehicle with the above moments of inertia and the control laws (5.16) and (5.18). The optimum gains K_{v1} and K_{p1} were used for (5.18). Initial conditions were

$$\omega_x = 0.1 \text{ sec}^{-1},$$

$$\omega_y = 0$$

$$\varphi = 0.1,$$

$$\theta = 0.1.$$

The control law (5.18) (based upon average lateral moments of inertia) did <u>not</u> produce a trajectory which converged to the origin. On the other hand, control law (5.16) always produces asymptotic stability if the gains K_1 to K_4 are positive.

CONCLUSIONS AND RECOMMENDATIONS FOR FURTHER STUDY

In conclusion, the synthesis procedure developed in this chapter has the following distinguishing points:

1. This technique allows the designer the freedom to choose the dynamic response that is desired to remove small attitude errors of an unsymmetric vehicle's spin axis.
2. This control can be continuously mechanized with constant gains.
3. The vehicle designer thus has more freedom to build an unsymmetric spacecraft intentionally. This freedom might ease the design tolerances in vehicle construction. Possibly it can provide the means for obtaining more precise control by making the disturbance torques fully observable.

This chapter by no means exhausts the possibilities for further study of continuous precision (including magnetic) control of nonsymmetric spinning vehicles. Cross-product-of-inertia terms and arbitrary nutation damping coefficients may still need to be taken into account in the control synthesis. A determination of power optimal control by a means less cumbersome than numerically solving the matrix Ricatti equations is highly desirable. Also, a demonstration that the control laws (including those of Chapters III and IV developed to remove small attitude errors produce asymptotic stability for large misalignment would be valuable for some spacecraft applications.

APPENDIX A

MATHEMATICAL MODEL OF THE NEAR EARTH MAGNETIC FIELD

A requirement for analyzing the earth's magnetic field for attitude control purposes is to have an adequate model of the field. The method of mathematically modeling the near-earth* magnetic field used today follows the work of Gauss and applies potential theory and spherical harmonic analysis. Discussions of this modeling can be found in Refs. 63, 64, and 65, and are summarized here.

It is assumed that if a region is removed from the magnetic sources, then the magnetic field $\vec{B}$ of that region is the negative gradient of the magnetic potential V_m of the sources,

$$\vec{B} = -\nabla V_m \quad . \tag{A.1}$$

This potential must satisfy Laplace's equation,

$$\nabla^2 V_m = 0 \quad . \tag{A.2}$$

The solution for this potential which describes the near-earth magnetic field is given as

$$V_m = a_e \sum_{n=1}^{\infty} \sum_{m=0}^{n} P_n^m(\cos \theta_p) \left\{ \left[g_{in}^m (a_e/R)^{n+1} + g_{en}^m (R/a_e)^n \right] \cos m\varphi_p + \left[h_{in}^m (a_e/R)^{n+1} + h_{en}^m (R/a_e)^n \right] \sin m\varphi_p \right\} . \tag{A.3}$$

---

* Satellite measurements have revealed that below synchronous altitude, the geomagnetic field strength is reasonably close to an earth-centered dipole field. Beyond this distance, the effect of the teardrop-shaped magnetosphere begins to be felt. See Ref. 64.

where

a_e	=	the mean earth radius;
R	=	the distance from the geocenter;
suffixes i, e on g and h	=	sources internal and external to the earth;
θ_p and φ_p	=	satellite position's earth-fixed colatitude and east longitude;
$P_n^m(\cos\theta_p)$	=	multiple of the associated Legendre function;
g_n^m and h_n^m	=	coefficients corresponding to the multiple and are selected to yield the best possible fit to measurement data of the magnetic field.

In the literature, the associated Legendre functions are usually normalized according to methods of Gauss or Schmidt [Ref. 63]. The latter normalization is utilized here because it seems to be the more prevalent one. (Care should be exercised when using published magnetic coefficients g_n^m and h_n^m to insure that they are normalized to the corresponding multiple of the associated Legendre function used.) The Schmidt normalized associated Legendre function is expressed as

$$P_n^m(\cos\theta_p) = \left(\frac{\delta_m(n+m)!}{2(n-m)!}\right)^{\frac{1}{2}} \frac{2^n n!(n-m)!}{(2n)!} \sin^m\theta_p \left[\cos^{n-m}\theta_p - \frac{(n-m)(n-m-1)}{2(2n-1)} \times \cos^{n-m-2}\theta_p + \frac{(n-m)(n-m-1)(n-m-2)(n-m-3)}{2\cdot 4(2n-1)(2n-3)}\cos^{n-m-4}\theta_p - \cdots\right], \quad (A.4)$$

where $\delta_m = 2$ for $m = 0$ and $= 1$ otherwise by the convention used in Ref. 63.

The Gauss normalized coefficients $P^{n,m}(\cos\theta_p)$, which are employed in Ref. 65, are obtained by the relationship

$$P^{n,m}(\cos\theta_p) = \left(\frac{2(n-m)!}{\delta_m(n+m)!}\right)^{\frac{1}{2}} \frac{(2n)!}{2^n n!(n-m)!} P_n^m(\cos\theta_p). \quad (A.5)$$

The main field is that portion of the geomagnetic field which originates within the earth. It represents greater than 99% of the measurable field and has a secular change of about 0.1% per year. The weak fields originating outside of the earth are quite variable with

fluctuations in periods of a few days or less. These fluctuations are discussed later. The extrapolated values of the main field can be considered correct up to synchronous altitude and time-varying external fields may be superimposed upon it.

Figure A.1 shows the components of the geomagnetic field and their associated angles. Here, B is the intensity of the field and X_m, Y_m, Z_m are its components with X_m pointing northward, Y_m pointing eastward, and Z_m pointing downward.

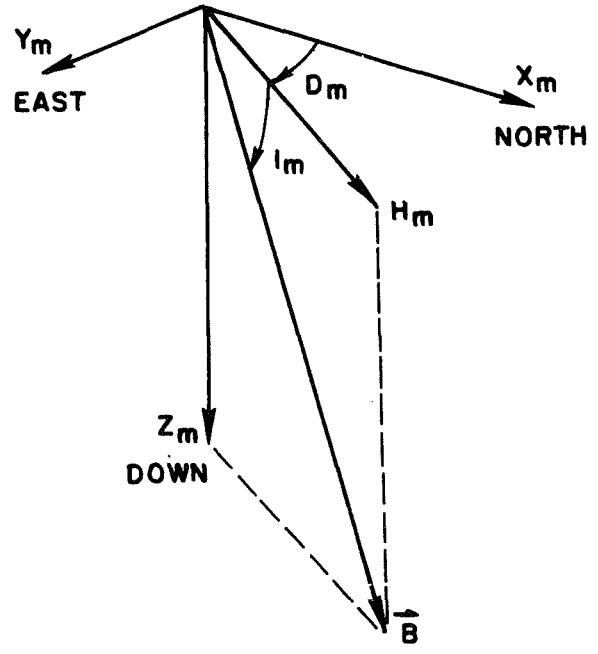

FIG. A.1. COMPONENTS OF THE GEOMAGNETIC FIELD AND THEIR ASSOCIATED ANGLES.

Also, I_m is the inclination or dip angle, D_m is the declination angle, and H_m is the horizontal component. From Eq. A.1, the components are found to be

$$X_m = \frac{1}{R}\frac{\partial V_m}{\partial \theta_p},$$

$$= \sum_{n=1}^{n_{max}} \sum_{m=0}^{n} \frac{dP_n^m}{d\theta_p} \left\{ \left[g_{in}^m (a_e/R)^{n+2} + g_{en}^m (R/a_e)^{n-1} \right] \cos m\varphi_p \right. \tag{A.6a}$$

$$\left. + \left[h_{in}^m (a_e/R)^{n+2} + h_{en}^m (R/a_e)^{n-1} \right] \sin m\varphi_p \right\}.$$

$$Y_m = -\frac{1}{R \sin \theta_p}\frac{\partial V_m}{\partial \varphi_p},$$

$$= \sum_{n=1}^{n_{max}} \sum_{m=0}^{n} \frac{mP_n^m}{\sin \theta_p} \left\{ \left[g_{in}^m (a_e/R)^{n+2} + g_{en}^m (R/a_e)^{n-1} \right] \sin m\varphi_p \right. \tag{A.6b}$$

$$\left. - \left[h_{in}^m (a_e/R)^{n+2} + h_{en}^m (R/a_e)^{n-1} \right] \cos m\varphi_p \right\}.$$

$$Z_m = \frac{\partial V_m}{\partial R},$$

$$= \sum_{n=1}^{n_{max}} \sum_{m=0}^{n} P_n^m \left\{ \left[-g_{in}^m (n+1)(a_e/R)^{n+2} + g_{en}^m n (R/a_e)^{n-1} \right] \cos m\varphi_p \right.$$

$$\left. + \left[-h_{in}^m (n+1)(a_e/R)^{n+2} + h_{en}^m (R/a_e)^{n-1} \right] \sin m\varphi_p \right\}. \tag{A.6c}$$

The magnitude of these components is commonly in gammas where 10^5 gammas = 1 gauss, the unit of induction.

A full set of the Schmidt normalized coefficients g_{in}^m, g_{en}^m, h_{in}^m, and h_{en}^m up to degree and order n=m=12 can be found in Ref. 66 for epoch 1965.0.

However, there are good reasons from the attitude control application standpoint to ignore the effects of external sources (the g_e and h_e coefficients) and use coefficients which are found by fitting the data to a model which assumes that the potential is due to an internal source only. First, satellite measurement data of the magnetic field are small in number compared to the amount of earth surface data. Secondly, the strength of measured external field sources is small (less than 1% of internal source) as can be seen by examining the coefficients of Ref. 66 for near-earth regions. Also, little has been proven as to the definite field contributions of the external fields. Finally, eliminating the external static contributions to the field considerably reduces the computation required to determine the field components.

When mechanizing Eqs. (A.6a) through A.6c) on a digital computer, a great deal of run time can be saved by making use of several recursion formulas which relate the terms of the summations. For $\theta_p \neq 0, \pi$ use

$$P_0^0 = 1 \quad , \tag{A.7a}$$

$$P_1^0 = \cos\theta_p \quad , \tag{A.7b}$$

$$\vdots$$

$$P_k^0 = \left(\frac{2k-1}{k}\right) \cos\theta_p \, P_{k-1}^0 - \left(\frac{k-1}{k}\right) P_{k-2}^0 \quad ; \tag{A.7c}$$

$$P_1^1 = \sin\theta_p \quad , \tag{A.8a}$$

$$\vdots$$

$$P_k^k = \left(\frac{2k-1}{2k}\right)^{\frac{1}{2}} \cos\theta_p \, P_{k-1}^{k-1} \quad \text{for} \quad k \geq 2 \quad ; \tag{A.8b}$$

$$P_k^{k-1} = (2k-1)^{\frac{1}{2}} \cos\theta_p \, P_{k-1}^{k-1} \quad \text{for} \quad k > 2 \quad , \tag{A.9a}$$

$$P_{n+1}^k = \left[(2n+1)\cos\theta_p P_n^k - (n^2-k^2)^{\frac{1}{2}} P_{n-1}^k\right] \Big/ \left[(n+1)^2-k^2\right]^{\frac{1}{2}} \tag{A.9b}$$

$$\text{for} \quad n \geq k+1 \quad ;$$

$$\frac{d}{d\theta_p}P_n^0 = -\left[\tfrac{1}{2}n(n+1)\right]^{\frac{1}{2}} P_n^1 \quad , \tag{A.10a}$$

$$\frac{d}{d\theta_p}P_n^k = \tfrac{1}{2}\left[\delta_{k-1}(n+k)(n-k+1)\right]^{\frac{1}{2}}P^{k-1} - \tfrac{1}{2}\left[(n+k+1)(n-k)\right]^{\frac{1}{2}}P_n^{k+1}$$

$$\text{for} \quad k \geqslant 0 \quad ;$$

$$\frac{kP_n^k}{\sin\theta_p} = \tfrac{1}{2}\left[\delta_{k-1}(n+k)(N+k-1)\right]^{\frac{1}{2}} P_{n-1}^{k-1} + \tfrac{1}{2}\left[(n-k)(n-k-1)\right]^{\frac{1}{2}} P_{n-1}^{k+1} \tag{A.11}$$

$$\text{for} \quad k > 0 \quad ,$$

where

$$\delta_{k-1} = \begin{bmatrix} 2 & k = 1 \\ 1 & k > 1 \end{bmatrix} \quad .$$

For $\theta_p = 0, \pi$ use the following:

$$\text{For} \quad \theta_p = 0, \quad P_n^0 = 1 \; ; \tag{A.12a}$$

$$\text{For} \quad \theta_p = \pi, \quad P_n^0 = (-1)^n \; . \tag{A.12b}$$

$$P_n^k = 0, \quad \text{for} \quad k > 0 \quad . \tag{A.12c}$$

Also,

$$\frac{d}{d\theta_p}P_n^k = 0 \qquad \text{for} \quad k = 0, \tag{A.13a}$$

$$= \tfrac{1}{2}[2n(n+1)]^{\frac{1}{2}} P_n^0 \qquad \text{for} \quad k = 1, \tag{A.13b}$$

$$= 0 \qquad \text{for} \quad k > 1 \quad , \tag{A.13c}$$

and

$$\frac{kP_n^k}{\sin \theta_p} = 0 \qquad \text{for} \quad k = 0, \tag{A.14a}$$

$$= \tfrac{1}{2}[2n(n+1)]^{\frac{1}{2}} P_{n-1}^0 \quad \text{for} \quad k = 1, \tag{A.14b}$$

$$= 0 \qquad \text{for} \quad k > 1 . \tag{A.14c}$$

X_m, Y_m, and Z_m are multiplied by 10^{-9} to convert from gammas to Webers/m^2 .

A suitable set of Schmidt coefficients of the geomagnetic field are those of Ref. 67 which are presented in Table A.1. The coefficients and their derivatives are in gammas and gammas/year and are for epoch 1960.0. They represent 197,000 observations fitted to an assumed internal source potential with a mean earth radius (a_e) of 6371.2 km.

VARIATION TO THE SLOWLY CHANGING MAGNETIC FIELD

The quantities which cause the earth's magnetic field to be distorted from that of a static symmetric dipole include those which are classified as (1) sun-line distortions, (2) secular variations, (3) diurnal variations, (4) daily lunar variations, (5) magnetic storm disturbances, and (6) local irregularities. The sun-line distortion is the tear-drop distortion spoken of earlier with the effect that the field lines are compressed in the subsolar direction and spread apart into a tail on the opposite side of the earth. This effect is insignificant, however, for distances, less than 5 earth radii. At synchronous altitude, the distortion in magnitude can be as large as 25%.

The secular variations in the geomagnetic field are accounted for by using the first-time derivatives of the Schmidt coefficients (g_n^m and h_n^m) as given in Table A.1 to update the coefficient to the epoch of interest. Use

TABLE A.1

SCHMIDT NORMALIZED HARMONIC COEFFICIENTS OF THE GEOMAGNETIC FIELD (EPOCH 1960.0) IN UNITS OF GAMMAS AND GAMMAS/YEAR.

Degree n	Order m	g_n^m	h_n^m	$\dot{g}_n^m$	$\dot{h}_n^m$
1	0	-30425	-0	20.6	-0.
1	1	-2162	5775	6.0	-3.9
2	0	-1536	-0	-29.1	-0.
2	1	3000	-1950	1.2	-13.7
2	2	1585	204	-0.7	-15.8
3	0	1301	-0	2.7	-0.
3	1	-1987	-431	-10.0	6.5
3	2	1290	231	1.6	2.9
3	3	871	-130	-1.3	-9.2
4	0	958	-0	-0.9	-0.
4	1	803	152	1.9	-1.8
4	2	503	-268	-1.2	-1.5
4	3	-394	3	-0.5	3.2
4	4	271	-251	-4.2	-5.5
5	0	-228	-0	2.6	-0.
5	1	360	9	-0.1	3.0
5	2	231	121	1.5	2.9
5	3	-31	-116	-0.4	-1.9
5	4	-157	-110	-0.7	1.2
5	5	-65	80	1.6	0.8
6	0	50	-0	-0.7	-0.
6	1	61	-12	1.0	-1.4
6	2	5	103	0.8	0.1
6	3	-242	61	2.1	1.5
6	4	-1	-27	1.6	-0.7
6	5	0	-12	-0.1	-0.1
6	6	-109	-12	0.1	0.4
7	0	71	-0		
7	1	-57	-54		
7	2	6	-24		
7	3	8	-9		
7	4	-24	2		
7	5	-2	28		
7	6	14	-21		
7	7	6	-20		
8	0	5	-0		
8	1	7	7		
8	2	-9	-12		
8	3	-14	6		
8	4	-3	-17		
8	5	7	3		
8	6	-6	24		
8	7	12	-3		
8	8	6	-16		
9	0	10	-0		
9	1	3	-22		
9	2	7	16		
9	3	-16	5		
9	4	11	-4		
9	5	11	-2		
9	6	1	10		
9	7	-0	12		
9	8	2	0		
9	9	2	-3		

$$g_n^m(t_y) = g_n^m(1960.0) + (t_y - 1960.0)\dot{g}_n^m \qquad (A.15)$$

and a similar expression to update $h_n^m(t_y)$ with t_y being the epoch in years.

Diurnal variations due to the sun result in cyclic variations of the field magnitude of up to 200 gammas. Near the earth, this variation is small compared to the total field and can be neglected from the control analysis standpoint. At distances of several earth radii, insufficient data is available to make any conclusions. The daily lunar variation can cause amplitude variations reaching 12 gammas but this also is small enough to neglect.

Theories exist on the cause and behavior of magnetic storms and their relationship to electric current systems in the lower ionosphere and the equatorial ring current which supposedly encircles the earth. However, because there is no general knowledge of the storm-time variations nor a general description of the ring current, geophysicists have found it impossible to include the storm effect in a model. During great magnetic storms, field variations can amount to 3500 gammas (or more than 5%) in the polar regions. Rapid variations of the magnetic field ranging in duration from a few minutes down to 0.1 seconds called 'micropulsations' also occur. Amplitude of these variations seem to be directly proportional to their duration. Fluctuations of up to 300 gammas have been recorded for durations of two minutes although the average fluctuation in amplitude is 20 gammas.

Local irregularities in the geomagnetic field are taken into account by using more than three terms in the harmonic expansion for the field.

It can be concluded that though variations exist in the earth's magnetic field, they can be usually neglected because they're small or can be taken into account by using a sufficient number of terms in the

harmonic representation of the field. Since this study is concerned with sub-synchronous orbits, the sun-line distortion can be neglected. Regarding the large variations due to magnetic storms, one can take the point of view that a magnetic control system should be made of sufficient power that it functions adequately in the presence of the weakest magnetic field probably encountered during an orbit. Thus, by designing the system so that it has a factor of safety in power over that required for operation in the average field, the fallibility of the magnetic model can be neglected.

FURTHER SIMPLICATION TO THE FIELD MODEL

When investigating the use of the magnetic field in conjunction with attitude control of spacecraft, it is often desirable to reduce the complexity of the field model. Using a simpler model results in easier visualization of the field characteristics. Also, a simple model often allows analytical solutions to questions which arise concerning the effect of the field.

The mathematical models of the geomagnetic field which have been used by control systems analysts include:

1. Constant field. Here one assumes the magnetic field is constant in magnitude and direction for a short duration of time.

2. Linearly changing field. The magnitude and direction of the field vector changes linearly with time.

3. Simple dipole. This model assumes the magnetic dipole lies along the earth's spin axis and points south. The potential used is $V_m = g_1^0 \cos \theta_p (a_e^3/R^2)$.

4. Tilted dipole. This is the most common model used. It uses the first three internal source terms of the potential given by Eq. A.3. The terms $g_1^1 a_e^3$ and $h_1^1 a_e^3$ represent dipoles lying in the equatorial plane and pointing toward 180° and 90°E longitude respectively. The resultant of the three orthogonal dipoles $B_0 a_e^3$ has a magnitude

$$B_0 = \sqrt{(g_1^0)^2 + (g_1^1)^2 + (h_1^1)^2}$$

and a polar angle $\Theta_0 = \cos^{-1} (g_1^0/B_0)$. The equatorial component

points toward longitude $\Phi_o = \tan^{-1}(h_1^1/g_1^1)$. The point (a_e, Θ_o, Φ_o) is the South geomagnetic pole. Its opposite, the North geomagnetic pole is approximately located at 79°N latitude (11° colatidue) and 69°W longitude. The potential of the tilted dipole is $V_m = B_o(a_e^3/R^2)\cos\theta_m$ where θ_m is the geomagnetic colatitude. Then the geomagnetic north and vertical components are $X_m = B_o(a_e/R)^3 \sin\theta_m$ and $Z_m = 2B_o(a_e/R)^3\cos\theta_m$.

5. Quadruple model. This model includes the first eight terms (up to $n_{max} = m_{max} = 2$) of the spherical harmonic expansion of V_m. Luke [Ref. 64] in his error analysis, uses the criterion that an acceptable model is one in which the magnitude and angular deviations of the field from that of the measured field are always less than 5% and 3° respectively. With this criterion, he concludes that for final analysis purposes, the tilted dipole is adequate at distances beyond 5 earth radii and the quadruple model is adequate beyond 3 earth radii. He recommends that below 3 earth radii, the full harmonic expansion model be used.

The decision of which model to be used at different points in the system design effort is largely one of judgment on the part of the analyst.

A mathematical average of the magnetic field components found in a circular orbit of variable inclination and altitude is shown in Fig. A.2. This figure, taken from Ref. 9, has the components coordinatized in the local (L) frame of Fig. 2.2. Figure A.2 is useful for estimating control gains and performance characteristics.

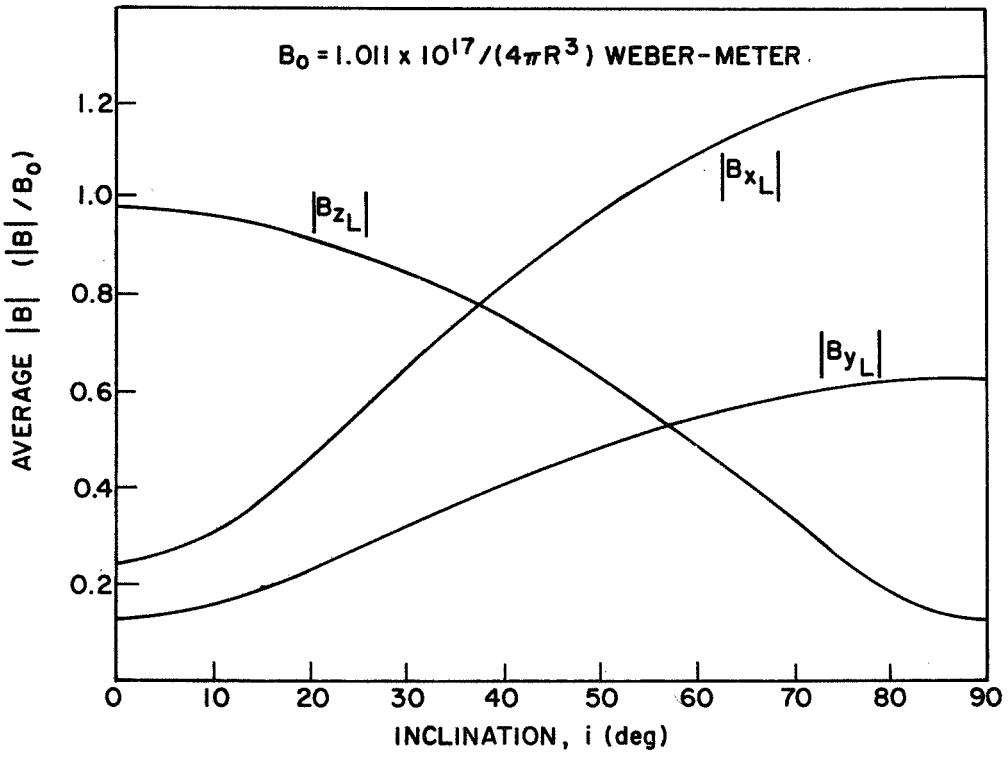

FIG. A.2. AVERAGE VALUE OF LOCAL COMPONENTS OF THE MAGNETIC FIELD FOR CIRCULAR ORBITS BASED UPON A SIMPLE DIPOLE MODEL.

APPENDIX B

DENSITY MODEL OF THE ATMOSPHERE ABOVE 120 KM

The atmospheric models derived from the analysis of satellite drag data of the recent past are variable in nature, in that density is a function of the height above sea level, the relative position of the sun with respect to the given point, and the energy being emitted from the sun. Models which account for the various fluctuations in density due to variables other than altitude change are termed "dynamic" models. Factors which affect the value of density in a dynamic model include:

1. The day-night effect,
2. The 27-day solar effect,
3. The 11-year solar cycle effect,
4. The semiannual effect, and
5. The magnetic storm effect.

Various models which account for each of these effects to some degree have been summarized by Bruce [Ref. 68].

The day-night or diurnal-bulge effect is due to the sun's ultraviolet radiation being maximum near the subsolar point. This radiation causes the atmosphere to heat and the density to increase. The resulting bulge lags the sun's path by about 30° in longitude (2 p.m. local time) because of the time required for the atmosphere to adjust to the heating. The bulge effect is not symmetric, however, and the minimum density (above 300 km) occurs on the dark side at about 4 a.m.

The sun's extreme ultraviolet emission is erratic in nature but tends to correspond to the sun's 27-day period of rotation. This emission, which also causes density fluctuations of the high-altitude atmosphere, is correlated with the 10.7 cm decimetric flux (2800 Mc) from the sun. This index, expressed in units of 10^{-22} Watts/m^2/cps bandwidth, is denoted by $F_{10.7}$.

The monthly average of the decimetric flux, denoted by $\bar{F}_{10.7}$, is correlated with the 11-year solar cycle which causes a slowly fluctuating corpuscular emission known as the solar wind. $\bar{F}_{10.7}$ ranges approximately between 70 and 280 during the quiet and active periods of the solar cycle. Figure B.1 taken from Ref. 69 shows the $F_{10.7}$ index average between the years 1947 and 1961. This effect can cause a variation in density by a factor of 3 at 100 n. miles altitude and even a greater effect at higher altitudes.

The density variation with annual and semiannual components known as the semiannual or plasma effect has also been hypothesized to be due to the solar wind. Figure B.2, also from Ref. 69, gives an indication of this effect for a 350 km altitude satellite over a four-year period.

The largest short-term fluctuation of the atmospheric density is due to magnetic storms. The 3-hour magnetic activity index a_p expressed in units of $2\gamma_m(\gamma_m = 10^{-5}$ gauss) normally fluctuates between 0 and 30 but can go as high as 400 during an intense storm.

Each of these five effects along with altitude variations has been incorporated into a model developed by Jacchia [Ref. 70] which is summarized here. The basic idea is to determine empirically the atmospheric temperature at a point as a function of the parameters $F_{10.7}$, $\bar{F}_{10.7}$, a_p, the day of the year, the local solar time, the latitudes of the sun and the point in question, and the altitude. Then with a fixed set of boundary conditions at the altitude of 120 km, the concentration of each of four gases are found at the point by integrating the static diffusion equation

$$\frac{dn_i}{n_i} = -\frac{dh_a}{H_i} - \frac{dT_m}{T_m}(1 + \alpha_d) \quad . \tag{B.1}$$

Here, n_i is the concentration of each of the gases N_2, O_2, O, and He, (the effect of hydrogen is also brought in above 500 km); h_a is the altitude, T_m is the temperature, and α_d is the thermal-diffusion

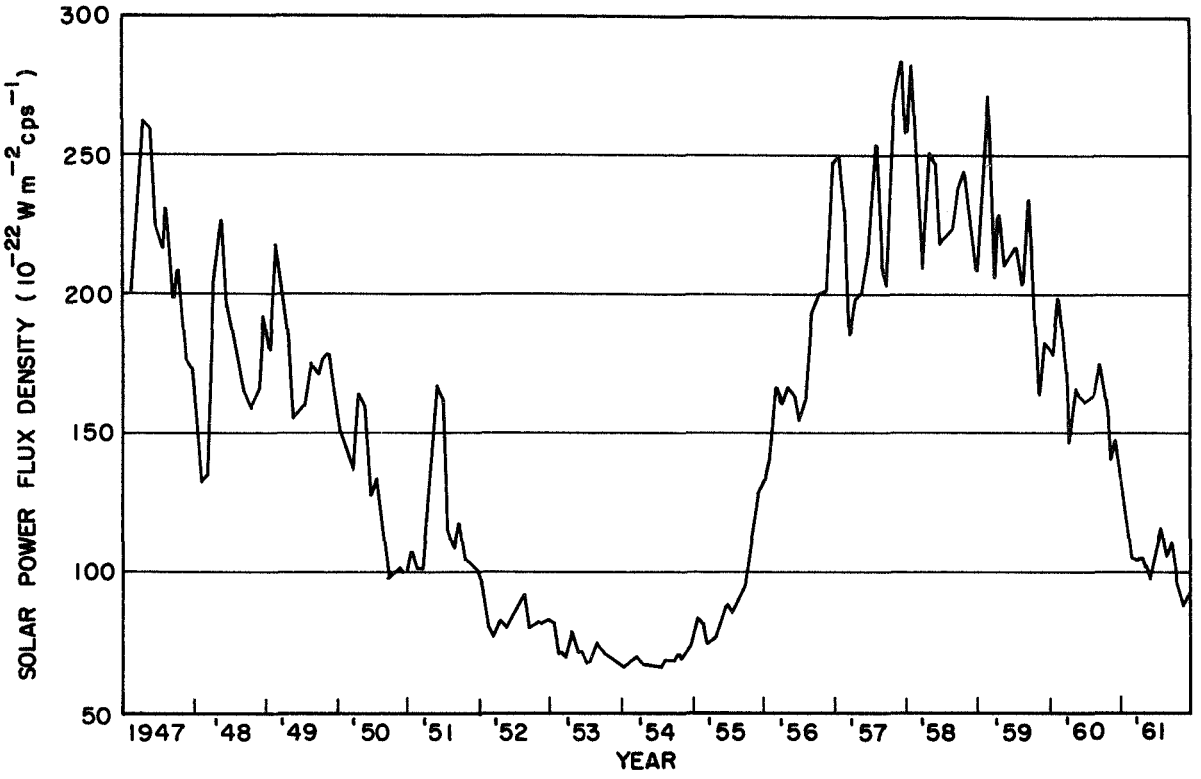

FIG. B.1. MONTHLY AVERAGES OF THE 10.7-CM SOLAR POWER FLUX DENSITY.

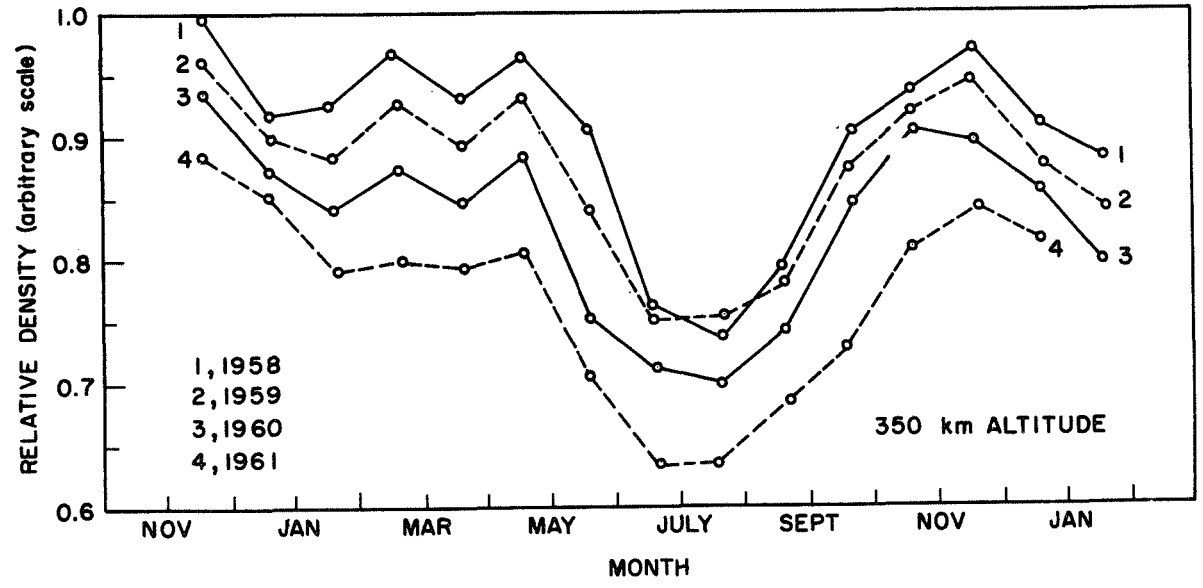

FIG. B.2. ANNUAL AND SEMIANNUAL RELATIVE ATMOSPHERIC DENSITY VARIATIONS.

factor. H_i is the scale height of the individual element defined as

$$H_i = \frac{kT_m}{m_i g_e} = \frac{k_B T_m (1+h_a/a_e)^2}{m_i g_{eo}} , \qquad (B.2)$$

where k_B is the Boltzmann constant, m_i is the molecular or atomic mass of the element, and g_e is the gravitational acceleration which is a function of h_a. Because this model is based on fixed boundary conditions at 120 km, there may be some doubt as to its usefulness for lower altitudes ($\leq$200 km). However, Jacchia compared his model with the results of Small [Ref. 71] and found excellent agreement between 130 km and 200 km for low-inclination orbits.

Since the time Jacchia published his results, data from flights of the Explorer 19 and 24 satellites in nearly polar orbits gave further information on density variations in the polar regions. Keating and Prior [Ref. 72] used the results of this data to modify Jacchia's model for the non-symmetry in the diurnal bulge. This later version minimizes the residuals between the observed and predicted exospheric temperatures in comparison with over 1000 other models.

This modified Jacchia model determines the exospheric temperature at 1000 km and uses an empirical equation to derive the resulting temperature at any other altitude. This temperature is then used in the solution to Eq.(B.1) to yield the desired density. The development proceeds as follows.

The night-time minimum temperature at 1000 km due to variations in the 11-year solar cycle can be expressed as

$$\bar{T}_o = 418^\circ + 3.6\,\bar{F}_{10.7} , \qquad (B.3)$$

where temperature is in degrees Kelvin. The fluctuation caused by the 27-day effect is accounted for by

$$T_o' = \bar{T}_o + 1.8\,(F_{10.7} - \bar{F}_{10.7}) . \qquad (B.4)$$

To this expression the semiannual effect is added;

$$T_o = T_o' + (0.37 + 0.14 \sin 2\pi \frac{d-151}{365}) \bar{F}_{10.7} \sin 4\pi \frac{d-59}{365} , \qquad (B.5)$$

where d is days from January 1. This temperature must be modified to account for variation at other locations in the bulge. This is done using the modification of Keating and Prior,

$$T_\infty' = T_o[1+0.28 \sin \eta_\odot + 0.28(\cos \theta_\odot - \sin \eta_\odot)\cos^{2.5} \frac{\tau_\odot}{2}] \qquad (B.6)$$

where

$\tau_\odot = H_a - 45° + 12° \sin (H_a + 45°) \quad (-\pi \leq \tau \leq \pi)$

H_a = hour angle of sun (deg) from the point,

$\eta = \frac{1}{2}|(\lambda_s - \lambda_\odot)|$,

$\theta_\odot = \frac{1}{2}|(\lambda_s + \lambda_\odot)|$,

λ_s = declination of point (deg),

$\lambda_\odot$ = sun's declination (deg).

This temperature is further modified to account for variation in the geomagnetic activity by

$$T_\infty = T_\infty' + 1.0 a_p + 125°[1 - \exp(-0.08 a_p)] . \qquad (B.7)$$

Combining Eqs. B.3 - B.7 yield the exospheric temperature at 1000 km and beyond. To find the temperature at any altitude h_a(in km), use

$$T_m = T_\infty - (T_\infty - 355°) \exp[-s_\odot(h_a - 120)] , \qquad (B.8)$$

where

$$s_\odot = 0.0291 \exp(-x_\odot^2/2) , \qquad (B.9)$$

$$x_\odot = \frac{(T_\infty - 800)}{750 + 1.722 \times 10^{-4}(T_\infty - 800)^2} , \qquad (B.10)$$

and

$$h_a = R - \frac{6378.165}{\sqrt{1 + 6.7385 \times 10^{-3} \sin^2\lambda'}} . \qquad (B.11)$$

R is the radial distance to the point from the geocenter (km).

The temperature of Eq. B.8 can be used with Eq. B.1 to determine the density at the point in question. Reference 70 contains a Table with the resulting densities at altitudes of from 120 to 1000 km and temperatures from 650° to 2100°K. Figure B.3 is a plot of these densities vs temperature with altitude as the parameter.

Rather than using Eq. B.1 or the Table for determining density, it was found that adequate accuracy could be obtained by using polynomials of the logarithm of density as a function of temperature. Third-order polynomials were fitted to the tabular values from Ref. 70 at altitudes of 200-1000 km in steps of 100 km. The resulting coefficients are presented in Table B.1.

After the temperature of the atmosphere at the point in question is found using Eqs. B.3 - B.11, the density from the polynomials at the neighboring altitudes can be found using

$$\ln \rho = A_1 + A_2 T_m + A_3 T_m^2 + A_4 T_m^3 . \qquad (B.12)$$

Then the density at the required altitude can be determined by simple interpolation, i.e., by

$$\rho = \exp\left[\frac{(h-h_{LO})}{100} (\ln \rho_{HI} - \ln \rho_{LO}) + \ln \rho_{LO}\right] \qquad (B.13)$$

where

h_{LO} = next lower altitude having a polynomial fit,

$\ln \rho_{LO}$ = logarithm (to base e) of density at h_{LO} and temperature T_m ,

$\ln \rho_{HI}$ = logarithm of density at $(h_{LO} + 100$ km) and temperature T_m.

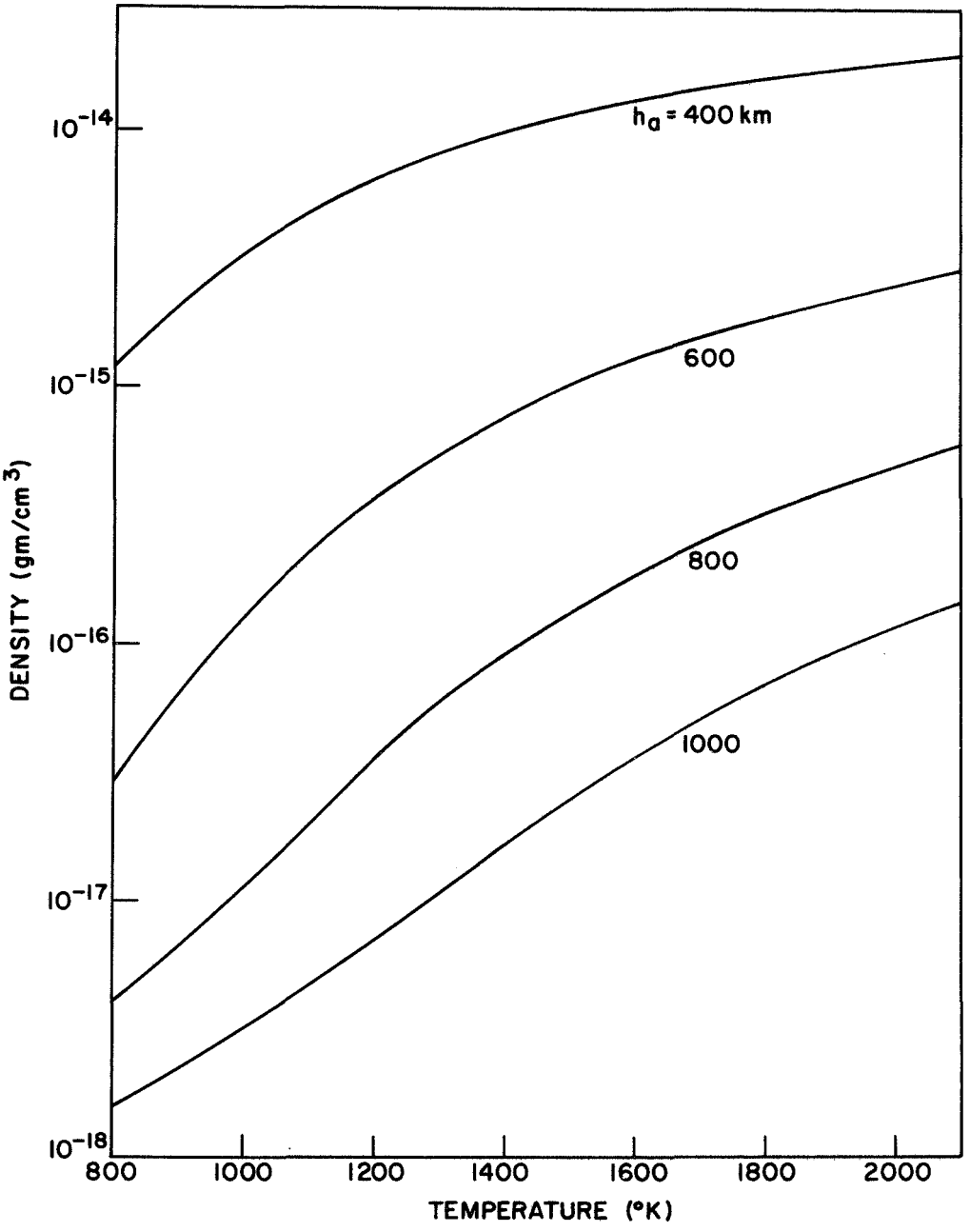

Fig. B.3. MEAN ATMOSPHERIC DENSITY AS A FUNCTION OF TEMPERATURE FOR DIFFERENT ALTITUDES.

TABLE B.1

POLYNOMIAL COEFFICIENTS USED TO YIELD ATMOSPHERIC DENSITY AS A FUNCTION OF TEMPERATURE

Density $\rho = \exp[A_1 + A_2 T_m + A_3 T_m^2 + A_4 T_m^3]$

ρ in gm/cm^3; T_m in °Kelvin.

Altitude km	$A_1 \times 10^{-1}$	$A_2 \times 10^{2}$	$A_3 \times 10^{6}$	$A_4 \times 10^{9}$
200	-3.054057	0.291475	-1.072323	0.003834
300	-3.817306	1.201897	-6.345819	1.150696
400	-4.194799	1.443336	-7.040865	1.204388
500	-4.568213	1.752301	-8.304390	1.396305
600	-4.907353	2.030690	-9.409241	1.559282
700	-5.089283	2.047103	-8.980082	1.424971
800	-4.968738	1.552572	-5.621701	0.733574
900	-4.595353	0.673299	-0.262906	-0.305830
1000	-4.250597	-0.050244	3.746130	-1.018655

For densities beyond 1000 km use

$$\rho = \rho_{1000} \exp\left[(h_a - 1000)(\ln \rho_{100} - \ln \rho_{900})/100\right] . \qquad (B.14)$$

Similarly, for densities between 120 km and 200 km, use

$$\rho = \rho_{120} \exp\left[(h_a - 120)(\ln \rho_{200} - \ln \rho_{120})/80\right] . \qquad (B.15)$$

Here, ρ_{200} is a function of T_m but ρ_{120} is fixed at 2.461×10^{-11} gm/cm^3.

Determining atmospheric density by the above procedure yields values with better than three-decimal place accuracy (as compared to the Table values) which is quite adequate when used for determining satellite disturbance torques.

As an indication of the change in atmospheric density as a function of the orbital position of a satellite, Figs. B.4 and B.5 are presented. Figure B.4 shows density variation in a 700 km polar, circular orbit with the 10.7 cm solar flux average set at values of 100, 200, and 300. Figure B.5 is a plot of density vs angular position of a resonating orbit with period 1/15 the rotational period of the earth showing the effect of varying eccentricity. In both figures, the starting point is near the minimum density point of the diurnal bulge.

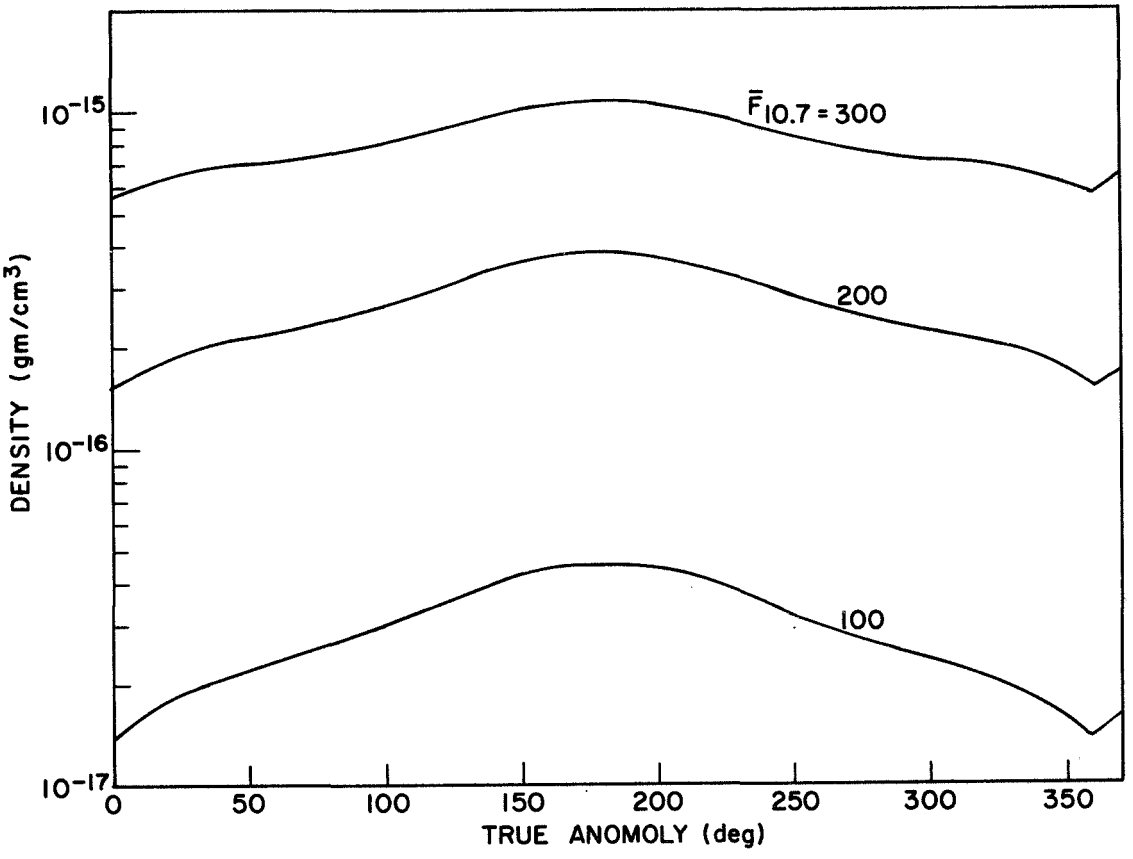

FIG. B.4. ATMOSPHERIC DENSITY VARIATIONS OF A 700 KM CIRCULAR ORBIT WITH DIFFERENT 10.7 CM SOLAR FLUX AVERAGES.

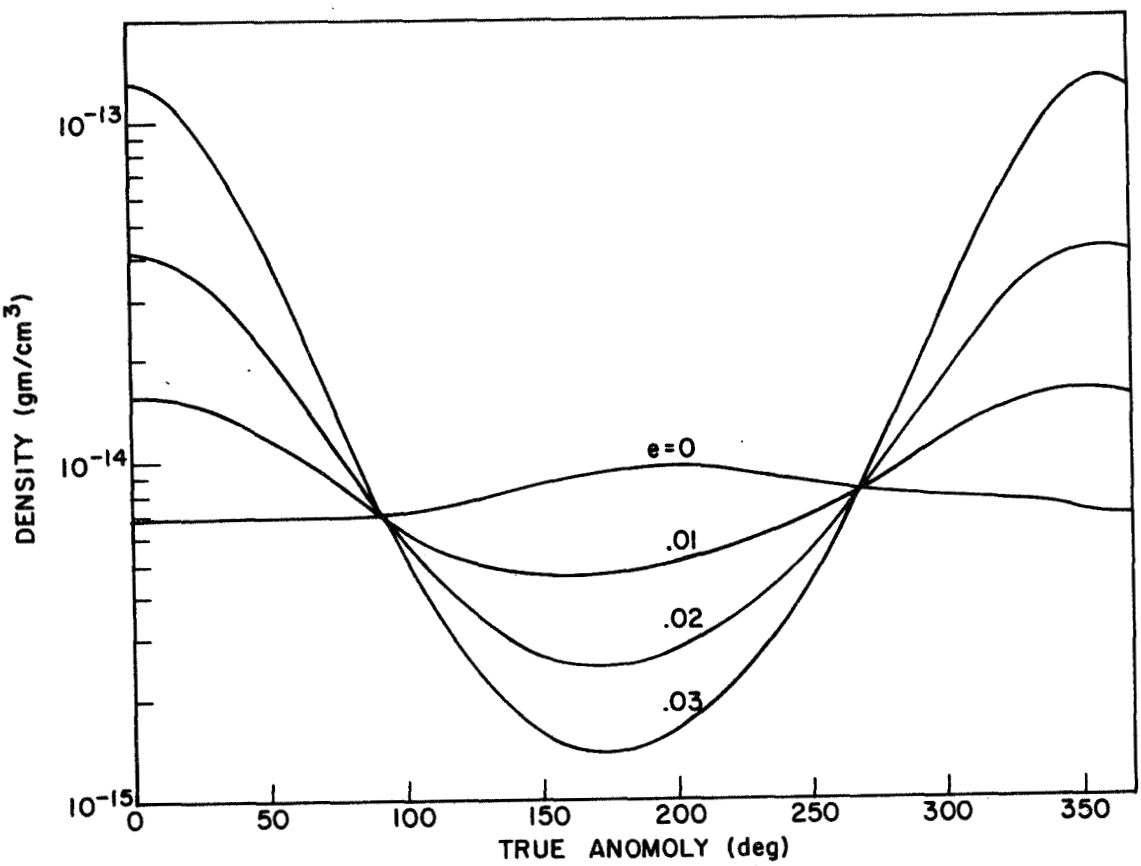

FIG. B.5. VARIATIONS IN ATMOSPHERIC DENSITY AS A FUNCTION OF THE ANGULAR POSITION OF A RESONANT ORBIT WITH PERIOD 1/15 THAT OF ROTATIONAL PERIOD OF THE EARTH.

a = 6840 km, i = 45°. ω_p = 0°. Ω = 180°. Date = March 21. $F_{10.7} = \bar{F}_{10.7} = 300$.

APPENDIX C

RADIATION PRESSURE MODEL FOR EARTH ORBITS

In the following section, analytical expressions are developed for the magnitude and direction of external radiation source vectors which cause attitude disturbances on earth-orbiting satellites. These sources include direct solar radiation, solar radiation reflected by the earth, and direct radiation emitted by the earth. Satellite-emitted radiation is not discussed here.

It must be noted that only direct solar radiation can be truly regarded as a vector (coming from the sun). The radiation reflected from and emitted by the earth is diffuse; its exact effect must be expressed in complicated integral form and can only be evaluated by computer techniques. It is possible for a cylindrically-shaped satellite to have every element of its surface reached by some portion of the earth-emitted radiation.

It is not the purpose of this analysis to produce exact expressions for the effect of the total radiation pressure force striking the satellite's surface. However, an attempt is made to present a reasonable approximation of the total effect so that the approximate disturbances can be expressed analytically or in a form which allows rapid computer determination. For this reason, it is assumed that the radiation from the earth can be adequately expressed as a vector pointing in the average direction of each incoming flux element to a point at the satellite's location. The vector magnitude equals the magnitude of the power input to a flat plate normal to the vector. As a result of this vector representation, the same technique can be used for obtaining the resulting radiation pressure forces and torques for all radiation sources.

DIRECT SOLAR RADIATION PRESSURE

The flux of radiant energy crossing unit area in unit time is

$$S_r = m_r c_\ell^2 \qquad (C.1)$$

where m_r is the mass of radiant energy and c_ℓ is the speed of light. The momentum flux is

$$m_r c_\ell = S_r/c_\ell \quad . \tag{C.2}$$

The sun's radiation disappears when the satellite is in the earth's shadow. This occurs when $\cos^{-1}(\hat{R}_\odot \cdot \hat{R}) > \pi/2 + \cos^{-1}(a_e/R)$ where $\hat{R}_\odot$ and $\hat{R}$ are unit vectors pointing from the geocenter to the sun and satellite respectively. According to Holl [Ref. 73], S_r varies between 0.1351 and 0.1397 Watts/cm^2 near the earth depending on the earth's position in its orbit. Thus, with c_ℓ = 299,850 km/sec., the solar radiation input force ranges between 4.50×10^{-5} and 4.66×10^{-5} dyne/cm^2.

EARTH EMITTED RADIATION PRESSURE

Assume the earth can be considered as a black body radiating uniformly at 250°K in a diffuse manner. The emitted power in any direction varies as the cosine of the angle between the given direction and the normal to the emitting element. Thus, the vector direction of this radiation source can be assumed to lie along the radius vector to the satellite. The general emittance is represented by the quantity Λ_e where

$$\Lambda_e \varepsilon = \sigma_{sb} T^4 \quad , \tag{C.3}$$

T is the absolute temperature of the black body, and σ_{sb} is the Stefan-Boltzmann constant. With the grey-body emissivity of the earth denoted by ε, the magnitude of the power input to the satellite is $\Lambda_e \varepsilon (a_e/R)^2$ with pressure $\Lambda_e \varepsilon\, a_e^2/(c_\ell R^2)$. For $\sigma_{sb} = 5.67 \times 10^{-12}$ Watts/cm^2 (deg K)^4 and T = 250°, Λ = 0.0226 Watts/cm^2. The resulting pressure on a flat plate normal to the radiation vector with $\varepsilon = 1$ is $7.53 \times 10^{-6}\ (a_e/R)^2$ dyne/cm^2. A general analysis of power input to a flat plate at an arbitrary angle to the earth-satellite radius vector can be found in Cunningham [Ref. 74].

EARTH REFLECTED RADIATION PRESSURE

The problem of determining the magnitude and direction of the solar radiation reflected from the earth and its atmosphere is compounded by

the fact that regions of the earth in the shadow of the sun contribute no radiation. In Ref. 75, Flandro indicated that a simplified model of the reflected radiant flux can be represented by a vector $\vec{D}_3$ such that its magnitude represents the equivalent flux at a given position relative to the earth. The vector's direction corresponds to the mean flux and is not usually in the $\vec{R}$ direction. This model is employed here.

Assume that the the albedo Γ of the earth is constant, that surface temperature adjustments occur rapidly, and that reflection is diffuse. Referring to Fig. C.1, define

- $\hat{R}_\odot$ - unit vector in direction of sun,
- $\vec{R}$ - radius vector from geocenter,
- $\hat{e}_{1,2}$ - unit vector forming right-hand system where $\hat{e}_2 = \hat{R}_\odot \times R/(R \sin \alpha)$,
- $\alpha_\odot$ - $\cos^{-1}(\hat{R}_\odot \cdot \vec{R}/|\vec{R}|)$,
- $\hat{n}$ - outward normal unit vector from dA,
- dA - incremental area of illuminated surface,
- $\vec{L}_\odot$ - vector from dA to vehicle,
- λ_n - $\cos^{-1}(\hat{R}_\odot \cdot \hat{n})$,
- θ_n - $\cos^{-1}(\hat{n} \cdot \vec{L}_\odot/|\vec{L}_\odot|)$,
- ϕ_n - angle from center to edge of illuminated circle.

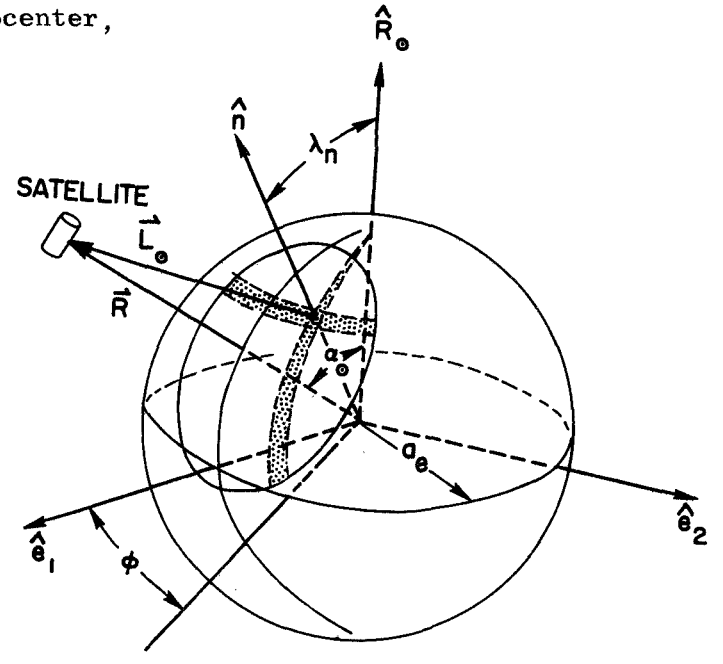

FIG. C.1 GEOMETRY OF THE SUN'S RADIATION REFLECTED BY THE EARTH.

The reflected flux per unit area is

$$d\vec{D}_3 = \frac{\Gamma S_r a_e^2 \sin 2\lambda_n \cos \theta_n \vec{L}_\odot}{2\pi c_\ell L_\odot^3} d\lambda_n d\varphi_n = \vec{C}_3 \, d\lambda_n d\varphi_n , \qquad (C.4)$$

where

$$L_\odot = (R \sin \alpha_\odot - a_e \sin \lambda_n \cos \varphi_n)\hat{e}_1 - (a_e \sin \lambda_n \sin \varphi_n)\hat{e}_2 + (R \cos \alpha_\odot - a_e \cos \lambda_n) R_\odot \quad , \tag{C.5}$$

$$L_\odot = R[1 + (a_e/R)^2 - 2(a_e/R)(\sin \alpha_\odot \cos \varphi_n \sin \lambda_n + \cos \alpha_\odot \cos \lambda_n)]^{\frac{1}{2}}, \tag{C.6}$$

$$\cos \theta_n = R[\sin \lambda_n \cos \varphi_n (\sin \alpha_\odot - (a_e/R) \sin \lambda_n \cos \varphi_n) - (a_e/R) \sin^2 \lambda_n \sin^2 \varphi_n + \cos \lambda_n (\cos \alpha_\odot - (a_e/R) \cos \lambda_n)]/L_\odot \quad . \tag{C.7}$$

The total vector $\vec{D}_3$ is found by integrating $d\vec{D}_3$ over the illuminated area seen by the spacecraft. Defining the angle δ_n as

$$\delta_n = \cos^{-1} (a_e/R) \quad , \tag{C.8}$$

and

$$\varphi_L = \cos^{-1}\left\{[(a_e/R) - \cos \lambda_n \cos \alpha_\odot]/\sin \lambda_n \sin \alpha_\odot\right\}, \tag{C.9}$$

one has the following integrals to evaluate depending on the vehicle's position with respect to the sun vector.

$$\vec{D}_3 = 2\left[\int_0^{\delta_n - \alpha_\odot} d\lambda_n \int_0^{\pi} \vec{C}_3 \, d\varphi_n + \int_{\delta_n - \alpha_\odot}^{\delta_n + \alpha_\odot} \alpha\lambda_n \int_0^{\varphi_L} \vec{C}_3 \, d\varphi_n\right] \tag{C.10a}$$

$$\text{for} \quad 0 \leq \alpha_\odot < \delta_n \quad ,$$

$$\vec{D}_3 = 2 \int_{\alpha_\odot - \delta_n}^{\alpha_\odot + \delta_n} d\lambda_n \int_0^{\varphi_L} \vec{C}_3 \, d\varphi_n \tag{C.10b}$$

$$\text{for} \quad \delta_n \leq \alpha_\odot \leq \frac{\pi}{2} - \delta_n \quad ,$$

and

$$\vec{D}_3 = 2 \int_{\alpha_\odot - \delta_n}^{\pi/2} d\lambda_n \int_0^{\varphi_L} \vec{C}_3 \, d\varphi_n \qquad \text{(C.10c)}$$

$$\text{for} \quad \frac{\pi}{2} - \delta_n \leq \alpha_\odot < \frac{\pi}{2} + \delta_n \quad .$$

For the case where $R > \sqrt{2}\, a_e$ one must also include the integral

$$\vec{D}_3 = 2 \left[\int_{\delta_n - \alpha_\odot}^{\pi/2} d\lambda_n \int_0^{\varphi_L} \vec{C}_3 \, d\varphi_n + \int_0^{\delta_n - \alpha_\odot} d\lambda_n \int_0^{\pi} \vec{C}_3 \, d\varphi_n \right] \qquad \text{(C.10d)}$$

$$\text{for} \quad \frac{\pi}{2} - \delta_n < \alpha_\odot < \delta_n \quad .$$

Integrals (C.10a-c) were integrated numerically using the expressions of (C.4) to (C.9) for altitudes ranging from 300 to 1800 km and an albedo $\Gamma = 0.4$. The results are plotted in Fig. C.2 which shows the magnitude of $\vec{D}_3$ and its deviation away from the radius vector $\vec{R}$. $\vec{D}_3$ lies in the plane of $\hat{R}_\odot$ and $\vec{R}$.

The magnitude of the reflected radiation flux can be represented quite well empirically by

$$\left|\vec{D}_3\right| = 5.40 \times 10^{-2} \exp(-3.0 \times 10^{-4} h_a) \cos \alpha_\odot \ \text{Watts/cm}^2 \ , \qquad \text{(C.11)}$$

$$\text{for} \quad \alpha_\odot \leq 90^\circ \ .$$

Defining the angle between the radius vector $\vec{R}$ and $\vec{D}_3$ as ν_n, its magnitude is approximately

$$\nu_n = f_n (\alpha_\odot / f_n)^{2.4} \ \text{rad} \, , \qquad \text{(C.12)}$$

where $f_n = 4.89 - h_a (5.82 \times 10^{-4})$ rad. In Eq. (C.11) and (C.12), h_a is the altitude in km. Dividing the expression in (C.11) by c_ℓ yields the resultant radiation pressure of

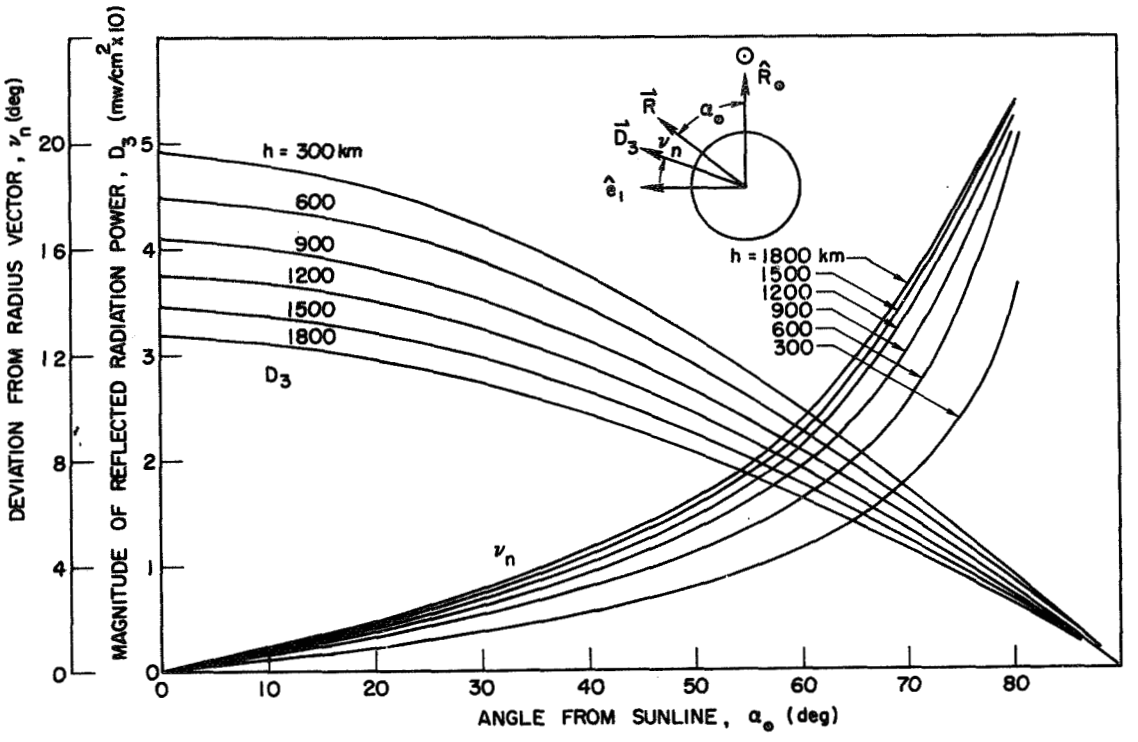

FIG. C.2. VECTOR REPRESENTATION OF THE EARTH-REFLECTED RADIATION AS A FUNCTION OF THE ANGLE FROM THE SUNLINE.

$$\overrightarrow{Ra3} = 1.80 \times 10^{-5} \exp(-3.0 \times 10^{-4} h_a) \cos \alpha_\odot \text{ dyne/cm}^2. \quad (C.13)$$

It can be assumed that reflected radiation pressure is negligible for $\alpha_\odot > 90°$.

/

APPENDIX D

THE CONSTRUCTION OF OBSERVERS FOR MULTIVARIABLE OUTPUT SYSTEMS

In this appendix, several theorems will be presented concerning the construction of observers for multivariable output systems. This material essentially comes from two recent publications [Refs. 76 and 77] and is necessary for the development of the reduced-order observer utilized in Chapter 4. The theorems which follow are stated without proof because of the length involved and for which the reader is referred to the indicated document location. Additional comments and procedures' outlines are included where appropriate to give the information presented necessary cohesiveness.

The state observers discussed are for linear constant systems which can be described by the equations

$$\begin{aligned} \dot{x}(t) &= Fx(t) + Gu(t) \quad , \\ y(t) &= Hx(t) \quad , \end{aligned} \tag{D.1}$$

where

$x(t)$ = $n \times 1$ state vector,

$u(t)$ = $r \times 1$ input vector,

$y(t)$ = $m \times 1$ output vector.

It is assumed that the system (F,H) is observable which implies that

$$\text{rank}[H^T \vdots F^T H^T \vdots F^{T^2} H^T \vdots \text{---} \vdots F^{T^{n-1}} H^T] = n \ .$$

Thus, it is possible to reconstruct $x(t)$ from $y(t)$ by means of adding an observer or state estimator to the system.

The concept of cyclic matrices and subspaces is used extensively in the theorems. Cyclicity can be defined as follows:

> Definition D.1 - cyclicity [Ref. 76]. A subspace S_n of R^n, the n-dimensional Euclidean space, is cyclic relative to the $n \times n$ matrix F if there exists an n-vector x such that the vectors x, Fx, ---, $F^{k-1}x$ where k is such that these k vectors are independent but that $F^k x$ is dependent on the preceding k vectors, forms a basis for S_n. S_n formed in this way is called the cyclic subspace generated by x relative to F. The matrix F

is cyclic if R^n is cyclic relative to F. F is cyclic if and only if it is similar to a Jordan matrix J in which no eigenvalue appears in more than one Jordan chain.∎

Any system matrix F can always be broken into cyclic subsystems governed by submatrices of F or a similar matrix. The usefulness of the cyclicity property of a matrix comes from the following theorem:

Theorem D.1 - Output Observability Theorem [Ref. 76, pg 62]. If the system matrix F is cyclic, then there exists a nonsingular transformation P_m of the output vector such that F is observable from every scalar component of the transformed output vector $y_1(t) = P_m y(t)$. Almost any nonsingular m × m matrix P_m assures this property.∎

Because of this property, almost any 1 × m row vector converts a cyclic multivariable output system into an observable, single output system. Obvious advantages to observer construction result from this theorem.

Another useful result is

Theorem D.2 [Lemma 4, Ref. 76, pg 67]. If F is similar to an n × n Jordan matrix J, and k is the maximum number of Jordan chains in which a given eigenvalue λ appears, then in order for (F,H) to be observable, it is necessary that H have at least k independent rows.∎

Thus, the minimum number of outputs which an observable system must have to maintain its observability is equal to the minimum number of cyclic subspaces which the system governed by F can be broken into.

In Ref. 76, Singer shows that any observable multivariable system can be transformed to a general canonical representation with state transformation $z(t) = T_1 x(t)$ and $y_1(t) = P_m y(t)$. This representation has features which are useful to the observer development of Chapter 4, so the procedure used to obtain the canonical form is now outlined.

1. Form the observability-type matrix M_1. The first $\alpha 1 + 1$ rows are formed by taking the first row of H (called h_1) and forming the rows $h_1, h_1F, \cdots, h_1F^{\alpha 1}$. Here, $\alpha 1$ is the smallest index such that $h_1F^{\alpha 1+1}$ is linearly dependent on the previous $\alpha 1 + 1$ rows. The next $\alpha 2 + 1$ rows of M_1 are $h_2, h_2F, \cdots, h_2F^{\alpha 2}$ where $\alpha 2$ is the smallest index such that $h_2F^{\alpha 2+1}$ is linearly dependent upon the previous

$\alpha 1 + \alpha 2 + 1$ rows. This procedure is repeated until M_1, of the form

$$M_1 = \begin{bmatrix} h_1 \\ h_1F \\ \vdots \\ h_1F^{\alpha 1} \\ \vdots \\ h_p \\ \vdots \\ h_pF^{\alpha p} \end{bmatrix} \qquad (D.2)$$

has rank n. The index **p** possibly may not equal m, the number of rows of H. Also, some intermediate row h_i of H may not contribute to M_1.

2. Reorder the outputs so that the first p outputs of the new output vector y_1 correspond in order to the p rows of H used to form M_1, i.e., form

$$y_1(t) = P_m y(t) = P_m Hx(t) , \qquad (D.3)$$

where P_m is a nonsingular matrix of zeros and ones which accomplishes this reordering.

3. Form the new systems matrix $F_1 = M_1 F M_1^{-1}$ which can be shown to have the form below. Here, $\emptyset$ represents a block of zeros, and x represents an arbitrary element. Since this matrix is quasi-lower-triangular, its characteristic equations is the product of the characteristic equations of the p diagonal blocks.

$$F_1 = \left[\begin{array}{c|c|c|c} \begin{matrix} 0 & 1 & 0 & \cdots & 0 \\ 0 & 0 & 1 & \cdots & 0 \\ \vdots & \vdots & \vdots & & \vdots \\ \beta_{10} & \beta_{11} & \beta_{12} & \cdots & \beta_{1,\alpha 1} \end{matrix} & & & \\ \hline & \begin{matrix} 0 & 1 & \cdots & 0 \\ 0 & 0 & \cdots & 0 \\ \vdots & \vdots & & \vdots \\ \beta_{20} & \beta_{21} & \cdots & \beta_{2,\alpha 2} \end{matrix} & & \\ \hline & & \ddots & \\ \hline & & & \begin{matrix} 0 & 1 & \cdots & 0 \\ 0 & 0 & \cdots & 0 \\ \vdots & \vdots & & \vdots \\ \beta_{p0} & \beta_{p1} & \cdots & \beta_{p,\alpha p} \end{matrix} \end{array}\right] \qquad \text{(D.4)}$$

4. Form the A matrix by inspection from elements of F_1 as

$$A = \left[\begin{array}{c|c|c|c} \begin{matrix} 1 & 0 & 0 & \cdots \\ -\beta_{1,\alpha 1} & 1 & 0 & \cdots \\ -\beta_{1,\alpha 1-1} & -\beta_{1,\alpha 1} & 1 & \cdots \\ \vdots & \vdots & \vdots & \\ \vdots & \vdots & \vdots & 0 \\ & & & 1 \end{matrix} & & & \\ \hline & \begin{matrix} 1 & 0 & \cdots & \cdots \\ -\beta_{2,\alpha 2} & 1 & \cdots & \cdots \\ -\beta_{2,\alpha 2-1} & -\beta_{2,\alpha 2} & \cdots & \cdots \\ \vdots & \vdots & & \\ \vdots & \vdots & & 1 \end{matrix} & & \\ \hline & & \ddots & \\ \hline & & & \begin{matrix} 1 & 0 & \cdots \\ -\beta_{p,\alpha p} & 1 & \cdots \\ \vdots & \vdots & \\ \vdots & & 1 \end{matrix} \end{array}\right] \qquad \text{(D.5)}$$

5. Use the A matrix to transform F_1 into the observable canonical form $F_2 = AF_1A^{-1} = AM_1FM_1^{-1}A^{-1}$, which is

$$F_2 = \left[\begin{array}{ccc|c|c} \beta_{1,\alpha 1} & 1\ 0\ \cdots & & & \\ \beta_{1,\alpha 1-1} & 0\ 1\ \cdots & & & \\ \vdots & \vdots & & & \\ \beta_{10} & 0\ 0\ \cdots & & & \\ \hline & & \beta_{2,\alpha 2} & 1\ \cdots & \\ & & \beta_{2,\alpha 2-1} & 0\ \cdots & \\ & \phi & \vdots & \vdots & \\ x & x\ x\ \cdots & \beta_{20} & 0\ \cdots & \\ \hline & & & \ddots & \\ \hline & & & & \beta_{p,\alpha p}\ 1\ \cdots \\ & & & & \beta_{p,\alpha p-1}\ 0\ \cdots \\ & \phi & \phi & & \vdots \\ x & x\ x\ \cdots & x & x\ \cdots & \beta_{po}\ 0\ \cdots \end{array}\right] \qquad \text{(D.6)}$$

This matrix has subblocks along the diagonal which are those of F_1 transposed about the perpendicular-to-the-diagonal axis.

6. An observer for this new system can be formed with arbitrary dynamics by forming

$$\begin{aligned} \dot{\hat{z}}(t) &= F_2\hat{z}(t) + K[P_m\hat{y}(t) - y(t)] + G_2u(t) \ , \\ \hat{y}(t) &= H_2\hat{z}(t) \ . \end{aligned} \qquad \text{(D.7)}$$

Here,

$$K = \begin{bmatrix} k_{1,\alpha 1} & \phi & \phi \\ k_{1,\alpha 1-1} & & \\ \vdots & & \\ k_{10} & & \\ \phi & k_{2,\alpha 2} \cdots & \phi \quad \phi \\ & k_{2,\alpha 2-1} & \\ & \vdots & \\ & k_{20} & \\ & & k_{p,\alpha p} \\ & & \vdots \\ & & k_{p0} \end{bmatrix} \qquad (D.8)$$

$G_2 = T_1 G = AM_1 G$, and $H_2 = P_m H T_1^{-1}$. In terms of the original system, then, the observer is

$$\dot{\hat{x}}(t) = (F - T_1^{-1} KPH)\hat{x}(t) + T_1^{-1} KP_m y(t) + Gu(t) \quad . \quad \blacksquare \qquad (D.9)$$

This construction procedure is straightforward and only M_1^{-1} cannot be formulated by inspection.

In Ref. 77, Gopinath shows that if the system is cyclic, then an observer can be constructed in a systematic way formalized as

Theorem D.3 [Modification of Theorem 5.1, Ref. 77, pg 79]. Let (F,H) be completely observable and F cyclic. Then the set of equations

$$
\begin{aligned}
\gamma_1 &= a_1 + \mathrm{tr}(HL) \\
\gamma_2 &= a_2 + a_1\mathrm{tr}(HL) + \mathrm{tr}\ HFL \\
\gamma_3 &= a_3 + a_2\mathrm{tr}(HL) + a_3\mathrm{tr}(HFL) + \mathrm{tr}(HF^2L) \\
&\ \ \vdots \\
\gamma_n &= a_n + \ . \ . \ . \qquad\qquad + \mathrm{tr}(HF^{n-1}L)
\end{aligned}
\tag{D.10}
$$

(subject to the condition that L be of rank one) has a unique solution for L almost surely. Here, the system has the characteristic equation

$$
s^n + \sum_{i=1}^{n} a_i s^{n-i} = 0 \ , \tag{D.11}
$$

and the desired observer characteristic equation is

$$
s^n + \sum_{i=1}^{n} \gamma_i s^{n-i} = 0 \ . \tag{D.12}
$$

Note that in Eq. (D.10), if $L = bc^T$ (where b and c are $n \times 1$ and $m \times 1$ column matrices),

$$
\mathrm{tr}(HF^jL) = \mathrm{tr}(c^THF^jb) = c^THF^jb \ .
$$

Also, note that if the definitions

$$
A \triangleq \begin{bmatrix}
1 & 0 & 0 & . & . & . \\
a_1 & 1 & 0 & . & . & . \\
a_2 & a_1 & 1 & . & . & . \\
. & . & . & & & \\
. & . & . & & & \\
a_{n-1} & a_{n-2} & . & & a_1 & 1
\end{bmatrix} ,
$$

$$
K \triangleq \begin{bmatrix}
\gamma_1 - a_1 \\
\gamma_2 - a_2 \\
\vdots \\
\gamma_n - a_n
\end{bmatrix} ,
$$

and

$$M_1 \triangleq \begin{bmatrix} c^T H \\ c^T HF \\ \vdots \\ c^T HF^n \end{bmatrix} ,$$

are used, then Eq. (D.10) can be solved for the column matrix b as

$$b = M_1^{-1} A^{-1} K \quad , \tag{D.13}$$

whenever M_1^{-1} exists. But this is a special form of the observer obtained by canonical forms. If one sets $P_m = c^T$ which is valid by Theorem D.1, then the observer for the cyclic system is

$$\begin{aligned} \dot{\hat{x}}(t) &= F\hat{x} + L[y(t) - H\hat{x}(t)] + Gu(t) \quad , \\ &= (F - M_1^{-1} A^{-1} K c^T H)\hat{x}(t) + M_1^{-1} A^{-1} K c^T y(t) + Gu(t) \quad , \end{aligned} \tag{D.14}$$

which is precisely Eq. (D.9). The matrix M_1 has an inverse almost always with the random selection of elements of c^T.

Reference 77 used the following theorem to show that noncyclic systems could usually be made cyclic.

> Theorem D.4 [Theorem 5.2, Ref. 77, pg 84]. Given a completely controllable and completely observable system which is not cyclic, the system (F-GK,G,H) is cyclic almost always, when the elements of K are picked from a distribution in which no finite mass is concentrated on a surface of dimension less than n. ∎

This method does not work for a noncontrollable system.

Reference 77 goes on to develop an ingenious method for the construction of reduced-order observers. If (F,H) is observable and H is m × n, then only an $(n-m)^{th}$-order observer needs to be constructed because the output y = Hx (where it is assumed that H has m independent rows) provides m of the n states directly. It is assumed that H is of the form

$$H = [I_m, 0]$$

which can always be mechanized, and that the F, G, and state matrices are partitioned as

$$x = \begin{bmatrix} x_1 \\ \hline x_2 \end{bmatrix} \begin{matrix} m \\ \\ n-m \end{matrix} ,$$

$$F = \left[\begin{array}{c|c} F_{11} & F_{12} \\ \hline F_{21} & F_{22} \end{array}\right] \begin{matrix} m \\ \\ n-m \end{matrix} ,$$

$$G = \begin{bmatrix} G_{11} \\ \hline G_{21} \end{bmatrix} \begin{matrix} m \\ \\ n-m \end{matrix} .$$

The reduced-order observer (which is referred to here as the Gopinath reduced-order observer), is constructed from a procedure which is presented in three theorems as follows:

Theorem D.5 [Theorem 5.3, Ref. 77, pg 88]. If (H,F) is completely observable, the pair (F_{12}, F_{22}) is completely observable.∎

Theorem D.6 [Theorem 5.4, Ref. 77, pg 90]. Let one system be defined as

$$\dot{x}_1 = Fx_1 + G\dot{u} ,$$

and the other as

$$\dot{x}_2 = Fx_2 + FGu ,$$

and let the eigenvalues of F have negative real parts. Then

$$x_1(t) = x_2(t) + Gu(t) \text{ as } t \to \infty .∎$$

Theorem D.7 [Theorem 5.5, Ref. 77, pg 91]. Given two observers of the form

$$\dot{\hat{x}}_2 = (F_{22} - LF_{12})\hat{x}_2 + G_{21}u + F_{21}x_1 + LF_{12}x_2 \quad ,$$

and

$$\dot{\bar{x}}_2 = (F_{22}-LF_{12})\bar{x}_2 + (F_{21}-LF_{11} + F_{22}L-LF_{12}L)x_1 + (G_{21}-LG_{11})u \quad ,$$

then if all eigenvalues of $F_{22} - LF_{12}$ have negative real parts, $\hat{x}_2 \rightarrow \bar{x}_2 + Lx_1$ as fast as $\exp(F_{22} - LF_{12})t$. Thus, the problem of designing an observer of dimension $(n - m)$ is reduced to designing one for the system

$$\dot{x}_2 = F_{22}x_2 + F_{21}x_1 + G_{21}u \quad .$$

It can be constructed as indicated in Fig. D.1. Here, $\hat{x}_z$ is the estimate of the unknown x_z . ∎

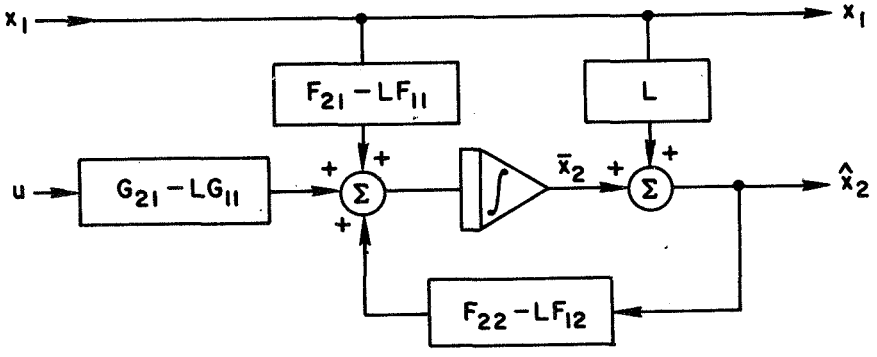

FIG. D.1. SCHEMATIC OF THE GOPINATH REDUCED-ORDER OBSERVER.

REFERENCES

1. Kamm, L.J., "Magnetorquer - A Satellite Orientation Device," ARS Journal, vol. 31, no. 6, June 1961.

2. White, J.S., F.H. Shigemoto, and K. Bourquin, "Satellite Attitude Control Utilizing the Earth's Magnetic Field," NASA TN D-1068, National Aeronautics and Space Administration, Washington, D.C., August 1961.

3. Westinghouse Electronics Corporation, "Electromagnetic Attitude Control System Study," NASA CR-24, National Aeronautics and Space Administration, Washington, D.C., March 1964.

4. Rennie, R.G., and H.H. Chanowitz, "A Magnetic Unloading System for an Ultra Stable Unmanned Spacecraft," IEEE Transactions on Aerospace, vol. 2, no. 2, April 1964.

5. Brown, S.C., "An Analytical Comparison of Some Electromagnetic Systems for Removing Momentum Stored by a Satellite Attitude Control System," NASA TR D-2693, National Aeronautics and Space Administration, Washington, D.C., March 1965.

6. Bodner, V.A., K.V. Alekseev, and G.G. Bebenin, "On One Class of Systems for Controlling the Orientation of Artificial Earth Satellites," Peaceful Uses of Automation in Outer Space, (J.A. Aseltine, ed.), Plenum Press, New York, New York, 1966.

7. Paiken, M. and R. Fleisig, "Momentum Control of the OAO Spacecraft Utilizing the Earth's magnetic Field," Proceedings of the 14th International Astronautical Congress, vol. 4, (Brun, E. and I. Hersey, eds.), Gauthier-Villars, Paris, 1965.

8. Hart, L.R., et al, "Application of Magnetic Torquing for Desaturation of Control Moment Gyros in Space Vehicle Control," Technical Report AFFDL-TR-67-8, Air Force Systems Command, Wright-Patterson Air Force Base, Ohio, June 1967.

9. Sonnabend, D., "A Magnetic Control System for an Earth Pointing Satellite," presented at the Symposium on Attitude Stabilization and Control of Dual-Spin Spacecraft, Aerospace Corporation, El Segundo, Calif., August 1967.

10. Arnesen, W.T., and J.P.C. Clark, "Magnetic Attitude Control of Synchronous Satellites," IEEE Transactions on Automatic Control, vol. AC-13, no. 5, October 1968.

11. Ergin, E.I., and P.C. Wheeler, "Magnetic Attitude Control of a Spinning Satellite," AIAA Paper No. 64-235, presented at AIAA First Annual Meeting, Washington, D.C., June 1964.

12. Mobley, F.F., "Attitude Control Systems for the Atmosphere Explorer-B Satellite," AIAA Paper No. 65-432, presented at AIAA Second Annual Meeting, San Francisco, Calif., July 1965.

13. Wheeler, P.C., "Magnetic Attitude Control of Rigid Axially Symmetric Spinning Satellites in Circular Earth Orbits," SUDAAR No. 224, Department of Aeronautics and Astronautics, Stanford University, Stanford, Calif., April 1965.

14. Renard, M.L., "Attitude Perturbations and Magnetic Control of a Spin-Stabilised Satellite," ESRO TR-1 (ESTEC), Noordwijk, The Netherlands, January 1966.

15. Vrablik, E.A., W.L. Black, and L.J. Travis, "LES-4 Spin Axis Orientation System," Lincoln Laboratory Technical Note, 1965-48, Lincoln Laboratory, Massachusetts Institute of Technology, Cambridge, Mass., October 1965.

16. Fischell, R.E., "Spin Control for Earth Satellites," Peaceful Uses of Automation in Outer Space, (J.A. Aseltine, ed.), Plenum Press, New York, N.Y., 1966.

17. Mobley, F.F., J.W. Teener, R.D. Brown, and B.E. Tossman, "Performance of the Spin Control System of the DME-A Satellite," presented at the AIAA Guidance and Control Conference, Seattle, Wash., August 1966.

18. Hecht, E., and W.P. Manager, "Magnetic Attitude Control of the TIROS Satellites," Torques and Attitude Sensing in Earth Satellites, (S. Fred Singer, ed.), Academic Press, New York, N.Y., 1964.

19. Tossman, B.E., "Magnetic Attitude Control System for the Radio Astronomy Explorer - a Satellite," AIAA Paper No. 68-855, presented at the AIAA Guidance, Control, and Flight Dynamics Conference, Pasadena, Calif., August 1968.

20. Fosth, D.C., and W.H. Zimmerman, "High Accuracy Attitude Control for Space Astronomy," presented at Joint Automatic Control Conference, Philadelphia, Penn., June 1967.

21. Liska, D.J., "A Two-Degree-of-Freedom Control Moment Gyro for High-Accuracy Attitude Control," Journal of Spacecraft and Rockets, vol. 5, no. 1, January 1968.

22. Goldstein, H., Classical Mechanics, Addison-Wesley Publishing Co., Inc., Reading, Mass., 1959.

23. Yu, E.Y., "Spin Decay, Spin-Precession Damping, and Spin-Axis Drift of the Telstar Satellite," Bell System Technical Journal, vol. 42, no. 5, September 1963.

24. Taylor, R.S., "Feasibility Study and Design of Passive Dampers for a Manned Rotating Space Station," NASA CR-163, Washington, D.C., March, 1965.

25. Spencer, T.M., "Cantilevered-Mass Nutation Damper for a Dual-Spin Spacecraft," Proceedings of the Symposium on Attitude Stabilization and Control of Dual-Spin Spacecraft, Aerospace Report No. TR-0158 (3307-01)-16, Aerospace Corp., El Segundo, Calif., November 1967.

26. Lange, B.O., "The Control and Use of Drag-Free Satellites," SUDAER No. 194, Department of Aeronautics and Astronautics, Stanford University, Stanford, Calif., June 1964.

27. Strange, W.E., F.M. Calabria, H.T. Rainey, and L.P. Gunshol, "Requirements for Resonant Satellites," AAS National Specialist Symposium on Orbital Resonance, January 1968.

28. Kaula, W.M., Theory of Satellite Geodesy, Blaisdell Publishing Company, Waltham, Mass., 1966.

29. Douglas, B.C., M.T. Palmiter, and G.S. Gedeon, "Resonant Satellite Study," TRW Report No. 09128.6001-R000, TRW Systems Group, Redondo Beach, Calif., 1968.

30. "Final Technical Report on a Preliminary Design of a Drag-Free Satellite and its Application to Geodesy," Contract No. NAS 12-695, NASA-ERC, Stanford University, Guidance and Control Laboratory, Stanford, Calif., May 1969.

31. Schaaf, S.A., and P.L. Chambre, "The Flow of Rarefied Gases," Fundamentals of Gas Dynamics, (H.W. Emmons, ed.), Princeton University Press, Princeton, New Jersey, 1958.

32. Schamberg, R., "A New Analytical Representation of Surface Interaction for Hyperthermal Free Molecule Flow with Application to Neutral-Particle Drag Estimates of Satellites," RM-2313, The Rand Corp., Santa Monica, Calif., January 1959.

33. Moe, K.O., "Recent Experimental Evidence Bearing on Satellite Drag Coefficients," AIAA Journal, vol. 6, no. 7, July, 1968.

34. Johnson, K.R., "Effect of Dissipative Aerodynamic Torque on Satellite Rotation," Journal of Spacecraft and Rockets, vol. 5, no. 4, April 1968.

35. King-Hele, D.G., "The Rotational Speed of the Upper Atmosphere Determined from Changes in Satellite Orbits," Space Research V, (King-Hele D.G., P. Muller, and G. Righini, eds.), North Holland Publishing Co., Amsterdam, 1965.

36. Evans, W.J., "Aerodynamic and Radiation Disturbance Torques on Satellites Having Complex Geometry," Torques and Attitude Sensing in Earth Satellites, (Singer, S.F., ed.), Academic Press, New York, 1964.

37. DeBra, D.B., "The Large Attitude Motions and Stability, Due to Gravity, of a Satellite with Passive Damping in an Orbit of Arbitrary Eccentricity about an Oblate Body," SUDAER No. 126, Department of Aeronautics and Astronautics, Stanford University, Stanford, Calif., May,1962.

38. Kaula, W.M., "Improved Geodetic Results From Camera Observations of Satellites," Journal of Geophysical Research, vol. 68, no. 18, 1963.

39. "Magnetic Torques," Vol. IV: Guidance and Control, NASA Space Vehicle Design Criteria, prepared under contract NAS 12-559, Exotech Incorporated, Washington, D.C., July 1, 1968.

40. Smith, G.L., "A Theoretical Study of the Torques Induced by a Magnetic Field on Rotating Cylinders and Spinning Thin-Wall Cones, Cone Frustums, and General Body of Revolution," NASA TR-129, Washington, D.C., 1962.

41. Fitzgerald, R.J., "Filtering Horizon-Sensor Measurements for Orbital Navigation," Journal of Spacecraft and Rockets, vol. 4, no. 4, April 1967.

42. Kalman, R.E., and R.S. Bucy, "New Results in Linear Filtering and Prediction Theory," Journal of Basic Engineering, Transactions of the ASME, vol. 83D, March 1961.

43. Wiener, N., The Extrapolation, Interpolation, and Smoothing of Stationary Time Series, John Wiley & Sons, Inc., New York, N. Y., 1949.

44. Oliver, B.M., J.R. Pierce, and C.E. Shannon, "The Philosophy of Pulse Code Modulation," Proceedings of the IRE, vol. 36, no. 11, November 1948.

45. Bryson, A.E., and Y.C. Ho, Applied Optimal Control, Blaisdell Publishing Company, Waltham, Mass., 1969.

46. Chikazumi, S., Physics of Magnetism, John Wiley & Sons, Inc., New York, N.Y., 1964.

47. Marshall, S.V., "An Analytic Model for the Fluxgate Magnetometer," IEEE Transactions on Magnetics, vol. MAG-3, no. 3, September 1967.

48. Lasalle, J.P., and S. Lefshetz, Stability by Lyapunov's Direct Method with Applications, Academic Press Inc., New York, N.Y., 1961.

49. Kalman, R.E., and J.E. Bertram, "Control System Analysis and Design Via the Second Method of Lyapunov," Journal of Basic Engineering, Transactions of the ASME, vol. 83D, June 1960.

50. Moore, J.B., and B.D.O. Anderson, "Generalizations of the Circle Criterion," Technical Report EE-6708, Department of Electrical Engineering, University of Newcastle, New South Wales, Australia, October 1967.

51. Potter, J.F., "Matrix Quadratic Solutions," Journal SIAM Applied Mathematics, vol. 14, no. 3, May 1966.

52. Hsu, C.S., "On a Restricted Class of Coupled Hill's Equations and Some Applications," Journal of Applied Mechanics, Transactions of the ASME, vol. 28E, December 1961.

53. Kryloff, N., and N. Bogoliuboff, Introduction to Nonlinear Mechanics, Princeton University Press, Princeton, J.J., 1943.

54. Moore, J.B., and B.D.O. Anderson, "Applications of the Multidimensional Popov Criterion," International Journal of Control, vol. 5, no. 4, April 1967.

55. Ling, S.C., "Magnetic Field Measurements in Space," Journal of Spacecraft and Rockets, vol. 1, no. 2, March-April 1964.

56. Munoz, R., "The Ames Magnetometer," Proceedings of the National Telemetering Conference, 1966.

57. Parker, E.N., "Dynamics of the Geomagnetic Storm," Space Science Reviews, vol. 1, 1962-1963.

58. Lapidus, L., and R. Luus, Optimal Control of Engineering Processes, Blaisdell Publishing Company, Waltham, Mass., 1967.

59. Silverman, L.M., and H.E. Meadows, "Controllability and Observability in Time-Variable Linear Systems," SIAM Journal on Control, vol. 5, no. 1, 1968.

60. Silverman, L.M., and B.D.O. Anderson, Controllability, Observability, and Stability of Linear Systems," SIAM Journal on Control, vol. 6, no. 1, 1968.

61. Lange, B.O., A.W. Fleming, and B.W. Parkinson, "Control Synthesis for Spinning Aerospace Vehicles," Journal of Spacecraft and Rockets, vol. 4, no. 2, February 1967.

62. Gantmacher, F.R., The Theory of Matrices, Vol. II, Chelsea Publishing Company, New York, N.Y., 1959.

63. Chapman, Sydney, and J. Bartels, Geomagnetism, Vol. 2, Oxford University Press, London, 1940.

64. Luke, R.K.C., "Descriptions of the Geomagnetic Field," Aerospace Report No. TR-1001(2307)-5, Aerospace Corporation, El Segundo, Calif., January 1967.

65. Chernosky, E.J., P.F. Fougere, and R.O. Hutchinson, "The Geomagnetic Field," Handbook of Geophysics and Space Environments, (Shea L. Valley, ed.), McGraw-Hill Book Co., Inc., New York, N.Y. 1965.

66. Hurwitz, L., D.G. Knapp, J.H. Nelson, and D.E. Watson, "Mathematical Model of the Geomagnetic Field for 1965," Journal of Geophysical Research, vol. 71, no. 9, May 1966.

67. Hendricks, S.J., and J.C. Cain, "Magnetic Field Data for Trapped-Particle Evaluations," Journal of Geophysical Research, vol. 71, no. 1, January 1966.

68. Bruce, R.W., "A Survey of Model Atmospheres Used in the Analysis of Satellite Orbits," Aerospace Report No. TDR-469(5540-10)-2, Aerospace Corporation, El Segundo, Calif., April 1965.

69. Stergis, C.G., "Atmospheric Temperature, Density, Pressure, and Moisture; Variations Above 200 Km.," Handbook of Geophysics and Space Environments, (S.L. Valley, ed.), McGraw-Hill Book Co., Inc., New York, N.Y., 1965.

70. Jacchia, L.G., "Static Diffusion Models of the Upper Atmosphere with Emperical Temperature Profiles," Smithsonian Contributions to Astrophysics, vol. 8, no. 9, Smithsonian Institution Astrophysical Observatory, Washington, D.C., 1965.

71. Small, H.W., "Atmospheric Densities Between 70 and 200 Nautical Miles from Satellite Observations," Tracking Note No. 23, Lockheed Missiles and Space Company, Sunnyvale, Calif., July 1964.

72. Keating, G.M., and E.J. Prior, "Latitude and Seasonal Variations in Atmospheric Densities Obtained During Low Solar Activity by Means of the Inflatable Air Density Satellite," Space Research VII, vol. 2, (Smith-Rose, R.L., and J.W. King, eds.), North Holland Publishing Co., Amsterdam, 1967.

73. Holl, H.B., "The Effect of Radiation Force on Satellites of Convex Shape," NASA TN D-604, National Aeronautics and Space Administration, Washington, D.C., May 1961.

74. Cunningham, F.G., "Power Input to a Small Flat Plate from a Diffusively Radiating Sphere with Application to Earth Satellites," NASA TN D-710, National Aeronautics and Space Administration, Washington, D.C., July 1961.

75. Flandro, G.A., "Non-gravitational Orbital Perturbations," Jet Propulsion Laboratory Space Programs Summary No. 37-30, Jet Propulsion Laboratory, California Institute of Technology, Pasadena, Calif., 1963.

76. Singer, R.A., "The Design and Synthesis of Linear Multivariable Systems with Application to State Estimation," SU-SEL-68-030, Stanford Electronics Labs., Stanford University, Stanford, Calif., June 1968.

77. Gopinath, B., and B.O. Lange, "On the Identification and Control of Linear Systems," SUDAAR 351, Department of Aeronautics and Astronautics, Stanford University, Stanford, Calif., June 1968.